University of Alberta

EFFECTS OF CORRELATION ON MULTIPLE ANTENNA SYSTEMS

by

Xiaodi Zhang 

A thesis submitted to the Faculty of Graduate Studies and Research in partial fulfillment of the requirements for the degree of **Doctor of Philosophy**.

Department of Electrical and Computer Engineering

Edmonton, Alberta

Spring 2007

Your file Votre référence
ISBN: 978-0-494-29777-3
Our file Notre référence
ISBN: 978-0-494-29777-3

Abstract

The use of multiple antennas in wireless systems is a key technology to meet the demand for high-speed data transmission with better quality of service (QoS). Unlike wired environments, wireless channels constitute a hostile propagation medium suffering from fading and interference. Spatial diversity employing independent multiple antennas can combat fading and interference effectively. However, in practice, the signals at antennas are often correlated, which influences system performance and cannot be ignored in many situations. In this dissertation, we provide insights into the effects of antenna correlation on the performance of various multiple receiver antenna systems through extensive theoretic analyses.

An exact and unified performance analysis framework for threshold-based hybrid selection/ maximal-ratio combining (T-HS/MRC) over generalized fading channels is presented. The average symbol error rate (SER) and outage probability in independent fading are obtained through the total probability theorem and moment generating function (MGF) method.

The exact SER and outage probability for selection combining (SC), hybrid selection/ maximal-ratio combining (H-S/MRC), and T-HS/MRC in Nakagami-m fading with a specific correlation structure are studied by transforming the correlated fading amplitudes into a set of independent Gaussian random variables (RVs).

Based on a Green's approximation method, an efficient approximate error rate analysis of H-S/MRC and T-HS/MRC in arbitrarily correlated Nakagami-m fading is proposed for positive integer values of fading parameter m. This method allows for different linear modulation schemes.

The outage and error rate of cellular systems with maximal ratio combining (MRC) in

cochannel interference (CCI) and correlated Rayleigh fading are provided when the correlation matrix is equally correlated or has different eigenvalues. The effect of channel estimation error on the system performance is examined rigorously.

The maximum number of receiver antennas that can be usefully deployed in a MRC diversity system with CCI and correlated Ricean fading is investigated. Three long-term output measures and the average bit error rate (BER) are evaluated. A widely applicable general rule of thumb, that the performance of a fixed-size antenna array containing the maximum number of independent antennas cannot be significantly improved by adding more than one additional antenna, is developed.

Acknowledgements

I am grateful to my supervisor Dr. Norman C. Beaulieu for his continual guidance, advice, support and encouragement throughout the duration of my Ph.D. study. His rigorous scholarship, clarity in thinking, and professional integrity will continue influence me in my future career.

I would like to thank my thesis committee members, Dr. George K. Karagiannidis from Aristotle University of Thessaloniki, Greece, Dr. Ioanis Nikolaidis from Department of Computer Science, Dr. Chintha Tellambura and Dr. Alan Lynch for their comments and suggestions with respect to this thesis.

I would like to thank all my colleagues in the iCORE Wireless Communications Laboratory for their help and friendship. Special thanks to Dr. Julian Cheng, Dr. Zheng Du, Dr. Bo Hu, Dr. Yunfei Chen, Dr. Peng Tan, and David Young for their technical discussions. I would also like to thank Feng Tao for his constant support and encouragement in my Ph.D. study.

Last, I owe my deepest gratitude to my parents, brothers and sisters for their unconditional love, patience, understanding, and support over all these years. They have always believed in me and encouraged me to pursue my dreams.

This work was sponsored by the Alberta Ingenuity and the Alberta Informatics Circle of Research Excellence (iCORE). Their financial support are greatly appreciated.

Contents

List of Tables

List of Figures

Acronyms

Acronyms	Definition
AISINR	Average instantaneous output signal-to-interference-plus noise ratio
AISIR	Average instantaneous output signal-to-interference ratio
AOA	Angle-of-arrival
AWGN	Additive white Gaussian noise
BER	Bit error rate
BFSK	Binary frequency-shift keying
BPSK	Binary phase-shift keying
CCI	Cochannel interference
CDF	Cumulative distribution function
CF	Characteristic function
DPSK	Differential phase-shift keying
EGC	Equal gain combining
GSC	Generalized selection combining
H-S/MRC	Hybrid selection/maximal-ratio combining
i.i.d.	Independent, identically distributed
i.n.d.	Independent, nonidentically distributed
INRP	Interference-power-to-noise-power ratio
LAN	Local area network
LOS	Line-of-sight

MC-CDMA	Multicarrier code-division multiple-access
MFSK	M-ary frequency-shift keying
MGF	Moment generating function
MIMO	Multiple input multiple output
MIMO-MU	MIMO multiuser
MIP	Multipath intensity profile
MISO	Multiple input single output
ML	Maximum likelihood
MQAM	M-ary quadrature-amplitude modulation
MPSK	M-ary phase-shift keying
MRC	Maximal ratio combining
PDF	Probability density function
PDP	Power delay profile
PSD	Power spectral density
QAM	Quadrature amplitude modulation
QoS	Quality of service
QPSK	Quadrature phase-shift keying
RF	Radio frequency
RV	Random variable
SAINPR	Signal amplitude to the square root of interference plus noise power ratio
SAPR	Signal amplitude to the square root of interference power ratio
SC	Selection combining
SER	Symbol error rate
SIMO	Single input multiple output
SINR	Signal-to-interference-plus-noise ratio
SINRP	Signal-power-to-interference-power-plus-noise-power ratio
SIR	Signal-to-interference ratio
SIRP	Signal-power-to-interference-power ratio

SISO	Single input single output
SNR	Signal-to-noise ratio
SW	Switch diversity
T-HS/MRC	Threshold-based hybrid selection/maximal-ratio combining
WAN	Wide area network
UWB	Ultra-wideband
2D	Two-dimensional
3D	Three-dimensional

List of Symbols

Symbol	Definition
$\chi_n(0,\sigma^2)$	Central chi-square distribution with n degrees of freedom and common Gaussian variance σ^2
$\chi_n(s,\sigma^2)$	Noncentral chi-square distribution with n degrees of freedom, noncentrality parameter s^2 and common Gaussian variance σ^2
$\delta(x)$	Kronecker delta funcion
γ_{AISIR}	Average instantaneous output SIR
$\gamma(\alpha,x)$	Incomplete gamma function
γ_{EGC}	Instantaneous EGC output SNR
γ_k	Instantaneous SNR of the kth diversity branch
$\gamma_{(k)}$ $(k=1,\cdots,N)$	Ordered instantaneous branch SNRs
$\gamma_{H-S/MRC}$	Instantaneous H-S/MRC output SNR
γ_{MRC}	Instantaneous MRC output SNR
γ_{SAPR}	Long-term output SAPR
γ_{SC}	Instantaneous SC output SNR
γ_{SINR}	Instantaneous output SINR
γ_{SIR}	Instantaneous output SIR
γ_{SIRP}	Long-term output SIRP
γ_{th}	Threshold of the output SNR or SINR
$\gamma_{T-HS/MRC(L_c)}$	Instantaneous T-HS/MRC output SNR when L_c branches are combined
Γ	Average diversity branch SNR

Γ_0	Ratio of the desired user signal power to the noise power
Γ_k	Average SNR of the kth diversity branch
Γ_I	Ratio of the desired user signal power to the total interference power
Γ_I^n	Ratio of the desired user signal power to the nth interfering user signal power
$\Gamma(\alpha)$	Gamma function
$\Gamma(\alpha, x)$	Incomplete Gamma function
λ_i	The ith matrix eigenvalue
Λ	Diagonal matrix composed of matrix eigenvalues
μ	Normalized threshold of T-HS/MRC
Ω	Average power of the fading envelope
$\phi_\gamma(j\omega)$	CF of RV γ
$\phi_\gamma(s)$	MGF of RV γ
$\phi_\gamma(s, x)$	Incomplete MGF of RV γ
Σ	Covariance matrix
$[A]^H$	Transpose and conjugate of matrix A
$[A]^T$	Transpose of matrix A
$\mathbf{c_n}$	Complex channel gain vector of the nth user
$\tilde{\mathbf{c_0}}$	Estimate of the channel gain vector for the desired user $\mathbf{c_0}$
C	Green's matrix
$C(\mu, \sigma^2)$	Complex Gaussian distribution with mean μ and variance σ^2
d_n	Information bits of the nth user signal
D	Decision variable
D_{N_I}	Transmitted data set $\{d_1, d_2, \cdots, d_{N_I}\}$
e_i	one specific permutation of the integers $\{1, \cdots, N\}$
E_s	Transmitted signal energy per symbol
$\mathbb{E}(\gamma)$	Expectation of RV γ
$f_\gamma(x)$	PDF of RV γ
$F_\gamma(x)$	CDF of RV γ

$\mathbb{F}(x)$	Fourier transform of x
h_k	Complex channel gain of the kth diversity branch
I	Identity matrix
$Im\{z\}$	Imaginary part of z
$I_v(x)$	The vth-order modified Bessel function of the first kind
$J_0(x)$	The zeroth-order Bessel function of the first kind
$\mathbb{K}$	Ricean factor
L_c	Number of branches to be combined
$\bar{L_c}$	Average number of branches combined of T-HS/MRC
$\mathbb{L}^{-1}(s)$	Inverse Laplace transform
m	Nakagami-m fading parameter
N	Number of diversity branches available
N_0	Power spectral density of AWGN
N_I	Number of interfering users
$N(\mu, \sigma^2)$	Gaussian distribution with mean μ and variance σ^2
P_0	Desired user signal power
P_I	Total interference power
P_n	Signal power of the nth user signal
P_e	Error probability
P_{outage}	Outage probability
$P(e, L_c = L)$	SER of T-HS/MRC when L branches are combined
$P(\gamma_{th}, L_c = L)$	Outage probability of T-HS/MRC when L branches are combined
$Q(x)$	Q function
$Q_v(a,b)$	The vth-order Marcum Q-function
$\mathbf{r}$	Received baseband signal vector
r_k	Received baseband signal RV of the kth diversity branch after match-filtering and sampling
$r_k(t)$	Received basedband signal of the kth diversity branch
r_{EGC}	EGC combiner output

r_{MRC}	MRC combiner output
r_{SC}	SC combiner output
$R_{\mathbf{c_n}}$	Correlation matrix of the channel gain vector of the nth user signal
$Re\{z\}$	Real part of z
$s(t)$	Complex baseband transmitted signal
s_k	Baseband transmitted signal RV of the kth diversity branch
S_N	A set of all permutations of the integers $\{1,\cdots,N\}$
T	Number of the primary antennas
$T_{N,L}$	A subset of S_N with element e_i satisfying $e_i[2] < e_i[3] < \cdots < e_i[L]$ and $e_i[L+1] < e_i[L+2] < \cdots < e_i[N]$
$tr(A)$	Trace of matrix A
$Var(\gamma)$	Variance of RV γ
W_{N,L_c}	A subset of S_N with element e_i satisfying $e_i[1] < e_i[2] < \cdots < e_i[L_c-1]$ and $e_i[L_c+1] < e_i[L_c+2] < \cdots < e_i[N]$
$\mathbf{z_0}$	Complex AWGN vector
z_k	Complex AWGN RV of the kth diversity branch after match-filtering and sampling
$z_k(t)$	Baseband additive white Gaussian noise process of the kth diversity branch

Chapter 1

Introduction

1.1 Multiple Antenna Systems

Over one hundred years ago, Guglielmo Marconi invented the radiotelegraphy, and the radio age began. Today, the rapid progress in radio technology is creating new and improved services at lower cost, which results in increases in air-time usage and the number of subscribers, and wireless industry has become a dominant force. From broadcast radio stations to cellular telephones to wireless Internet, there are more wireless applications than ever before. Wireless revenues are currently growing between 20% and 30% each year. On the other hand, wireless industry is faced with a number of challenges including the limited availability of radio frequency spectrum and a complex time varying wireless environment (fading and interference). In addition, the increasing demand for seamless, high-speed applications with better quality of service (QoS), such as multimedia wireless transmission, etc., requires larger capacity, greater user coverage and lower transmission error rate. This makes higher spectral efficiency and better link reliability become two major concerns for future broadband wireless systems. As a break-through technique, the use of multiple antennas at the receiver and/or the transmitter in the system, namely, multiple antenna systems, can achieve significant improvements in these measures by employing spatial multiplexing and diversity schemes [1]. Some aspects of this technology have al-

ready been incorporated into 3G mobile and fixed wireless standards. As a core technique for future mobile networks (Beyond 3G or 4G), wireless LANs and WANs, multiple antenna system attracts lots of interest both from academia and industry.

As shown in Fig. 1.1, there are different antenna configurations for multiple antenna systems. The SISO (single input single output) system is the familiar wireless configuration; SIMO (single input multiple output) has a single transmitter antenna and multiple receiver antennas; MISO (multiple input single output) has multiple transmitter antennas and a single receiver antenna; and MIMO (multiple input multiple output) has multiple transmitter antennas and multiple receiver antennas. The MIMO-MU (MIMO multiuser) configuration refers to the case where a base-station with multiple antennas communicates with N_I users each with one or more antennas.

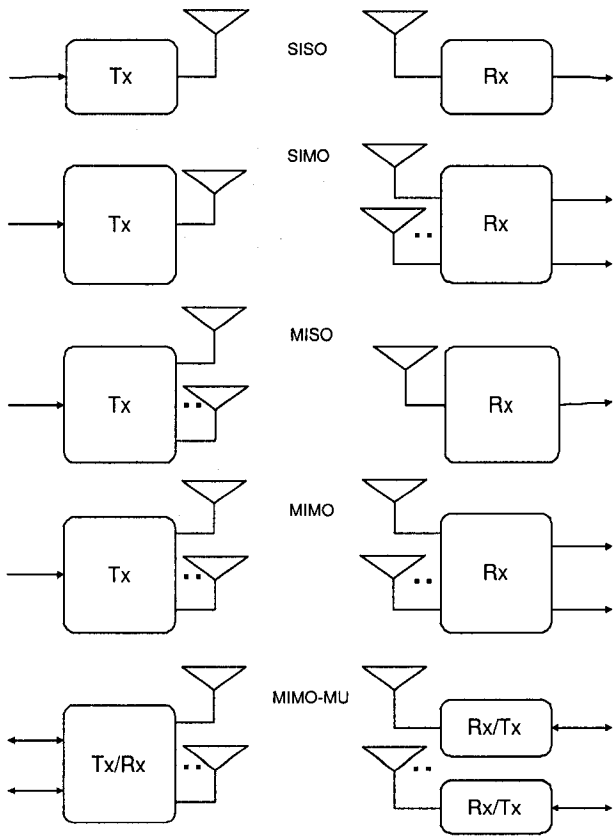

Fig. 1.1. Antenna configurations in multiple antenna systems.

In the field of multiple antenna systems, there are mainly three study areas :

1) the electromagnetic design of the antennas and antenna arrays is involved in designing antennas to meet requirements for gain, polarization, beamwidth, sidelobe level, efficiency and radiation pattern, etc.;

2) the angle-of-arrival (AOA) estimation focuses on estimating arrival angles of wavefronts impinging on the antenna array with minimum error and high resolution;

3) the use of antenna arrays improves spectral efficiency, coverage and quality of wireless links [1]. In this dissertation, we mainly focus on the third area. Concretely, we study the performance of multiple antenna systems with various receiver diversity combining schemes in the presence of correlated fading and cochannel interference (CCI). The results will be useful for better system design.

1.2 Wireless Transmission Environment

In this section, we first briefly describe fading and interference, which are two main sources deteriorating wireless system performance. Then we introduce fading correlation, an important factor which cannot be ignored in many situations. In Section 1.2.1, three basic types of fading channels studied in this thesis are presented. In Section 1.2.2, the basic concepts of cellular systems and cochannel interference are introduced. In Section 1.2.3, fading correlation among antenna signals in practical systems is emphasized.

1.2.1 Multipath Fading

Radiowave propagation through wireless channels is complicated and characterized by various effects such as multipath fading and shadowing. Multipath fading is due to the constructive and destructive combination of randomly delayed, reflected, scattered, and diffracted signal components. This type of fading is responsible for the short-term signal variations, where both of the signal envelope and signal phase fluctuate over time.

Depending on the relative relation between the symbol period of the transmitted signal

and the coherence time of fading channels, fading is classified into slow fading and fast fading [2], [3]. Coherence time is the period of time over which the fading process is correlated. Coherence time T_c is approximated by the inverse of the channel Doppler spread f_d, namely, $T_c \approx 1/f_d$. When the symbol time duration T_s is smaller than the channel's coherence time T_c, the fading is considered as slow fading; otherwise, the fading is fast fading. Similarly, according to the relative relation between the transmitted signal bandwidth and the channel coherence bandwidth, fading is classified into frequency-nonselective fading and frequency-selective fading. Coherence bandwidth measures the frequency range over which the fading process is correlated. The channel's coherence bandwidth f_c is related to the maximum delay spread τ_{max} by $f_c \approx 1/\tau_{max}$. When the bandwidth of the transmitter signal is much smaller than the channel's coherence bandwidth, the fading is frequency-nonselective or equivalently frequency-flat; otherwise, the fading is frequency-selective. In this thesis, we mainly focus on slow and frequency-nonselective fading channels.

Depending on the nature of the radio propagation environment, there are different models describing the statistical behavior of the multipath fading envelope. In the following, we introduce three fading envelope models [2] used in our work.

Rayleigh Fading

In mobile radio channels without a direct line-of-sight (LOS) path, the Rayleigh distribution is commonly used to describe the statistical time varying nature of the received envelope of a flat fading signal, or the envelope of an individual multipath component. It is well known that the envelope of the sum of two independent, identically distributed (i. i. d.) Gaussian signals with zero mean and variance σ^2 obeys a Rayleigh distribution. The probability density function (PDF) of Rayleigh distribution is given by

$$\begin{aligned} f_\alpha(x) &= \frac{x}{\sigma^2}\exp\left(-\frac{x^2}{2\sigma^2}\right) \\ &= \frac{2x}{\Omega}\exp\left(-\frac{x^2}{\Omega}\right), \qquad x \geq 0 \end{aligned} \tag{1.1}$$

where $\Omega = \mathbb{E}(\alpha^2) = 2\sigma^2$, is the average power of the received signal envelope. The corresponding squared envelope α^2 is exponentially distributed with distribution given by

$$f_{\alpha^2}(x) = \frac{1}{\Omega}\exp\left(-\frac{x}{\Omega}\right), \qquad x \geq 0. \tag{1.2}$$

Ricean Fading

Where there is a dominant stationary (no fading) signal component, such as a LOS propagation path, arriving with many weaker random multipath signal components, the small-scale fading envelope distribution is Ricean given by

$$f_{\alpha}(x) = \frac{x}{\sigma^2}\exp\left(-\frac{x^2+A^2}{2\sigma^2}\right) I_0\left(\frac{Ax}{\sigma^2}\right), \qquad x \geq 0 \tag{1.3}$$

where A denotes the peak amplitude of the dominant signal and $I_v(x)$ denotes the vth-order modified Bessel function of the first kind given at [4, eq. (2-1-120)]. As the strength of the dominant signal diminishes, the Ricean distribution degenerates to a Rayleigh distribution. As the strength of the dominant signal becomes large relative to the strength of the scattering component, the channel does not exhibit any fading at all. The Ricean distribution can also be rewritten using the Ricean factor as follows

$$f_{\alpha}(x) = \frac{2x(\mathbb{K}+1)}{\Omega}\exp\left(-\mathbb{K}-\frac{(\mathbb{K}+1)x^2}{\Omega}\right) I_0\left(2x\sqrt{\frac{\mathbb{K}(\mathbb{K}+1)}{\Omega}}\right) \qquad x \geq 0 \tag{1.4}$$

where $\mathbb{K} = A^2/(2\sigma^2)$ is the Ricean factor defined as the ratio of the specular power A^2 to the scattered power $2\sigma^2$, and the average envelope power $\Omega = \mathbb{E}(\alpha^2) = A^2 + 2\sigma^2$. Note that $A^2 = K\Omega/(K+1)$ and $2\sigma^2 = \Omega/(\mathbb{K}+1)$. The squared envelope has a non-central chi-square distribution with two degrees of freedom given by

$$f_{\alpha^2}(x) = \frac{(\mathbb{K}+1)}{\Omega}\exp\left(-\mathbb{K}-\frac{(\mathbb{K}+1)x}{\Omega}\right) I_0\left(2\sqrt{\frac{\mathbb{K}(\mathbb{K}+1)x}{\Omega}}\right), \qquad x \geq 0. \tag{1.5}$$

Nakagami-*m* Fading

Introduced by Nakagami in the early 1940's [5], the Nakagami-*m* distribution is frequently used to characterize the statistics of signals transmitted through multipath fading channels. Empirical data show that the Nakagami fading model fits observed data better than

Rayleigh, Ricean or log-normal distributions. The Nakagami-m faded signal envelope has a PDF as

$$f_\alpha(x) = \frac{2}{\Gamma(m)}\left(\frac{m}{\Omega}\right)^m x^{2m-1}\exp\left(-\frac{mx^2}{\Omega}\right), \qquad x \geq 0,\ m \geq \frac{1}{2} \tag{1.6}$$

where $\Omega = \mathbb{E}(\alpha^2)$, m is the fading parameter defined as $m = \Omega^2/\mathbb{E}[(\alpha^2 - \Omega)^2]$, and $\Gamma(x)$ is the gamma function given at [6, eq. (8.310.1)]. The corresponding squared envelope has a Gamma distribution as

$$f_{\alpha^2}(x) = \left(\frac{m}{\Omega}\right)^m \frac{x^{m-1}}{\Gamma(m)}\exp\left(-\frac{mx}{\Omega}\right), \qquad x \geq 0. \tag{1.7}$$

The Nakagami-m distribution can be used to model fading conditions more or less severe than Rayleigh fading. When $m = 1$, the Nakagami-m distribution becomes the Rayleigh distribution. When $m = 0.5$, it becomes a one-sided Gaussian distribution, and when $m \to \infty$, the distribution becomes an impulse (no fading). In addition, the Ricean distribution can be closely approximated by the Nakagami distribution with $\mathbb{K} = \sqrt{m^2 - m}/(m - \sqrt{m^2 - m})$ and $m = (\mathbb{K}+1)^2/(2\mathbb{K}+1)$, for $m > 1$ [2].

1.2.2 Cochannel Interference

Spectrum resource is limited. To achieve a high spectral efficiency to accommodate more and more users while maintaining a certain QoS, the cellular concept is introduced in solving the spectral congestion problem and the user capacity problem [7]. The basic idea of cellular communications is first to divide the target coverage area into cells. Each cell is allocated a portion of the total number of channels available to the entire system. Different sets of channels are assigned to adjacent cells and the same set of channels is reused in different cells that are separated sufficiently apart, as illustrated in Fig. 1.2, where the cells labeled with the same letters use the same set of frequencies (channels). These cells are called cochannel cells. Therefore, the desired mobile user signal is subject to the corruption of the interference generated by other user signals in the cochannel cells operating at the same carrier frequency. This kind of interference is called cochannel interference. To accommodate increasing number of users, the cell sizes are often reduced (a microcellular

environment) in order to meet this capacity demand. As a result, the radio link performance in a microcellular system is limited dominantly by CCI rather than thermal noise.

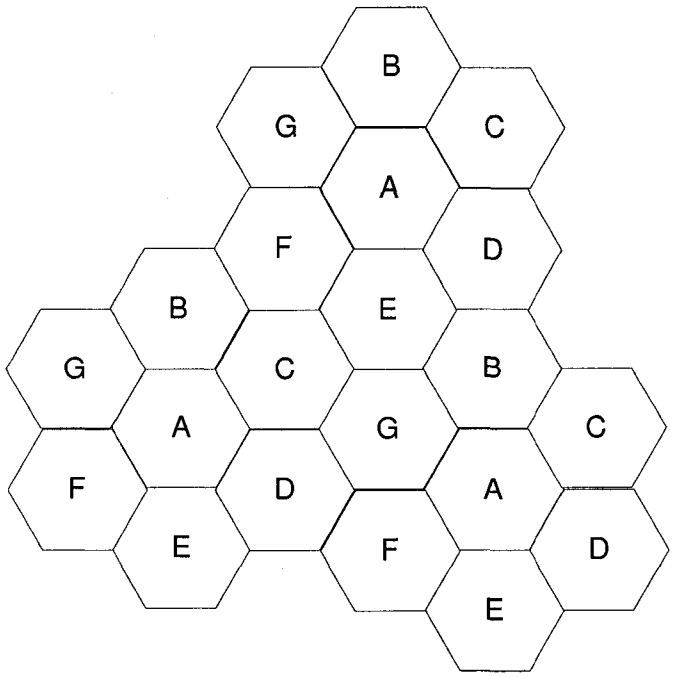

Fig. 1.2. A two-tier cellular system layout with hexagon cell shape.

1.2.3 Fading Correlation

When all of the antennas are independent, using multiple antennas improves system performance greatly [8], [9]. However, in practice, there are often exist applications where independent antenna signals are not available. For example, in compact antenna systems, such as small-size mobile handsets [10], the antenna fadings are correlated due to space limitations. It is indicated that the capacity of a fixed-volume multiple antenna system approaches a finite limit, which is independent of the number of antennas placed into this fixed-space antenna array due to antenna correlation [11]. For multipath diversity over frequency-selective channels, correlation coefficients up to 0.6 between adjacent and second adjacent paths in the channel impulse response of frequency-selective channels were observed in [12] and [13]. These early observations were confirmed by the propagation

campaign of Patenaude *et al.* [14], [15]. Based on a thorough statistical analysis of several macrocellular, microcellular, and indoor wideband channel impulse response measurements, they reported correlation coefficients sometimes higher than 0.8 with no significant reduction in the correlation even for large path delay differences. As a result, the maximum theoretical diversity gain promised by RAKE reception cannot be achieved [3]. On the other hand, some papers suggest that substantial benefits can be obtained from adding additional, correlated antennas [16–19]. For example, in the case of space diversity where the correlation depends on the distance between the antennas, expressed in terms of wavelength, the results in [16] show that when the separation between two adjacent antennas is greater than one fifth of the wavelength, most of the diversity gain is still obtained and the penalty due to the residual correlation is on the order of 1-2 dB. Reference [17] indicates that the spatial diversity gain of combating multipath fading for the desired signal is reduced due to the correlation of the received signal among the antenna branches. However, the degradation in performance can be small even for correlations as high as 0.7 [19]. From the foregoing discussions, we note that fading correlation has significant impact on the system performance and cannot be ignored in many practical systems. Motivated by this, we explore the effects of antenna correlation on the performance of multiple antenna systems in this thesis.

1.3 Receiver Diversity

Unlike stationary and more predictable wired environments, a wireless channel constitutes a hostile propagation medium, which typically suffers from the extremely random fading and interference from other users. To combat multipath fading and cochannel interference, many of the current and emerging wireless systems use one form or another of diversity. The use of multiple receiver antennas for diversity goes back to Marconi and the early radio pioneers, and leads to a considerable performance gain, both in terms of a better link budget and in terms of tolerance to CCI [20–22]. In the following, we introduce the basic concept of diversity and then describe various diversity combining schemes studied in this thesis.

1.3.1 Diversity Concept

The principle of diversity is that, if a number of copies of the same information bearing signal are available, and they all experience independent fading, then the probability that all copies are in deep fades simultaneously, is small. If signal copies are properly combined at the receiver end, one can reduce the effect of channel fading and improve the performance of communication systems.

Fig. 1.3 shows a diagram of a linear diversity combiner structure. Assume that there are N available diversity branches experiencing slow and flat fading. The received baseband signal at the kth diversity branch, $r_k(t)$, is given by

$$r_k(t) = h_k s(t) + z_k(t), \qquad k = 1, \cdots, N \tag{1.8}$$

where $s(t)$ is the baseband transmitted signal with average signal energy per symbol E_s, h_k is the complex channel gain for the kth diversity branch, and $z_k(t)$ is a zero-mean complex additive white Gaussian noise (AWGN) process with power spectral density (PSD) N_0 Watt/Hz. After match-filtering and sampling at the kth branch receiver, the received branch signal variable r_k is given by

$$r_k = h_k s_k + z_k, \qquad k = 1, \cdots, N \tag{1.9}$$

where s_k is the transmitted signal random variable (RV), and z_k is a complex AWGN RV with zero mean and variance N_0. Then the instantaneous signal-to-noise ratio (SNR) for the kth diversity branch is given by [23–25]

$$\gamma_k = |h_k|^2 \frac{E_s}{N_0}, \qquad k = 1, \cdots, N. \tag{1.10}$$

All of the received variables r_k $(k = 1, \cdots, N)$ are then linearly combined as the combiner output represented by [22]

$$r = \sum_{k=1}^{N} a_k r_k \tag{1.11}$$

where the combining coefficient a_k $(k = 1, \cdots, N)$ is proportional to the channel gain and may be allowed to vary with the fluctuating local statistics of r_k. In our work, we take a_k to be locally constant or at least approximately so.

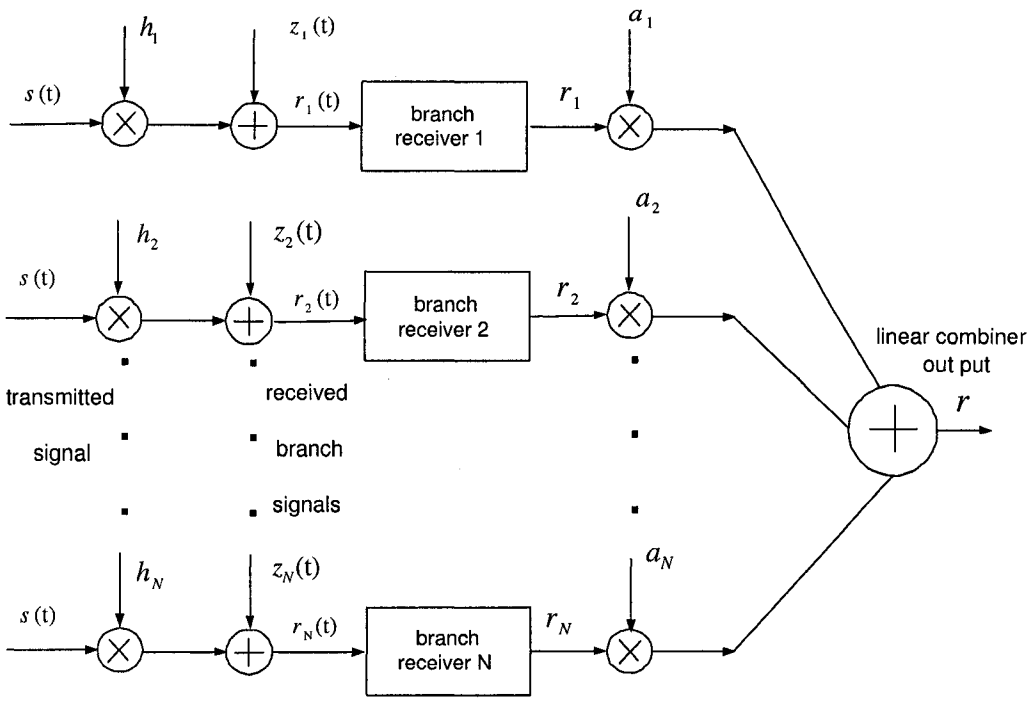

Fig. 1.3. A diagram of a linear diversity combiner structure.

There are several known methods to obtain the independent copies of the signal [22], [26]. Space diversity, most commonly used and preferred for mobile communication engineering, places antennas far enough apart to achieve independent fading signals. Frequency diversity transmits the same information on two or more carrier frequencies. If these are sufficiently separated, the fading on the different frequency channels is approximately independent, as in the case of space diversity. Time diversity transmits the same information at two or more distinct times to obtain independent fading signals in the time domain. Multipath diversity, or the RAKE technique, can be achieved in multipath situations when wideband signals are transmitted. The multipath ray reception is obtained by resolving multipath components at different delays [4, 27, 28]. In addition, polarization diversity, feedback diversity, and diversity reception of signals arriving with different angles, have also been developed. In this thesis, we mainly focus on space diversity.

1.3.2 Classic Diversity Combining Methods

Various diversity combining schemes have been developed to capitalize on the uncorrelated fading signals. The following are three classic types of linear combining schemes that have been widely used in practice.

Maximal Ratio Combining

First proposed by Kahn [21], a maximal ratio combining (MRC) scheme co-phases, weights and combines the received signals from multiple branches. In the absence of interference, MRC is the optimum combining scheme to maximize the combiner output SNR when local noise is Gaussian [22]. However, MRC is also considered as the most complicated to implement due to the fact that phase-lock and amplitude weighting must be performed. Assuming the noise components of the input branches are mutually independent, the MRC combiner output signal is obtained by replacing the combining coefficient a_k in (1.11) with the conjugate of the complex branch gain h_k

$$r_{MRC} = \sum_{k=1}^{N} h_k^* r_k = \sum_{k=1}^{N} |h_k|^2 s_k + h_k^* z_k \tag{1.12}$$

where $\{\cdot\}^*$ denotes complex conjugation. Then the instantaneous MRC output SNR, γ_{MRC}, is given by

$$\gamma_{MRC} = \frac{(\sum_{k=1}^{N} |h_k|^2)^2 E_s}{(\sum_{k=1}^{N} |h_k|^2) N_0} = \sum_{k=1}^{N} \frac{|h_k|^2 E_s}{N_0} = \sum_{k=1}^{N} \gamma_k \tag{1.13}$$

where $\gamma_k = |h_k|^2 E_s / N_0$ denotes the instantaneous SNR of the kth diversity branch as defined previously.

Equal Gain Combining

It may not always be convenient or desirable to provide the variable weighting capability required for true maximal ratio combining. Instead, the weights may all be set equal to a constant amplitude value resulting in equal gain combining (EGC). Concretely, EGC sets the weights a_k in (1.11) as $h_k^*/|h_k|$, namely, just co-phases the branch signals with equal

weights. Assuming equal noise powers in all the branches, the instantaneous output signal of EGC is given by

$$r_{EGC} = \sum_{k=1}^{N} \frac{h_k^*}{|h_k|} r_k = \sum_{k=1}^{N} |h_k| s_k + \frac{h_k^*}{|h_k|} z_k. \tag{1.14}$$

The instantaneous EGC output SNR, γ_{EGC}, is given by

$$\gamma_{EGC} = \frac{(\sum_{k=1}^{N} |h_k|)^2 E_s}{N N_0}. \tag{1.15}$$

Selection Combining

For selection combining (SC), the system just picks the best out of the N noisy signals r_k $(k = 1, \cdots, N)$. Let α_k $(k = 1, \cdots, N)$ represent the received noiseless signal envelope at the kth branch, and assume all of the N branches have the same noise power spectral density N_0. Then the output of SC can be expressed as

$$r_{SC} = r_{index(max\{\alpha_k\}_{k=1}^{N})} \tag{1.16}$$

where $index(x_k)$ denotes the index k corresponding to x_k. Then the instantaneous output SNR of SC is given by

$$\gamma_{SC} = \max\{\gamma_k\}_{k=1}^{N}. \tag{1.17}$$

Selection combining is the simplest method of all, and can be applied for noncoherent detection where no phase information is required. However, since SC ignores information provided by other diversity branches, its performance is poorer than other schemes.

1.3.3 Hybrid Selection/Maximal-Ratio Combining

From the previous discussion, we know that SC is the simplest combining scheme by using only one of the N available branch signals, and hence does not fully exploit the amount of diversity offered by the fading channel. MRC is the optimal combining scheme implemented by weighting and combining the received signals to maximize the instantaneous SNR at the combiner output. However, MRC is complicated and sensitive to channel estimation errors when the instantaneous SNR is low. On the other hand, though a high diversity order is possible in many situations, it may not be feasible to utilize all of the available

branches. For example, the main limitation for a handset is typically the power consumption and the cost of the radio frequency (RF) electronics in each diversity branch. For spread spectrum receivers operating in dense multipath environments, such as a wideband receiver, the available correlator resources limit the number of paths that can be utilized in a Rake receiver. This has motivated studies of diversity combining techniques that process only a subset of the available diversity branches with limited resources, less complexity but good performance close to MRC. Proposed by Eng *et al.* as SC2 and SC3 in [29], hybrid selection/maximal-ratio combining (H-S/MRC) is such a combining scheme to achieve a good compromise between system performance and system complexity by first selecting a subset of the best branch signals and then combining these branch signals using MRC. Concretely, H-S/MRC chooses from N received branch signals the L_c best ones and optimally weights and sums the L_c best signal replicas to produce the receiver decision statistics. The output instantaneous SNR of a H-S/MRC combiner is given by [23]

$$\gamma_{H-S/MRC} = \sum_{k=1}^{L_c} \gamma_{(k)}, \qquad L_c = 1, \cdots, N \tag{1.18}$$

where $\gamma_{(k)}$ $(k = 1, \cdots, N)$ are the descending-ordered instantaneous branch SNRs, γ_k $(k = 1, \cdots, N)$, satisfying $\gamma_{(1)} \geq \gamma_{(2)} \geq \cdots \geq \gamma_{(N)} \geq 0$.

1.3.4 Threshold-Based Hybrid Selection/Maximal-Ratio Combining

Since, in conventional H-S/MRC, the number of selected diversity branches, L_c, is predetermined, this scheme has a fixed complexity; however, at times of deep fade, the combiner may potentially include branches whose instantaneous SNRs may be small and could be discarded, or alternatively, discard many branches whose instantaneous SNRs may be close in value to those of the branches selected and could contribute to the performance improvement in good channel conditions [30]. This makes H-S/MRC not very suitable for use in a channel that improves or degrades from time to time, as is the case in mobile communications channels. For example,in ultra-wideband (UWB) systems, the power delay profile (PDP) depends on the severity of scattering and usually differs from one fading environment to another [31].

To alleviate the above-mentioned problem associated with conventional H-S/MRC, a new diversity combining scheme was proposed in [30]. This new method allows the number of combined branches to be a variable whose value is determined in accordance with the instantaneous SNR of each branch and a predetermined normalized threshold. Here we call this combining scheme threshold-based hybrid selection/maximal-ratio combining (T-HS/MRC). Concretely, at the front end of a T-HS/MRC receiver, the ratio of the instantaneous SNR of each branch to that of the best branch with the largest instantaneous SNR is first tested against a fixed normalized threshold μ whose value is chosen in the interval [0, 1]. Then, MRC is applied only to those diversity branches whose ratio values equal or exceed the value of μ. Then the instantaneous output SNR of a T-HS/MRC combiner is given by

$$\gamma_{T-HS/MRC(L_c)} = \sum_{k=1}^{L_c} \gamma_{(k)}, \qquad L_c = 1, \cdots, N \tag{1.19}$$

where L_c is an integer RV that represents the number of branches being combined in order of decreasing instantaneous SNR starting with the one having the largest instantaneous SNR. The event that L_c diversity branches are selected, means that the ordered instantaneous branch SNRs, at the selection time, satisfy $\gamma_{(1)} > \gamma_{(2)} > \cdots > \gamma_{(L_c)} \geq \mu\gamma_{(1)} > \gamma_{(L_c+1)} > \gamma_{(L_c+2)} > \cdots > \gamma_{(N)}$. Therefore, a T-HS/MRC combiner can be viewed as a conventional H-S/MRC combiner whose number of combined diversity branches, L_c, is a RV related to the normalized threshold μ and the ordered instantaneous branch SNRs $\gamma_{(k)}$ $(k = 1, \cdots, N)$, rather than a fixed number. Particularly, when the value of the normalized threshold μ equals 0 and 1, T-HS/MRC becomes MRC and SC, respectively.

1.4 Thesis Outline and Contributions

In this thesis, we mainly focus on the performance analysis of multiple antenna systems using various diversity schemes with CCI in various fading channels. The effects of antenna correlation on system performance and system design are studied. This thesis consists of five major chapters. Each chapter corresponds to one major contribution. At the begin-

ning of each chapter, we review, in detail, some background and literature which are most relevant to the subject of that chapter.

In Chapter 2, we present an exact and unified performance analysis framework for T-HS/MRC systems over generalized fading channels. We first review the previous works on T-HS/MRC, which give an inaccurate performance evaluation of this scheme. Then using the total probability theorem and moment generating function (MGF) method, the exact average symbol error rate (SER) and outage probability of T-HS/MRC in generalized fading channels are derived. This theoretical analysis applies for different M-ary linear modulation schemes in various fading models. For the case of independent fading, we simplify the MGF of T-HS/MRC output SNR and obtain exact expressions for the average SER and outage probability. Both independent, identically distributed case and independent, nonidentically distributed (i. n. d.) case are considered. In particular, closed-form SER and outage probability in independent Rayleigh fading are obtained. In addition, we compare our theory, the previous inaccurate analysis, and Monte Carlo simulations for different fading models with different numbers of diversity branches. The effect of the normalized threshold μ on the system performance is also investigated.

In Chapter 3, we study the performances of SC, H-S/MRC and T-HS/MRC in correlated Nakagami-m fading when the fading parameter m is a positive integer value. Since all of the three combining methods are involved in order statistics, we call them here generalized selection combining (GSC). The exact average SER and outage probability of the three combining schemes in Nakagami-m fading with a particular correlation structure are presented. This correlation model though not general, is much more general than the equal correlation case and includes equal correlation as a special case. Based on a representation of correlated Nakagami-m fading amplitudes with multivariate Gaussian RVs, we simplify the performance analysis by first transforming the correlated branch gains into a set of conditionally independent branch gains, then averaging the conditional SER and outage probability to obtain the final results. The numerical and simulation results show that our theory is in excellent agreement with the Monte Carlo simulations.

Due to the very complicated nature of order statistics involved in analyzing GSC, cur-

rently there are no exactly theoretical works on GSC in arbitrarily correlated fading channels. In Chapter 4, we propose an approximate SER analysis of H-S/MRC and T-HS/MRC in arbitrarily correlated Nakagami-m fading with positive integer values of fading parameter m. We first approximate the covariance matrix of the channel fadings to a Green's matrix, whose inverse is tridiagonal. The elements of the approximate Green's matrix are found using nonlinear approximation methods. Then the approximate SER of H-S/MRC and T-HS/MRC is derived through the MGF method. The approximate analysis allows for different M-ary linear modulation schemes. The efficiency of this approximate analysis are examined through different correlation models.

In Chapter 5, explicit expressions for outage probability of MRC with an arbitrary number of antennas in the presence of an arbitrary number of cochannel interferers and thermal noise are first derived when the branch gains of the desired user signal and interfering signals experience correlated Rayleigh fading and have the same correlation matrix. Two special cases, when the correlation matrix is equi-correlated and when the correlation matrix has different eigenvalues, are considered. The results apply to both the equal-power cochannel interferers case and the unequal-power cochannel interferers case. We also obtain a closed-form outage probability expression for MRC in CCI-limited environments. Further, the average bit error rate (BER) of a coherent binary phase-shift keying (BPSK) modulated cellular system using MRC in the presence of CCI and correlated Rayleigh fading is presented in closed-form for both of the two correlation structures. Different from the outage probability, the average BER in Rayleigh fading depends on the total interfering power instead of the individual interfering user powers. Besides, the case when the channel estimation is not perfect is also studied. Closed-form BERs of BPSK with a special channel estimator are provided. The effect of channel estimation error on the BER performance is examined.

The question of how many receiver antennas to employ effectively in a diversity system operating in CCI and fading is studied in Chapter 6. Three output measures and the average BER of a MRC diversity system in the presence of an arbitrary number of cochannel interferers are evaluated when the desired user signal and the interfering user signals are

independent, and each of them experiences arbitrarily correlated Ricean fading at the receiver antennas. Our goal is to investigate the best number of antennas required for a fixed-size antenna array to achieve a good compromise between system performance and system cost. To illustrate the problem clearly, we first consider a system model for CCI-limited environments, then the more practical model including the effect of noise is examined. For the CCI-limited case, a widely applicable general rule of thumb that the performance of a fixed-size antenna array containing the maximum number of independent antennas cannot be significantly improved by adding more than one additional antenna is developed. Some special cases where particular gains can be achieved by adding additional correlated antennas are also discussed. Further, the results show that this rule still applies when the interference dominates the noise. In addition, the asymptotic limits for the long-term output measures are unchanged when noise is neglected.

Finally, we summarize the contributions of this thesis and suggest future work in Chapter 7.

Chapter 2

Unified Performance Analysis of T-HS/MRC over Generalized Fading Channels

2.1 Introduction

As discussed in Chapter 1, H-S/MRC first ranks the instantaneous branch output SNRs, then selects a subset of these with the largest values, and finally combines them in the fashion of MRC. Since in H-S/MRC, the number of selected branches is predetermined, the scheme has a fixed processing complexity. However, it suffers from the fact that it potentially discards many branches whose SNRs might be close in value to the ones selected, or alternatively, includes the branches whose SNRs might be low. In 2000, Sulyman and Kousa proposed a new combining scheme, namely, T-HS/MRC, to alleviate this problem associated with H-S/MRC by allowing the number of combined branches to be a variable whose value is determined in accordance with the instantaneous SNR of each branch and a predetermined normalized threshold [30]. The average BER of a particular embodiment of this scheme in a Nakagami-*m* fading channel was presented and compared with that of H-S/MRC by simulation in their paper. The results show that T-HS/MRC gives a BER per-

formance close to the optimum performance at a threshold μ around 0.25. This indicates that other diversity branches left uncombined at this level render no appreciable degradation compared to the optimum performance regardless of the type of channels involved.

The performance analysis of T-HS/MRC systems was first studied for the case of independent Nakagami-m diversity branches in [32,33], and was later extended to generalized independent fading environments in [34]. In these works, a T-HS/MRC combiner is viewed as a conventional H-S/MRC combiner whose number of branches being combined, L_c, is random rather than fixed. Since the T-HS/MRC combiner outputs corresponding to each integer value of L_c represent disjoint events and form a partition of the probability space, the average SER and outage probability of T-HS/MRC are calculated using the total probability theorem [35]. Specifically, the average SER and outage probability conditioned on the number of combined diversity branches, L_c, are weighted by the probability of occurrence of the corresponding value of L_c. However, in the analyses of [32–34] , when calculating the average SER and outage probability conditioned on L_c, the corresponding results for conventional H-S/MRC are directly used by ignoring the fact that in T-HS/MRC systems, the number of combined branches, L_c, is actually a function of the ordered instantaneous branch SNRs and the normalized threshold. Thus, the joint PDF of the ordered instantaneous branch SNRs conditioned on L_c may change and is not the same as that of conventional H-S/MRC where the number of selected branches, L_c, is a fixed number independent of the ordered instantaneous branch SNRs. Therefore, the results for T-HS/MRC in [32–34] are inaccurate except for two special cases, namely, conventional MRC and SC, corresponding to the value of the normalized threshold equaling 0 and 1, respectively.

In this chapter, we present an exact and unified analysis framework for T-HS/MRC over generalized fading environments [36, 37]. The average SER and outage probability with i.i.d. and i.n.d. diversity branches are derived using the total probability theorem and MGF method. Our analytical method can be applied to generalized slow and frequency-nonselective fading channels including Rayleigh fading, Nakagami-m fading and Ricean fading, as well as different M-ary linear modulation schemes. For the purpose of illustration, we consider the performance of coherent M-ary phase-shift keying (MPSK) with

T-HS/MRC in Nakagami-m fading as an example.

The remainder chapter is organized as follows. The system model is described in Section 2.2. In Section 2.3, a unified analysis of the average SER and outage probability of T-HS/MRC in generalized fading environments is performed. Explicit expressions for the two performance measures in the cases of i.i.d. and i.n.d. diversity branches are derived in Section 2.4. Numerical results and discussion are presented in Section 2.5. In Section 2.6, we summarize the chapter results.

2.2 System Model

We assume that there are N available diversity branches experiencing slow and frequency-nonselective fading. The channel gains and the noise processes are assumed independent. Recall in Chapter 1 that $\gamma_k = |h_k|^2 E_s/N_0$ denotes the instantaneous SNR per symbol of the kth diversity branch defined by (1.10), and $\gamma_{(k)}$ $(k = 1, \cdots, N)$ represent the instantaneous branch SNRs in descending order, that is, $\gamma_{(1)} > \gamma_{(2)} > \cdots > \gamma_{(N)}$. A T-HS/MRC combiner coherently combines the branches whose instantaneous SNRs equal or exceed the product of the normalized threshold μ and the largest instantaneous branch SNR $\gamma_{(1)}$. Then the output instantaneous SNR of a T-HS/MRC combiner is given by (1.19) [32–34, 36]

$$\gamma_{T-HS/MRC(L_c)} = \sum_{k=1}^{L_c} \gamma_{(k)}, \qquad L_c = 1, \cdots, N \tag{2.1}$$

where L_c is an integer random variable that represents the number of branches being combined in order of decreasing instantaneous SNR starting with the one having the largest instantaneous SNR. The event that L_c diversity branches are selected, means that the ordered instantaneous branch SNRs, at the selection time, satisfy $\gamma_{(1)} > \gamma_{(2)} > \cdots > \gamma_{(L_c)} \geq \mu\gamma_{(1)} > \gamma_{(L_c+1)} > \gamma_{(L_c+2)} > \cdots > \gamma_{(N)}$. Therefore, a T-HS/MRC combiner can be viewed as a conventional H-S/MRC combiner whose number of combined diversity branches, L_c, is a RV related to the normalized threshold μ and the ordered instantaneous branch SNRs $\gamma_{(k)}$ $(k = 1, \cdots, N)$, rather than a fixed number. Specifically, when the value of the normalized threshold μ equals 0 and 1, T-HS/MRC becomes MRC and SC, respectively.

2.3 Unified Performance Analysis of T-HS/MRC

2.3.1 Average SER

Since the T-HS/MRC combiner outputs corresponding to each integer value of L_c represent disjoint events [33] and form a partition of probability space, the average SER of T-HS/MRC, P_e, can be calculated using the total probability theorem [35] according to

$$P_e = \sum_{L=1}^{N} P(e, L_c = L) \tag{2.2}$$

where $P(e, L_c = L)$ is the average SER of T-HS/MRC corresponding to the joint event that L branches are selected and that they satisfy $\gamma_{(1)} > \gamma_{(2)} > \cdots > \gamma_{(L)} \geq \mu\gamma_{(1)} > \gamma_{(L+1)} > \gamma_{(L+2)} > \cdots > \gamma_{(N)}$. The probability, $P(e, L_c = L)$, can be calculated using the MGF method for different linearly modulated signals [38]. Here we just consider coherent MPSK as an example; results for other modulation formats can be derived similarly. The probability $P(e, L_c = L)$ for coherent MPSK is given by [24]

$$P(e, L_c = L) = \frac{1}{\pi} \int_0^{\Theta} \phi_{\gamma_{T-HS/MRC(L)}} \left(-\frac{c_{MPSK}}{\sin^2 \theta} \right) d\theta \tag{2.3}$$

where $c_{MPSK} = \sin^2(\pi/M)$, $\Theta = \pi(M-1)/M$, $\phi_\gamma(s) = \mathbb{E}(e^{s\gamma})$ is the MGF of the random variable γ, and $\gamma_{T-HS/MRC(L)} = \sum_{k=1}^{L} \gamma_{(k)}$, is defined by (2.1), where the ordered instantaneous branch SNRs satisfy $\gamma_{(1)} > \gamma_{(2)} > \cdots > \gamma_{(L)} \geq \mu\gamma_{(1)} > \gamma_{(L+1)} > \gamma_{(L+2)} > \cdots > \gamma_{(N)}$.

2.3.2 Outage Probability

Similar to the previous analysis of the average SER of T-HS/MRC, since the T-HS/MRC combiner outputs corresponding to each integer value of L_c represent disjoint events [33] and form a partition of probability space, the outage probability of T-HS/MRC, $P_{outage}(\gamma_{th})$, can be calculated as [3]

$$\begin{aligned} P_{outage}(\gamma_{th}) &= P(\gamma_{T-HS/MRC(L_c)} < \gamma_{th}) \\ &= \sum_{L=1}^{N} P(\gamma_{T-HS/MRC(L)} < \gamma_{th},\ L_c = L) \end{aligned} \tag{2.4}$$

where γ_{th} is the specified threshold of the combiner output instantaneous SNR, $\gamma_{T-HS/MRC(L_c)}$, and $P(\gamma_{T-HS/MRC(L)} < \gamma_{th}, L_c = L)$ is the outage probability of T-HS/MRC corresponding to the joint event that L branches are selected and that they satisfy $\gamma_{(1)} > \gamma_{(2)} > \cdots > \gamma_{(L)} \geq \mu\gamma_{(1)} > \gamma_{(L+1)} > \gamma_{(L+2)} > \cdots > \gamma_{(N)}$. For notational convenience, denote $P(\gamma_{T-HS/MRC(L)} < \gamma_{th}, L_c = L)$ by $P(\gamma_{th}, L_c = L)$. According to [3, eqs. (1.5), (1.6) and (9B.5)], the probability, $P(\gamma_{th}, L_c = L)$, can be calculated as

$$\begin{aligned} P(\gamma_{th}, L_c = L) &= \frac{1}{2\pi j}\int_{\eta - j\infty}^{\eta + j\infty} \frac{\phi_{\gamma_{T-HS/MRC(L)}}(-s)}{s} e^{s\gamma_{th}} ds \\ &= \frac{2e^{\eta\gamma_{th}}}{\pi}\int_0^{\infty} Re\left\{\frac{\phi_{\gamma_{T-HS/MRC(L)}}[-(\eta + j\omega)]}{\eta + j\omega}\right\}\cos(\omega\gamma_{th})d\omega \end{aligned} \quad (2.5)$$

where γ_{th} and $\phi_{\gamma_{T-HS/MRC(L)}}(s)$ were defined previously, $Re\{\cdot\}$ denotes the real part of a complex number, and η is chosen in the region of convergence of the integral of (2.5) in the complex s-plane.

2.3.3 MGF

According to (2.1), the MGF of $\gamma_{T-HS/MRC(L)}$ is given by

$$\begin{aligned} \phi_{\gamma_{T-HS/MRC(L)}}(s) &= \mathbb{E}\left(e^{s\gamma_{T-HS/MRC(L)}}\right) \\ &= \int_0^{\infty} d\gamma_{(1)} \int_{\mu\gamma_{(1)}}^{\gamma_{(1)}} d\gamma_{(2)} \cdots \int_{\mu\gamma_{(1)}}^{\gamma_{(L-1)}} d\gamma_{(L)} \int_0^{\mu\gamma_{(1)}} d\gamma_{(L+1)} \int_0^{\gamma_{(L+1)}} d\gamma_{(L+2)} \\ &\quad \cdots \times \int_0^{\gamma_{(N-1)}} e^{s\sum_{k=1}^{L}\gamma_{(k)}} f_{\gamma_{(1)},\cdots,\gamma_{(N)}}(\gamma_{(1)}, \cdots, \gamma_{(N)}) d\gamma_{(N)} \end{aligned} \quad (2.6)$$

where $f_{\gamma_{(1)},\cdots,\gamma_{(N)}}(\gamma_{(1)}, \cdots, \gamma_{(N)})$ is the joint PDF of the ordered instantaneous branch SNRs. If the joint PDF, $f_{\gamma_{(1)},\cdots,\gamma_{(N)}}(\gamma_{(1)}, \cdots, \gamma_{(N)})$, is known, we can obtain the average SER and outage probability of T-HS/MRC by calculating the MGF of $\gamma_{T-HS/MRC(L)}$ and then substituting the result into (2.3), (2.2) and (2.5), (2.4) respectively. So far we have developed a general analysis framework for T-HS/MRC, which can be applied for arbitrary fading models and various modulation schemes.

2.4 Independent Fading Channels

When the space among the antennas is large enough, the fadings among the antennas can be taken as independent. In the following, we analyze the performance of T-HS/MRC for the cases of i.i.d. diversity branches and i.n.d. diversity branches, respectively.

2.4.1 I. I. D. Case

Assume there are N independent and identically distributed diversity branches available. Let $\Gamma = \mathbb{E}(\gamma_k)$ $(k = 1, \cdots, N)$ represent the average branch SNR. Then the joint PDF of the ordered instantaneous branch SNRs is given by [23–25, 39]

$$f_{\gamma_{(1)},\cdots,\gamma_{(N)}}(\gamma_{(1)},\cdots,\gamma_{(N)}) = \begin{cases} N!\prod_{k=1}^{N} f_\gamma(\gamma_{(k)}) & , \quad \gamma_{(1)} > \gamma_{(2)} > \cdots > \gamma_{(N)} \\ 0 & , \quad otherwise \end{cases} \tag{2.7}$$

where $f_\gamma(\cdot)$ is the common PDF of the instantaneous branch SNR, γ_k $(k = 1, \cdots, N)$.

Substituting (2.7) into (2.6), the MGF of $\gamma_{T-HS/MRC(L)}$ becomes

$$\begin{aligned} \phi_{\gamma_{T-HS/MRC(L)}}(s) &= \int_0^\infty d\gamma_{(1)} \int_{\mu\gamma_{(1)}}^{\gamma_{(1)}} d\gamma_{(2)} \cdots \int_{\mu\gamma_{(1)}}^{\gamma_{(L-1)}} d\gamma_{(L)} \int_0^{\mu\gamma_{(1)}} d\gamma_{(L+1)} \\ &\quad \times \int_0^{\gamma_{(L+1)}} d\gamma_{(L+2)} \cdots \int_0^{\gamma_{(N-1)}} e^{s\Sigma_{k=1}^{L}\gamma_{(k)}} N! \prod_{k=1}^{N} f_\gamma(\gamma_{(k)}) d\gamma_{(N)} \\ &= N! \int_0^\infty e^{s\gamma_{(1)}} f_\gamma(\gamma_{(1)}) d\gamma_{(1)} \int_{\mu\gamma_{(1)}}^{\gamma_{(1)}} e^{s\gamma_{(2)}} f_\gamma(\gamma_{(2)}) d\gamma_{(2)} \cdots \\ &\quad \times \int_{\mu\gamma_{(1)}}^{\gamma_{(L-1)}} e^{s\gamma_{(L)}} f_\gamma(\gamma_{(L)}) d\gamma_{(L)} \int_0^{\mu\gamma_{(1)}} f_\gamma(\gamma_{(L+1)}) d\gamma_{(L+1)} \\ &\quad \times \int_0^{\gamma_{(L+1)}} f_\gamma(\gamma_{(L+2)}) d\gamma_{(L+2)} \cdots \int_0^{\gamma_{(N-1)}} f_\gamma(\gamma_{(N)}) d\gamma_{(N)}. \end{aligned} \tag{2.8}$$

Using [40, eq. (3)], (2.8) can be further simplified as

$$\phi_{\gamma_{T-HS/MRC(L)}}(s) = L\binom{N}{L} \int_0^\infty e^{st} f_\gamma(t) [F_\gamma(\mu t)]^{N-L} [\phi_\gamma(s, \mu t) - \phi_\gamma(s, t)]^{L-1} dt \tag{2.9}$$

where $\binom{N}{L} = N!/(L!(N-L)!)$, $\phi_\gamma(s,x)$ and $F_\gamma(x)$ are the incomplete MGF and the cumulative distribution function (CDF) of random variable γ, respectively given by

$$\phi_\gamma(s,x) = \int_x^\infty e^{st} f_\gamma(t) dt \tag{2.10}$$

TABLE 2.1

PDF and incomplete MGF of instantaneous SNR for the kth diversity branch

Fading Channel	PDF $f_\gamma(x)$ $(x \geq 0)$	incomplete MGF $\phi_\gamma(s,x)$ $(x \geq 0)$
Rayleigh	$\frac{1}{\Gamma}\exp(-x/\Gamma)$	$\frac{\exp[-x(1/\Gamma - s)]}{1-s\Gamma}$
Nakagami-m	$\frac{1}{\Gamma(m)}\left(\frac{m}{\Gamma}\right)^m x^{m-1}\exp\left(\frac{-mx}{\Gamma}\right)$	$\frac{1}{\Gamma(m)}\left(\frac{m}{m-s\Gamma}\right)^m \Gamma(m, x(\frac{m}{\Gamma}-s))$
Ricean	$\frac{1+\mathbb{K}}{\Gamma}\exp\left[-\mathbb{K}-\frac{(1+\mathbb{K})x}{\Gamma}\right]$ $\times I_0\left[2\sqrt{\frac{\mathbb{K}(\mathbb{K}+1)x}{\Gamma}}\right]$	$\frac{1+\mathbb{K}}{1+\mathbb{K}-s\Gamma}\exp\left[\frac{s\mathbb{K}\Gamma}{1+\mathbb{K}-s\Gamma}\right]$ $\times Q\left(\sqrt{\frac{2\mathbb{K}(\mathbb{K}+1)}{1+\mathbb{K}-s\Gamma}}, \sqrt{\frac{2(1+\mathbb{K}-s\Gamma)x}{\Gamma}}\right)$

and

$$F_\gamma(x) = \int_0^x f_\gamma(t)dt = 1 - \phi_\gamma(0,x). \tag{2.11}$$

Expressions for the PDF and the incomplete MGF of the instantaneous branch SNR γ_k, $(k = 1,\cdots,N)$ for various channel fadings, based on the results in [41] are listed in Table 2.1.

Substituting (2.9) into (2.3) and (2.2), the average SER of coherent MPSK with T-HS/MRC in the case of i.i.d. diversity branches becomes

$$\begin{aligned} P_e &= \frac{1}{\pi}\sum_{L=1}^{N} L\binom{N}{L}\int_0^{\pi(M-1)/M} d\theta \int_0^\infty e^{-\frac{c_{MPSK}}{\sin^2\theta}t} f_\gamma(t)[F_\gamma(\mu t)]^{N-L} \\ &\quad \times \left[\phi_\gamma\left(-\frac{c_{MPSK}}{\sin^2\theta}, \mu t\right) - \phi_\gamma\left(-\frac{c_{MPSK}}{\sin^2\theta}, t\right)\right]^{L-1} dt. \end{aligned} \tag{2.12}$$

Similarly, substituting (2.9) into (2.5) and (2.4), the outage probability of T-HS/MRC

in the case of i.i.d. diversity branches becomes

$$P_{outage}(\gamma_{th}) = \frac{2e^{\eta\gamma_{th}}}{\pi}\sum_{L=1}^{N} L\binom{N}{L}\int_0^{\infty} d\omega \int_0^{\infty} e^{-\eta t} f_\gamma(t)[F_\gamma(\mu t)]^{N-L}\cos(\omega\gamma_{th}) \times Re\left\{\frac{e^{-j\omega t}[\phi_\gamma(-(\eta+j\omega),\mu t)-\phi_\gamma(-(\eta+j\omega),t)]^{L-1}}{\eta+j\omega}\right\} dt. \tag{2.13}$$

To illustrate (2.9), (2.12) and (2.13), let us consider the case that there are N available diversity branches experiencing i.i.d. Rayleigh fading. Results for other channel fading can be derived similarly by using corresponding fading statistics. Then for each branch in Rayleigh fading, the instantaneous branch SNR, γ_k $(k = 1,\cdots,N)$, follows an exponential distribution with

$$f_\gamma(t) = \begin{cases} \frac{1}{\Gamma}\exp(-\frac{t}{\Gamma}) & , \quad t \geq 0 \\ 0 & , \quad t < 0 \end{cases} \tag{2.14}$$

where $\Gamma = \mathbb{E}(\gamma)$ is the average SNR for each diversity branch as defined previously. The incomplete MGF and CDF of γ are given, respectively, by

$$\begin{aligned} \phi_\gamma(s,x) &= \int_x^{\infty} e^{st} f_\gamma(t)dt \\ &= \frac{1}{1-s\Gamma}e^{-(\frac{1}{\Gamma}-s)x}, \qquad x \geq 0 \end{aligned} \tag{2.15}$$

and

$$\begin{aligned} F_\gamma(x) &= 1-\phi_\gamma(0,x) \\ &= 1-e^{-\frac{1}{\Gamma}x}, \qquad x \geq 0. \end{aligned} \tag{2.16}$$

Substituting (2.14), (2.15) and (2.16) into (2.9) gives the MGF of $\gamma_{T-HS/MRC(L)}$, $\phi_{\gamma_{T-HS/MRC(L)}}(s)$ in closed-form as

$$\phi_{\gamma_{T-HS/MRC(L)}}(s) = L\binom{N}{L}\sum_{q=0}^{N-L}\sum_{p=0}^{L-1}\binom{N-L}{q}\binom{L-1}{p}(-1)^{p+q} \times \frac{1}{(1-s\Gamma)^L[1+(1-\mu)p+\mu(L-1)]+q\mu(1-s\Gamma)^{L-1}}. \tag{2.17}$$

Substituting (2.17) into (2.3) and (2.2), the average SER of coherent MPSK with T-HS/MRC in i.i.d. Rayleigh fading, becomes in closed form

$$P_e = \frac{1}{\pi}\sum_{L=1}^{N}\sum_{q=0}^{N-L}\sum_{p=0}^{L-1} L\binom{N}{L}\binom{N-L}{q}\binom{L-1}{p}(-1)^{p+q}\int_0^{\pi(M-1)/M} \frac{\sin^{2L}\theta}{\left(\sin^2\theta + c_{MPSK}\Gamma\right)^L[1+(1-\mu)p+\mu(L-1)]+q\mu\sin^2\theta\left(\sin^2\theta+c_{MPSK}\Gamma\right)^{L-1}} d\theta. \tag{2.18}$$

Similarly, the outage probability of T-HS/MRC in i.i.d. Rayleigh fading is obtained by substituting (2.17) into (2.5) and (2.4) to give

$$P_{outage}(\gamma_{th}) = \frac{2e^{\eta\gamma_{th}}}{\pi}\sum_{L=1}^{N}\sum_{q=0}^{N-L}\sum_{p=0}^{L-1} L\binom{N}{L}\binom{N-L}{q}\binom{L-1}{p}(-1)^{p+q}\times \int_0^{\infty}\cos(\omega\gamma_{th})\times Re\left\{\frac{1}{(\eta+j\omega)[1+(\eta+j\omega)\Gamma]^{L-1}}\times \frac{1}{[1+(\eta+j\omega)\Gamma][1+(1-\mu)p+\mu(L-1)]+q\mu}\right\} d\omega. \tag{2.19}$$

Alternatively, the outage probability of T-HS/MRC in i.i.d. Rayleigh fading can be derived in closed form as follows.

Rewrite (2.4) as

$$P_{outage}(\gamma_{th}) = \sum_{L=1}^{N} P(\gamma_{T-HS/MRC(L)} < \gamma_{th}, L_c = L) = \sum_{L=1}^{N}\int_0^{\gamma_{th}} f_{\gamma_{T-HS/MRC(L)}}(\gamma)d\gamma \tag{2.20}$$

where $f_{\gamma_{T-HS/MRC(L)}}(\gamma)$ denotes the PDF of $\gamma_{T-HS/MRC(L)}$, which can be calculated by [3]

$$f_{\gamma_{T-HS/MRC(L)}}(\gamma) = \mathbb{L}^{-1}\{\phi_{\gamma_{T-HS/MRC(L)}}(-s)\} \tag{2.21}$$

where $\mathbb{L}^{-1}(\cdot)$ denotes the inverse Laplace transform. Substituting (2.17) into (2.21), the PDF, $f_{\gamma_{T-HS/MRC(L)}}(\gamma)$ $(\gamma \geq 0)$, in i.i.d. Rayleigh fading, is given by

$$f_{\gamma_{T-HS/MRC(L)}}(\gamma)|_{\mu=0} = \begin{cases} 0 & , \quad L = 1,\cdots,N-1 \\ \frac{\gamma^{N-1}e^{-\gamma/\Gamma}}{(N-1)!\Gamma^N} & , \quad L = N \end{cases} \tag{2.22a}$$

$$f_{\gamma_{T-HS/MRC(L)}}(\gamma)|_{\mu=1} = \begin{cases} \frac{N}{\Gamma} e^{-\gamma/\Gamma}\left(1-e^{-\gamma/\Gamma}\right)^{N-1} & , \quad L=1 \\ 0 & , \quad L=2,\cdots,N \end{cases} \tag{2.22b}$$

$$\begin{aligned} f_{\gamma_{T-HS/MRC(L)}}(\gamma)|_{0<\mu<1} &= L\binom{N}{L}\sum_{p=0}^{L-1}\binom{L-1}{p}\frac{(-1)^p\gamma^{L-1}e^{-\gamma/\Gamma}}{\Gamma^L c_p(L-1)!} + \\ & L\binom{N}{L}\sum_{q=0}^{N-L}\sum_{p=0}^{L-1}\binom{N-L}{q}\binom{L-1}{p}\frac{(-1)^{p+q+L-1}c_p^{L-2}}{\Gamma(q\mu)^{L-1}} \\ & \times\left[e^{-\frac{c_p+q\mu}{\Gamma c_p}\gamma} - e^{-\frac{\gamma}{\Gamma}}\sum_{i=0}^{L-2}\frac{(-q\mu)^i\gamma^i}{i!(\Gamma c_p)^i}\right], \\ & \qquad\qquad L=1,\cdots,N \end{aligned} \tag{2.22c}$$

where $c_p = [1+(1-\mu)p+\mu(L-1)]$.

Substituting (2.22) into (2.20), the outage probability of T-HS/MRC in i.i.d. Rayleigh fading is obtained in closed form as

$$P_{outage}(\gamma_{th})|_{\mu=0} = 1-e^{-\gamma_{th}/\Gamma}\sum_{i=0}^{N-1}\frac{{\gamma_{th}}^i}{i!\Gamma^i} \tag{2.23a}$$

$$P_{outage}(\gamma_{th})|_{\mu=1} = (1-e^{-\gamma_{th}/\Gamma})^N \tag{2.23b}$$

$$\begin{aligned} P_{outage}(\gamma_{th})|_{0<\mu<1} &= \sum_{L=1}^{N} L\binom{N}{L}\sum_{p=0}^{L-1}\frac{(-1)^p\gamma(L,\gamma_{th}/\Gamma)}{p!(L-1-p)!c_p} + \\ & \sum_{L=1}^{N} L\binom{N}{L}\sum_{q=0}^{N-L}\sum_{p=0}^{L-1}\binom{N-L}{q}\binom{L-1}{p}\frac{(-1)^{p+q+L-1}c_p^{L-1}}{(q\mu)^{L-1}}\times \\ & \left[\frac{1-e^{-\frac{(c_p+q\mu)}{c_p\Gamma}\gamma_{th}}}{c_p+q\mu} - \sum_{i=0}^{L-2}\frac{(-q\mu)^i}{i!c_p^{i+1}}\gamma(i+1,\gamma_{th}/\Gamma)\right] \end{aligned} \tag{2.23c}$$

where $\gamma(n,x)$ is the incomplete Gamma function given by

$$\gamma(n,x) = \int_0^x t^{n-1}e^{-t}dt = (n-1)!\left(1-e^{-x}\sum_{q=0}^{n-1}\frac{x^q}{q!}\right), \qquad x\geq 0,\ n=1,2,\cdots. \tag{2.24}$$

Eqs. (2.23a) and (2.23b) correspond to the outage probability of MRC and SC [3, eq. (9.322)], respectively, which verifies this special case of T-HS/MRC.

2.4.2 I. N. D. Case

In some situations, the statistics of the N independent diversity branches are not the same. For example, based on IMT-2000 channel models [42] and JTC channel models [43], the channel multipath intensity profile (MIP) is variable, namely, the average SNR of each diversity branch is different [44]. In this section, the performance of T-HS/MRC with N independent but nonidentically distributed diversity branches is analyzed.

The joint PDF of the ordered instantaneous branch SNRs of i.n.d. diversity branches is given by [34], [45]

$$f_{\gamma_{(1)},\cdots,\gamma_{(N)}}(\gamma_{(1)},\cdots,\gamma_{(N)}) = \begin{cases} \Sigma_{e_i \in S_N} \prod_{k=1}^{N} f_{\gamma_{e_i[k]}}(\gamma_{(k)}) & , \quad \gamma_{(1)} > \gamma_{(2)} > \cdots > \gamma_{(N)} \\ 0 & , \quad otherwise \end{cases} \tag{2.25}$$

where $f_{\gamma_k}(\cdot)$ is the PDF of the instantaneous SNR of the kth branch, γ_k $(k = 1,\cdots,N)$. All of these PDFs are not necessarily identical; S_N is the set of all permutations of the integers $\{1,\cdots,N\}$ and $e_i \in S_N$ denotes $e_i = \{e_i[1], e_i[2],\cdots, e_i[N]\}$, one specific permutation of the integers $\{1,\cdots,N\}$.

Substituting (2.25) into (2.6), the MGF of $\gamma_{T-HS/MRC(L)}$ for i.n.d. diversity branches, becomes

$$\begin{aligned} \phi_{\gamma_{T-HS/MRC(L)}}(s) &= \sum_{e_i \in S_N} \int_0^{\infty} d\gamma_{(1)} \int_{\mu\gamma_{(1)}}^{\gamma_{(1)}} d\gamma_{(2)} \cdots \int_{\mu\gamma_{(1)}}^{\gamma_{(L-1)}} d\gamma_{(L)} \int_0^{\mu\gamma_{(1)}} d\gamma_{(L+1)} \\ &\quad \times \int_0^{\gamma_{(L+1)}} d\gamma_{(L+2)} \cdots \int_0^{\gamma_{(N-1)}} e^{s\Sigma_{k=1}^{L}\gamma_{(k)}} \prod_{k=1}^{N} f_{\gamma_{e_i[k]}}(\gamma_{(k)}) d\gamma_{(N)} \\ &= \sum_{e_i \in S_N} \int_0^{\infty} e^{s\gamma_{(1)}} f_{\gamma_{e_i[1]}}(\gamma_{(1)}) d\gamma_{(1)} \int_{\mu\gamma_{(1)}}^{\gamma_{(1)}} e^{s\gamma_{(2)}} f_{\gamma_{e_i[2]}}(\gamma_{(2)}) d\gamma_{(2)} \cdots \\ &\quad \times \int_{\mu\gamma_{(1)}}^{\gamma_{(L-1)}} e^{s\gamma_{(L)}} f_{\gamma_{e_i[L]}}(\gamma_{(L)}) d\gamma_{(L)} \int_0^{\mu\gamma_{(1)}} f_{\gamma_{e_i[L+1]}}(\gamma_{(L+1)}) d\gamma_{(L+1)} \\ &\quad \times \int_0^{\gamma_{(L+1)}} f_{\gamma_{e_i[L+2]}}(\gamma_{(L+2)}) d\gamma_{(L+2)} \cdots \int_0^{\gamma_{(N-1)}} f_{\gamma_{e_i[N]}}(\gamma_{(N)}) d\gamma_{(N)}. \end{aligned} \tag{2.26}$$

Using [41, eqs. (11), (12) and (A.1)], (2.26) can be further simplified as

$$\phi_{\gamma_{T-HS/MRC(L)}}(s) = \sum_{e_i \in T_{N,L}} \int_0^\infty e^{st} f_{\gamma_{e_i[1]}}(t) \prod_{k=2}^{L} \left[\phi_{\gamma_{e_i[k]}}(s,\mu t) - \phi_{\gamma_{e_i[k]}}(s,t) \right] \times \prod_{k=L+1}^{N} F_{\gamma_{e_i[k]}}(\mu t) dt \tag{2.27}$$

where $\phi_{\gamma_{e_i[k]}}(s,x)$ and $F_{\gamma_{e_i[k]}}(x)$ are respectively the incomplete MGF and CDF of $\gamma_{e_i[k]}$ as defined at (2.10) and (2.11); and $T_{N,L}$ is a subset of S_N, whose element e_i satisfies $e_i[2] < e_i[3] < \cdots < e_i[L]$ and $e_i[L+1] < e_i[L+2] < \cdots < e_i[N]$.

Substituting (2.27) into (2.3) and (2.2), the average SER of coherent MPSK with T-HS/MRC in the case of i. n. d. diversity branches becomes

$$P_e = \frac{1}{\pi} \sum_{L=1}^{N} \sum_{e_i \in T_{N,L}} \int_0^{\pi(M-1)/M} d\theta \int_0^\infty e^{-\frac{c_{MPSK}}{\sin^2\theta} t} f_{\gamma_{e_i[1]}}(t) \prod_{k=L+1}^{N} F_{\gamma_{e_i[k]}}(\mu t) \times \prod_{k=2}^{L} \left[\phi_{\gamma_{e_i[k]}}\left(-\frac{c_{MPSK}}{\sin^2\theta}, \mu t \right) - \phi_{\gamma_{e_i[k]}}\left(-\frac{c_{MPSK}}{\sin^2\theta}, t \right) \right] dt. \tag{2.28}$$

The outage probability of T-HS/MRC in the case of i.n.d. diversity branches is obtained by substituting (2.27) into (2.5) and (2.4) to give

$$P_{outage}(\gamma_{th}) = \frac{2e^{\eta\gamma_{th}}}{\pi} \sum_{L=1}^{N} \sum_{e_i \in T_{N,L}} \int_0^\infty d\omega \int_0^\infty e^{-\eta t} \cos(\omega\gamma_{th}) f_{\gamma_{e_i[1]}}(t) \prod_{k=L+1}^{N} F_{\gamma_{e_i[k]}}(\mu t) \times Re\left\{ \frac{e^{-j\omega t}}{\eta + j\omega} \times \prod_{k=2}^{L} [\phi_{\gamma_{e_i[k]}}(-(\eta+j\omega),\mu t) - \phi_{\gamma_{e_i[k]}}(-(\eta+j\omega),t)] \right\} dt. \tag{2.29}$$

Consider the case that N diversity branches experience i.n.d. Rayleigh fading with different average branch SNRs, $\Gamma_k = \mathbb{E}(\gamma_k)$ $(k = 1, \cdots, N)$. We shall need the following result given in (2.30):

$$\prod_{k=1}^{N}(1-c_k) = 1 + \sum_{p=1}^{N} (-1)^p \sum_{v \in S_{(\{1,\cdots,N\},p)}} \prod_{q=1}^{p} c_{v(q)} \tag{2.30}$$

where $S_{(\{1,\cdots,N\},p)}$ denotes the set of total combinations of the integers $\{1,\cdots,N\}$ taken $p\,(1 \le p \le N)$ numbers at a time, and $v = \{v(1),\cdots,v(p)\} \in S_{(\{1,\cdots,N\},p)}$ denotes a specific

combination of the integers $\{1,\cdots,N\}$ taken p $(1 \le p \le N)$ numbers at a time. Eq. (2.30) is derived in Appendix A.

Substituting (2.14), (2.15) and (2.16) into (2.27) and using (2.30), the MGF of $\gamma_{T-HS/MRC(L)}$ becomes

$$\begin{aligned}\phi_{\gamma_{T-HS/MRC(L)}}(s) &= \sum_{e_i \in T_{N,L}} \frac{1}{\Gamma_{e_i[1]} \prod_{k=2}^{L}(1-s\Gamma_{e_i[k]})} \times \\ &\left[\frac{1}{\left(\frac{1}{\Gamma_{e_i[1]}} - s\right) + \mu \sum_{k=2}^{L}\left(\frac{1}{\Gamma_{e_i[k]}} - s\right)} + \sum_{p=1}^{N-1} (-1)^p \times \right. \\ &\left. \sum_{v \in S_{(\{2,\cdots,N\},p)}} \frac{1}{\left(\frac{1}{\Gamma_{e_i[1]}} - s\right) + \mu \sum_{k=2}^{L}\left(\frac{1}{\Gamma_{e_i[k]}} - s\right) + \sum_{q=1}^{p} a_{v(q)}(s)} \right]\end{aligned} \tag{2.31}$$

where μ is the normalized threshold, $T_{N,L}$ and e_i were defined previously, and $a_k(s)$ $(k = 2,\cdots,N)$ is defined by

$$a_k(s) = \begin{cases} \left(\frac{1}{\Gamma_{e_i[k]}} - s\right)(1-\mu) & , \quad 2 \le k \le L \\ \frac{\mu}{\Gamma_{e_i[k]}} & , \quad L+1 \le k \le N. \end{cases} \tag{2.32}$$

Combining (2.31) with (2.3) and (2.2) gives the average SER of coherent MPSK subjected to i.n.d. Rayleigh fading in closed form as

$$\begin{aligned}P_e &= \frac{1}{\pi} \sum_{L=1}^{N} \sum_{e_i \in T_{N,L}} \int_0^{\pi(M-1)/M} \frac{1}{\Gamma_{e_i[1]} \prod_{k=2}^{L}\left(1 + \frac{c_{MPSK}}{\sin^2\theta}\Gamma_{e_i[k]}\right)} \times \\ &\left[\frac{1}{\left(\frac{1}{\Gamma_{e_i[1]}} + \frac{c_{MPSK}}{\sin^2\theta}\right) + \mu \sum_{k=2}^{L}\left(\frac{1}{\Gamma_{e_i[k]}} + \frac{c_{MPSK}}{\sin^2\theta}\right)} + \sum_{p=1}^{N-1} (-1)^p \times \right. \\ &\left. \sum_{v \in S_{(\{2,\cdots,N\},p)}} \frac{1}{\left(\frac{1}{\Gamma_{e_i[1]}} + \frac{c_{MPSK}}{\sin^2\theta}\right) + \mu \sum_{k=2}^{L}\left(\frac{1}{\Gamma_{e_i[k]}} + \frac{c_{MPSK}}{\sin^2\theta}\right) + \sum_{q=1}^{p} a_{v(q)}\left(-\frac{c_{MPSK}}{\sin^2\theta}\right)} \right] d\theta.\end{aligned} \tag{2.33}$$

Substituting (2.31) into (2.5) and (2.4) gives the outage probability of T-HS/MRC in

i.n.d. Rayleigh fading as

$$
\begin{aligned}
P_{outage}(\gamma_{th}) = & \frac{2e^{\eta\gamma_{th}}}{\pi}\sum_{L=1}^{N}\sum_{e_i\in T_{N,L}}\int_0^{\infty}\frac{\cos(\omega\gamma_{th})}{\Gamma_{e_i[1]}}\times \\
& Re\left\{\frac{1}{(\eta+j\omega)\prod_{k=2}^{L}[1+(\eta+j\omega)\Gamma_{e_i[k]}]}\times\right. \\
& \left[\frac{1}{\left(\frac{1}{\Gamma_{e_i[1]}}+\eta+j\omega\right)+\mu\sum_{k=2}^{L}\left(\frac{1}{\Gamma_{e_i[k]}}+\eta+j\omega\right)}+\right. \\
& \sum_{p=1}^{N-1}(-1)^p\sum_{v\in S_{(\{2,\cdots,N\},p)}} \\
& \left.\left.\frac{1}{\left(\frac{1}{\Gamma_{e_i[1]}}+\eta+j\omega\right)+\mu\sum_{k=2}^{L}\left(\frac{1}{\Gamma_{e_i[k]}}+\eta+j\omega\right)+\sum_{q=1}^{p}a_{v(q)}(-\eta-j\omega)}\right]\right\}d\omega.
\end{aligned}
\tag{2.34}
$$

2.5 Numerical Results

In this section, some examples of the average symbol error rate and outage probability of T-HS/MRC for the cases of i.i.d and i.n.d. diversity branches in Nakagami-m fading, are given. Results computed using our theoretical analysis, the theoretical analysis of [32–34] and Monte Carlo simulation are compared. In particular, the effect of the normalized threshold μ on the performance of T-HS/MRC is examined. In the following figures, the notation T-HS/MRC denotes the results of our theory and S-TGSC represents the analytical results of [32–34].

Fig. 2.1 shows the average SER of coherent QPSK using T-HS/MRC versus the average branch SNR with $N = 5$ diversity branches experiencing i.i.d. Nakagami-m fading with fading parameter $m = 3$ and normalized threshold μ =0.0, 0.25, 0.5, 0.8 and 1.0. The diamonds denote the average SER obtained using Monte Carlo simulation. As a special case of T-HS/MRC, MRC and SC correspond to μ =0.0 and 1.0 respectively. It is seen that our analytical results and the simulation results are in excellent agreement, but there

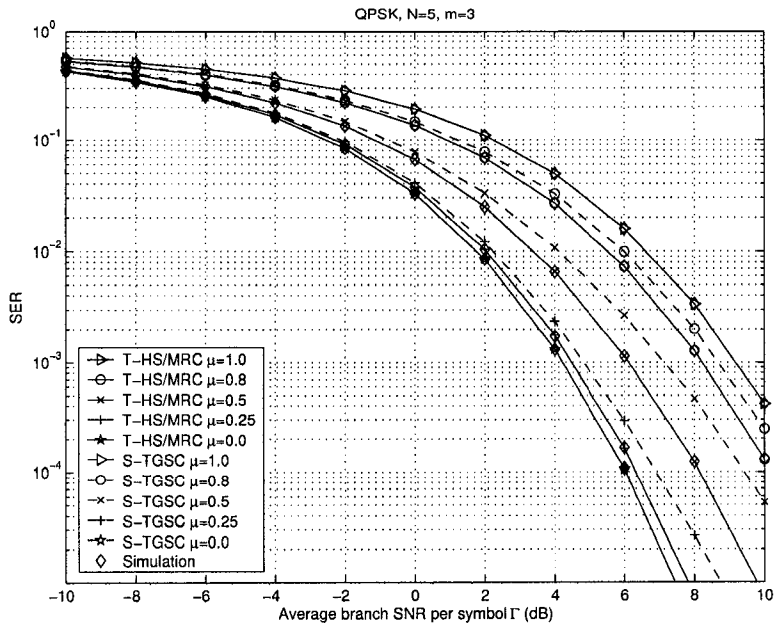

Fig. 2.1. The average SER of coherent QPSK with T-HS/MRC versus the average branch SNR Γ with N=5 diversity branches in i.i.d. Nakagami-m fading with fading parameter $m = 3$ and normalized threshold μ=0.0, 0.25, 0.5, 0.8 and 1.0.

are significant differences between the simulation results and the results of [32–34] (except for MRC and SC) when the average branch SNR, Γ, becomes large. For example, when the normalized threshold $\mu = 0.5$ and the average branch SNR $\Gamma = 8$ dB, the difference between the correct result and the result of [32–34] is about 1.3 dB. The differences show that the analyses of average SER of T-HS/MRC for the case of i.i.d. diversity branches in [32–34] are not correct.

Fig. 2.2 shows the average BER of coherent BPSK using T-HS/MRC versus the average branch SNR per bit with $N = 6$ diversity branches in i.i.d. Rayleigh fading for various values of the average number of branches combined, $\bar{L_c} = \mathbb{E}(L_c)$, defined in [33, eq. (44)]. For convenience of comparison with the results in [33], the same values of normalized threshold, μ, corresponding to the average number of branches combined, $\bar{L_c}$, are used according to [33, Table II]. The cases of SC and MRC correspond to $\bar{L_c} = 1$ and $\bar{L_c} = 6$, respectively.

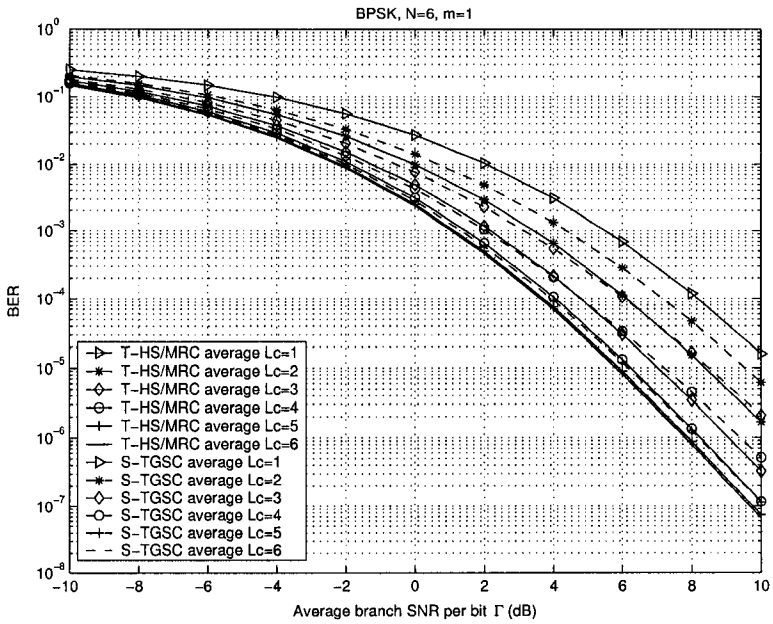

Fig. 2.2. The average BER of coherent BPSK with T-HS/MRC versus the average branch SNR per bit Γ with N=6 diversity branches in i.i.d. Rayleigh fading and average number of combined branches $\bar{L_c}$ =1, 2, 3, 4, 5 and 6.

From Fig. 2.2, one can observe that for a fixed number of available diversity branches, N, the gain obtained from increasing $\bar{L_c}$ by decreasing the normalized threshold μ, increases, but the benefit is subject to diminishing returns as $\bar{L_c}$ increases. In addition, one can see that (except for MRC and SC) there are significant differences between the results of our analysis and those of [33]. For example, when the average number of branches combined $\bar{L_c}$ equals 3, for large average branch SNR Γ, the difference in the results obtained from the two methods is about 1.1 dB to 1.6 dB.

To examine the effect of the normalized threshold, μ, on the performance of T-HS/MRC, the average BER of coherent BPSK versus the normalized threshold μ for i.i.d. Nakagami-m fading with fading parameter $m = 2$ and average branch SNR per bit $\Gamma = 6$ dB is shown in Fig. 2.3. One can see that the BER increases with increasing μ due to fewer diversity branches satisfying the condition of T-HS/MRC and being excluded from the combining. Also, the incremental benefit of decreasing the value of μ decreases as μ decreases. This is

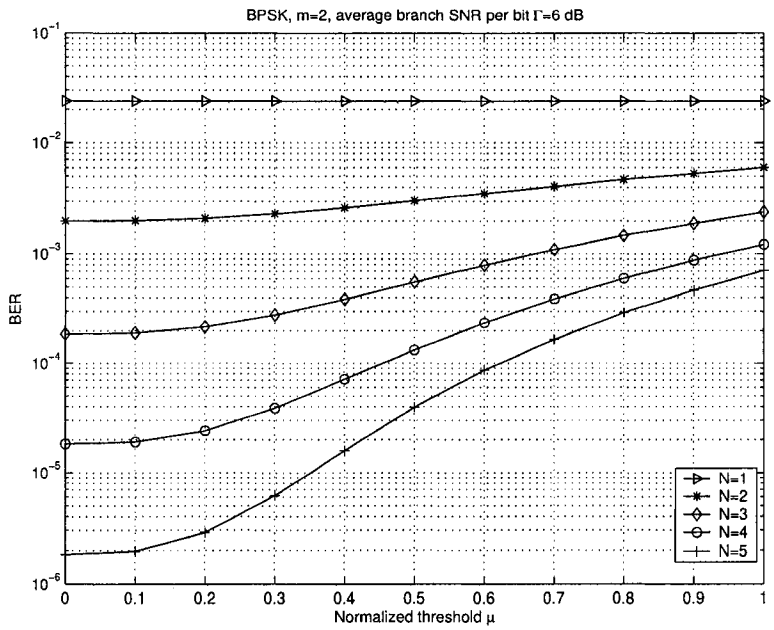

Fig. 2.3. The average BER of coherent BPSK versus the normalized threshold μ for i.i.d. Nakagami-m fading with fading parameter $m = 2$, average branch SNR per bit $\Gamma = 6$ dB and N =1, 2, 3, 4, and 5 available diversity branches.

because the BER of MRC is achieved when $\mu = 0$ and represents an ultimate lower bound below which the BER cannot be reduced.

Fig. 2.4 shows the average SER of coherent QPSK using T-HS/MRC versus the average branch SNR for i.i.d. Nakagami-m fading with fading parameter $m = 2$ and normalized threshold $\mu = 0.3$. Different numbers of available diversity branches, N, are considered. From this figure, we note the substantial benefits of increasing N for fixed normalized threshold, μ, as expected.

Fig. 2.5 shows the outage probability of T-HS/MRC versus the average branch SNR with $N = 4$ diversity branches for i.i.d. Nakagami-m fading with fading parameter $m = 2$ and normalized threshold values, μ =0.0, 0.3, 0.6, 0.9 and 1.0. The diamonds denote the outage probability obtained using Monte Carlo simulation. As a special case of T-HS/MRC, MRC and SC correspond to μ =0.0 and 1.0, respectively. It is seen that our analytical results and the simulation results are in excellent agreement, but there are signif-

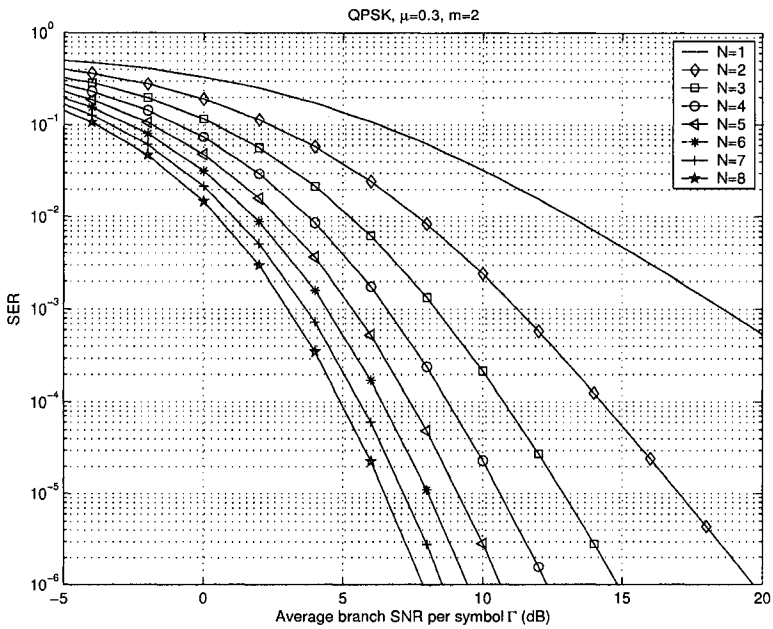

Fig. 2.4. The average SER of coherent QPSK using T-HS/MRC versus the average branch SNR Γ for i.i.d. Nakagami-m fading with fading parameter $m = 2$, normalized threshold $\mu = 0.3$ and N =1, 2, 3, 4, 5, 6, 7 and 8 available diversity branches.

icant differences (except for MRC and SC) between the simulation results and the analytical results of [32–34] when the average branch SNR, Γ, becomes large . For example, when the normalized threshold $\mu = 0.6$ and the average branch SNR $\Gamma = 4$ dB, the difference between the correct result and the result of [32–34] is more than 1.0 dB. When $\mu = 0.3$ and $\Gamma = 2$ dB, the difference is more than 1.5 dB. Hence, the outage probability of T-HS/MRC for the case of i.i.d. diversity branches in [32–34] is not correct.

Fig. 2.6 shows the outage probability of T-HS/MRC versus the average branch SNR with $N = 6$ diversity branches in i.i.d. Rayleigh fading for different values of average number of combined branches, $\bar{L_c}$. The corresponding values of normalized threshold, μ, are the same as those of Fig. 2.2. It is seen that for a fixed number of available diversity branches, N, the gain obtained from increasing $\bar{L_c}$ by decreasing the normalized threshold μ, increases, but the benefit is subject to diminishing returns as $\bar{L_c}$ increases. Again, one can see that (except for MRC and SC), the differences between the results of our analysis and

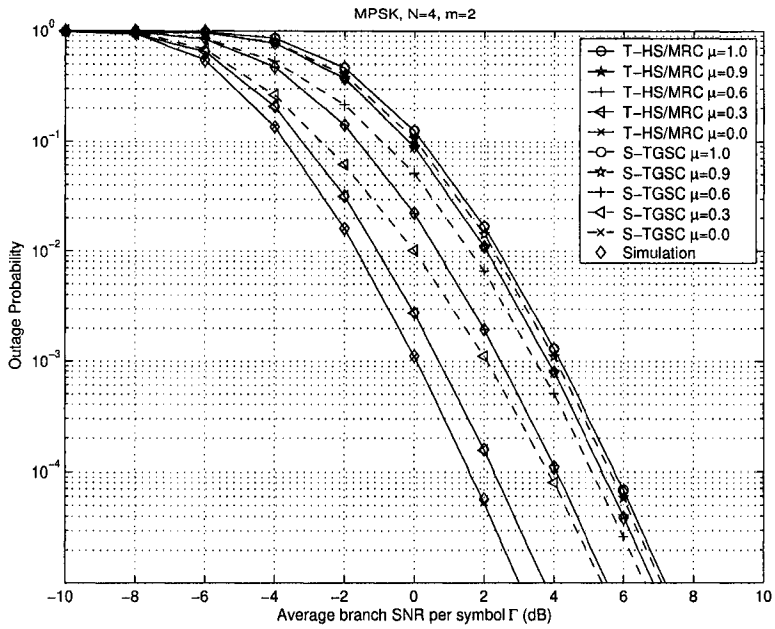

Fig. 2.5. The outage probability of T-HS/MRC versus the average branch SNR Γ with N=4 diversity branches in i.i.d. Nakagami-m fading with fading parameter $m = 2$ and normalized threshold μ =0.0, 0.3, 0.6, 0.9 and 1.0.

those of [33] are significant. For example, when the average number of branches combined $\bar{L_c}$ equals 3, for large average branch SNR Γ, the difference in the results obtained using the two methods is about 1.6 dB to 1.9 dB.

As two examples of the case of i.n.d. diversity branches, Fig. 2.7 and Fig. 2.8 examine the performances of T-HS/MRC in Rayleigh fading with exponentially decaying average branch SNR, namely, $\Gamma_k = \mathbb{E}(\gamma_k) = \Gamma_1 \exp[-\eta(k-1)]$ $(k = 1, \cdots, N)$, as defined in [45, eq. (23)]. The number of available diversity branches, N, equals 4 for both of the two figures. Fig. 2.7 shows the average SER of coherent QPSK versus the largest average branch SNR, Γ_1, with normalized threshold, μ =0.25, and the average fading power decay factor values, η =0.0, 0.3, 0.7 and 1.0. Fig. 8 shows the outage probability of T-HS/MRC versus the largest average branch SNR, Γ_1, with normalized threshold, μ =0.2, and the average fading power decay factor values, η =0.0, 0.2, 0.5 and 1.0. The case of i.i.d. diversity branches corresponds to $\eta = 0.0$. It is seen that the results obtained using our

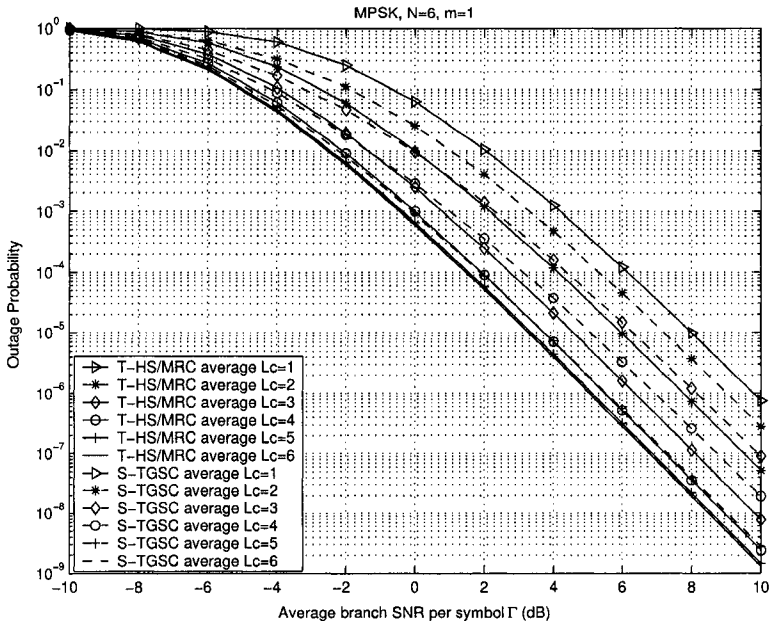

Fig. 2.6. The outage probability of T-HS/MRC versus the average branch SNR Γ with N=6 diversity branches in i.i.d. Rayleigh fading and average number of combined branches $\bar{L}_c$ =1, 2, 3, 4, 5 and 6.

theory are in excellent agreement with results obtained using Monte Carlo simulation. The results show, for example, that the performance deteriorates with increasing η, as expected. Fig. 2.7 and 2.8 can be used to accurately assess the amount of the degradation. However, there are significant differences between the correct results and the results obtained using the analyses in [32–34] when the largest average branch SNR, Γ_1, becomes large. Thus, the analyses of T-HS/MRC for the case of i.n.d. diversity branches in [32–34] are not correct.

2.6 Summary

In this chapter, the exact average symbol error rate and outage probability of threshold-based hybrid selection/maximal-ratio combining in generalized fading environments were analyzed. Using the total probability theorem and moment generating function method, a unified analysis framework of T-HS/MRC was developed. Explicit expressions of SER and

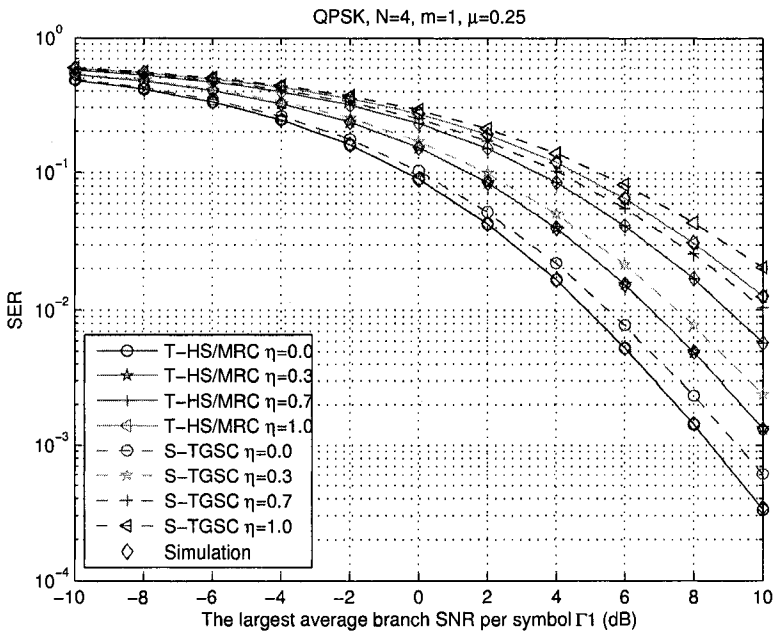

Fig. 2.7. The average SER of coherent QPSK using T-HS/MRC versus the largest average branch SNR Γ_1 for N=4 diversity branches with exponentially decaying average branch SNRs in Rayleigh fading, normalized threshold μ=0.25 and average fading power decay factor η=0.0, 0.3, 0.7 and 1.0.

outage probability for the cases of independent, identically distributed and independent, nonidentically, distributed diversity branches were presented. The derivation accommodates different M-ary linear modulation schemes and various slow and flat fading channels. For independent Rayleigh fading, closed-form expressions for SER and outage probability were obtained. The results show that previous published results are inaccurate.

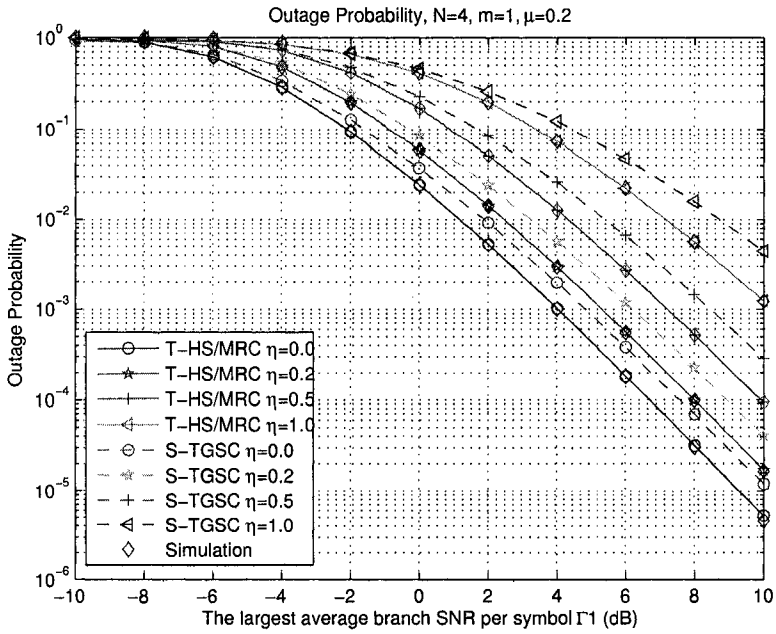

Fig. 2.8. The outage probability of T-HS/MRC versus the largest average branch SNR Γ_1 for N=4 diversity branches with exponentially decaying average branch SNRs in Rayleigh fading, normalized threshold $\mu = 0.2$ and average fading power decay factor η=0.0, 0.2, 0.5 and 1.0.

Chapter 3

Performance Analysis of Generalized Selection Combining in Correlated Nakagami-*m* Fading

3.1 Introduction

Diversity combining is an effective technique for combatting signal fading in wireless communications. Various combining schemes representing different levels of performance and different cost are used. As one of the classic combining methods, selection combining has been widely used in practice due to its simplicity which entails choosing a best branch signal from N available diversity branches, such as choosing the branch with the largest instantaneous SNR. However, its performance is poorer than some other schemes since it ignores the information provided by the remaining branch signals. The performance of SC in independent fading has been studied in [22], [46]. Most of the available results on SC in correlated fading focus on two or three branches [47–51]. A general approach for studying N-branch SC in correlated fading was proposed in [52]. However, it requires N-dimensional integration and the computation complexity increases exponentially with N. In [53], an expression for the joint PDF of multivariate Nakagami-m random variables with

exponential correlation was derived and applied to the theoretical analysis of SC.

Hybrid selection/maximal-ratio combining is considered as an effective combining technique for achieving a good compromise between system performance and complexity by coherently combining L_c largest signals from N available diversity branches. In the literature, the performance of H-S/MRC has been extensively studied when the diversity branch gains are independent. Based on the assumption of independent Rayleigh fading with equal branch average SNR, Win and Winters analyzed H-S/MRC using a novel technique named "virtual branch", which results in a simple derivation and formula for the mean, variance of the combiner output SNR and SER for arbitrary values of L_c and N in [23], [24]. The "virtual branch" method transforms the ordered branch SNRs into a new set of conditionally independent virtual branches and expresses the ordered branch SNRs as a linear function of the unordered virtual branch SNRs. This method permits the combiner output SNR to be represented in terms of the conditional independent virtual branch SNRs. Therefore, the derivations of the analysis involving in the evaluation of nested L_c-fold integrals, essentially reduce to the evaluation of a single integral. Concurrent and independent work on the performance analysis of H-S/MRC was done in [54]. Starting with the MGF of the H-S/MRC output SNR, Alouini and Simon provided a general analytical framework for the performance evaluation of H-S/MRC in terms of the output average SNR, outage probability and average error probability for a wide variety of modulation schemes over independent Rayleigh fading. According to their method, a simple closed-form expression for the MGF of the H-S/MRC output SNR was obtained. By taking inverse Laplace transform on the MGF, one can get the PDF of the H-S/MRC output SNR. In [25, 55, 56], the performance of H-S/MRC over independent Nakagami-m fading was analyzed. Two different methods were developed to derive the MGF expressions for H-S/MRC output SNR in generalized Nakagami fading channels with distinct and noninteger fading severity parameters, as well as different average branch SNRs. More recently, unified approaches were presented for H-S/MRC over generalized fading channels, where the channel statistics in different branches are independent but may be nonidentical, or even distributed according to different distribution families in [40, 41, 57, 58]. All of the previous works of H-S/MRC

focus on independent fading. There are very few works for the case of correlated fading. The average SER of H-S/MRC in equally correlated Nakagami-m fading, where the correlation between any pair of the branch powers is the same, was analyzed in [39]. The average SER of triple H-S/MRC in exponentially correlated Rayleigh fading was given in [59].

As discussed in detail in Chapter 2, since the number of selected branches L_c is fixed, H-S/MRC may potentially discard many branches whose instantaneous SNRs may be close in value to those of the branches selected, or alternatively, potentially include branches whose SNRs may be small. To alleviate this problem, threshold-based hybrid selection/maximal-ratio combining was proposed in [30], which allows the number of the combined branches to be a variable whose value is determined in accordance with the instantaneous SNR of each branch and a predetermined normalized threshold μ $(0 \leq \mu \leq 1)$. The performance of T-HS/MRC with independent diversity branches has been studied in [32–34]. An exact analysis of T-HS/MRC over generalized fading channels was presented in [36]. When the fading is equally correlated Nakagami-m distributed, the average SER of T-HS/MRC was given in [60].

Since the performance analyses for SC, H-S/MRC and T-HS/MRC are involved in the very complicated nature of order statistics, there are very few works that study the three generalized selection combining schemes with arbitrary number of branches in arbitrarily correlated fading channels. Recently, a novel approach for deriving the CDFs of the N-branch SC output in equally correlated fading was proposed in [61], where the problem of deriving the SC output CDF in equally correlated fading is transformed into the problem of deriving the SC output CDF in conditionally independent fading by noting that a set of equally correlated complex Gaussian RVs can be obtained by linearly combining a set of independent Gaussian RVs. The analysis of SC in equally correlated fading including Rayleigh, Nakagami-m and Ricean channels is simplified substantially with this method in [61].

In this chapter, we extend the approach in [61] to a more general correlated case, where the correlation coefficient matrix is determined by N real numbers whose values are between 0 and 1. This particular correlation structure is examined in [62, eqs. (8.1.5) and

(8.1.6)], and includes equal correlation studied in [61] as a special case [62, eq. (8.1.4)]. The exact average SER and outage probability of SC, H-S/MRC and T-HS/MRC in Nakagami-m fading for positive integer values of m, are obtained for this correlation structure [63].

The remainder of this chapter is organized as follows. The system model is described in Section 3.2. Representations of Rayleigh fading amplitudes and Nakagami-m fading amplitudes with the particular correlation structure are presented in Section 3.3.1 and Section 3.3.2, respectively. The performances of SC, H-S/MRC and T-HS/MRC are analyzed in Section 3.4. Numerical results and discussion are provided in Section 3.5. Finally, we give our conclusions in Section 3.6.

3.2 System Model

Assume that there are N available diversity branches experiencing slow and flat Nakagami-m fading with the same positive integer values of fading parameter m. The instantaneous SNR of the kth diversity branch, γ_k, is defined as (1.10)

$$\gamma_k = |h_k|^2 \frac{E_s}{N_0}, \qquad k = 1, \cdots, N \tag{3.1}$$

where E_s is the average symbol energy, h_k is the instantaneous branch gain, and N_0 is the power spectral density of complex white Gaussian noise on the kth branch. Further, we assume that all of the branches have the same average branch SNR, namely, $\Gamma = \mathbb{E}(\gamma_k) = \mathbb{E}(|h_k|^2)E_s/N_0 \ (k = 1, \cdots, N)$.

Let $\sum_\gamma$ denote the branch power covariance coefficient matrix, whose element $\sum_\gamma^{k,j}$ $(k, j = 1, \cdots, N)$ satisfies [62, eq. (8.1.5)]

$$\sum_\gamma^{k,j} = \frac{\mathbb{E}(\gamma_k\gamma_j) - \mathbb{E}(\gamma_k)\mathbb{E}(\gamma_j)}{\sqrt{Var(\gamma_k)Var(\gamma_j)}} = \begin{cases} \rho_k\rho_j & (k \neq j) \\ 1 & (k = j) \end{cases}, \quad k, j = 1, \cdots, N \tag{3.2}$$

where $0 \leq \rho_k < 1$ $(k = 1, \cdots, N)$, and $Var(\cdot)$ is the variance of a random variable. Obviously, when all of ρ_k $(k = 1, \cdots, N)$ are equal to ρ, the covariance matrix becomes equally correlated as studied in [61].

Recall in Chapter 1 that for SC, the branch with the largest instantaneous SNR is selected as the combiner output given by (1.17)

$$\gamma_{SC} = \max_{k=1,\cdots,N}(\gamma_k). \tag{3.3}$$

For H-S/MRC, assume that the L_c $(1 \leq L_c \leq N)$ branches having the largest values of instantaneous SNR are chosen at the selection time. Then the output instantaneous SNR of a H-S/MRC combiner is given by (1.18)

$$\gamma_{H-S/MRC} = \sum_{k=1}^{L_c} \gamma_{(k)}, \qquad L_c = 1,\cdots,N \tag{3.4}$$

where $\gamma_{(k)}$ $(k = 1,\cdots,N)$ are the descending-ordered instantaneous branch SNRs, satisfying $\gamma_{(1)} > \gamma_{(2)} > \cdots > \gamma_{(N)} \geq 0$.

For T-HS/MRC, denote the predetermined normalized threshold by μ $(0 \leq \mu \leq 1)$. The branches whose instantaneous SNRs exceed or equal the multiplication of the normalized threshold μ and the largest instantaneous branch SNR $\gamma_{(1)}$, are combined at the receiver end. Then the output instantaneous SNR of a T-HS/MRC combiner is given by (1.19)

$$\gamma_{T-HS/MRC(L_c)} = \sum_{k=1}^{L_c} \gamma_{(k)}, \qquad L_c = 1,\cdots,N \tag{3.5}$$

where L_c is an integer RV that represents the number of branches being combined in order of decreasing instantaneous SNR starting with the one having the largest SNR. The event L_c diversity branches are selected, means that the ordered instantaneous branch SNRs, at the selecting time, satisfy $\gamma_{(1)} > \gamma_{(2)} > \cdots > \gamma_{(L_c)} \geq \mu\gamma_{(1)} > \gamma_{(L_c+1)} > \gamma_{(L_c+2)} > \cdots > \gamma_{(N)}$.

3.3 Representation of Correlated Branch Gain Amplitudes

In this section, we extend the representation in [61] of equally correlated Nakagami-*m* fading by a set of independent Gaussian RVs to a more general case, where the covariance coefficient matrix satisfies (3.2). First, we introduce some notations used in the following. $N(\mu, \sigma^2)$ denotes a Gaussian distribution with mean μ and variance σ^2, $C(\mu, \sigma^2)$ denotes a complex Gaussian distribution with mean $\mu = \mathbb{E}(z)$ and variance $\sigma^2 = (1/2)\mathbb{E}[(z -$

$\mu)(z-\mu)^*]$, $\chi_n(0,\sigma^2)$ denotes a central chi-square distribution with n degrees of freedom and the common variance of the corresponding Gaussian components σ^2 given at [4, eq. (2-1-110)], $\chi_n(s,\sigma^2)$ denotes a noncentral chi-square distribution with n degrees of freedom, noncentrality parameter s^2 and the common variance of the corresponding Gaussian components σ^2 given at [4, eq. (2-1-118)], and $Q_v(a,b)$ denotes the vth-order Marcum Q-function given at [4, eq. (2-1-122)]

$$Q_v(a,b) = \int_b^\infty x\left(\frac{x}{a}\right)^{v-1} \exp\left(-\frac{x^2+a^2}{2}\right) I_{v-1}(ax)dx \tag{3.6}$$

where $I_v(\cdot)$ is the vth-order modified Bessel function of the first kind given at [4, eq. (2-1-120)]. For brevity, we write $Q(a,b)$ to denote $Q_1(a,b)$.

3.3.1 Correlated Rayleigh Fading Amplitudes

Similar to [61, eq.(2)], the channel gain of the kth branch in Rayleigh fading can be represented by extending [62, eq. (8.1.6)] to the complex plane

$$G_k = (\sqrt{1-\rho_k}X_k + \sqrt{\rho_k}X_0) + i(\sqrt{1-\rho_k}Y_k + \sqrt{\rho_k}Y_0), \qquad k = 1,\cdots,N \tag{3.7}$$

where $i = \sqrt{-1}$, $0 \le \rho_k < 1$, and X_k, Y_k $(k = 0,\cdots,N)$ are independent Gaussian RVs with distribution $N(0,1/2)$, and for any $k,j \in \{0,\cdots,N\}$, $\mathbb{E}(X_kY_j) = 0$, and $\mathbb{E}(X_kX_j) = \mathbb{E}(Y_kY_j) = (1/2)\delta_{k,j}$, where $\delta_{k,j}$ is the Kronecker delta with

$$\delta_{k,j} = \begin{cases} 0 & (k \neq j) \\ 1 & (k = j). \end{cases}$$

Since G_k is zero-mean complex Gaussian distributed with distribution $C(0,1/2)$, $|G_k|$ $(k = 1,\cdots,N)$ is a set of Rayleigh RVs with mean-square value $\mathbb{E}(|G_k|^2) = 1$. The correlation coefficient between any G_k and G_j $(k \neq j)$ can be derived as

$$\begin{aligned} \rho_{k,j} &= \frac{\mathbb{E}(G_kG_j^*) - \mathbb{E}(G_k)\mathbb{E}(G_j^*)}{\sqrt{Var(G_k)Var(G_j)}} \\ &= \frac{\sqrt{\rho_k\rho_j}\mathbb{E}(X_0^2+Y_0^2)}{\sqrt{\mathbb{E}(|G_k|^2)\mathbb{E}(|G_j|^2)}} \\ &= \sqrt{\rho_k\rho_j}. \end{aligned} \tag{3.8}$$

Combining (3.7) and (3.1) with the definition of the branch power covariance coefficient $\Sigma_\gamma^{k,j}$ in (3.2), one can show that

$$\begin{aligned}
\Sigma_\gamma^{k,j} &= \frac{\mathbb{E}(|G_k|^2|G_j|^2)-\mathbb{E}(|G_k|^2)\mathbb{E}(|G_j|^2)}{\sqrt{Var(|G_k|^2)Var(|G_j|^2)}} \\
&= \mathbb{E}\Big\{[(\sqrt{1-\rho_k}X_k+\sqrt{\rho_k}X_0)^2+(\sqrt{1-\rho_k}Y_k+\sqrt{\rho_k}Y_0)^2]\times \\
&\quad [(\sqrt{1-\rho_j}X_j+\sqrt{\rho_j}X_0)^2+(\sqrt{1-\rho_j}Y_j+\sqrt{\rho_j}Y_0)^2]\Big\}-1 \\
&= (1-\rho_k)(1-\rho_j)+\rho_k(1-\rho_j)+\rho_j(1-\rho_k)+\rho_k\rho_j\mathbb{E}[(X_0^2+Y_0^2)^2]-1 \\
&= \begin{cases} \rho_k\rho_j=\rho_{k,j}^2 & (k\neq j) \\ 1 & (k=j). \end{cases}
\end{aligned} \tag{3.9}$$

Therefore, the correlated N-branch Rayleigh fadings with power covariance matrix Σ_γ given by (3.2) can be represented by a set of complex Gaussian RVs given by (3.7). When ρ_k $(k=1,\cdots,N)$ are all equal to ρ, the branch fadings become equally correlated N-branch Rayleigh fadings.

3.3.2 Correlated Nakagami-*m* Fading Amplitudes

Similar to [61, eq. (5)], we can express the N Nakagami-m fading amplitudes with positive integer values of m by a set of Nm zero-mean complex Gaussian RVs

$$\begin{aligned}
G_{kl} = (\sqrt{1-\rho_k}X_{kl}+\sqrt{\rho_k}X_{0l}) \quad &+ \quad i(\sqrt{1-\rho_k}Y_{kl}+\sqrt{\rho_k}Y_{0l}), \\
&k=1,\cdots,N,\ l=1,\cdots,m
\end{aligned} \tag{3.10}$$

where X_{kl} and Y_{kl} $(k=0,\cdots,N,\ l=1,\cdots,m)$ are independent Gaussian RVs with distribution $N(0,1/2)$. For any $k,j\in\{0,1,\cdots,N\}$, $l,n\in\{1,\cdots,m\}$, $\mathbb{E}(X_{kl}Y_{jn})=0$, $\mathbb{E}(X_{kl}X_{jn})=\mathbb{E}(Y_{kl}Y_{jn})=(1/2)\delta_{k,j}\delta_{l,n}$. Then the correlation coefficient between any G_{kl} and G_{jn} $(k\neq j)$ can be derived as

$$\begin{aligned}
\rho_{kl,\,jn} &= \frac{\mathbb{E}(G_{kl}G_{jn}^*)-\mathbb{E}(G_{kl})\mathbb{E}(G_{jn}^*)}{\sqrt{\mathbb{E}(|G_{kl}|^2)\mathbb{E}(|G_{jn}|^2)}} \\
&= \begin{cases} \sqrt{\rho_k\rho_j} & (k\neq j \text{ and } l=n) \\ 0 & (l\neq n). \end{cases}
\end{aligned} \tag{3.11}$$

Let R_k denote the summation of the squared magnitudes of G_{kl}, namely,

$$R_k = \sum_{l=1}^{m} |G_{kl}|^2. \tag{3.12}$$

Then R_k $(k = 1, \cdots, N)$ is the sum of squares of m independent Rayleigh envelopes with distribution $\chi_{2m}(0, 1/2)$ [61]. One can show that the cross-covariance coefficient between R_k and R_j $(k \neq j)$ is given by

$$\begin{aligned}
\rho_{R_k,R_j} &= \frac{\mathbb{E}(R_k R_j) - \mathbb{E}(R_k)\mathbb{E}(R_j)}{\sqrt{Var(R_k)Var(R_j)}} \\
&= \frac{\sum_{l=1}^{m}\sum_{n=1}^{m}\mathbb{E}(|G_{kl}|^2|G_{jn}|^2) - m^2}{\sqrt{m^2}} \\
&= \frac{\sum_{l=1}^{m}\mathbb{E}(|G_{kl}|^2|G_{jl}|^2) + \sum_{l=1}^{m}\sum_{n=1\, n\neq l}^{m}\mathbb{E}(|G_{kl}|^2|G_{jn}|^2) - m^2}{m} \\
&= \frac{m(1+\rho_k\rho_j) + m(m-1) - m^2}{m} \\
&= \rho_k\rho_j, \qquad (k \neq j).
\end{aligned} \tag{3.13}$$

Note that $\sqrt{R_k}$ $(k = 1, \cdots, N)$ is a set of correlated Nakagami-m fading amplitudes with mean-square value $\mathbb{E}(R_k) = m$. Combining (3.10) and (3.12) with the definition of the branch power correlation coefficient in (3.2), we have

$$\Sigma_{\gamma}^{k,j} = \begin{cases} \rho_{R_k,R_j} = \rho_k\rho_j & (k \neq j) \\ 1 & (k = j). \end{cases} \tag{3.14}$$

The branch power covariance coefficient $\Sigma_{\gamma}^{k,j}$ is the square of the complex gain correlation coefficient $\rho_{kl,jn}$ when $k \neq j$ and $l = n$ in (3.11). Therefore, the correlated N branch Nakagami-m fading amplitudes with positive integer values of m and power covariance matrix Σ_{γ} given by (3.2) can be represented by the set of complex Gaussian RVs in (3.10). Again, when ρ_k $(k = 1, \cdots, N)$ are equal, the fadings become equally correlated N-branch Nakagami-m fadings. Eq. (3.14) specializes to (3.9) when the fading is Rayleigh with $m = 1$.

3.4 Performance Analysis

In this section, we analyze the performance of SC, H-S/MRC and T-HS/MRC in correlated Rayleigh and Nakagami-m fading with the power covariance structure given in (3.2). Using the representations of Rayleigh and Nakagami-m amplitudes in Section 3.3, our analysis is simplified greatly.

3.4.1 SER and Outage Probability of SC

CDF of SC Output SNR in Rayleigh Fading

Assume that the branches experience Rayleigh fading with covariance matrix given by (3.2). Let $\mathscr{T} = X_0^2 + Y_0^2$. When $X_0 = x_0$ and $Y_0 = y_0$ are fixed, $|G_k|^2$ $(k = 1, \cdots, N)$ are independent with noncentral chi-square distribution $\chi_2(\sqrt{\rho_k(x_0^2+y_0^2)}, (1-\rho_k)/2)$, whose CDF is given by [61, eq.(12)]

$$\begin{aligned} F_{|G_k|^2|\mathscr{T}}(y|t) &= \Pr(|G_k|^2 \le y|t) \\ &= 1 - Q\left(\sqrt{\frac{2\rho_k t}{1-\rho_k}}, \sqrt{\frac{2y}{1-\rho_k}}\right), \qquad k = 1, \cdots, N \end{aligned} \tag{3.15}$$

where $Q(\cdot,\cdot)$ denotes $Q_1(\cdot,\cdot)$, the first order Marcum Q-function. Then the CDF of the SC output for fixed $X_0^2 + Y_0^2 = t$, can be calculated as [61, eq. (13)]

$$\begin{aligned} F_{\gamma_{SC}|\mathscr{T}}(y|t) &= \Pr(\gamma_1 \le y, \cdots, \gamma_N < y|t) \\ &= \Pr\left(|G_1|^2 \le \frac{y}{\Gamma}, \cdots, |G_N|^2 \le \frac{y}{\Gamma}|t\right) \\ &= \prod_{k=1}^{N}\left[1 - Q\left(\sqrt{\frac{2\rho_k t}{1-\rho_k}}, \sqrt{\frac{2y}{\Gamma(1-\rho_k)}}\right)\right]. \end{aligned} \tag{3.16}$$

Observing that $\mathscr{T} = X_0^2 + Y_0^2$ follows a central chi-square distribution $\chi_2(0, 1/2)$, the PDF of $\mathscr{T}$ is given by [61, eq.(14)]

$$f_{\mathscr{T}}(t) = e^{-t}, \qquad t \ge 0. \tag{3.17}$$

Averaging the conditional CDF in (3.16) across the PDF of $\mathscr{T}$ in (3.17), the CDF of the SC output in correlated Rayleigh fading is given by

$$\begin{aligned} F_{\gamma_{SC}}(y) &= \int_0^\infty F_{\gamma_{SC}|\mathscr{T}}(y|t) f_{\mathscr{T}}(t) dt \\ &= \int_0^\infty \prod_{k=1}^{N} \left[1 - Q\left(\sqrt{\frac{2\rho_k t}{1-\rho_k}}, \sqrt{\frac{2y}{\Gamma(1-\rho_k)}} \right) \right] e^{-t} dt. \end{aligned} \tag{3.18}$$

When $\rho_k = \rho$ $(k = 1, \cdots, N)$, (3.18) becomes [61, eq. (15)], corresponding to N-branch equally correlated Rayleigh fading.

CDF of SC Output SNR in Nakagami-m Fading

For Nakagami-m fading with positive integer values of m, similar derivations can be done. Let $\mathscr{T} = \sum_{l=1}^{m} (X_{0l}^2 + Y_{0l}^2)$. For fixed values of $X_{0l} = x_{0l}$ and $Y_{0l} = y_{0l}$ $(l = 1, \cdots, m)$, the branch powers R_k are independent and follow a noncentral chi-square distribution denoted by $\chi_{2m}(\sqrt{\rho_k \sum_{l=1}^{m} (x_{0l}^2 + y_{0l}^2)}, (1-\rho_k)/2)$. Observing that $\mathscr{T} = \sum_{l=1}^{m} (X_{0l}^2 + Y_{0l}^2)$, follows a central chi-square distribution $\chi_{2m}(0, 1/2)$, the PDF of $\mathscr{T}$ is given by

$$f_{\mathscr{T}}(t) = \frac{t^{m-1} e^{-t}}{(m-1)!}, \qquad t \geq 0. \tag{3.19}$$

The conditional CDF of the SC output becomes

$$F_{\gamma_{SC}|\mathscr{T}}(y|t) = \prod_{k=1}^{N} \left[1 - Q_m\left(\sqrt{\frac{2\rho_k t}{1-\rho_k}}, \sqrt{\frac{2my}{\Gamma(1-\rho_k)}} \right) \right]. \tag{3.20}$$

Averaging the conditional CDF of the SC output over $\mathscr{T}$, the CDF of the SC output in correlated Nakagami-m fading, is given by

$$F_{\gamma_{SC}}(y) = \frac{1}{(m-1)!} \int_0^\infty \prod_{k=1}^{N} \left[1 - Q_m\left(\sqrt{\frac{2\rho_k t}{1-\rho_k}}, \sqrt{\frac{2my}{\Gamma(1-\rho_k)}} \right) \right] t^{m-1} e^{-t} dt. \tag{3.21}$$

Again, when $\rho_k = \rho$ $(k = 1, \cdots, N)$, (3.21) becomes [61, eq. (22)], namely the CDF of N-branch SC output in equally correlated Nakagami-m fading. For numerical computation in (3.21), we use the function NCX2CDF provided by Matlab to compute the CDF of a noncentral chi-square distributed RV, which is in form of the mth-order Marcum Q-function in (3.21) [61].

Performance Analysis of SC

The outage probability of SC is defined by [3]

$$P_{Outage} = P(0 \leq \gamma_{SC} \leq \gamma_{th}) = F_{\gamma_{SC}}(\gamma_{th}) \tag{3.22}$$

where γ_{th} is the threshold of the SC output SNR. When the channel experiences Rayleigh or Nakagami-m fading with power covariance matrix $\sum_{\gamma}$ in (3.2), the outage probability of SC can be calculated by (3.18) and (3.21), respectively.

The average SER of SC for different modulation formats in Nakagami-m fading with covariance matrix $\sum_{\gamma}$ in (3.2), can be obtained by combining [61, eqs. (31)-(42)] with (3.18) and (3.21), respectively. For example, for BPSK, the average BER of SC in Rayleigh fading is given by substituting (3.18) and [61, eq. (33)] into [61, eq. (32)] to obtain

$$P_e = \frac{1}{2\sqrt{\pi}} \int_0^{\infty} \int_0^{\infty} \frac{e^{-\gamma - t}}{\sqrt{\gamma}} \prod_{k=1}^{N} \left[1 - Q\left(\sqrt{\frac{2\rho_k t}{1-\rho_k}}, \sqrt{\frac{2\gamma}{\Gamma(1-\rho_k)}} \right) \right] dt d\gamma. \tag{3.23}$$

Similarly, when the branches are subject to Nakagami-m fading, the average BER of BPSK with SC is given by

$$P_e = \frac{1}{2\sqrt{\pi}(m-1)!} \int_0^{\infty} \int_0^{\infty} \frac{t^{m-1} e^{-\gamma - t}}{\sqrt{\gamma}} \prod_{k=1}^{N} \left[1 - Q_m\left(\sqrt{\frac{2\rho_k t}{1-\rho_k}}, \sqrt{\frac{2m\gamma}{\Gamma(1-\rho_k)}} \right) \right] dt d\gamma. \tag{3.24}$$

For noncoherent M-ary frequency-shift keying (MFSK), the average BER using SC in correlated Nakagami-m fading, is given by substituting (3.21) and [4, eqs. (5-4-46) and (5-4-48)] into [61, eq. (32)] to obtain

$$\begin{aligned} P_e = & \frac{2^{\log_2 M - 1}}{(m-1)!(2^{\log_2 M} - 1)} \sum_{n=1}^{M-1} \frac{(-1)^{n+1} n(\log_2 M)}{(n+1)^2} \binom{M-1}{n} \int_0^{\infty} \int_0^{\infty} t^{m-1} e^{-\frac{n(\log_2 M)\gamma}{n+1} - t} \\ & \times \prod_{k=1}^{N} \left[1 - Q_m\left(\sqrt{\frac{2\rho_k t}{1-\rho_k}}, \sqrt{\frac{2m\gamma}{\Gamma(1-\rho_k)}} \right) \right] dt d\gamma. \end{aligned} \tag{3.25}$$

For M-ary quadrature-amplitude modulation (MQAM), such as 16-QAM and 64-QAM adopted in the IEEE 802.11a standard, the average SER using SC in correlated Nakagami-

m fading, is given by substituting (3.21) and [4, eq. (5-2-79)] into [61, eq. (32)] to obtain

$$P_e(\gamma) = \frac{1}{(m-1)!}\sqrt{\frac{b}{2\pi}}\int_0^\infty\int_0^\infty \frac{t^{m-1}e^{-\frac{b\gamma}{2}-t}}{\sqrt{\gamma}}\left(\frac{a}{2}-cQ(\sqrt{b\gamma})\right) \times\prod_{k=1}^{N}\left[1-Q_m\left(\sqrt{\frac{2\rho_k t}{1-\rho_k}},\sqrt{\frac{2m\gamma}{\Gamma(1-\rho_k)}}\right)\right]dtd\gamma \tag{3.26}$$

where $(a,b,c)=(4(\sqrt{M}-1)/\sqrt{M},3\log_2 M/(M-1),4(\sqrt{M}-1)^2/M)$, and $Q(\cdot)$ is the Q function, denoting the area under the tail of the Gaussian PDF given at [4, eq. (2-1-97)].

3.4.2 SER of H-S/MRC

In this part, we will use the MGF method to study the average SER of H-S/MRC in correlated N-branch Nakagami-m fading for positive integer values of fading parameter m and the power covariance matrix Σ_γ given by (3.2).

As mentioned previously, for fixed $\mathscr{T}=\sum_{l=1}^{m}(X_{0l}^2+Y_{0l}^2)$, the branch powers R_k are independent and follow a noncentral chi-square distribution $\chi_{2m}(\sqrt{\rho_k\sum_{l=1}^{m}(x_{0l}^2+y_{0l}^2)},(1-\rho_k)/2)$. Thus, one can show that the branch SNRs γ_k conditioned on $\mathscr{T}$, are independent with distribution $\chi_{2m}(\sqrt{\rho_k\Gamma t/m},\Gamma(1-\rho_k)/(2m))$

$$f_{\gamma_k|\mathscr{T}}(y|t)=\frac{1}{2\sigma_k^2}\left(\frac{y}{c_k^2}\right)^{\frac{m-1}{2}}\exp\left(-\frac{y+c_k^2}{2\sigma_k^2}\right)I_{m-1}\left(\frac{c_k}{\sigma_k^2}\sqrt{y}\right) \tag{3.27}$$

where $c_k^2=\rho_k\Gamma t/m$, $\sigma_k^2=\Gamma(1-\rho_k)/(2m)$, and $I_v(\cdot)$ is the vth-order modified Bessel function of the first kind. The PDF in (3.27) can be computed using the function NCX2PDF provided in Matlab.

Since the branch SNRs γ_k conditioned on $\mathscr{T}$ are independent, the joint PDF of the ordered branch SNRs $\gamma_{(k)}$ $(k=1,\cdots,N)$ conditioned on $\mathscr{T}$ can be calculated according to [58, eq. (3)]

$$f_{\gamma_{(1)},\cdots,\gamma_{(N)}|\mathscr{T}}(\gamma_{(1)},\cdots,\gamma_{(N)}|t) = \sum_{e_i\in S_N}\prod_{k=1}^{N}f_{\gamma_{e_i[k]}|\mathscr{T}}(\gamma_{(k)}|t), \quad \gamma_{(1)}>\gamma_{(2)}>\cdots>\gamma_{(N)}\geq 0 \tag{3.28}$$

where S_N is the set of all permutations of the integers $\{1,2,\cdots,N\}$, and $e_i\in S_N=\{e_i[1],e_i[2],\cdots,e_i[N]\}$ denotes the specific permutation of the integers $\{1,2,\cdots,N\}$.

Then the MGF of $\gamma_{H-S/MRC}$ conditioned on $\mathscr{T}$ is given by

$$\begin{aligned}
\phi_{\gamma_{H-S/MRC}|\mathscr{T}}(s|t) &= \mathbb{E}(e^{s\gamma_{H-S/MRC}}|\mathscr{T}) \\
&= \mathbb{E}\left(e^{s\sum_{k=1}^{L_c}\gamma_{(k)}}|\mathscr{T}\right) \\
&= \int_0^\infty d\gamma_{(1)}\int_0^{\gamma_{(1)}} d\gamma_{(2)}\cdots\int_0^{\gamma_{(N-1)}} e^{s\sum_{k=1}^{L_c}\gamma_{(k)}}\times \\
&\quad f_{\gamma_{(1)},\cdots,\gamma_{(N)}|\mathscr{T}}(\gamma_{(1)},\cdots,\gamma_{(N)}|t)d\gamma_{(N)} \\
&= \sum_{e_i\in S_N}\int_0^\infty d\gamma_{(1)}\int_0^{\gamma_{(1)}} d\gamma_{(2)}\cdots\int_0^{\gamma_{(N-1)}} e^{s\sum_{k=1}^{L_c}\gamma_{(k)}}\times \\
&\quad \prod_{k=1}^{N} f_{\gamma_{e_i[k]}|\mathscr{T}}(\gamma_{(k)}|t)d\gamma_{(N)}. \qquad (3.29)
\end{aligned}$$

Using [58, eq. (6)], the conditional MGF of $\gamma_{H-S/MRC}$ can be simplified as

$$\phi_{\gamma_{H-S/MRC}|\mathscr{T}}(s|t) = \sum_{e_i\in W_{N,L_c}}\int_0^\infty e^{s\gamma} f_{\gamma_{e_i[L_c]}|\mathscr{T}}(\gamma|t)\prod_{k=1}^{L_c-1}\phi_{\gamma_{e_i[k]}|\mathscr{T}}(s,\gamma|t)\prod_{k=L_c+1}^{N}F_{\gamma_{e_i[k]}|\mathscr{T}}(\gamma|t)d\gamma \qquad (3.30)$$

where W_{N,L_c} is a subset of S_N, whose element e_i satisfies $e_i[1] < e_i[2] < \cdots < e_i[L_c-1]$ and $e_i[L_c+1] < e_i[L_c+2] < \cdots < e_i[N]$. $F_{\gamma_{e_i[k]}|\mathscr{T}}(x|t)$ and $\phi_{\gamma_{e_i[k]}|\mathscr{T}}(s,x|t)$, are the CDF and the incomplete MGF of $\gamma_{e_i[k]}$ conditioned on $\mathscr{T}$, respectively, given by

$$F_{\gamma_{e_i[k]}|\mathscr{T}}(x|t) = \int_0^x f_{\gamma_{e_i[k]}|\mathscr{T}}(\gamma|t)d\gamma = 1 - Q_m\left(\sqrt{\frac{2\rho_{e_i[k]}t}{1-\rho_{e_i[k]}}}, \sqrt{\frac{2mx}{\Gamma(1-\rho_{e_i[k]})}}\right) \qquad (3.31)$$

and

$$\begin{aligned}
\phi_{\gamma_{e_i[k]}|\mathscr{T}}(s,x|t) &= \int_x^\infty e^{s\gamma} f_{\gamma_{e_i[k]}|\mathscr{T}}(\gamma|t)d\gamma \\
&= \frac{\exp\left(\frac{c_{e_i[k]}^2 s}{1-2s\sigma_{e_i[k]}^2}\right)}{(1-2\sigma_{e_i[k]}^2 s)^m} Q_m\left(\frac{c_{e_i[k]}}{\sigma_{e_i[k]}\sqrt{1-2s\sigma_{e_i[k]}^2}}, \sqrt{\frac{(1-2\sigma_{e_i[k]}^2 s)x}{\sigma_{e_i[k]}^2}}\right) \\
&= \left(\frac{m}{m-\Gamma s(1-\rho_{e_i[k]})}\right)^m \exp\left(\frac{\rho_{e_i[k]}\Gamma t s}{m-\Gamma s(1-\rho_{e_i[k]})}\right)\times \\
&\quad Q_m\left(\sqrt{\frac{2m\rho_{e_i[k]}t}{(1-\rho_{e_i[k]})(m-\Gamma s(1-\rho_{e_i[k]}))}}, \sqrt{\frac{2(m-\Gamma s(1-\rho_{e_i[k]}))x}{\Gamma(1-\rho_{e_i[k]})}}\right). \qquad (3.32)
\end{aligned}$$

Substituting (3.31) and (3.32) into (3.30), and averaging (3.30) over $\mathscr{T}$, the MGF of $\gamma_{H-S/MRC}$ becomes

$$\begin{aligned}\phi_{\gamma_{H-S/MRC}}(s) &= \int_0^\infty \frac{t^{m-1}e^{-t}}{(m-1)!}\phi_{\gamma_{H-S/MRC}|\mathscr{T}}(s|t)dt \\ &= \frac{1}{(m-1)!}\sum_{e_i\in W_{N,L_c}}\prod_{k=1}^{L_c-1}\left(\frac{m}{m-\Gamma s(1-\rho_{e_i[k]})}\right)^m \times \\ &\quad \int_0^\infty t^{m-1}e^{-t}\times\exp\left(\sum_{k=1}^{L_c-1}\frac{\Gamma\rho_{e_i[k]}ts}{m-\Gamma s(1-\rho_{e_i[k]})}\right)\int_0^\infty e^{s\gamma}f_{\gamma_{e_i[L_c]}|\mathscr{T}}(\gamma|t)\times \\ &\quad \prod_{k=1}^{L_c-1}Q_m\left(\sqrt{\frac{2m\rho_{e_i[k]}t}{(1-\rho_{e_i[k]})(m-\Gamma s(1-\rho_{e_i[k]}))}},\sqrt{\frac{2(m-\Gamma s(1-\rho_{e_i[k]}))\gamma}{\Gamma(1-\rho_{e_i[k]})}}\right)\times \\ &\quad \prod_{k=L_c+1}^{N}\left[1-Q_m\left(\sqrt{\frac{2\rho_{e_i[k]}t}{1-\rho_{e_i[k]}}},\sqrt{\frac{2m\gamma}{\Gamma(1-\rho_{e_i[k]})}}\right)\right]d\gamma dt \end{aligned} \tag{3.33}$$

where $f_{\gamma_{e_i[k]}|\mathscr{T}}(\cdot)$ is given by (3.27).

When all of $\rho_k=\rho$ $(k=1,\cdots,N)$, the MGF of $\gamma_{H-S/MRC}$ in equally correlated Nakagami-m fading becomes

$$\begin{aligned}\phi_{\gamma_{H-S/MRC}}(s) &= L_c\binom{N}{L_c}\frac{1}{(m-1)!}\left(\frac{m}{m-\Gamma s(1-\rho)}\right)^{m(L_c-1)} \\ &\quad \times\int_0^\infty t^{m-1}e^{-t}\times\exp\left(\frac{(L_c-1)\Gamma\rho ts}{m-\Gamma(1-\rho)s}\right)dt\int_0^\infty e^{s\gamma}f_{\gamma|\mathscr{T}}(\gamma|t)\times \\ &\quad \left[Q_m\left(\sqrt{\frac{2m\rho t}{(1-\rho)(m-\Gamma s(1-\rho))}},\sqrt{\frac{2(m-\Gamma s(1-\rho))\gamma}{\Gamma(1-\rho)}}\right)\right]^{L_c-1}\times \\ &\quad \left[1-Q_m\left(\sqrt{\frac{2\rho t}{1-\rho}},\sqrt{\frac{2m\gamma}{\Gamma(1-\rho)}}\right)\right]^{N-L_c}d\gamma \end{aligned} \tag{3.34}$$

where $f_{\gamma|\mathscr{T}}(\gamma|t)$ is given by (3.27) with $c^2=\rho\Gamma t/m$ and $\sigma^2=\Gamma(1-\rho)/(2m)$. This result is new and not available in [61].

The average SER can be calculated using the MGF method for different linearly modulated signals [38]. Here we consider coherent MPSK as an example; results for other modulation formats can be derived similarly. The average SER of coherent MPSK, P_e, is given by

$$P_e=\frac{1}{\pi}\int_0^\Theta\phi_{\gamma_{H-S/MRC}}\left(-\frac{c_{MPSK}}{\sin^2\theta}\right)d\theta \tag{3.35}$$

where $c_{MPSK} = \sin^2(\pi/M)$, $\Theta = \pi(M-1)/M$, and $\phi_{\gamma_{H-S/MRC}}(s) = \mathbb{E}\left(e^{s\sum_{k=1}^{L_c}\gamma_{(k)}}\right)$ is the MGF of $\gamma_{H-S/MRC}$ as given by (3.33).

3.4.3 SER of T-HS/MRC

Recall in Chapter 2 that since the T-HS/MRC combiner outputs corresponding to each integer value of L_c represent disjoint events and form a partition of probability space, the average SER of T-HS/MRC can be calculate using the total probability theorem (2.2)

$$P_e = \sum_{L=1}^{N} P(e, L_c = L) \tag{3.36}$$

where $P(e, L_c = L)$ is the average SER of T-HS/MRC corresponding to the joint event that L branches are selected and they satisfy $\gamma_{(1)} > \gamma_{(2)} > \cdots \geq \mu\gamma_{(1)} > \gamma_{(L+1)} > \cdots > \gamma_{(N)}$. The probability $P(e, L_c = L)$ can be calculated using the MGF method for different linearly modulated signals. Here we just consider coherent MPSK as an example. The probability $P(e, L_c = L)$ of coherent MPSK is given by (2.3)

$$P(e, L_c = L) = \frac{1}{\pi}\int_0^{\Theta} \phi_{\gamma_{T-HS/MRC(L)}}\left(-\frac{c_{MPSK}}{\sin^2\theta}\right) d\theta \tag{3.37}$$

where c_{MPSK} and Θ were defined previously, and $\phi_{\gamma_{T-HS/MRC(L)}}(s) = \mathbb{E}\left(e^{s\sum_{k=1}^{L}\gamma_{(k)}}\right)$ is the MGF of $\gamma_{T-HS/MRC(L)}$ defined by (3.5), where the ordered instantaneous branch SNRs satisfy $\gamma_{(1)} > \gamma_{(2)} > \cdots \geq \mu\gamma_{(1)} > \gamma_{(L+1)} > \cdots > \gamma_{(N)}$.

Since the branch SNRs conditioned on $\mathscr{T} = \sum_{l=1}^{m}(X_{0l}^2 + Y_{0l}^2)$ are independent, the conditional MGF of $\gamma_{T-HS/MRC(L)}$ defined in (3.5) can be calcuated as [36, eqs. (25) and (26)]

$$\begin{aligned}
\phi_{\gamma_{T-HS/MRC(L)|\mathscr{T}}}(s|t) &= \sum_{e_i \in S_N} \int_0^{\infty} d\gamma_{(1)} \int_{\mu\gamma_{(1)}}^{\gamma_{(1)}} d\gamma_{(2)} \cdots \int_{\mu\gamma_{(1)}}^{\gamma_{(L-1)}} d\gamma_{(L)} \int_0^{\mu\gamma_{(1)}} d\gamma_{(L+1)} \\
&\quad \times \int_0^{\gamma_{(L+1)}} d\gamma_{(L+2)} \cdots \int_0^{\gamma_{(N-1)}} e^{s\sum_{k=1}^{L}\gamma_{(k)}} \prod_{k=1}^{N} f_{\gamma_{e_i[k]}|\mathscr{T}}(\gamma_{(k)}|t) d\gamma_{(N)} \\
&= \sum_{e_i \in T_{N,L}} \int_0^{\infty} e^{s\gamma} f_{\gamma_{e_i[1]}|\mathscr{T}}(\gamma|t) \prod_{k=2}^{L} \left[\phi_{\gamma_{e_i[k]}|\mathscr{T}}(s, \mu\gamma|t) - \phi_{\gamma_{e_i[k]}|\mathscr{T}}(s, \gamma|t)\right] \\
&\quad \times \prod_{k=L+1}^{N} F_{\gamma_{e_i[k]}|\mathscr{T}}(\mu\gamma|t) d\gamma
\end{aligned} \tag{3.38}$$

where e_i and S_N were defined previously, $T_{N,L}$ is a subset of S_N, whose element e_i satisfies $e_i[2] < e_i[3] < \cdots < e_i[L]$ and $e_i[L+1] < e_i[L+2] < \cdots < e_i[N]$. The functions $f_{\gamma_{e_i[k]}|\mathscr{T}}(x|t)$, $F_{\gamma_{e_i[k]}|\mathscr{T}}(x|t)$ and $\phi_{\gamma_{e_i[k]}|\mathscr{T}}(s,x|t)$, are the PDF, CDF and the incomplete MGF of $\gamma_{e_i[k]}$ conditioned on $\mathscr{T}$, respectively, given by (3.27), (3.31) and (3.32).

Averaging (3.38) over $\mathscr{T}$, the MGF of $\gamma_{T-HS/MRC(L)}$ is given by

$$\begin{aligned}\phi_{\gamma_{T-HS/MRC(L)}}(s) &= \frac{1}{(m-1)!}\sum_{e_i\in T_{N,L}}\prod_{k=2}^{L}\left(\frac{m}{m-\Gamma s(1-\rho_{e_i[k]})}\right)^m \\ &\times\int_0^\infty t^{m-1}e^{-t}\exp\left(\sum_{k=2}^{L}\frac{\Gamma\rho_{e_i[k]}ts}{m-\Gamma s(1-\rho_{e_i[k]})}\right)dt\int_0^\infty e^{s\gamma}f_{\gamma_{e_i[1]}|\mathscr{T}}(\gamma|t)\times \\ &\prod_{k=2}^{L}\left[Q_m\left(\sqrt{\frac{2m\rho_{e_i[k]}t}{(1-\rho_{e_i[k]})(m-\Gamma s(1-\rho_{e_i[k]}))}},\sqrt{\frac{2(m-\Gamma s(1-\rho_{e_i[k]}))\mu\gamma}{\Gamma(1-\rho_{e_i[k]})}}\right)\right. \\ &\left.-Q_m\left(\sqrt{\frac{2m\rho_{e_i[k]}t}{(1-\rho_{e_i[k]})(m-\Gamma s(1-\rho_{e_i[k]}))}},\sqrt{\frac{2(m-\Gamma s(1-\rho_{e_i[k]}))\gamma}{\Gamma(1-\rho_{e_i[k]})}}\right)\right] \\ &\times\prod_{k=L+1}^{N}\left[1-Q_m\left(\sqrt{\frac{2\rho_{e_i[k]}t}{1-\rho_{e_i[k]}}},\sqrt{\frac{2m\mu\gamma}{\Gamma(1-\rho_{e_i[k]})}}\right)\right]d\gamma. \end{aligned} \tag{3.39}$$

When all of $\rho_k = \rho$ $(k = 1,\cdots,N)$, the MGF of $\gamma_{T-HS/MRC(L)}$ in equally correlated Nakgami-m fading becomes

$$\begin{aligned}\phi_{\gamma_{T-HS/MRC(L)}}(s) &= \frac{L\binom{N}{L}}{(m-1)!}\times\left(\frac{m}{m-\Gamma s(1-\rho)}\right)^{(L-1)m}\int_0^\infty t^{m-1}e^{-t} \\ &\times\exp\left(\frac{(L-1)\Gamma\rho ts}{m-\Gamma s(1-\rho)}\right)dt\int_0^\infty e^{s\gamma}f_{\gamma|\mathscr{T}}(\gamma|t)\times\left[1-Q_m\left(\sqrt{\frac{2\rho t}{1-\rho}},\sqrt{\frac{2m\mu\gamma}{\Gamma(1-\rho)}}\right)\right]^{N-L} \\ &\times\left[Q_m\left(\sqrt{\frac{2m\rho t}{(1-\rho)(m-\Gamma s(1-\rho))}},\sqrt{\frac{2(m-\Gamma s(1-\rho))\mu\gamma}{\Gamma(1-\rho)}}\right)\right. \\ &\left.-Q_m\left(\sqrt{\frac{2m\rho t}{(1-\rho)(m-\Gamma s(1-\rho))}},\sqrt{\frac{2(m-\Gamma s(1-\rho))\gamma}{\Gamma(1-\rho)}}\right)\right]^{L-1}d\gamma. \end{aligned} \tag{3.40}$$

Substituting (3.39) into (3.37) and (3.36), one can obtain the average SER of coherent MPSK with T-HS/MRC in correlated Nakagami-m fading for positive integer values of m and power covariance matrix (3.2).

3.5 Numerical Results

In this section, some numerical examples and simulation results for SC, H-S/MRC and T-HS/MRC in correlated Nakagami-m fading with positive integer values of m and power covariance matrix (3.2), are provided. In the examples, we use $\vec{\rho} = [\rho_1, \rho_2, \cdots, \rho_N]$ to denote a vector whose elements $0 \leq \rho_k < 1$ $(k = 1, \cdots, N)$ comprise the covariance matrix Σ_γ in (3.2).

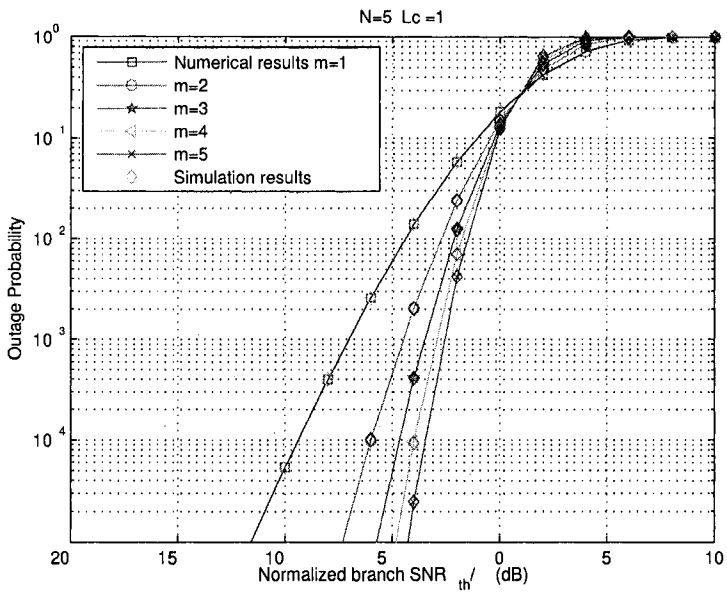

Fig. 3.1. The outage probability versus the normalized branch SNR threshold γ_{th}/Γ of SC with $N = 5$ for different values of fading parameter m.

Fig. 3.1 shows the outage probability of SC in Nakagami-m fading versus the normalized SNR threshold γ_{th}/Γ. The number of diversity branches $N = 5$. The covariance matrix is constituted by the vector $\vec{\rho} = [0.9\ 0.3\ 0.7\ 0.6\ 0.1]$. The diamonds denote the outage probability estimated using Monte Carlo simulation. One can see that our theoretical results are in excellent agreement with the simulation results. Observe that when the normalized branch SNR threshold $\gamma_{th}/\Gamma \leq 1.1$ dB, the outage probability decreases with increasing fading parameter m; however, when $\gamma_{th}/\Gamma > 1.1$ dB, the outage probability increases with

increasing fading parameter m.

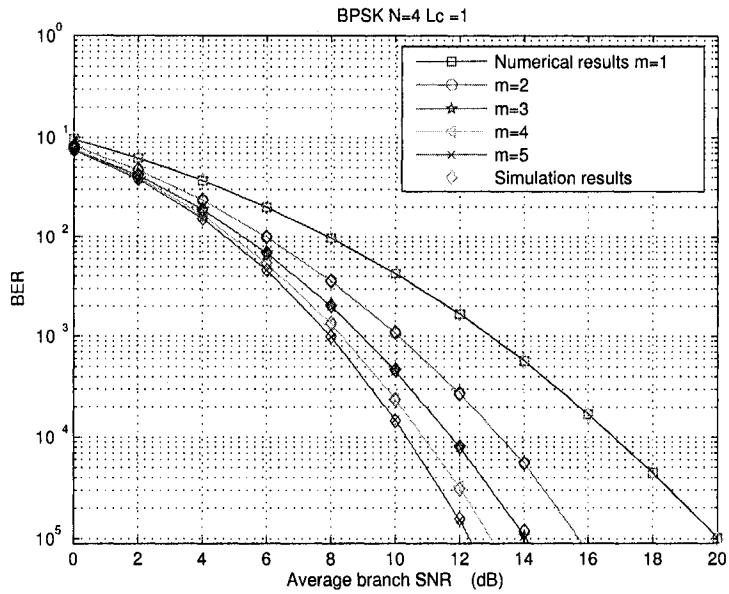

Fig. 3.2. The average BER versus the average branch SNR Γ of coherent BPSK using SC with $N = 4$ for different values of fading parameter m.

Fig. 3.2 shows the average BER versus the average branch SNR, Γ, of a coherent BPSK system with SC in correlated Nakagami-m fading with $N = 4$ and $\vec{\rho} = [0.95\ 0.9\ 0.95\ 0.9]$. Different values of fading parameter m are considered. The diamonds denote the average BER obtained using Monte Carlo simulation. One can again see that the theoretical results are in excellent agreement with the simulation results. High-order coherent modulation formats can be accommodated by the analysis. Fig. 3.3 shows the average SER versus the average branch SNR, Γ, of a coherent 16-QAM system with SC in correlated Nakagami-m fading with $N = 4$ and $\vec{\rho} = [0.745\ 0.913\ 0.884\ 0.721]$. The analysis and results apply equally to noncoherent reception. Fig. 3.4 shows the average BER versus the average branch SNR per bit, Γ, of a noncoherent MFSK system with SC in $N = 4$ correlated Nakagami fading with $m = 2$ and $\vec{\rho} = [0.95\ 0.9\ 0.95\ 0.9]$.

Fig. 3.5 shows an example of a H-S/MRC system, where the average SER versus the average branch SNR, Γ, of a coherent QPSK system with H-S/MRC in correlated Nakagami-

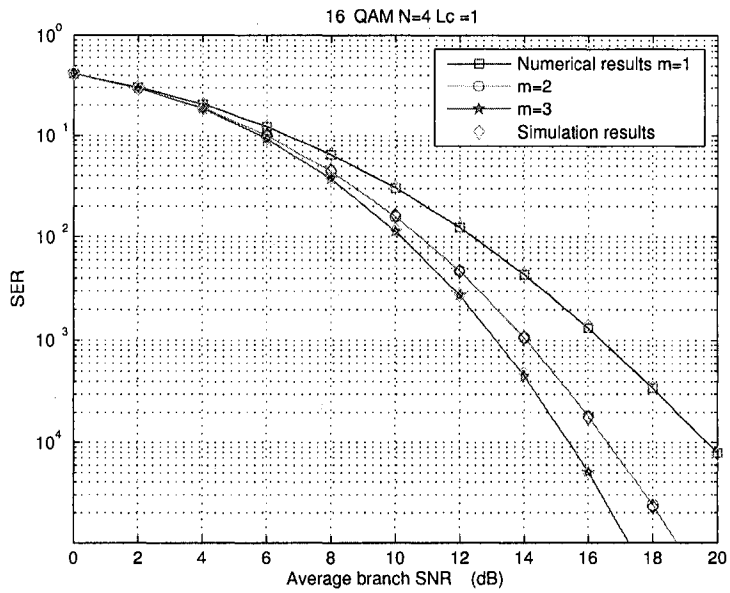

Fig. 3.3. The average SER versus the average branch SNR Γ of coherent 16-QAM using SC with $N = 4$ for different values of fading parameter m.

m fading is considered. The $L_c = 2$ best branch signals out of $N = 4$ available branches are selected. The corresponding vector $\vec{\rho} = [0.745\ 0.913\ 0.884\ 0.721]$. Again, the simulation results denoted by the diamonds support our theoretical results for different values of fading parameter m. One sees that a more lightly faded environment, represented by $m = 3$ offers better performance than a Rayleigh faded environment, represented by $m = 1$, by about 4.6 dB in SNR at SER=10^{-4}.

The amount of performance gain that can be achieved by adding an additional branch is of interest. Fig. 3.6 shows the average SER versus the average branch SNR, Γ, of a coherent QPSK system with H-S/MRC in correlated Rayleigh fading with $N = 4$ and $\vec{\rho} = [0.9\ 0.3\ 0.7\ 0.6]$. Different numbers of the selected branches L_c are considered. As expected, the SER decreases when more branches are selected. However, the benefit from choosing one more branch decreases with increasing L_c. For example, when the SER is 10^{-4}, about 2 dB gain in SNR is obtained in going from $L_c = 1$ to $L_c = 2$, while only 0.3 dB in SNR is gained in going from $L_c = 3$ to $L_c = 4$.

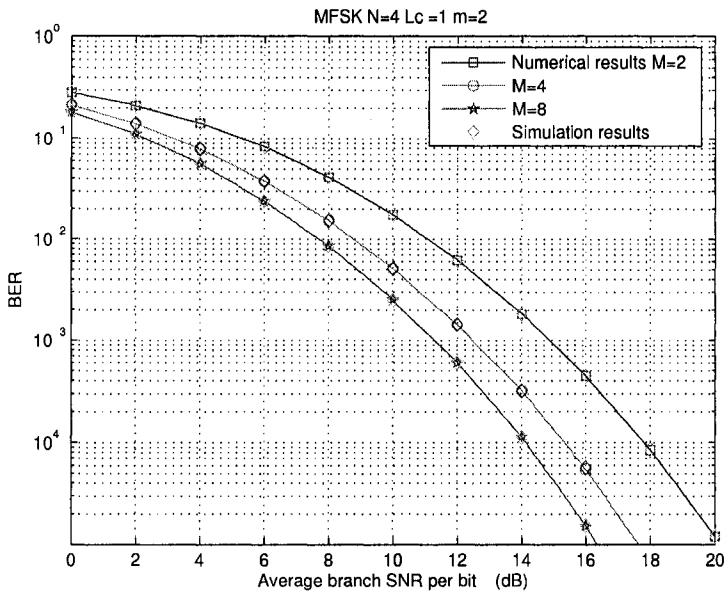

Fig. 3.4. The average BER versus the average branch SNR per bit Γ of coherent MFSK using SC with $N = 4$ for different values of modulation order M.

The effect of the normalized threshold, μ, on the SER of T-HS/MRC in correlated Nakagami-m fading can be investigated using our theoretical results. Fig. 3.7 shows the average SER versus the average branch SNR, Γ, of a coherent QPSK system with T-HS/MRC in correlated Nakagami-m fading with $N = 4$, $m = 2$, and $\vec{\rho} = [0.745\ 0.913\ 0.884\ 0.721]$. Different values of normalized threshold μ are considered. One can see that our numerical results are in excellent agreement with the simulation results. Observe that the SER decreases when μ decreases, as expected.

To further examine the effect of the normalized threshold μ on the performance of T-HS/MRC, the average BER of coherent BPSK versus the normalized threshold μ for correlated Nakagami-m fading with $N = 5$ and $\vec{\rho} = [0.9\,0.3\,0.7\,0.6\,0.1]$ is shown in Fig. 3.8. The average branch SNR $\Gamma = 10$ dB. One can see that the BER increases with increasing μ due to fewer diversity branches satisfying the condition of T-HS/MRC and being excluded from the combining. Also, the incremental benefit of decreasing the value of μ decreases as μ decreases. This is because the BER of MRC is achieved when $\mu = 0$, and represents

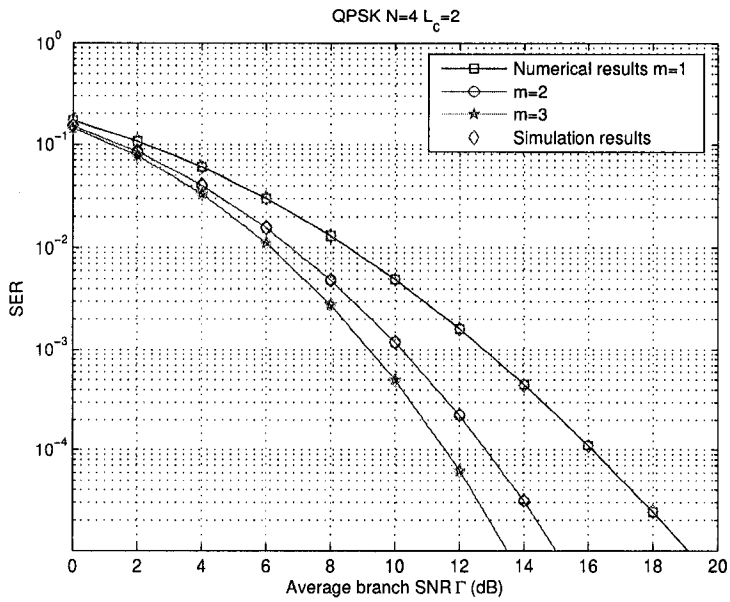

Fig. 3.5. The average SER versus the average branch SNR Γ of coherent QPSK using H-S/MRC with $N = 4$ and $L_c = 2$ for different values of fading parameter m.

an ultimate lower bound below which the BER cannot be reduced.

3.6 Summary

In this chapter, exact performance analyses of selection combining, hybrid selection/maximal-ratio combining, and threshold-based hybrid selection/maximal-ratio combining operating in correlated Nakagami-m branch fading with positive integer values of fading parameter m, were derived for a particular correlation structure. This correlation model includes equal correlation as a special case. The theoretical analyses are performed possible by transforming the correlated branch gains into a set of conditionally independent complex Gaussian random variables. Our analyses are simplified compared to other analyses for special cases of branch correlation and accommodate different M-ary linear modulation schemes. Numerical and simulation results show excellent agreement with theoretical results.

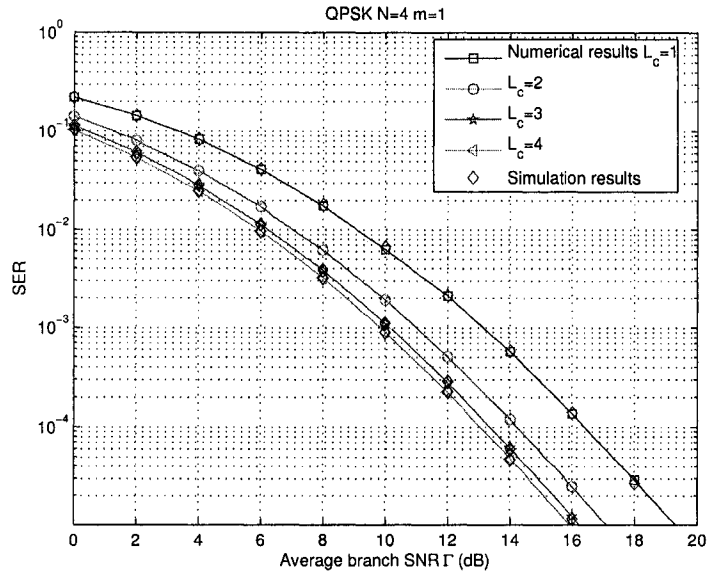

Fig. 3.6. The average SER versus the average branch SNR Γ of coherent QPSK using H-S/MRC in Rayleigh fading with $N = 4$ for different values of active branches L_c.

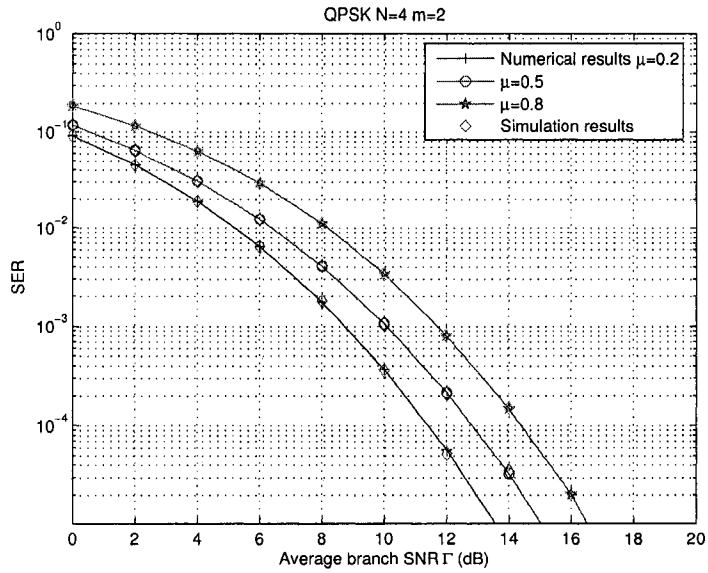

Fig. 3.7. The average SER versus the average branch SNR Γ of coherent QPSK using T-HS/MRC with $N = 4$ and $m = 2$ for different values of normalized threshold μ.

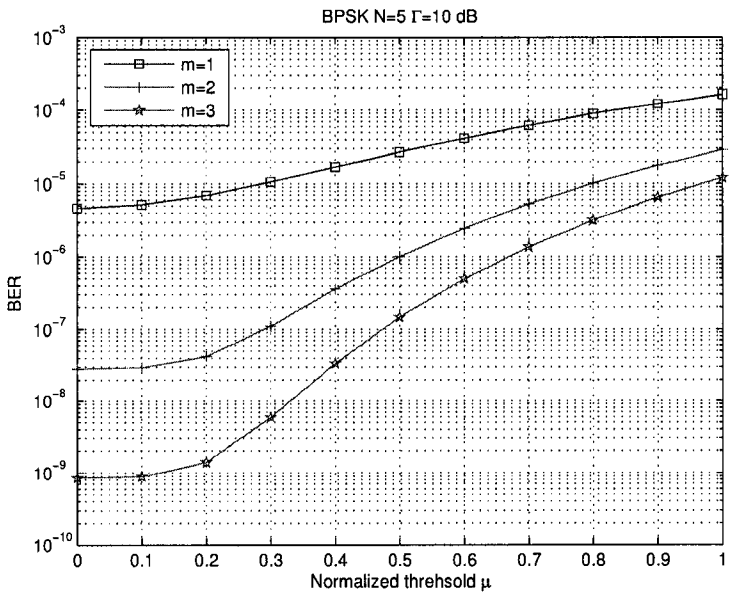

Fig. 3.8. The average BER versus the normalized threshold μ, of coherent BPSK using T-HS/MRC with $N = 5$, and the average branch SNR $\Gamma = 10$ dB for different values of fading parameter m.

Chapter 4

Approximate SER of H-S/MRC and T-HS/MRC in Arbitrarily Correlated Nakagami-*m* Fading

4.1 Introduction

The performance analyses of H-S/MRC and T-HS/MRC in independent fading environments have been extensively studied. However, in practice, there often exist applications where independent diversity branches are not available. For example, in compact antenna systems, such as employed in handsets, the diversity branch fadings are correlated due to space limitations. However, currently, there are no works providing exact theoretical results of H-S/MRC and T-HS/MRC with arbitrary number of diversity branches in arbitrarily correlated fading due to the very complicated nature of the order statistics involved in performance analysis. Recently, combining the results for the generalized Rayleigh distribution in [64] and the approximate correlation matrix with a Green's matrix in [65], Karagiannidis, *et al.* proposed a useful approach to evaluate the multivariate Nakagami-*m* PDF and CDF using a Green's approximation method in [66]. The main idea of their work is as follows. Recall that when the fading parameter m is a positive integer, a Nakagami-*m*

random variable can be considered as the square root of the sum of squares of m independent Rayleigh or $2m$ independent Gaussian random variables [5]. When the inverse of the covariance matrix is a tridiagonal matrix with nonzero elements only on the diagonal and slots horizontally or vertically adjacent the diagonal (i.e. along the subdiagonal and superdiagonal), the joint PDF of multivariate Nakagami-m RVs can be derived from the joint PDF of multivariate Gaussian RVs [64]. However, in general cases, the inverse of the covariance matrix does not have the tridiagonal property. In this case, [66] approximates the covariance matrix with a Green's matrix whose elements are the closest to the entries of the covariance matrix by observing that the inverse of a Green's matrix is tridiagonal. Then the approximate joint PDF and CDF of multivariate Nakagami-m RVs with an arbitrary covariance matrix can be obtained by applying the results in [64]. Using this method, an efficient approximate analysis of SC in arbitrarily correlated Nakagami-m fading with positive integer values of fading parameter m was given in [66]. The applicability and the usefulness of the proposed analysis was examined by numerical examples and simulation results for various correlation models well known in practical diversity systems in [66].

Based on the Green's matrix approximation approach in [66], an approximate SER analysis of H-S/MRC and T-HS/MRC in arbitrarily correlated Nakagami-m fading when the fading parameter m is positive integer, is developed in this chapter [67, 68]. Further, an exact solution for the average SER of T-HS/MRC in correlated Nakagami-m fading when the inverse of the covariance matrix is tridiagonal, is also given.

The remainder of this chapter is organized as follows. The system model is described in Section 4.2. In Section 4.3, an approximation to the joint PDF of the branch SNRs is developed using the Green's matrix method. The approximate SER analysis of H-S/MRC and T-HS/MRC is presented in Section 4.4. Some numerical results are shown in Section 4.5 and finally, we conclude this chapter in Section 4.6.

4.2 System Model

Based on the system model in [66], we assume that there are N diversity branches experiencing slow and flat Nakagami-m fading, and the branch fadings are arbitrarily correlated. The fading parameter, m, is assumed a positive integer. Let $\gamma_k = |h_k|^2 E_s/N_0$ denote the instantaneous SNR of the kth diversity branch, as defined in (1.10). Further we assume that the branch SNRs, γ_k $(k = 1, \cdots, N)$, have the same average SNR, i.e., $\Gamma = \mathbb{E}(\gamma_k)$. Then, the amplitudes of the branch gains, $|h_k|$ $(k = 1, \cdots, N)$, can be equivalently obtained from $2m$ independent Gaussian distributed N-dimensional column vectors Y_l $(l = 1, \cdots, 2m)$ with zero mean and power covariance coefficient matrix Σ. The entries of the matrix Σ, $\Sigma_{i,j}$ $(i, j = 1, \cdots, N)$, are defined by [66]

$$\Sigma_{i,j} = \frac{\mathbb{E}(|Y_l^i|^2 |Y_l^j|^2) - \mathbb{E}(|Y_l^i|^2)\mathbb{E}(|Y_l^j|^2)}{\sqrt{Var(|Y_l^i|^2) Var(|Y_l^j|^2)}} = \begin{cases} \rho_{i,j} & (i \neq j) \\ 1 & (i = j). \end{cases} \tag{4.1}$$

where $0 \leq \rho_{i,j} < 1$, and Y_l^i denotes the the ith element of the Gaussian vector Y_l.

4.3 Joint PDF of Branch SNRs

4.3.1 Exact Joint PDF of Branch SNRs

According to [66], let $W = \Sigma^{-1}$ denote the inverse of the power covariance coefficient matrix of the N-dimensional Gaussian RVs as defined in (4.1). When W is tridiagonal, the elements of W satisfy

$$W = \begin{bmatrix} p_{1,1} & p_{1,2} & 0 & 0 & \cdots & 0 & 0 & 0 \\ p_{2,1} & p_{2,2} & p_{2,3} & 0 & \ddots & 0 & 0 & 0 \\ 0 & p_{3,2} & p_{3,3} & p_{3,4} & \ddots & 0 & 0 & 0 \\ \vdots & \ddots & \ddots & \ddots & \ddots & \vdots & \vdots & \vdots \\ 0 & 0 & 0 & 0 & \cdots & p_{N-1,N-2} & p_{N-1,N-1} & p_{N-1,N} \\ 0 & 0 & 0 & 0 & \cdots & 0 & p_{N,N-1} & p_{N,N} \end{bmatrix}. \tag{4.2}$$

Then the exact joint PDF of branch SNRs, γ_k $(k = 1, \cdots, N)$ in correlated Nakagami-m fading with the inverse of the covariance matrix, W, can be derived using [66, eq. (2)] as

$$f_{\gamma_1,\cdots,\gamma_N}(\gamma_1,\cdots,\gamma_N) = \frac{f(\sqrt{\frac{2m}{\Gamma}\gamma_1},\cdots,\sqrt{\frac{2m}{\Gamma}\gamma_N})}{(2\Gamma/m)^{N/2}\prod_{k=1}^{N}\sqrt{\gamma_k}} \tag{4.3}$$

where $f(\cdot)$ is the joint PDF of the N-dimensional Nakagami-m RVs given by [66, eq. (2)]

$$\begin{aligned} f(x_1,x_2,\cdots,x_N) &= \frac{|W|^m x_1^{m-1} x_N^m e^{-p_{N,N}x_N^2/2}}{2^{m-1}\Gamma(m)} \times \\ &\prod_{k=1}^{N-1}\left[|p_{k,k+1}|^{-(m-1)} x_k e^{-p_{k,k}x_k^2/2} I_{m-1}(|p_{k,k+1}|x_k x_{k+1})\right] \end{aligned} \tag{4.4}$$

where $|W|$ is the determinant of W and $p_{i,j}$ $(i,j = 1,\cdots,N)$ are the elements of W, and $I_v(\cdot)$ is the vth-order modified Bessel function of the first kind [4], [69].

When m is a positive integer, one can expand the modified Bessel functions in (4.4) into an infinite series following [69], and (4.3) becomes

$$\begin{aligned} f_{\gamma_1,\cdots,\gamma_N}(\gamma_1,\cdots,\gamma_N) &= \frac{|W|^m \prod_{k=1}^{N-1}|p_{k,k+1}^{-(m-1)}|}{(m-1)!} \sum_{v_1=0}^{\infty}\sum_{v_2=0}^{\infty}\cdots\sum_{v_{N-1}=0}^{\infty} \frac{\prod_{k=1}^{N-1}|p_{k,k+1}|^{m-1+2v_k}}{\prod_{k=1}^{N-1}[v_k!(m+v_k-1)!]} \\ &\times\left(\frac{\gamma_1^{v_1+m-1}e^{-\frac{mp_{1,1}}{\Gamma}\gamma_1}}{\left(\frac{\Gamma}{m}\right)^{v_1+m}}\right)\times\left(\frac{\gamma_N^{v_{N-1}+m-1}e^{-\frac{mp_{N,N}}{\Gamma}\gamma_N}}{\left(\frac{\Gamma}{m}\right)^{v_{N-1}+m}}\right) \\ &\times\prod_{k=2}^{N-1}\left(\frac{\gamma_k^{v_{k-1}+v_k+m-1}e^{-\frac{mp_{k,k}}{\Gamma}\gamma_k}}{\left(\frac{\Gamma}{m}\right)^{v_{k-1}+v_k+m}}\right) \\ &= \frac{|W|^m}{\prod_{k=1}^{N}p_{k,k}{}^m}\sum_{v_1=0}^{\infty}\sum_{v_2=0}^{\infty}\cdots\sum_{v_{N-1}=0}^{\infty}\prod_{k=1}^{N-2}\binom{v_k+v_{k+1}+m-1}{v_k} \\ &\times\binom{v_{N-1}+m-1}{v_{N-1}}\times\prod_{k=1}^{N-1}\left(\frac{p_{k,k+1}^2}{p_{k,k}p_{k+1,k+1}}\right)^{v_k} \\ &\times g\left(\gamma_1;v_1+m-1,\frac{\Gamma}{p_{1,1}m}\right) \\ &\times g\left(\gamma_N;v_{N-1}+m-1,\frac{\Gamma}{p_{N,N}m}\right) \\ &\times\prod_{k=2}^{N-1}g\left(\gamma_k;v_{k-1}+v_k+m-1,\frac{\Gamma}{p_{k,k}m}\right) \end{aligned} \tag{4.5}$$

where $g(x;n,a)$ is given by

$$g(x;n,a) = \frac{x^n e^{-\frac{x}{a}}}{n!a^{n+1}}, \qquad x \geq 0,\ Re\{a\} > 0. \tag{4.6}$$

For the purpose of brevity, rewrite (4.5) as

$$f_{\gamma_1,\cdots,\gamma_N}(\gamma_1,\cdots,\gamma_N) = \frac{|W|^m}{\prod_{k=1}^{N} p_{k,k}{}^m} \sum_{\nu_1=0}^{\infty}\sum_{\nu_2=0}^{\infty}\cdots\sum_{\nu_{N-1}=0}^{\infty} A\prod_{k=1}^{N} g(\gamma_k;l_k,a_k) \tag{4.7}$$

where $a_k = \Gamma/(p_{k,k}m)$ $(k=1,\cdots,N)$, A and l_k are given, respectively, by

$$A = \binom{\nu_{N-1}+m-1}{\nu_{N-1}} \prod_{q=1}^{N-2} \binom{\nu_q+\nu_{q+1}+m-1}{\nu_q} \prod_{q=1}^{N-1} \left(\frac{p_{q,q+1}^2}{p_{q,q}p_{q+1,q+1}}\right)^{\nu_q}$$

and

$$l_k = \begin{cases} \nu_1+m-1 & , \quad k=1 \\ \nu_{k-1}+\nu_k+m-1 & , \quad k=2,\cdots,N-1 \\ \nu_{N-1}+m-1 & , \quad k=N \end{cases}.$$

4.3.2 Approximate Joint PDF of Branch SNRs

In the general case, the inverse of the covariance matrix $\sum$, W, does not have a tridiagonal structure. In this case, we approximate $\sum$ with a Green's matrix, C, whose elements are the closest possible values to the entries of $\sum$. Note that the inverse of a Green's matrix is tridiagonal. Then the approximate matrix C is in format as [66, eq. (9)]

$$C = \begin{bmatrix} u_1w_1 & u_1w_2 & u_1w_3 & u_1w_4 & \cdots & u_1w_N \\ u_1w_2 & u_2w_2 & u_2w_3 & u_2w_4 & \cdots & u_2w_N \\ u_1w_3 & u_2w_3 & u_3w_3 & u_3w_4 & \cdots & u_3w_N \\ \vdots & \vdots & \vdots & \vdots & \ddots & \vdots \\ u_1w_N & u_2w_N & u_3w_N & u_4w_N & \cdots & u_Nw_N \end{bmatrix} \tag{4.8}$$

where u_i and w_i $(i=1,\cdots,N)$ are two sequences of real numbers and $u_iw_i = 1$ $(i = 1,\cdots,N)$ due to the form of $\sum$. Equating $\sum$ with C, a linear system equation is produced as

shown in [66, eq. (10)]

$$\begin{array}{lllll} w_2 = \Sigma_{2,1} w_1 & & & & \\ w_3 = \Sigma_{3,1} w_1 & w_3 = \Sigma_{3,2} w_2 & & & \\ w_4 = \Sigma_{4,1} w_1 & w_4 = \Sigma_{4,2} w_2 & w_4 = \Sigma_{4,3} w_3 & & \\ \vdots & \vdots & \vdots & \ddots & \ddots \\ w_N = \Sigma_{N,1} w_1 & w_N = \Sigma_{N,2} w_2 & w_N = \Sigma_{N,3} w_3 & \cdots & w_N = \Sigma_{N,N-1} w_{N-1} \end{array} . \quad (4.9)$$

Eq. (4.9) can be rewritten in matrix format as follows

$$A\mathbf{w} = \begin{bmatrix} \Sigma_{2,1} & -1 & 0 & \cdots & 0 & 0 \\ \Sigma_{3,1} & 0 & -1 & \cdots & 0 & 0 \\ 0 & \Sigma_{3,2} & -1 & \cdots & 0 & 0 \\ \vdots & \vdots & \vdots & \ddots & \ddots & \\ \Sigma_{N,1} & 0 & 0 & \cdots & 0 & -1 \\ 0 & \Sigma_{N,2} & 0 & \cdots & 0 & -1 \\ 0 & 0 & \Sigma_{N,3} & \cdots & 0 & -1 \\ \vdots & \vdots & \vdots & \ddots & \vdots & \vdots \\ 0 & 0 & 0 & \cdots & \Sigma_{N,N-1} & -1 \end{bmatrix} \begin{bmatrix} w_1 \\ w_2 \\ w_3 \\ \vdots \\ w_N \end{bmatrix} = 0. \quad (4.10)$$

Note that to satisfy the definitions of the normalized covariance matrix and the Green's matrix, all of w_i should be non-zero values with the same sign. Therefore, it becomes a linear system of equations with constraints that either all of $w_i > 0$ $(i = 1, \cdots, N)$ or all of $w_i < 0$ $(i = 1, \cdots, N)$. This constrained system equation can be solved for w_i using well-known methods such as Levenberg-Marquards, quasi-Newton, or conjugate gradient methods, available in most mathematical software packages such as Mathematica, Matlab, Maple, etc. [66]. In our examples, we use Levenberg-Marquards method, which finds the optimal solutions for w_i to minimize the Euclidean norm of the vector $(A\mathbf{w})$, namely $\min_{(\mathbf{w}>0) \cup (\mathbf{w}<0)} f = \|A\mathbf{w}\|_2$, where $\|\mathbf{v}\|_2$ denotes the Euclidean norm of the vector $\mathbf{v}$. This problem is a convex optimization problem and hence the global optimum exists. Since $u_i = 1/w_i$, C can be obtained.

Substituting C for Σ in (4.7), one can obtain an approximate joint PDF for arbitrarily

correlated branch SNRs, which can be used to make an approximate analysis of H-S/MRC and T-HS/MRC in Nakagmi-m fading with arbitrary covariance matrix. In the following, we will use W to represent a matrix possessing the tridiagonal structure; thus, W represents the inverse of $\sum$ with tridiagonal property, and represents the inverse of the corresponding Green's matrix approximation, C, as indicated by the context.

4.4 SER of H-S/MRC and T-HS/MRC

Appendix B gives a general result for expressing the joint PDF of ordered random variables in terms of the joint PDF of the unordered random variables. From Appendix B, one can obtain the joint PDF of the ordered branch SNRs $\gamma_{(1)}, \cdots, \gamma_{(N)}$, as

$$\begin{aligned} f_{\gamma_{(1)},\cdots,\gamma_{(N)}}(\gamma_{(1)},\cdots,\gamma_{(N)}) &= \sum_{e_i \in S_N} f_{\gamma_1,\cdots,\gamma_N}(\gamma_{(e_i[1])},\cdots,\gamma_{(e_i[N])}) \\ &= \frac{|W|^m}{\prod_{k=1}^{N} p_{k,k}{}^m} \sum_{v_1=0}^{\infty}\sum_{v_2=0}^{\infty}\cdots\sum_{v_{N-1}=0}^{\infty} A \sum_{e_i \in S_N} \prod_{k=1}^{N} g\left(\gamma_{(k)}; l_{e_i[k]}, a_{e_i[k]}\right) \\ &\qquad \gamma_{(1)} > \gamma_{(2)} > \cdots > \gamma_{(N)} > 0 \end{aligned} \tag{4.11}$$

where $e_i \in S_N$ denotes $e_i = \{e_i[1], e_i[2], \cdots, e_i[N]\}$, one specific permutation of the integers $\{1, \cdots, N\}$, and W, A, a_k, l_k and $g(\cdot;\cdot,\cdot)$ were defined previously. With this joint PDF, the average SER of H-S/MRC and T-HS/MRC can be calculated using the MGF method for different linearly modulated signals [38] as done in Chapter 3. Here, we take coherent MPSK as an example; results for other modulation formats can be derived similarly.

4.4.1 Approximate SER of H-S/MRC

Substituting (4.11) into (3.29), one obtains

$$\begin{aligned} \phi_{\gamma_{H-S/MRC}}(s) &= \int_0^{\infty} d\gamma_{(1)} \int_0^{\gamma_{(1)}} d\gamma_{(2)} \cdots \int_0^{\gamma_{(N-1)}} e^{s\sum_{k=1}^{Lc}\gamma_{(k)}} \times \\ &\quad f_{\gamma_{(1)},\cdots,\gamma_{(N)}}(\gamma_{(1)},\cdots,\gamma_{(N)}) d\gamma_{(N)} \\ &= \frac{|W|^m}{\prod_{k=1}^{N} p_{k,k}{}^m} \sum_{v_1=0}^{\infty}\sum_{v_2=0}^{\infty}\cdots\sum_{v_{N-1}=0}^{\infty} A \sum_{e_i \in S_N} \int_0^{\infty} g\left(\gamma_{(1)}; l_{e_i[1]}, a_{e_i[1]}\right) e^{s\gamma_{(1)}} d\gamma_{(1)} \end{aligned}$$

$$\times \cdots \int_0^{\gamma_{(L_c-1)}} g\left(\gamma_{(L_c)}; l_{e_i[L_c]}, a_{e_i[L_c]}\right) e^{s\gamma_{(L_c)}} d\gamma_{(L_c)}$$
$$\times \int_0^{\gamma_{(L_c)}} g\left(\gamma_{(L_c+1)}; l_{e_i[L_c+1]}, a_{e_i[L_c+1]}\right) d\gamma_{(L_c+1)} \cdots$$
$$\times \int_0^{\gamma_{(N-1)}} g\left(\gamma_{(N)}; l_{e_i[N]}, a_{e_i[N]}\right) d\gamma_{(N)}. \tag{4.12}$$

Using [34, eqs. (11), (12) and (A.1)], (4.12) can be further simplified as

$$\begin{aligned}\phi_{\gamma_{H-S/MRC}}(s) &= \frac{|W|^m}{\prod_{k=1}^{N} p_{k,k}{}^m} \sum_{\nu_1=0}^{\infty} \sum_{\nu_2=0}^{\infty} \cdots \sum_{\nu_{N-1}=0}^{\infty} A \sum_{e_i \in W_{N,L_c}} \int_0^{\infty} g\left(\gamma_{(L_c)}; l_{e_i[L_c]}, a_{e_i[L_c]}\right) e^{s\gamma_{(L_c)}} \\ &\times \prod_{k=1}^{L_c-1} \phi_{e_i[k]}(s; \gamma_{(L_c)}) \times \prod_{k=L_c+1}^{N} F_{e_i[k]}(\gamma_{(L_c)}) d\gamma_{(L_c)} \end{aligned} \tag{4.13}$$

where W_{N,L_c} is a subset of S_N, whose element e_i satisfies $e_i[1] < e_i[2] < \cdots < e_i[L_c - 1]$ and $e_i[L_c+1] < e_i[L_c+2] < \cdots < e_i[N]$, as defined previously. $\phi_{e_i[k]}(s,x)$ and $F_{e_i[k]}(x)$ are given respectively by

$$\begin{aligned}\phi_{e_i[k]}(s,x) &= \int_x^{\infty} e^{s\gamma} g(\gamma; l_{e_i[k]}, a_{e_i[k]}) d\gamma \\ &= \frac{e^{-\left(\frac{1}{a_{e_i[k]}} - s\right)x}}{(1 - a_{e_i[k]} s)^{l_{e_i[k]}+1}} \sum_{q=0}^{l_{e_i[k]}} \frac{\left[\left(\frac{1}{a_{e_i[k]}} - s\right)x\right]^q}{q!} \\ &= \frac{\Gamma\left(1 + l_{e_i[k]}, \left(\frac{1}{a_{e_i[k]}} - s\right)x\right)}{l_{e_i[k]}!(1 - a_{e_i[k]} s)^{1+l_{e_i[k]}}} \end{aligned} \tag{4.14}$$

and

$$\begin{aligned}F_{e_i[k]}(x) &= \int_0^{x} g(\gamma; l_{e_i[k]}, a_{e_i[k]}) d\gamma \\ &= 1 - \phi_{e_i[k]}(0; x) \\ &= 1 - e^{-\frac{x}{a_{e_i[k]}}} \sum_{q=0}^{l_{e_i[k]}} \frac{x^q}{q! a_{e_i[k]}{}^q} \\ &= \frac{\gamma\left(1 + l_{e_i[k]}, \frac{x}{a_{e_i[k]}}\right)}{l_{e_i[k]}!} \end{aligned} \tag{4.15}$$

where $\Gamma(\alpha,x)$ and $\gamma(\alpha,x)$ are incomplete Gamma functions given by [6, eq. (8.352.1)] and [6, eq. (8.352.2)], respectively.

Substituting (4.14), (4.15) and (4.12) into (3.35), an approximate average SER of coherent MPSK in arbitrarily correlated Nakagami-m fading for positive integer values of m is obtained as

$$
\begin{aligned}
P_e &= \frac{|W|^m}{\prod_{k=1}^{N} p_{k,k}{}^m} \sum_{v_1=0}^{\infty} \sum_{v_2=0}^{\infty} \cdots \sum_{v_{N-1}=0}^{\infty} \binom{v_{N-1}+m-1}{v_{N-1}} \prod_{k=1}^{N-2} \binom{v_k+v_{k+1}+m-1}{v_k} \\
&\times \prod_{k=1}^{N-1} \left(\frac{p_{k,k+1}^2}{p_{k,k}p_{k+1,k+1}} \right)^{v_k} \sum_{e_i \in W_{N,L_c}} \frac{1}{\pi} \int_0^{\Theta} d\theta \int_0^{\infty} g\left(\gamma_{(L_c)}; l_{e_i[L_c]}, a_{e_i[L_c]}\right) e^{-\frac{c_{MPSK}}{\sin^2\theta}\gamma_{(L_c)}} \\
&\times \prod_{k=1}^{L_c-1} \phi_{e_i[k]}\left(-\frac{c_{MPSK}}{\sin^2\theta}; \gamma_{(L_c)}\right) \times \prod_{k=L_c+1}^{N} F_{e_i[k]}(\gamma_{(L_c)}) d\gamma_{(L_c)}. \qquad (4.16)
\end{aligned}
$$

Since $\phi_{e_i[k]}(-c_{MPSK}/\sin^2\theta; \gamma_{(L_c)}) \leq 1$ and $F_{e_i[k]}(\gamma_{(L_c)}) \leq 1$, then the SER in (4.16) satisfies

$$
\begin{aligned}
P_e &\leq \frac{L_c}{\pi}\binom{N}{L_c} \frac{|W|^m}{\prod_{k=1}^{N} p_{k,k}{}^m} \sum_{v_1=0}^{\infty} \sum_{v_2=0}^{\infty} \cdots \sum_{v_{N-1}=0}^{\infty} \binom{v_{N-1}+m-1}{v_{N-1}} \prod_{k=1}^{N-2} \binom{v_k+v_{k+1}+m-1}{v_k} \\
&\times \prod_{k=1}^{N-1} \left(\frac{p_{k,k+1}^2}{p_{k,k}p_{k+1,k+1}} \right)^{v_k}. \qquad (4.17)
\end{aligned}
$$

Empirically, using Matlab, we numerically testified the infinite series $Y = \sum_{v_1=0}^{\infty} \cdots \sum_{v_{N-1}=0}^{\infty} \binom{v_{N-1}+m-1}{v_{N-1}} \times \prod_{k=1}^{N-2} \binom{v_k+v_{k+1}+m-1}{v_k} \prod_{k=1}^{N-1} \left(\frac{p_{k,k+1}^2}{p_{k,k}p_{k+1,k+1}} \right)^{v_k}$ to converge for all tested values of N and correlation models we use. Observe that $p_{k,k+1}^2/(p_{k,k}p_{k+1,k+1}) < 1/2$ $(k = 1, \cdots, N-1)$, which aids the convergence of the infinite series. However, the convergence becomes slow when N is large and/or the values of $p_{k,k+1}^2/(p_{k,k}p_{k+1,k+1})$ $(k = 1, \cdots, N-1)$ are close to 1/2. Then, for larger values of N, the convergence of (4.16) is slow and the computation time of (4.16) is much longer. For the examples in the next section, we truncate each v_k $(k = 1, \cdots, N-1)$ at 10 to achieve a relative error tolerance less than 5%.

4.4.2 SER of T-HS/MRC

Substituting (4.11) into (2.6), the MGF of $\gamma_{T-HS/MRC(L)}$ can be derived as

$$\begin{aligned}\phi_{\gamma_{T-HS/MRC(L)}}(s) &= \mathbb{E}\{e^{s\gamma_{T-HS/MRC(L)}}\} \\ &= \frac{|W|^m}{\prod_{k=1}^{N} p_{k,k}{}^m} \sum_{v_1=0}^{\infty}\sum_{v_2=0}^{\infty}\cdots\sum_{v_{N-1}=0}^{\infty} A \sum_{e_i\in S_N} \\ &\quad \times \int_0^{\infty} g\left(\gamma_{(1)}; l_{e_i[1]}, a_{e_i[1]}\right) e^{s\gamma_{(1)}} d\gamma_{(1)} \cdots \\ &\quad \times \int_{\mu\gamma_{(1)}}^{\gamma_{(L-1)}} g\left(\gamma_{(L)}; l_{e_i[L]}, a_{e_i[L]}\right) e^{s\gamma_{(L)}} d\gamma_{(L)} \\ &\quad \times \int_0^{\mu\gamma_{(1)}} g\left(\gamma_{(L+1)}; l_{e_i[L+1]}, a_{e_i[L+1]}\right) d\gamma_{(L+1)} \cdots \\ &\quad \times \int_0^{\gamma_{(N-1)}} g\left(\gamma_{(N)}; l_{e_i[N]}, a_{e_i[N]}\right) d\gamma_{(N)}. \end{aligned} \tag{4.18}$$

With [34, eqs. (11), (12) and (A. 1)], (4.18) can be further simplified as

$$\begin{aligned}\phi_{\gamma_{T(L)}}(s) &= \frac{|W|^m}{\prod_{k=1}^{N} p_{k,k}{}^m} \sum_{v_1=0}^{\infty}\sum_{v_2=0}^{\infty}\cdots\sum_{v_{N-1}=0}^{\infty} A \sum_{e_i\in T_{N,L}} \int_0^{\infty} g\left(\gamma_{(1)}; l_{e_i[1]}, a_{e_i[1]}\right) e^{s\gamma_{(1)}} \\ &\quad \times \prod_{k=2}^{L}\left[\phi_{e_i[k]}(s,\mu\gamma_{(1)}) - \phi_{e_i[k]}(s,\gamma_{(1)})\right] \times \prod_{k=L+1}^{N} F_{e_i[k]}(\mu\gamma_{(1)}) d\gamma_{(1)} \end{aligned} \tag{4.19}$$

where $T_{N,L}$ is a subset of S_N, whose element e_i satisfies $e_i[2] < e_i[3] < \cdots < e_i[L]$ and $e_i[L+1] < e_i[L+2] < \cdots < e_i[N]$, as defined previously. $\phi_{e_i[k]}(s,x)$ and $F_{e_i[k]}(x)$ were given respectively by (4.14) and (4.15).

Substituting (4.14), (4.15) and (4.19) into (2.3) and (2.2), the average SER of coherent MPSK using T-HS/MRC in correlated Nakagami-m fading, is given by

$$\begin{aligned}P_e &= \frac{|W|^m}{\pi\prod_{k=1}^{N} p_{k,k}{}^m} \sum_{v_1=0}^{\infty}\sum_{v_2=0}^{\infty}\cdots\sum_{v_{N-1}=0}^{\infty} A \sum_{e_i\in T_{N,L}} \sum_{L=1}^{N} \int_0^{\Theta} d\theta \\ &\quad \times \int_0^{\infty} g\left(\gamma_{(1)}; l_{e_i[1]}, a_{e_i[1]}\right) e^{-\frac{c_{MPSK}}{\sin^2\theta}\gamma_{(1)}} \times \prod_{k=L+1}^{N} F_{e_i[k]}(\mu\gamma_{(1)}) \\ &\quad \times \prod_{k=2}^{L}\left[\phi_{e_i[k]}\left(-\frac{c_{MPSK}}{\sin^2\theta}, \mu\gamma_{(1)}\right) - \phi_{e_i[k]}\left(-\frac{c_{MPSK}}{\sin^2\theta}, \gamma_{(1)}\right)\right] d\gamma_{(1)} \end{aligned} \tag{4.20}$$

where $c_{MPSK} = \sin^2(\pi/M)$, and $\Theta = \pi(M-1)/M$, as defined previously. When the inverse of the covariance matrix is tridiagonal, (4.20) gives the exact average SER of coherent MPSK with T-HS/MRC in correlated Nakagami-m fading.

4.5 Numerical Results

In this section, some examples of the average SERs of coherent MPSK with H-S/MRC and T-HS/MRC in Nakagami-m fading with positive integer values of m are given. The accuracy of the SER analyses of H-S/MRC and T-HS/MRC using the Green's matrix approximation is also examined. In the following examples, we truncate each v_k $(k = 1, \cdots, N-1)$ at 10 to achieve a relative error tolerance less than 5%.

Fig. 4.1 shows the average SER versus the average branch SNR, Γ, of a coherent QPSK system with H-S/MRC in correlated Nakagami-m fading with $N = 3$ and fading parameter $m = 2$. The linearly arbitrary model, Σ_{3_lin} and the corresponding approximate matrix C_{3_lin} in [66] are used. Different values of the number of the selected diversity branches, L_c, are considered. The dashed curves denote exact average SERs obtained using Monte Carlo simulation. One can see that the approximate SERs using Green's matrix are very close to the simulation results.

$$\Sigma_{3_{\text{lin}}} = \begin{bmatrix} 1.000 & 0.795 & 0.605 \\ 0.795 & 1.000 & 0.795 \\ 0.605 & 0.795 & 1.000 \end{bmatrix}$$

$$C_{3_{\text{lin}}} = \begin{bmatrix} 1.000 & 0.786 & 0.617 \\ 0.786 & 1.000 & 0.786 \\ 0.617 & 0.786 & 1.000 \end{bmatrix}$$

Fig. 4.2 shows the average SER versus the average branch SNR, Γ, of a coherent QPSK system with H-S/MRC in correlated Rayleigh fading with $N = 4$. The linearly arbitrary model, Σ_{4_lin} in [66] ($\Sigma_{4\_\text{lin}}(3,1)$ should be 0.617 instead of 0.620.), is considered here. The dashed curves denote the exact average SER obtained using Monte Carlo simulation. One can see that the approximate SERs obtained using Green's matrix are close to the simulation results. For example, when $L_c = 3$ and $\Gamma = 6$ dB, the difference between the

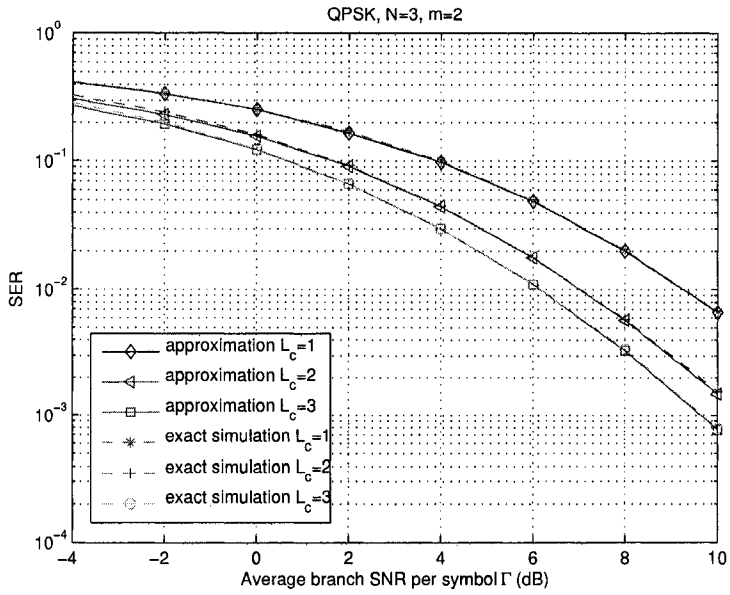

Fig. 4.1. The approximate average SER versus the average branch SNR Γ of coherent QPSK with H-S/MRC in a linearly arbitrary model with the number of diversity branches $N = 3$ and Nakagami-m fading parameter $m = 2$.

approximate SER and the exact SER is about 0.22 dB.

$$\sum_{4_{\text{lin}}} = \begin{bmatrix} 1.000 & 0.786 & 0.617 & 0.450 \\ 0.786 & 1.000 & 0.750 & 0.620 \\ 0.617 & 0.750 & 1.000 & 0.750 \\ 0.450 & 0.620 & 0.750 & 1.000 \end{bmatrix}$$

$$C_{4_{\text{lin}}} = \begin{bmatrix} 1.000 & 0.700 & 0.538 & 0.377 \\ 0.700 & 1.000 & 0.769 & 0.538 \\ 0.538 & 0.769 & 1.000 & 0.700 \\ 0.377 & 0.538 & 0.700 & 1.000 \end{bmatrix}$$

Fig. 4.3 shows the average SER versus the average branch SNR, Γ, of a coherent QPSK system with H-S/MRC in correlated Rayleigh fading with $N = 5$. The linearly

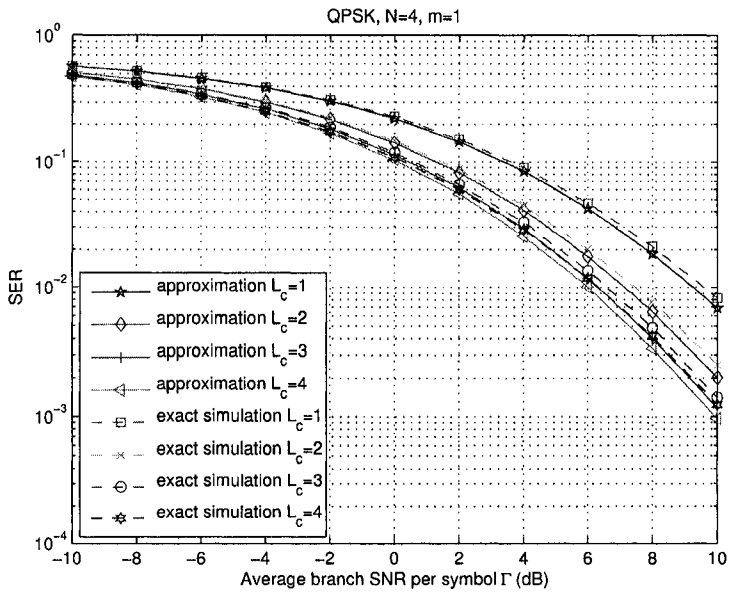

Fig. 4.2. The approximate average SER versus the average branch SNR Γ of coherent QPSK with H-S/MRC in Rayleigh fading with the linearly arbitrary model when the number of diversity branches $N = 4$.

arbitrary model, R_r in [70, eq. (40)], is considered here. We approximate R_r with C_{R_r} as given below. The dashed curves denote the exact average SER obtained using Monte Carlo simulation. One can see that the approximate SERs obtained using the Green's matrix are close to the simulation results with the discrepancies being less than 0.48 dB in SNR. For example, when $L_c = 2$ and $\Gamma = 8$ dB, the difference between the approximate SER and the exact SER is about 0.28 dB.

$$\sum_{R_r} = \begin{bmatrix} 1.000 & 0.795 & 0.605 & 0.375 & 0.283 \\ 0.795 & 1.000 & 0.795 & 0.605 & 0.375 \\ 0.605 & 0.795 & 1.000 & 0.795 & 0.605 \\ 0.375 & 0.605 & 0.795 & 1.000 & 0.795 \\ 0.283 & 0.375 & 0.605 & 0.795 & 1.000 \end{bmatrix}$$

$$C_{R_r} = \begin{bmatrix} 1.000 & 0.764 & 0.587 & 0.434 & 0.318 \\ 0.764 & 1.000 & 0.769 & 0.568 & 0.417 \\ 0.587 & 0.769 & 1.000 & 0.740 & 0.542 \\ 0.434 & 0.568 & 0.740 & 1.000 & 0.733 \\ 0.318 & 0.417 & 0.542 & 0.733 & 1.000 \end{bmatrix}$$

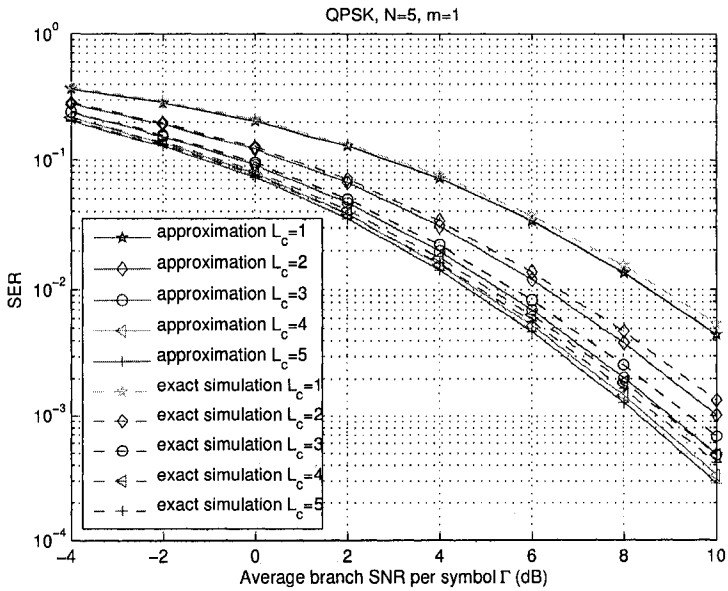

Fig. 4.3. The approximate average SER versus the average branch SNR Γ of coherent QPSK with H-S/MRC in Rayleigh fading with the linearly arbitrary model when the number of diversity branches $N = 5$.

Similar observations can also be drawn from Fig. 4.4, which shows the average SER versus the average branch SNR, Γ, of a coherent QPSK system with H-S/MRC in Nakagami fading with $N = 4$ and $L_c = 2$ for different values of fading parameter m. The constant model Σ_{4_con} and the corresponding approximate matrix C_{4_con} in [66] are considered here. The dashed curves denote exact average SERs obtained using Monte Carlo simulation. When $\Gamma = 8$ dB and $m = 1$, the difference between the approximate SER and the exact SER computed with the constant model is less than 0.24 dB. In addition, for the larger

values of average branch SNR, the approximation with $m = 2$ and $m = 3$ is better than the approximation with $m = 1$, namely, Rayleigh fading. Therefore, the approximate analysis with Green's matrix can be used to effectively evaluate H-S/MRC in arbitrarily correlated Nakagami-m fading for positive integer values of m.

$$\sum_{4_{con}} = \begin{bmatrix} 1.000 & 0.500 & 0.500 & 0.500 \\ 0.500 & 1.000 & 0.500 & 0.500 \\ 0.500 & 0.500 & 1.000 & 0.500 \\ 0.500 & 0.500 & 0.500 & 1.000 \end{bmatrix}$$

$$C_{4_{con}} = \begin{bmatrix} 1.000 & 0.641 & 0.434 & 0.278 \\ 0.641 & 1.000 & 0.676 & 0.434 \\ 0.434 & 0.676 & 1.000 & 0.641 \\ 0.278 & 0.434 & 0.641 & 1.000 \end{bmatrix}$$

Fig. 4.5 shows the exact average SER versus the average branch SNR, Γ, of a coherent QPSK system using T-HS/MRC with $N = 3$ in exponentially correlated Nakagami-m fading with fading parameter $m = 2$ and correlation coefficient $\rho = 0.5$. The exponential model, whose inverse of covariance matrix is tridiagonal, is given in [66]. Different values of normalized threshold, μ, are considered. The diamonds denote the average SERs obtained using Monte Carlo simulation. As a special case of T-HS/MRC, MRC and SC corresponds to μ =0.0 and 1.0 respectively. From Fig. 4.5, one can see that our analytical results are in excellent agreement with the simulation results. The performance of T-HS/MRC degrades with increasing μ as expected.

To examine the accuracy of the approximate analysis of T-HS/MRC in arbitrarily correlated Nakagami-m fading, Fig. 4.6 shows the average SER versus the average branch SNR, Γ, of a coherent QPSK system using T-HS/MRC in a linearly arbitrary Nakagami-m correlation model with fading parameter $m = 2$ and $N = 3$. The linearly arbitrary model $\sum_{3\_lin}$ used in Fig. 4.1 is considered here. Different values of normalized threshold μ are considered. The dashed curves with diamonds denote the exact average SERs obtained

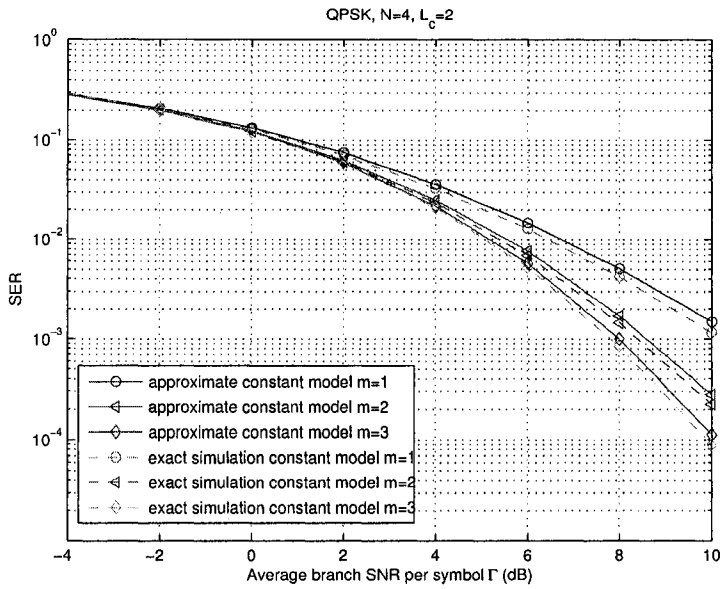

Fig. 4.4. The approximate average SER versus the average branch SNR Γ of coherent QPSK with H-S/MRC in Nakagami fading with fading parameter $m = 1$, 2 and 3, and the number of diversity branches $N = 4$ for the constant model.

using Monte Carlo simulation. One can see that the approximate SERs using the Green's matrix are very close to the simulation results.

Fig. 4.7 shows the average SER versus the average branch SNR, Γ, of a coherent QPSK system using T-HS/MRC in correlated Nakagami fading with the number of diversity branches $N = 4$ for different values of Nakagami fading parameter m. The constant model, Σ_{4_con}, and the circular model, Σ_{4_circ} in [66], are considered. The dashed curves denote the exact average SERs obtained using Monte Carlo simulation. It is seen that the approximate SERs calculated using Green's matrix are close to the simulation results. For example, when $\Gamma = 14$ dB and $m = 1$, the difference between the approximate SER and the exact SER for the two models is less than 0.45 dB in SNR. The approximation accuracy is affected by the approximation accuracy of the closest possible Green's matrix and the values of fading parameter m. Further, this apparent greatest discrepancy occurs for $m = 1$. When $m = 2$ and 3, much better accuracy is achieved for both of the two models

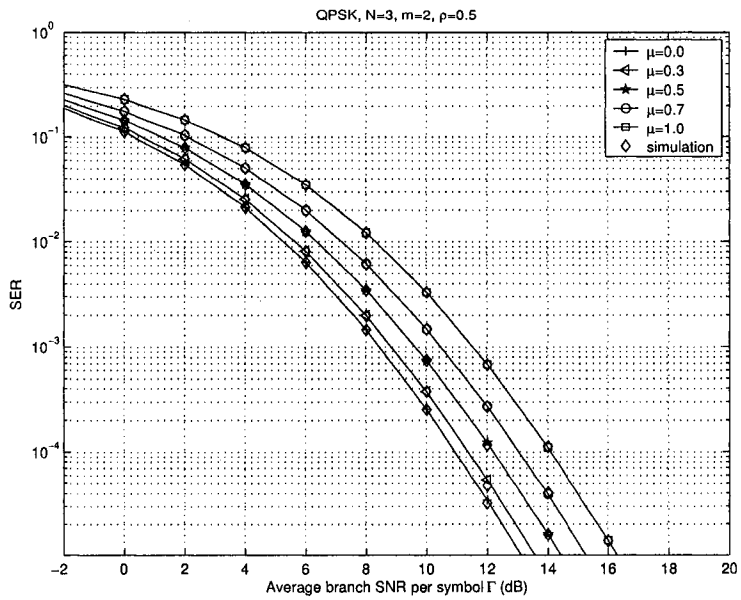

Fig. 4.5. The average SER versus the average branch SNR Γ of coherent QPSK using T-HS/MRC with the number of diversity branches $N = 3$, Nakagami-m fading parameter $m = 2$, exponential correlation coefficient $\rho = 0.5$, and normalized threshold μ =0.0, 0.3, 0.5, 0.7 and 1.0.

as observed in Fig. 4.4. Therefore, this approximation method using the Green's matrix is effective in evaluating the performance of T-HS/MRC with diversity branches having arbitrary Nakagami-m correlations.

$$\Sigma_{4_{\text{circ}}} = \begin{bmatrix} 1.000 & 0.700 & 0.500 & 0.700 \\ 0.700 & 1.000 & 0.700 & 0.500 \\ 0.500 & 0.700 & 1.000 & 0.700 \\ 0.700 & 0.500 & 0.700 & 1.000 \end{bmatrix}$$

$$C_{4_{\text{circ}}} = \begin{bmatrix} 1.000 & 0.786 & 0.572 & 0.453 \\ 0.786 & 1.000 & 0.732 & 0.576 \\ 0.572 & 0.732 & 1.000 & 0.786 \\ 0.453 & 0.576 & 0.786 & 1.000 \end{bmatrix}$$

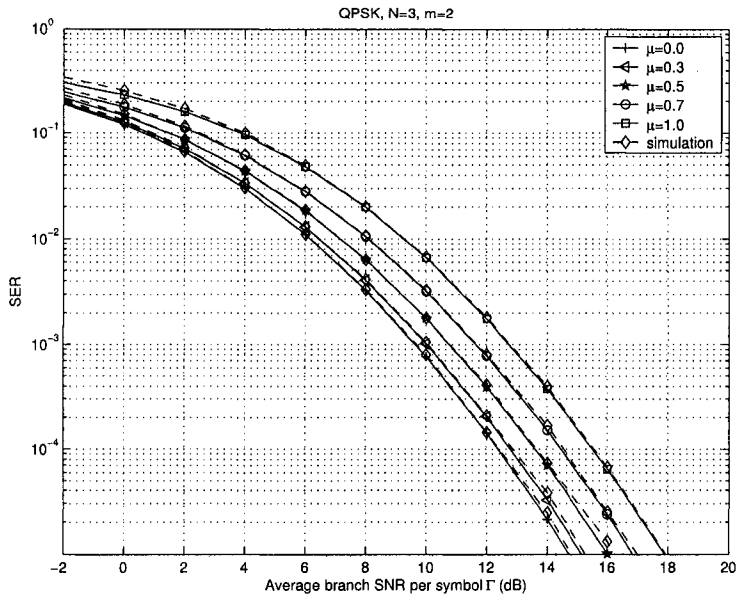

Fig. 4.6. The approximate average SER versus the average branch SNR Γ of coherent QPSK using T-HS/MRC in a linearly arbitrary model with the number of diversity branches $N = 3$, Nakagami-m fading parameter $m = 2$, and normalized threshold μ =0.0, 0.3, 0.5, 0.7 and 1.0.

4.6 Summary

In this chapter, an efficient approximate symbol error rate analysis of H-S/MRC and T-HS/MRC in arbitrarily correlated Nakagami-m fading channels with positive integer values of fading parameter m was developed using a Green's matrix approximation. This method is suitable for arbitrary number of branches and accommodates various linear modulation schemes.

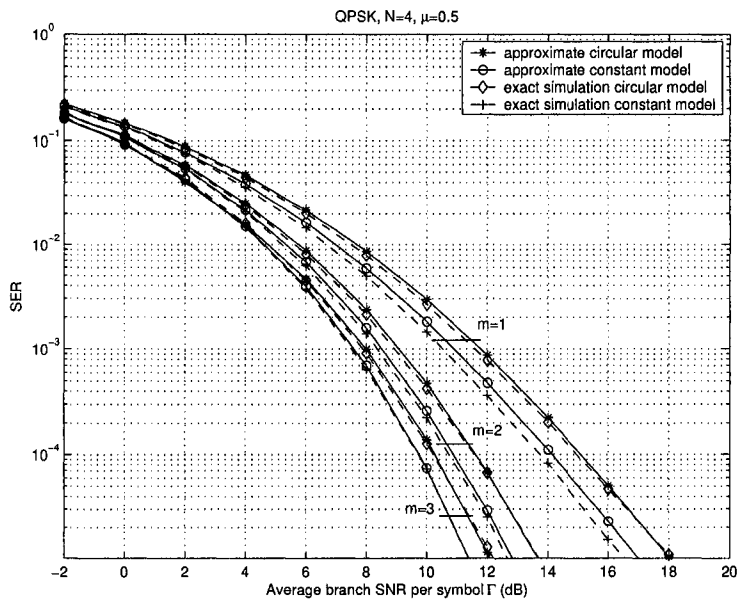

Fig. 4.7. The approximate average SER versus the average branch SNR Γ of coherent QPSK using T-HS/MRC in Nakagami fading with fading parameter $m = 1$, 2 and 3, the number of diversity branches $N = 4$, and normalized threshold $\mu = 0.5$ for the constant model and circular model.

Chapter 5

Outage and Error Rate of MRC Cellular Systems in Multiple Interferers and Correlated Rayleigh Fading

5.1 Introduction

In wireless cellular systems, data transmission is mainly limited by fading and cochannel interference. Fading is due to multipath propagation and cochannel interference is due to frequency reuse in different cells. There are several techniques proposed to mitigate the effects of fading and CCI, and improve the system performance. Among them, diversity reception using multiple antennas at the receiver has been recognized as an effective method. When the noise is additive white Gaussian, MRC is an optimal combining scheme that maximizes the output SNR by coherently combining all of the branch signals [22]. However, this combining scheme is suboptimal when non-Gaussian interference is present, such as CCI [71]. Therefore, it is of interest to analyze the performance of MRC diversity systems in the presence of fading and CCI.

In the literature, the outage probabilities of cellular systems using SC, EGC and switched diversity (SW) with CCI in independent Nakagami fading were analyzed in [72]. The out-

age probability of MRC in CCI for the case of independent fading diversity branches has been extensively studied in [73–77]. However, in practice, there often exist applications where fading correlation has significant impact on the system performance and cannot be ignored. In this area, a performance analysis assuming that either only the desired user diversity branch signals, or only the interfering diversity branch signals experience correlated fading was presented in [78]. Recently, dual-branch MRC in a CCI-limited environment where both the desired user signal and the interfering user signals experience correlated Rayleigh fading was considered in [79]. Based on [79] and using a joint characteristic function method, more general results for an arbitrary number of antennas with equal-power cochannel interferers and unequal-power cochannel interferers were given in [80] and [81], respectively. However, these results ignore the effect of noise and only apply for CCI-limited environments. Moreover, only outage probability is considered in [79–81].

The average error rate of digital modulations in fading and CCI is another important performance measure of cellular systems. In [82], approximations for the average BER of both coherent BPSK and noncoherent binary frequency-shift keying (BFSK) in an interference-limited system were derived for i.i.d. Nakagami interferers. Exact solutions for the average BER of a single branch receiver system with CCI in Nakagami-m fading were given in [83]. The performance of diversity receiver systems with CCI in independent Nakagami fading was studied in [84, 85]. The average BER of coherent BPSK and binary differential phase-shift keying (DPSK) in correlated Ricean fading channels with multiple cochannel interferers was studied by expressing the decision variables as Gaussian quadratic forms and using the MGF approach in [86]. However, the BER calculation requires recursively finding the saddle points and no explicit closed-from BER expression was given for the case of Rayleigh fading. Different from the method used in [86], in our work, an exact and closed-form BER expression for coherent BPSK in correlated Rayleigh fading and cochannel interferers is provided [87].

All of the above-mentioned works assume perfect channel estimation for MRC diversity systems. However, in practical systems, the branch gains estimated at the receiver are often imperfect, which degrades the system performance. The performance of MRC

with channel estimation error in noise-limited environments has been extensively analyzed in [88–93]. The effect of interference was taken into account in [94], where a multicarrier code-division multiple-access (MC-CDMA) BPSK system is studied. In [95], the outage probability of MRC with Gaussian channel estimation error in independent Rayleigh fading and equal-power interferers was considered. Their result was extended to the case of unequal-power cochannel interferers in [96]. Here, we investigate the effect of imperfect channel estimation on the BER performance when the branch gains of the desired user signal and interfering signals experience correlated Rayleigh fading.

In this chapter, the outage probability of MRC diversity with an arbitrary number of branches is presented when the branch gains of the desired user signal and interfering signals experience correlated Rayleigh fading and have the same correlation matrix. Two cases, when the correlation matrix is equi-correlated and when the correlation matrix has different eigenvalues, are considered. Equi-correlation corresponds to the situation of closely packed and symmetrically placed diversity antennas [39]. The correlation matrix with different eigenvalues includes more general correlation models, such as the model used in [18] with different correlation eigenvalues, exponential correlation with different correlation eigenvalues, etc.. On the other hand, closed-form BER expressions of a coherent BPSK system using MRC with CCI in correlated Rayleigh fading are derived. Further, the effect of imperfect channel estimation on the BER performance in correlated Rayleigh fading and CCI is investigated where a special channel estimator is applied.

The remainder of this chapter is organized as follows. The system model is described in Section 5.2. In Section 5.3, the outage probability of the MRC combiner output is presented. The average BER of coherent BPSK using MRC with perfect channel estimation is analyzed in Section 5.4. The effect of imperfect channel estimation on the error rate of BPSK using MRC in CCI and correlated Rayleigh fading is examined in Section 5.5. Finally, we give our conclusions in Section 5.6.

5.2 System Model

Assume that a receiver with an N-element antenna array operates in N_I cochannel interfering users [79]. Further, assume that the desired user signal and the interfering user signals are independent and experience slow and flat Rayleigh fading. However, the fadings for each user at the N receiver antennas are assumed correlated with the same correlation coefficient matrix. Then the received signal vector consists of components from the desired user and the N_I interfering users, and is given by [3, eq. (11.1)], [96]

$$\mathbf{r} = \sqrt{P_0}\mathbf{c_0}d_0 + \sum_{n=1}^{N_I} \sqrt{P_n}\mathbf{c_n}d_n + \mathbf{z_0} \tag{5.1}$$

where P_0 and P_n $(n = 1, \cdots, N_I)$ represent the powers of the desired user and the nth interfering user, respectively. The powers of the N_I interfering users may not be equal. The symbols d_0 and d_n $(n = 1, \cdots, N_I)$, denote the information bits of the desired user signal and the nth interfering user signal, respectively, and have zero mean and unit variance. The normalized circularly complex Gaussian vectors $\mathbf{c_0}$ and $\mathbf{c_n}$ $(n = 1, \cdots, N_I)$ represent the channel gains experiencing Rayleigh fading for the desired user and the nth interfering user, respectively. Further, the fadings for each user are assumed correlated with the same covariance matrix $\mathbb{E}(\mathbf{c_n}\mathbf{c_n}^H) = \sum (n = 0, \cdots, N_I)$, where $[A]^H$ denotes the transpose and conjugate of matrix A. The noise vector $\mathbf{z_0}$ is complex white (both temporally and spatially) Gaussian with zero mean and variance matrix $N_0 I$, where I is the identity matrix. Then the output of a MRC combiner with weighting vector $\mathbf{w_0}$ is given by

$$r = \mathbf{w_0}^H\mathbf{r} = \sqrt{P_0}(\mathbf{w_0}^H\mathbf{c_0})d_0 + \sum_{n=1}^{N_I} \sqrt{P_n}(\mathbf{w_0}^H\mathbf{c_n})d_n + (\mathbf{w_0}^H\mathbf{z_0}). \tag{5.2}$$

When the channel estimation is perfect, namely, $\mathbf{w_0} = \mathbf{c_0}$, (5.2) becomes

$$r = \mathbf{c_0}^H\mathbf{r} = \sqrt{P_0}(\mathbf{c_0}^H\mathbf{c_0})d_0 + \sum_{n=1}^{N_I} \sqrt{P_n}(\mathbf{c_0}^H\mathbf{c_n})d_n + (\mathbf{c_0}^H\mathbf{z_0}). \tag{5.3}$$

The interference plus noise covariance of the MRC output conditioned on the fading gains is given by [3]

$$\sum_{IN} = \mathbb{E}\left\{ \left(\sum_{n=1}^{N_I} \sqrt{P_n}(\mathbf{c_0}^H\mathbf{c_n})d_n + (\mathbf{c_0}^H\mathbf{z_0}) \right) \left(\sum_{n=1}^{N_I} \sqrt{P_n}(\mathbf{c_0}^H\mathbf{c_n})d_n + (\mathbf{c_0}^H\mathbf{z_0}) \right)^H \right\}. \tag{5.4}$$

The instantaneous output signal-to-interference-plus-noise ratio (SINR) after the MRC combiner, γ_{SINR}, is defined as the ratio of the signal power to the interference plus noise covariance conditioned on fading gains $\mathbf{c_n}$ $(n = 0, 1, \cdots, N_I)$ given by [3,73,79]

$$\gamma_{SINR} = \frac{|\sqrt{P_0}(\mathbf{c_0}^H \mathbf{c_0}) d_0|^2}{\sum_{IN}}. \tag{5.5}$$

Since the information bits of the users are assumed independent with zero mean and unit variance, and are independent of noise, (5.4) becomes

$$\begin{aligned}
\sum_{IN} &= \mathbb{E}\left\{ \sum_{n=1}^{N_I} P_n |\mathbf{c_0}^H \mathbf{c_n}|^2 |d_n|^2 + \sum_{n=1}^{N_I} \sum_{q=1, q\neq n}^{N_I} \sqrt{P_n P_q} d_n d_q^H \mathbf{c_0}^H \mathbf{c_n} \mathbf{c_q}^H \mathbf{c_0} + \right. \\
&\quad \left(\sum_{n=1}^{N_I} \sqrt{P_n} (\mathbf{c_0}^H \mathbf{c_n}) d_n \right)^H (\mathbf{c_0}^H \mathbf{z_0}) + \left(\sum_{n=1}^{N_I} \sqrt{P_n} (\mathbf{c_0}^H \mathbf{c_n}) d_n \right) (\mathbf{c_0}^H \mathbf{z_0})^H \\
&\quad \left. + \mathbf{c_0}^H \mathbf{z_0} \mathbf{z_0}^H \mathbf{c_0} \right\} \\
&= \sum_{n=1}^{N_I} P_n |\mathbf{c_0}^H \mathbf{c_n}|^2 + N_0 (\mathbf{c_0}^H \mathbf{c_0})
\end{aligned} \tag{5.6}$$

where the terms $\mathbb{E}\{\sqrt{P_n P_q} d_n d_q^H \mathbf{c_0}^H \mathbf{c_n} \mathbf{c_q}^H \mathbf{c_0}\} = 0$ for $n \neq q$, $\mathbb{E}\{\sqrt{P_n}(\mathbf{c_0}^H \mathbf{c_n}) d_n (\mathbf{c_0}^H \mathbf{z_0})^H\} = 0$, and $\mathbb{E}\{\sqrt{P_n}(\mathbf{c_n}^H \mathbf{c_0}) d_n^H (\mathbf{c_0}^H \mathbf{z_0})\} = 0$.

Substituting (5.6) into (5.5), the instantaneous SINR becomes

$$\gamma_{SINR} = \frac{P_0 |\mathbf{c_0}^H \mathbf{c_0}|^2}{\sum_{n=1}^{N_I} P_n |\mathbf{c_0}^H \mathbf{c_n}|^2 + N_0 (\mathbf{c_0}^H \mathbf{c_0})}. \tag{5.7}$$

5.3 Outage Probability

Then the outage probability of the SINR, γ_{SINR}, is defined by [3]

$$F_{\gamma_{SINR}}(\gamma_{th}) = \Pr(\gamma_{SINR} \leq \gamma_{th}), \qquad \gamma_{th} > 0 \tag{5.8}$$

where γ_{th} is the output SINR threshold. Substituting (5.7) into (5.8) and combining with $\mathbf{c_0}^H \sum \mathbf{c_0} > 0$, one obtains

$$\begin{aligned}
F_{\gamma_{SINR}}(\gamma_{th}) &= \Pr\left(\frac{P_0 |\mathbf{c_0}^H \mathbf{c_0}|^2}{\sum_{n=1}^{N_I} P_n |\mathbf{c_0}^H \mathbf{c_n}|^2 + N_0 (\mathbf{c_0}^H \mathbf{c_0})} \leq \gamma_{th} \right) \\
&= \Pr\left(\frac{\frac{P_0}{\gamma_{th}} |\mathbf{c_0}^H \mathbf{c_0}|^2 - N_0 (\mathbf{c_0}^H \mathbf{c_0})}{\mathbf{c_0}^H \sum \mathbf{c_0}} \leq K \right)
\end{aligned} \tag{5.9}$$

where

$$K = \sum_{n=1}^{N_I} P_n \left| \frac{(\mathbf{c_0}^H \mathbf{c_n})}{\sqrt{\mathbf{c_0}^H \sum \mathbf{c_0}}} \right|^2 . \tag{5.10}$$

Since $\mathbf{c_n}$ $(n = 0, 1, \cdots, N_I)$ are independent zero-mean complex Gaussian random vectors, conditioned on $\mathbf{c_0}$, the random variable $(\mathbf{c_0}^H \mathbf{c_n})/\sqrt{\mathbf{c_0}^H \sum \mathbf{c_0}}$ is complex Gaussian with zero mean and unit variance, and hence is independent of the fading vector $\mathbf{c_0}$. Therefore, the summation of the squares of these RVs, K, is independent of $\mathbf{c_0}$ [79]. Assume that the N_I interferers can be divided into p groups, each of them having the same power P_n and $\sum_{n=1}^{p} t_n = N_I$. Then the PDF of K can be represented by [77, eqs. (13), (14)]

$$f_K(k) = \sum_{n=1}^{p} \sum_{l_n=1}^{t_n} \frac{\alpha_{nl_n}}{(l_n - 1)!} \frac{k^{l_n - 1} e^{-k/P_n}}{{P_n}^{l_n}}, \qquad k \geq 0 \tag{5.11}$$

where t_n denotes the number of interfering users with the same power P_n, and α_{nl_n} is given by

$$\alpha_{nl_n} = (-1)^{t_n + l_n} \sum_{\tau(n,l_n)} \prod_{i=1, i \neq n}^{p} \frac{C_{t_i+q_i-1}^{q_i} \left(\frac{P_i}{P_n}\right)^{q_i}}{\left(1 - \frac{P_i}{P_n}\right)^{t_i+q_i}} \tag{5.12}$$

where $C_n^{l_n} = n!/(l_n!(n - l_n)!)$ and $\tau(n, l_n)$ denotes a set of p-tuples such that $\tau(n, l_n) = \{(q_1, \cdots, q_p) : q_i \in \mathbb{N}_0,\ q_n = 0, \sum_{i=1}^{p} q_i = t_n - l_n\}$, with $\mathbb{N}_0$ signifying the set of nonnegative integers [77].

Let Λ denote a diagonal matrix composed of the eigenvalues of the correlation matrix $\sum$, λ_i $(i = 1, \cdots, N)$ such that $\sum = U \Lambda U^H$, where U is the corresponding eigenvector matrix with $U^H U = U U^H = I$. Further, let $u = \mathbf{v}^H \Lambda \mathbf{v}$, and $w = \mathbf{v}^H \Lambda^2 \mathbf{v}$, where $\mathbf{v} = \Lambda^{-1/2} U^H \mathbf{c_0}$ is a $N \times 1$ complex Gaussian vector with zero mean and unit variance matrix I. Then (5.9) can be rewritten as

$$\begin{aligned} F_{\gamma_{SINR}}(\gamma_{th}) &= \Pr\left(\frac{\frac{P_0}{\gamma_{th}} u^2 - N_0 u}{w} \leq K \right) \\ &= \Pr\left(w \geq \frac{P_0}{K \gamma_{th}} u^2 - \frac{N_0}{K} u \right). \end{aligned} \tag{5.13}$$

Since K is independent of $\mathbf{c_0}$, and hence independent of $\mathbf{v}$, the CDF of the SINR, γ_{SINR}, conditioned on K can be expressed as

$$F_{\gamma_{SINR}|K}(\gamma_{th}|k) = \Pr\left(w \geq \frac{P_0}{k \gamma_{th}} u^2 - \frac{N_0}{k} u | k \right). \tag{5.14}$$

If the conditional CDF in (5.14) is known, the outage probability of SINR can be obtained by averaging (5.14) over K.

5.3.1 Joint PDF of u and w

Note that due to the fading correlation, the random variables u and w are correlated. To obtain the conditional outage probability given in (5.14), one has to get the joint PDF of u and w first. Since $u = \sum_{i=1}^{N} \lambda_i |v_i|^2$, and $w = \sum_{i=1}^{N} \lambda_i{}^2 |v_i|^2$, where $2|v_i|^2$ $(i = 1, \cdots, N)$ are i.i.d. chi-square distributed with two degrees of freedom [79], the joint CF of u and w is given by [35]

$$\begin{aligned} \phi_{u,w}(j\omega_1, j\omega_2) &= \mathbb{E}\left\{e^{j\omega_1 u + j\omega_2 w}\right\} \\ &= \mathbb{E}\left\{e^{\sum_{i=1}^{N}(j\omega_1\lambda_i + j\omega_2\lambda_i^2)|v_i|^2}\right\} \\ &= \prod_{i=1}^{N} \mathbb{E}_{v_i}\left\{e^{(j\omega_1\lambda_i + j\omega_2\lambda_i^2)|v_i|^2}\right\} \\ &= \prod_{i=1}^{N} \frac{1}{1 - j\lambda_i\omega_1 - j\lambda_i^2\omega_2}. \end{aligned} \tag{5.15}$$

According to the relation between the CF and the Fourier transform, one has $\phi_x(-j\omega) = \mathbb{F}(x)$, where $\phi_x(j\omega)$ denotes the CF of x, and $\mathbb{F}(x)$ denotes taking Fourier transform on x [35]. Then, the joint PDF of u and w can be derived by taking the two-dimensional inverse Fourier transform on $\phi_{u,w}(-j\omega_1, -j\omega_2)$ [97]. In the following, the joint PDF of u and w will be considered for the case that the correlation matrix has different eigenvalues and the case that the correlation matrix is equi-correlated, respectively.

Case I: Correlation Matrix With Different Eigenvalues

Assume all of the eigenvalues λ_i are not equal, and satisfy $\lambda_1 > \lambda_2 > \cdots > \lambda_N > 0$. Then, the joint PDF of u and w can be derived by taking the two-dimensional inverse Fourier

transform on $\phi_{u,w}(-j\omega_1, -j\omega_2)$ resulting in

$$f_{u,w}(u,w) = \sum_{i,j\in\{1,\cdots,N\},\, i<j} \frac{(\lambda_i\lambda_j)^{N-3} e^{-\left(\frac{1}{\lambda_i}+\frac{1}{\lambda_j}\right)u+\frac{w}{\lambda_i\lambda_j}}}{(\lambda_i-\lambda_j)\prod_{l=1,\, l\neq i,j}^{N}(\lambda_i-\lambda_l)(\lambda_j-\lambda_l)} \times \left[U(\lambda_i u-w) - U(\lambda_j u-w) + \delta(\lambda_j u-w)\right], \quad u \geq 0 \tag{5.16}$$

where $\delta(x)$ is the Kronecker delta function, and $U(x)$ is defined by

$$U(x) = \begin{cases} 1, & x \geq 0 \\ 0, & x < 0. \end{cases}$$

The detailed derivation from (5.15) to (5.16) is given in Appendix C.

Case II: Equi-Correlated Correlation Matrix

When all of the users experience equi-correlated Rayleigh fading with correlation coefficient ρ $(0 < \rho < 1)$, the elements of correlation matrix satisfy $\Sigma_{i,j} = \rho$ $(i, j = 1, \cdots N,\ i \neq j)$ and $\Sigma_{i,i} = 1$ $(i = 1, \cdots, N)$. Since the eigenvalues of matrix Σ are $\lambda_1 = 1 + (N-1)\rho$ and $\lambda_i = 1 - \rho$ $(i = 2, \cdots, N)$ [3, eq.(9.172)], (5.15) becomes

$$\phi_{u,w}(j\omega_1, j\omega_2) = \frac{1}{(1 - j\lambda_1\omega_1 - j\lambda_1^2\omega_2)} \times \frac{1}{(1 - j\lambda_2\omega_1 - j\lambda_2^2\omega_2)^{N-1}}. \tag{5.17}$$

According to the definitions of the two-dimensional Fourier transform and two-dimensional convolution [97], for $N \geq 2$, we have

$$\mathbb{F}\left\{\frac{u^{N-2}e^{-\frac{1}{\lambda}u}\delta(w-\lambda u)}{(N-2)!\lambda^{N-1}}\right\} = \frac{1}{(1 + j\lambda\omega_1 + j\lambda^2\omega_2)^{N-1}}, \qquad u \geq 0. \tag{5.18}$$

Taking the two-dimensional inverse Fourier transform of $\phi_{u,w}(-j\omega_1, -j\omega_2)$ given in (5.17) and combining with (5.18) and (C.3), the joint PDF of u and w in equi-correlated Rayleigh fading is derived as

$$f(u,w) = \frac{(\lambda_1 u - w)^{N-2} e^{\frac{w}{\lambda_1\lambda_2} - \left(\frac{1}{\lambda_1}+\frac{1}{\lambda_2}\right)u}}{(N-2)!\lambda_1\lambda_2^{N-1}(\lambda_1-\lambda_2)^{N-1}}, \qquad 0 \leq \lambda_2 u \leq w \leq \lambda_1 u. \tag{5.19}$$

In the following, we use the joint PDF of u and w obtained for the case that the correlation matrix has different eigenvalues and for the case that the correlation matrix is equi-correlated to derive the outage probability of MRC in the presence of CCI and correlated Rayleigh fading.

5.3.2 Case I: Correlation Matrix With Different Eigenvalues

When the correlation matrix has different eigenvalues, substituting (5.16) into (5.14) and combining with (C.6) in Appendix C, the conditional CDF of the SINR, γ_{SINR}, can be derived as

$$
\begin{aligned}
F_{\gamma_{SINR}|K}(\gamma_{th}|k) &= \sum_{i,j\in\{1,\cdots,N\},\, i<j} \frac{(\lambda_i\lambda_j)^{N-3}}{(\lambda_i-\lambda_j)\prod_{l=1,\, l\neq i,j}^{N}(\lambda_i-\lambda_l)(\lambda_j-\lambda_l)} \times \\
&\quad \left[\int_0^{\left(\lambda_j+\frac{N_0}{k}\right)\frac{k\gamma_{th}}{P_0}} du \int_{\lambda_j u}^{\lambda_i u} e^{\frac{w}{\lambda_i\lambda_j}-u\left(\frac{1}{\lambda_i}+\frac{1}{\lambda_j}\right)} dw + \right. \\
&\quad \left. \int_{\left(\lambda_j+\frac{N_0}{k}\right)\frac{k\gamma_{th}}{P_0}}^{\left(\lambda_i+\frac{N_0}{k}\right)\frac{k\gamma_{th}}{P_0}} du \int_{\frac{P_0u^2}{k\gamma_{th}}-\frac{N_0u}{k}}^{\lambda_i u} e^{\frac{w}{\lambda_i\lambda_j}-u\left(\frac{1}{\lambda_i}+\frac{1}{\lambda_j}\right)} dw\right] \\
&= \sum_{i,j\in\{1,\cdots,N\},\, i<j} \frac{(\lambda_i\lambda_j)^{N-2}}{\prod_{l=1,\, l\neq i,j}^{N}(\lambda_i-\lambda_l)(\lambda_j-\lambda_l)} - \\
&\quad e^{-k\gamma_{th}/P_0} \sum_{i,j\in\{1,\cdots,N\},\, i<j} \frac{(\lambda_i\lambda_j)^{N-2}\left(\lambda_i e^{-N_0\gamma_{th}/(\lambda_i P_0)} - \lambda_j e^{-N_0\gamma_{th}/(\lambda_j P_0)}\right)}{(\lambda_i-\lambda_j)\prod_{l=1,l\neq i,j}^{N}(\lambda_i-\lambda_l)(\lambda_j-\lambda_l)} \\
&\quad - \sum_{i,j\in\{1,\cdots,N\},\, i<j} \frac{(\lambda_i\lambda_j)^{N-2}}{(\lambda_i-\lambda_j)\prod_{l=1,l\neq i,j}^{N}(\lambda_i-\lambda_l)(\lambda_j-\lambda_l)} \times \\
&\quad \int_{(k\lambda_j+N_0)\gamma_{th}/P_0}^{(k\lambda_i+N_0)\gamma_{th}/P_0} \exp\left(\frac{P_0u^2}{\lambda_i\lambda_j k\gamma_{th}} - u\left(\frac{1}{\lambda_i}+\frac{1}{\lambda_j}+\frac{N_0}{\lambda_i\lambda_j k}\right)\right) du \\
&= 1 - e^{-k\gamma_{th}/P_0} \sum_{i,j\in\{1,\cdots,N\},\, i<j} \frac{(\lambda_i\lambda_j)^{N-2}\left(\lambda_i e^{-N_0\gamma_{th}/(\lambda_i P_0)} - \lambda_j e^{-N_0\gamma_{th}/(\lambda_j P_0)}\right)}{(\lambda_i-\lambda_j)\prod_{l=1,l\neq i,j}^{N}(\lambda_i-\lambda_l)(\lambda_j-\lambda_l)} \\
&\quad - \sum_{i,j\in\{1,\cdots,N\},\, i<j} \frac{(\lambda_i\lambda_j)^{N-2}}{(\lambda_i-\lambda_j)\prod_{l=1,l\neq i,j}^{N}(\lambda_i-\lambda_l)(\lambda_j-\lambda_l)} \times \\
&\quad \int_{(k\lambda_j+N_0)\gamma_{th}/P_0}^{(k\lambda_i+N_0)\gamma_{th}/P_0} \exp\left(\frac{P_0u^2}{\lambda_i\lambda_j k\gamma_{th}} - u\left(\frac{1}{\lambda_i}+\frac{1}{\lambda_j}+\frac{N_0}{\lambda_i\lambda_j k}\right)\right) du, \\
&\qquad \gamma_{th} > 0. \quad (5.20)
\end{aligned}
$$

Averaging (5.20) on K, the outage probability of the SINR becomes

$$
\begin{aligned}
F_{\gamma_{SINR}}(\gamma_{th}) \;=\; & \\
& 1-\sum_{n=1}^{p}\sum_{l_n=1}^{t_n}\frac{\alpha_{nl_n}}{\left(1+\frac{\gamma_{th}}{\Gamma_I^n}\right)^{l_n}}\sum_{i,j\in\{1,\cdots,N\},\, i<j}\frac{(\lambda_i\lambda_j)^{N-2}(\lambda_i e^{-\gamma_{th}/(\lambda_i\Gamma_0)}-\lambda_j e^{-\gamma_{th}/(\lambda_j\Gamma_0)})}{(\lambda_i-\lambda_j)\prod_{l=1,l\neq i,j}^{N}(\lambda_i-\lambda_l)(\lambda_j-\lambda_l)} \\
& -\sum_{i,j\in\{1,\cdots,N\},\, i<j}\frac{(\lambda_i\lambda_j)^{N-2}}{(\lambda_i-\lambda_j)\prod_{l=1,l\neq i,j}^{N}(\lambda_i-\lambda_l)(\lambda_j-\lambda_l)}\sum_{n=1}^{p}\sum_{l_n=1}^{t_n}\frac{\alpha_{nl_n}}{(l_n-1)!} \\
& \int_0^{\infty}dk\int_{(\frac{k\lambda_j}{\Gamma_I^n}+\frac{1}{\Gamma_0})\gamma_{th}}^{(\frac{k\lambda_i}{\Gamma_I^n}+\frac{1}{\Gamma_0})\gamma_{th}}k^{l_n-1}\exp\left(\frac{\Gamma_I^n u^2}{\lambda_i\lambda_j k\gamma_{th}}-u\left(\frac{1}{\lambda_i}+\frac{1}{\lambda_j}+\frac{\Gamma_I^n}{\lambda_i\lambda_j k\Gamma_0}\right)-k\right)du
\end{aligned}
\tag{5.21}
$$

where $\Gamma_I^n = P_0/P_n$ $(n=1,\cdots,N_I)$, is the ratio of the desired user signal power to the nth interfering user signal power, and $\Gamma_0 = P_0/N_0$ is the ratio of the desired user signal power to the noise power, namely, the average power SNR. Eq. (5.21) is a new result for outage probability of MRC with unequal-power CCI and thermal noise in correlated Rayleigh fading, and requires a double numerical integration.

When $\Gamma_0 = \infty$, namely, the noise is negligible, (5.21) becomes the outage probability of the signal-to-interference ratio (SIR) in CCI-limited correlated Rayleigh fading given by [81, eq. (8)]

$$
\begin{aligned}
F_{\gamma_{SIR}}(\gamma_{th}) \;=\; & \\
& 1-\sum_{n=1}^{p}\sum_{l_n=1}^{t_n}\frac{\alpha_{nl_n}}{\left(1+\frac{\gamma_{th}}{\Gamma_I^n}\right)^{l_n}}-\sum_{i,j\in\{1,\cdots,N\},\, i<j}\frac{(\lambda_i\lambda_j)^{N-2}}{(\lambda_i-\lambda_j)\prod_{l=1,l\neq i,j}^{N}(\lambda_i-\lambda_l)(\lambda_j-\lambda_l)} \\
& \times\sum_{n=1}^{p}\sum_{l_n=1}^{t_n}\frac{\alpha_{nl_n}}{(l_n-1)!}\int_0^{\infty}dk\int_{k\lambda_j\gamma_{th}/\Gamma_I^n}^{k\lambda_i\gamma_{th}/\Gamma_I^n}k^{l_n-1}\exp\left(\frac{u^2\Gamma_I^n}{\lambda_i\lambda_j k\gamma_{th}}-\frac{(\lambda_i+\lambda_j)u}{\lambda_i\lambda_j}-k\right)du.
\end{aligned}
\tag{5.22}
$$

Letting $u = kx$, using [98, eq. (1) and (3)], (5.22) can be further simplified in closed form

as

$$
\begin{aligned}
F_{\gamma_{SIR}}(\gamma_{th}) &= 1-\sum_{n=1}^{p}\sum_{l_n=1}^{t_n}\frac{\alpha_{nl_n}}{\left(1+\frac{\gamma_{th}}{\Gamma_I^n}\right)^{l_n}}-\sum_{i,j\in\{1,\cdots,N\},\,i<j}\frac{(\lambda_i\lambda_j)^{N-2}}{(\lambda_i-\lambda_j)\prod_{l=1,l\neq i,j}^{N}(\lambda_i-\lambda_l)(\lambda_j-\lambda_l)} \\
&\quad\times\sum_{n=1}^{p}\sum_{l_n=1}^{t_n}\frac{\alpha_{nl_n}}{(l_n-1)!}\int_{\lambda_j\gamma_{th}/\Gamma_I^n}^{\lambda_i\gamma_{th}/\Gamma_I^n}dx\int_0^{\infty}k^{l_n}\exp\left(\frac{kx^2\Gamma_I^n}{\lambda_i\lambda_j\gamma_{th}}-\frac{(\lambda_i+\lambda_j)kx}{\lambda_i\lambda_j}-k\right)dk \\
&= 1-\sum_{n=1}^{p}\sum_{l_n=1}^{t_n}\frac{\alpha_{nl_n}}{\left(1+\frac{\gamma_t}{\Gamma_I^n}\right)^{l_n}}-\sum_{i,j\in\{1,\cdots,N\},\,i<j}\frac{(\lambda_i\lambda_j)^{N-2}}{(\lambda_i-\lambda_j)\prod_{l=1,l\neq i,j}^{N}(\lambda_i-\lambda_l)(\lambda_j-\lambda_l)} \\
&\quad\times\sum_{n=1}^{p}\sum_{l_n=1}^{t_n}l_n\alpha_{nl_n}\int_{A_3^{j,n}}^{A_4^{i,n}}\left(1+A_2^{i,j}x-A_1^{i,j,n}x^2\right)^{-1-l_n}dx \\
&= 1-\sum_{n=1}^{p}\sum_{l_n=1}^{t_n}\frac{\alpha_{nl_n}}{\left(1+\frac{\gamma_t}{\Gamma_n}\right)^{l_n}}-\sum_{i,j\in\{1,\cdots,N\},\,i<j}\frac{(\lambda_i\lambda_j)^{N-2}}{(\lambda_i-\lambda_j)\prod_{l=1,l\neq i,j}^{N}(\lambda_i-\lambda_l)(\lambda_j-\lambda_l)} \\
&\quad\times\sum_{n=1}^{p}\sum_{l_n=1}^{t_n}l_n\alpha_{nl_n}[S_{l_n}(A_4^{i,n})-S_{l_n}(A_3^{j,n})] \qquad (5.23)
\end{aligned}
$$

where $A_1^{i,j,n}=\Gamma_I^n/(\lambda_i\lambda_j\gamma_{th})$, $A_2^{i,j}=(1/\lambda_i+1/\lambda_j)$, $A_3^{j,n}=\lambda_j\gamma_{th}/\Gamma_I^n$, $A_4^{i,n}=\lambda_i\gamma_{th}/\Gamma_I^n$, and

$$
S_{l_n}(x)=\int\frac{1}{(1+A_2^{i,j}x-A_1^{i,j,n}x^2)^{l_n+1}}dx. \qquad (5.24)
$$

$S_{l_n}(x)$ can be calculated in closed form by [6, eq. (2.171.4) and (2.172)]

$$
\begin{aligned}
\int\frac{dx}{R^{n+1}} &= \int\frac{1}{(a+bx+cx^2)^{n+1}}dx \\
&= \frac{2cx+b}{2n+1}\sum_{k=0}^{n-1}\frac{2k(2n+1)(2n-1)(2n-3)\cdots(2n-2k+1)c^k}{n(n-1)\cdots(n-k)\Delta^{k+1}R^{n-k}} \\
&\quad+2^n\frac{(2n-1)!!c^n}{n!\Delta^n}\int\frac{dx}{R} \qquad (5.25)
\end{aligned}
$$

and

$$
\int\frac{dx}{R}=\begin{cases}\frac{1}{\sqrt{-\Delta}}ln\frac{\sqrt{-\Delta-(b+2cx)}}{(b+2cx)+\sqrt{-\Delta}}, & \Delta<0\\ \frac{-2}{b+2cx}, & \Delta=0\\ \frac{2}{\sqrt{\Delta}}arctan\frac{b+2cx}{\sqrt{\Delta}}, & \Delta>0\end{cases} \qquad (5.26)
$$

where $\Delta=4ac-b^2$.

When all interfering signals have equal powers, that is, $P_n = P_I/N_I$ $(n = 1, \cdots, N_I)$, where $P_I = \sum_{n=1}^{N_I} P_n$ is the total interfering power, one has $\Gamma_I^n = N_I\Gamma_I$, and $\Gamma_I = P_0/P_I$ is the ratio of the desired user signal power to the total interference power. Then (5.21) becomes

$$\begin{aligned} F_{\gamma_{SINR}}(\gamma_{th}) &= 1 - \sum_{i,j\in\{1,\cdots,N\},\, i<j} \frac{(\lambda_i\lambda_j)^{N-2}(\lambda_i e^{-\gamma_{th}/(\lambda_i\Gamma_0)} - \lambda_j e^{-\gamma_{th}/(\lambda_j\Gamma_0)})}{\left(1+\frac{\gamma_{th}}{N_I\Gamma_I}\right)^{N_I}(\lambda_i-\lambda_j)\prod_{l=1,l\neq i,j}^{N}(\lambda_i-\lambda_l)(\lambda_j-\lambda_l)} \\ &\quad - \sum_{i,j\in\{1,\cdots,N\},\, i<j} \frac{(\lambda_i\lambda_j)^{N-2}}{(N_I-1)!(\lambda_i-\lambda_j)\prod_{l=1,l\neq i,j}^{N}(\lambda_i-\lambda_l)(\lambda_j-\lambda_l)} \int_0^\infty dk \\ &\quad \int_{(\frac{k\lambda_j}{N_I\Gamma_I}+\frac{1}{\Gamma_0})\gamma_{th}}^{(\frac{k\lambda_i}{N_I\Gamma_I}+\frac{1}{\Gamma_0})\gamma_{th}} k^{N_I-1}\exp\left(\frac{N_I\Gamma_I u^2}{\lambda_i\lambda_j k\gamma_{th}} - u\left(\frac{1}{\lambda_i}+\frac{1}{\lambda_j}+\frac{N_I\Gamma_I}{\lambda_i\lambda_j k\Gamma_0}\right) - k\right) du. \end{aligned} \tag{5.27}$$

Further, when $\Gamma_0 = \infty$, (5.27) becomes the outage probability corresponding to the case of equal-power CCI-limited correlated Rayleigh fading given by [80, eq. (10)], and can be further calculated in closed form as

$$\begin{aligned} &F_{\gamma_{SIR}}(\gamma_{th}) = \\ &1 - \left(\frac{1}{\frac{\gamma_{th}}{N_I\Gamma_I}+1}\right)^{N_I} - \sum_{i,j\in\{1,\cdots,N\},\, i<j} \frac{(\lambda_i\lambda_j)^{N-2}}{(N_I-1)!(\lambda_i-\lambda_j)\prod_{l=1,l\neq i,j}^{N}(\lambda_i-\lambda_l)(\lambda_j-\lambda_l)} \\ &\times \int_0^\infty dk \int_{k\lambda_j\gamma_{th}/(N_I\Gamma_I)}^{k\lambda_i\gamma_{th}/(N_I\Gamma_I)} k^{N_I-1}\exp\left(\frac{u^2 N_I\Gamma_I}{\lambda_i\lambda_j k\gamma_{th}} - \frac{(\lambda_i+\lambda_j)u}{\lambda_i\lambda_j} - k\right) du \\ &= 1 - \left(\frac{1}{\gamma_{th}/(N_I\Gamma_I)+1}\right)^{N_I} - \sum_{i,j\in\{1,\cdots,N\},\, i<j} \frac{N_I(\lambda_i\lambda_j)^{N-2}}{(\lambda_i-\lambda_j)\prod_{l=1,l\neq i,j}^{N}(\lambda_i-\lambda_l)(\lambda_j-\lambda_l)} \\ &\times \int_{\lambda_j\gamma_{th}/(N_I\Gamma_I)}^{\lambda_i\gamma_{th}/(N_I\Gamma_I)} \frac{1}{\left(1+\left(\frac{1}{\lambda_i}+\frac{1}{\lambda_j}\right)x - \frac{N_I\Gamma_I x^2}{\lambda_i\lambda_j\gamma_{th}}\right)^{N_I+1}} dx \\ &= 1 - \left(\frac{1}{\gamma_{th}/(N_I\Gamma_I)+1}\right)^{N_I} - \sum_{i,j\in\{1,\cdots,N\},\, i<j} \frac{N_I(\lambda_i\lambda_j)^{N-2}}{(\lambda_i-\lambda_j)\prod_{l=1,l\neq i,j}^{N}(\lambda_i-\lambda_l)(\lambda_j-\lambda_l)} \\ &\times \left[S_{N_I}\left(\frac{\lambda_i\gamma_{th}}{N_I\Gamma_I}\right) - S_{N_I}\left(\frac{\lambda_j\gamma_{th}}{N_I\Gamma_I}\right)\right] \end{aligned} \tag{5.28}$$

where $S_{N_I}(x)$ can be calculated in closed form as done in (5.24). Eq. (5.28) is a new result for the outage probability in CCI-limited correlated Rayleigh fading with different eigenvalues for the correlation matrix when the interfering users have equal signal powers.

5.3.3 Case II: Equi-Correlated Correlation Matrix

When all of the users experience equi-correlated Rayleigh fading with correlation coefficient ρ $(0 < \rho < 1)$, the CDF of the SINR conditioned on K becomes by substituting (5.19) into (5.14)

$$\begin{aligned} F_{\gamma_{SINR}|K}(\gamma_{th}|k) &= 1-\left(\frac{\lambda_1}{\lambda_1-\lambda_2}\right)^{N-1}\exp\left(-\left(\frac{k\gamma_{th}}{P_0}+\frac{N_0\gamma_{th}}{\lambda_1 P_0}\right)\right)+\frac{\lambda_2}{\lambda_1}\sum_{q=0}^{N-2}\sum_{l=0}^{q} \\ &\left(\frac{\lambda_1}{\lambda_1-\lambda_2}\right)^{N-1-q}\frac{1}{l!}\left(\frac{k\gamma_{th}}{P_0}+\frac{N_0\gamma_{th}}{\lambda_2 P_0}\right)^{l}\exp\left(-\left(\frac{k\gamma_{th}}{P_0}+\frac{N_0\gamma_{th}}{\lambda_2 P_0}\right)\right) \\ &-\frac{{\lambda_1}^{N-2}}{(\lambda_1-\lambda_2)^{N-1}}\sum_{q=0}^{N-2}\frac{1}{q!}\int_{\frac{k\lambda_2\gamma_{th}+N_0\gamma_{th}}{P_0}}^{\frac{k\lambda_1\gamma_{th}+N_0\gamma_{th}}{P_0}}\left(\frac{u}{\lambda_2}+\frac{N_0 u}{\lambda_1\lambda_2 k}-\frac{P_0u^2}{\lambda_1\lambda_2 k\gamma_{th}}\right)^{q} \\ &\times\exp\left(\frac{P_0u^2}{\lambda_1\lambda_2 k\gamma_{th}}-\left(\frac{1}{\lambda_1}+\frac{1}{\lambda_2}+\frac{N_0}{\lambda_1\lambda_2 k}\right)u\right)du. \end{aligned} \tag{5.29}$$

Averaging (5.29) over K, the outage probability of the SINR is given by

$$\begin{aligned} F_{\gamma_{SINR}}(\gamma_{th}) &= 1-\left(\frac{\lambda_1}{\lambda_1-\lambda_2}\right)^{N-1}e^{-\gamma_{th}/(\lambda_1\Gamma_0)}\sum_{n=1}^{p}\sum_{l_n=1}^{t_n}\frac{\alpha_{nl_n}}{\left(1+\frac{\gamma_{th}}{\Gamma_I^n}\right)^{l_n}}+ \\ &\frac{\lambda_2 e^{-\gamma_{th}/(\lambda_2\Gamma_0)}}{\lambda_1}\sum_{q=0}^{N-2}\sum_{l=0}^{q}\left(\frac{\lambda_1}{\lambda_1-\lambda_2}\right)^{N-1-q}\sum_{n=1}^{p}\sum_{l_n=1}^{t_n}\alpha_{nl_n} \\ &\sum_{i=0}^{l}C_{l_n+i-1}^{l_n-1}\frac{1}{(l-i)!}\left(\frac{\gamma_{th}}{\lambda_2\Gamma_0}\right)^{l-i}\left(\frac{\gamma_{th}}{\Gamma_I^n}\right)^{i}\left(1+\frac{\gamma_{th}}{\Gamma_I^n}\right)^{-l_n-i} \\ &-\frac{{\lambda_1}^{N-2}}{(\lambda_1-\lambda_2)^{N-1}}\sum_{q=0}^{N-2}\frac{1}{q!}\sum_{n=1}^{p}\sum_{l_n=1}^{t_n}\frac{\alpha_{nl_n}}{(l_n-1)!}\int_0^{\infty}dk \\ &\int_{\frac{k\lambda_2\gamma_{th}}{\Gamma_I^n}+\frac{\gamma_{th}}{\Gamma_0}}^{\frac{k\lambda_1\gamma_{th}}{\Gamma_I^n}+\frac{\gamma_{th}}{\Gamma_0}}k^{l_n-1}\times\left(\frac{u}{\lambda_2}+\frac{u\Gamma_I^n}{\lambda_1\lambda_2\Gamma_0 k}-\frac{\Gamma_I^n u^2}{\lambda_1\lambda_2 k\gamma_{th}}\right)^{q} \\ &\times\exp\left(\frac{\Gamma_I^n u^2}{\lambda_1\lambda_2 k\gamma_{th}}-\left(\frac{1}{\lambda_1}+\frac{1}{\lambda_2}+\frac{\Gamma_I^n}{\lambda_1\lambda_2 k\Gamma_0}\right)u-k\right)du. \end{aligned} \tag{5.30}$$

Similarly, when $\Gamma_0 = \infty$, namely the noise is negligible, (5.30) becomes [81, eq. (13)]

$$\begin{aligned} F_{\gamma_{SIR}}(\gamma_{th}) &= 1-\left(\frac{\lambda_1}{\lambda_1-\lambda_2}\right)^{N-1}\sum_{n=1}^{p}\sum_{l_n=1}^{t_n}\frac{\alpha_{nl_n}}{\left(1+\frac{\gamma_{th}}{\Gamma_I^n}\right)^{l_n}} \\ &+\frac{\lambda_2}{\lambda_1}\sum_{q=0}^{N-2}\sum_{l=0}^{q}\left(\frac{\lambda_1}{\lambda_1-\lambda_2}\right)^{N-1-q}\sum_{n=1}^{p}\sum_{l_n=1}^{t_n}C_{l_n+l-1}^{l_n-1}\alpha_{nl_n} \\ &\times\left(\frac{\gamma_{th}}{\Gamma_I^n}\right)^{l}\left(1+\frac{\gamma_{th}}{\Gamma_I^n}\right)^{-l-l_n}-\frac{{\lambda_1}^{N-2}}{(\lambda_1-\lambda_2)^{N-1}}\sum_{q=0}^{N-2}\frac{1}{q!} \\ &\sum_{n=1}^{p}\sum_{l_n=1}^{t_n}\frac{\alpha_{nl_n}}{(l_n-1)!}\int_0^{\infty}dk\int_{\frac{k\lambda_2\gamma_{th}}{\Gamma_I^n}}^{\frac{k\lambda_1\gamma_{th}}{\Gamma_I^n}}\exp\left(\frac{\Gamma_I^n u^2}{\lambda_1\lambda_2 k\gamma_{th}}-\left(\frac{1}{\lambda_1}+\frac{1}{\lambda_2}\right)u-k\right) \\ &\times\left(\frac{u}{\lambda_2}-\frac{\Gamma_I^n u^2}{\lambda_1\lambda_2 k\gamma_{th}}\right)^{q}k^{l_n-1}du. \end{aligned} \tag{5.31}$$

Letting $u = kx$, (5.31) can be further simplified in closed form as

$$\begin{aligned} F_{\gamma_{SIR}}(\gamma_{th}) &= 1-\left(\frac{\lambda_1}{\lambda_1-\lambda_2}\right)^{N-1}\sum_{n=1}^{p}\sum_{l_n=1}^{t_n}\frac{\alpha_{nl_n}}{\left(1+\frac{\gamma_{th}}{\Gamma_I^n}\right)^{l_n}} \\ &+\frac{\lambda_2}{\lambda_1}\sum_{q=0}^{N-2}\sum_{l=0}^{q}\left(\frac{\lambda_1}{\lambda_1-\lambda_2}\right)^{N-1-q}\sum_{n=1}^{p}\sum_{l_n=1}^{t_n}C_{l_n+l-1}^{l_n-1}\alpha_{nl_n} \\ &\times\left(\frac{\gamma_{th}}{\Gamma_I^n}\right)^{l}\left(1+\frac{\gamma_{th}}{\Gamma_I^n}\right)^{-l-l_n}-\frac{{\lambda_1}^{N-2}}{(\lambda_1-\lambda_2)^{N-1}}\sum_{q=0}^{N-2}\frac{1}{q!} \\ &\sum_{n=1}^{p}\sum_{l_n=1}^{t_n}\frac{(l_n+q)!\alpha_{nl_n}}{(l_n-1)!}\int_{B_3^n}^{B_4^n}\frac{(B_5x-B_1^nx^2)^q}{(1+B_2x-B_1^nx^2)^{l_n+q+1}}dx \\ &= 1-\left(\frac{\lambda_1}{\lambda_1-\lambda_2}\right)^{N-1}\sum_{n=1}^{p}\sum_{l_n=1}^{t_n}\frac{\alpha_{nl_n}}{\left(1+\frac{\gamma_{th}}{\Gamma_I^n}\right)^{l_n}} \\ &+\frac{\lambda_2}{\lambda_1}\sum_{q=0}^{N-2}\sum_{l=0}^{q}\left(\frac{\lambda_1}{\lambda_1-\lambda_2}\right)^{N-1-q}\sum_{n=1}^{p}\sum_{l_n=1}^{t_n}C_{l_n+l-1}^{l_n-1}\alpha_{nl_n} \\ &\times\left(\frac{\gamma_{th}}{\Gamma_I^n}\right)^{l}\left(1+\frac{\gamma_{th}}{\Gamma_I^n}\right)^{-l-l_n}-\frac{{\lambda_1}^{N-2}}{(\lambda_1-\lambda_2)^{N-1}}\sum_{q=0}^{N-2}\frac{1}{q!} \\ &\sum_{n=1}^{p}\sum_{l_n=1}^{t_n}\frac{(l_n+q)!\alpha_{nl_n}}{(l_n-1)!}[Y_{q,l_n+q}(B_4^n)-Y_{q,l_n+q}(B_3^n)] \end{aligned} \tag{5.32}$$

where $B_1^n = \Gamma_I^n/(\lambda_1\lambda_2\gamma_{th})$, $B_2 = (1/\lambda_1 + 1/\lambda_2)$, $B_3^n = \lambda_2\gamma_{th}/\Gamma_I^n$, $B_4^n = \lambda_1\gamma_{th}/\Gamma_I^n$, and $B_5 =$

$1/\lambda_2$. The integration term $Y_{q,l_n+q}(x) = \int (B_5 x - B_1^n x^2)^q / (1 + B_2 x - B_1^n x^2)^{l_n+q+1} dx$ can be calculated by [6, eqs. (2.171.3), (2.172), (2.18.3)].

When all interfering signals have equal powers, namely $\Gamma_I^n = N_I \Gamma_I$, (5.30) becomes

$$
\begin{aligned}
F_{\gamma_{SINR}}(\gamma_{th}) \;=\; & \\
& 1 - \left(\frac{\lambda_1}{\lambda_1 - \lambda_2}\right)^{N-1} \frac{e^{-\frac{\gamma_{th}}{\lambda_1 \Gamma_0}}}{\left(1 + \frac{\gamma_{th}}{N_I \Gamma_I}\right)^{N_I}} + \frac{\lambda_2 e^{-\frac{\gamma_{th}}{\lambda_2 \Gamma_0}}}{\lambda_1} \sum_{q=0}^{N-2} \sum_{l=0}^{q} \left(\frac{\lambda_1}{\lambda_1 - \lambda_2}\right)^{N-1-q} \\
& \sum_{i=0}^{l} \frac{C_{N_I+i-1}^{N_I-1}}{(l-i)!} \left(\frac{\gamma_{th}}{\lambda_2 \Gamma_0}\right)^{l-i} \left(\frac{\gamma_{th}}{N_I \Gamma_I}\right)^{i} \left(1 + \frac{\gamma_{th}}{N_I \Gamma_I}\right)^{-N_I - i} - \frac{{\lambda_1}^{N-2}}{(\lambda_1 - \lambda_2)^{N-1}} \sum_{q=0}^{N-2} \frac{1}{q!(N_I - 1)!} \\
& \int_0^{\infty} dk \int_{\frac{k\lambda_2 \gamma_{th}}{N_I \Gamma_I} + \frac{\gamma_{th}}{\Gamma_0}}^{\frac{k\lambda_1 \gamma_{th}}{N_I \Gamma_I} + \frac{\gamma_{th}}{\Gamma_0}} \exp\left(\frac{N_I \Gamma_I u^2}{\lambda_1 \lambda_2 k \gamma_{th}} - \left(\frac{1}{\lambda_1} + \frac{1}{\lambda_2} + \frac{N_I \Gamma_I}{\lambda_1 \lambda_2 k \Gamma_0}\right) u - k\right) \\
& \times \left(\frac{u}{\lambda_2} + \frac{u N_I \Gamma_I}{\lambda_1 \lambda_2 \Gamma_0 k} - \frac{N_I \Gamma_I u^2}{\lambda_1 \lambda_2 k \gamma_{th}}\right)^q \times k^{N_I - 1} du. \qquad (5.33)
\end{aligned}
$$

Further, when $\Gamma_0 = \infty$, (5.33) becomes [81, eq. (14)] corresponding to the equal-power CCI-limited case, which can be further simplified in closed form as

$$
\begin{aligned}
F_{\gamma_{SIR}}(\gamma_{th}) \;=\; & 1 - \left(\frac{\lambda_1}{\lambda_1 - \lambda_2}\right)^{N-1} \frac{1}{\left(1 + \frac{\gamma_{th}}{N_I \Gamma_I}\right)^{N_I}} + \frac{\lambda_2}{\lambda_1} \sum_{q=0}^{N-2} \\
& \sum_{l=0}^{q} \left(\frac{\lambda_1}{\lambda_1 - \lambda_2}\right)^{N-1-q} C_{N_I+l-1}^{N_I-1} \left(\frac{\gamma_{th}}{N_I \Gamma_I}\right)^{l} \left(1 + \frac{\gamma_{th}}{N_I \Gamma_I}\right)^{-l-N_I} \\
& - \frac{{\lambda_1}^{N-2}}{(\lambda_1 - \lambda_2)^{N-1}} \sum_{q=0}^{N-2} \frac{1}{q!(N_I - 1)!} \int_0^{\infty} dk \int_{\frac{k\lambda_2 \gamma_{th}}{N_I \Gamma_I}}^{\frac{k\lambda_1 \gamma_{th}}{N_I \Gamma_I}} \\
& \exp\left(\frac{N_I \Gamma_I u^2}{\lambda_1 \lambda_2 k \gamma_{th}} - \left(\frac{1}{\lambda_1} + \frac{1}{\lambda_2}\right) u - k\right) \times \left(\frac{u}{\lambda_2} - \frac{N_I \Gamma_I u^2}{\lambda_1 \lambda_2 k \gamma_{th}}\right)^q \times k^{N_I - 1} du \\
= \; & 1 - \left(\frac{\lambda_1}{\lambda_1 - \lambda_2}\right)^{N-1} \frac{1}{\left(1 + \frac{\gamma_{th}}{N_I \Gamma_I}\right)^{N_I}} + \frac{\lambda_2}{\lambda_1} \sum_{q=0}^{N-2} \\
& \sum_{l=0}^{q} \left(\frac{\lambda_1}{\lambda_1 - \lambda_2}\right)^{N-1-q} C_{N_I+l-1}^{N_I-1} \left(\frac{\gamma_{th}}{N_I \Gamma_I}\right)^{l} \left(1 + \frac{\gamma_{th}}{N_I \Gamma_I}\right)^{-l-N_I} \\
& - \frac{{\lambda_1}^{N-2}}{(\lambda_1 - \lambda_2)^{N-1}} \sum_{q=0}^{N-2} N_I C_{N_I+q}^{q} \int_{\lambda_2 \gamma_{th}/(N_I \Gamma_I)}^{\lambda_1 \gamma_{th}/(N_I \Gamma_I)} \frac{\left(\frac{x}{\lambda_2} - \frac{N_I \Gamma_I x^2}{\lambda_1 \lambda_2 \gamma_{th}}\right)^q}{\left(1 + (\frac{1}{\lambda_1} + \frac{1}{\lambda_2}) x - \frac{N_I \Gamma_I x^2}{\lambda_1 \lambda_2 \gamma_{th}}\right)^{N_I + q + 1}} dx. \qquad (5.34)
\end{aligned}
$$

5.3.4 Numerical Results

In this section, some numerical examples of the outage probability of MRC in CCI and correlated Rayleigh fading are given. In our examples, we assume that the channel gain vector $\mathbf{c_n} = [x_{n,1} + jy_{n,1} \cdots x_{n,N} + jy_{n,N}]^T$ $(n = 0, \cdots, N_I)$ satisfies $\mathbb{E}[x_{n,i}x_{n,j}] = \mathbb{E}[y_{n,i}y_{n,j}]$ and $\mathbb{E}[x_{n,i}y_{n,j}] = \mathbb{E}[y_{n,i}x_{n,j}] = 0$ $(i, j = 1, \cdots, N)$ where $[A]^T$ denotes the transpose of matrix A. For the outage probability, a wireless cellular system in which the desired signal is corrupted by $N_I = 6$ cochannel interferers in correlated Rayleigh fading with outage SINR threshold $\gamma_{th} = 12$ dB, is considered. Given the total interference power $P_I = \sum_{n=1}^{N_I} P_n$, the average power SIR is defined as SIR$= P_0/P_I$, and the average power SNR is defined as SNR$= P_0/N_0$. Two cases are considered: 1) all interfering users have the same powers; 2) the powers of the interfering users are unequal with $P_n = P$ $(n = 1, \cdots, 5)$ and $P_6 = 5P$.

Fig. 5.1 shows the outage probability of MRC with unequal-power interferers as a function of the power SIR using the channel model from [18] with $\Delta = \pi$, where $\mathbb{E}[x_{n,i}x_{n,j}] = \mathbb{E}[y_{n,i}y_{n,j}] = 0.5J_0(2\pi(i-j)d)$, and d is the ratio of the spacing to the wavelength between two adjacent antennas. Here, we consider $d = 0.382$, which represents the minimum normalized spacing between any two adjacent antenna elements yielding zero correlation. Different values of average power SNR are considered, among which, average power SNR$= \infty$ corresponds to the CCI-limited case. In this figure, the diamond markers denote the outage probability obtained using Monte Carlo simulation. It is seen that the analytical results and the simulation results are in excellent agreement. Observe that an outage floor appears for a fixed value of SNR when the power SIR is large. This is because the outage probability at large values of average power SIR is mainly affected by the fixed value of average power SNR when the noise dominates the cochannel interference. As expected, the outage floor decreases with increasing average power SNR.

Fig. 5.2 shows the outage probability of MRC as a function of the average SNR in equicorrelated Rayleigh fading with $N_I = 6$ unequal-power interferers, $N = 4$ receiver antennas and correlation coefficient $\rho = 0.5$. Different values of average power SIR are considered. In this figure, one sees that when the interference dominates the noise, an outage floor is

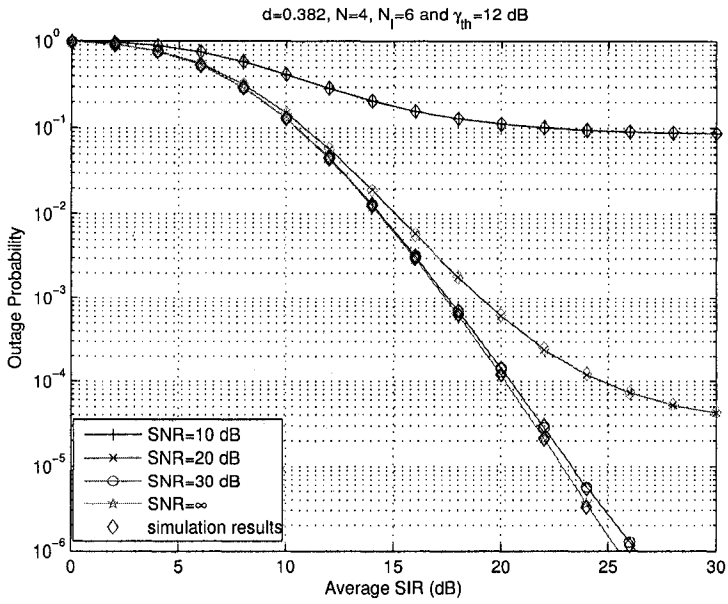

Fig. 5.1. The outage probability of MRC versus the average power SIR with $N = 4$, $d = 0.382$, $\gamma_{th} = 12$ dB, and $N_I = 6$ unequal-power interferers for different values of average power SNR.

established by the value of the SIR. The floor can be reduced by increasing the power SIR, as expected.

The effect of the normalized spacing between two adjacent antennas, d, on the outage probability is examined in Fig. 5.3. The channel model from [18] with $\Delta = \pi$ is considered for $N_I = 6$ equal-power interferers with average power SIR=20 dB. From this figure, one can see that the outage probabilities when $d = 0.382$ and $d = 0.4$ are close to the globally minimum outage probability at $d = 0.9$. From the viewpoint of system design, Fig. 5.3 indicates that one may set $d = 0.382$ or 0.4 to achieve a good compromise between outage performance and space limitations.

Fig. 5.4 shows the outage probability versus the average power SNR in equi-correlated Rayleigh fading with $N = 4$ receiver antennas, and $N_I = 6$ equal-power interferers. Different values of correlation coefficient ρ are considered. It is seen that the outage floors when the SIR= 10 dB are much greater than those when the SIR= 20 dB. Further, while

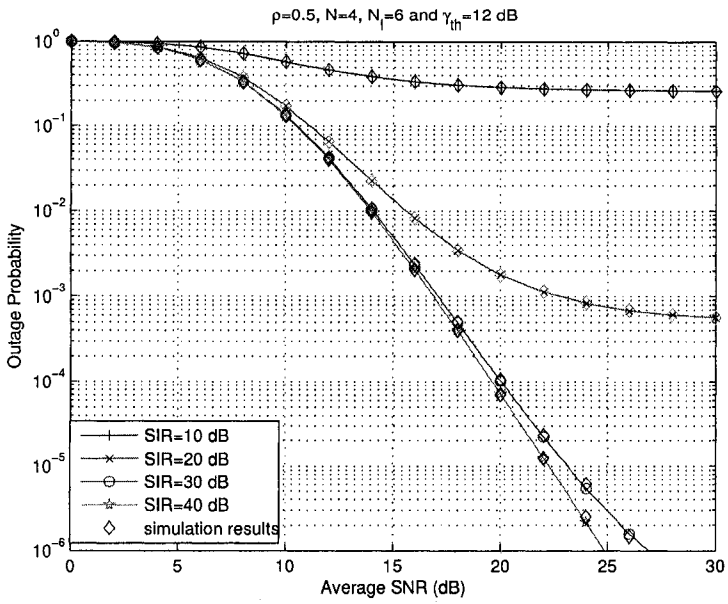

Fig. 5.2. The outage probability of MRC versus the average power SNR in equi-correlated Rayleigh fading with $N = 4$, $\rho = 0.5$, $\gamma_{th} = 12$ dB, and $N_I = 6$ unequal-power interferers for different values of average power SIR.

the performance generally improves with decreasing correlation coefficient ρ, as expected, it is seen that a large value of correlation coefficient causes significantly more performance degradation at large values of SIR than at small values of SIR.

5.4 BER of BPSK with Perfect Channel Estimation

In this section, the average BER of a coherent BPSK system using MRC diversity in the presence of multiple interferers and correlated Rayleigh fading is studied. We assume that all of the user signals are BPSK modulated, namely, the information bits of the desired user signal,d_0, and the nth interfering user signal, d_n $(n = 1, \cdots, N_I)$, take values from $\{+1, -1\}$ with equal probability. Then the decision variable after the MRC combiner is given by

$$D = Re\{r\} = \sqrt{P_0}(\mathbf{c_0}^H \mathbf{c_0})d_0 + \sum_{n=1}^{N_I} \sqrt{P_n} Re\{(\mathbf{c_0}^H \mathbf{c_n})\} d_n + Re\{(\mathbf{c_0}^H \mathbf{z_0})\}. \quad (5.35)$$

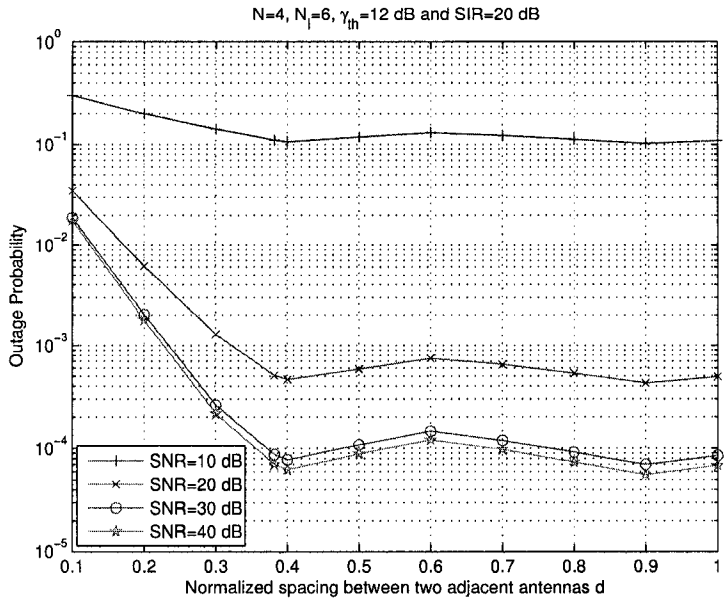

Fig. 5.3. The outage probability of MRC versus the normalized spacing between two adjacent antennas, d, with $N = 4$, $\gamma_{th} = 12$ dB, $N_I = 6$ equal-power interferers, and average power SIR=20 dB for different values of average power SNR.

Without loss of generality, assume that $d_0 = +1$ is transmitted, then the average BER conditioned on $\mathbf{c_0}$ for the desired user, is given by

$$\begin{aligned} P_{e|\mathbf{c_0}} &= \Pr(D < 0 | d_0 = +1, \mathbf{c_0}) \\ &= \Pr\left(\sqrt{P_0}(\mathbf{c_0}^H \mathbf{c_0}) + \sum_{n=1}^{N_I} \sqrt{P_n} Re\{(\mathbf{c_0}^H \mathbf{c_n})\} d_n + Re\{(\mathbf{c_0}^H \mathbf{z_0})\} < 0 | \mathbf{c_0} \right). \end{aligned} \tag{5.36}$$

Since the quadratic form $\mathbf{c_0}^H \sum \mathbf{c_0} > 0$, the error probability of (5.36) can be rewritten as

$$P_{e|\mathbf{c_0}} = \Pr\left(\frac{\sqrt{P_0}(\mathbf{c_0}^H \mathbf{c_0})}{\sqrt{\mathbf{c_0}^H \sum \mathbf{c_0}}} + \sum_{n=1}^{N_I} \sqrt{P_n} g_n d_n + n_0 < 0 | \mathbf{c_0} \right) \tag{5.37}$$

where $g_n = Re\left\{ (\mathbf{c_0}^H \mathbf{c_n}) / \sqrt{\mathbf{c_0}^H \sum \mathbf{c_0}} \right\}$ $(n = 1, \cdots, N_I)$ and $n_0 = Re\left\{ (\mathbf{c_0}^H \mathbf{z_0}) / \sqrt{\mathbf{c_0}^H \sum \mathbf{c_0}} \right\}$. Since $\mathbf{c_n}$ $(n = 0, \cdots, N_I)$ are independent zero-mean complex Gaussian vectors, one can show that $(\mathbf{c_0}^H \mathbf{c_n}) / \sqrt{\mathbf{c_0}^H \sum \mathbf{c_0}}$ $(n = 1, \cdots, N_I)$ are independent complex Gaussian distributed

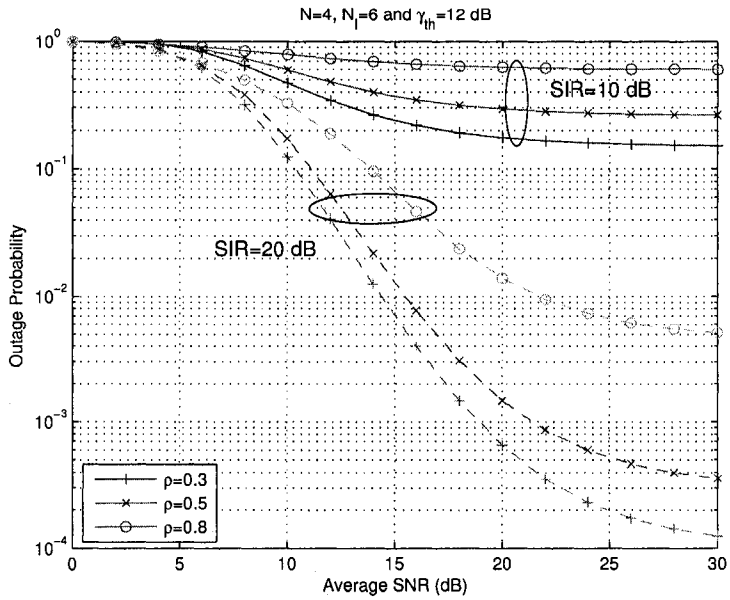

Fig. 5.4. The outage probability of MRC versus the average power SNR in equi-correlated Rayleigh fading with $N = 4$, $\gamma_{th} = 12$ dB, and $N_I = 6$ equal-power interferers for different values of correlation coefficient $\rho = 0.3$, 0.5 and 0.8.

with zero mean and unit variance [79], and independent of $\mathbf{c_0}$. Therefore, g_n $(n = 1, \cdots, N_I)$ are independent Gaussian distributed with zero mean and variance $\sigma_{g_n}^2 = 1/2$, and independent of $\mathbf{c_0}$. In addition, n_0 conditioned on $\mathbf{c_0}$ can be shown to be Gaussian distributed with zero mean and variance $\sigma_{n_0}^2 = N_0(\mathbf{c_0}^H\mathbf{c_0})/(2(\mathbf{c_0}^H\Sigma\mathbf{c_0}))$.

Let $Y = \sum_{n=1}^{N_I}\sqrt{P_n}g_n d_n + n_0$. Since g_n $(n = 1, \cdots, N_I)$ and n_0 conditioned on $\mathbf{c_0}$ are independent, the CF of Y conditioned on $\mathbf{c_0}$ is calculated by [35]

$$\phi_Y(j\omega) = \mathbb{E}(e^{j\omega Y}) = \phi_{\mathscr{X}}(j\omega)\phi_{n_0}(j\omega) \tag{5.38}$$

where $\mathscr{X} = \sum_{n=1}^{N_I} I_n = \sum_{n=1}^{N_I}\sqrt{P_n}g_n d_n$, and $\phi_\gamma(j\omega)$ denotes the CF of the random variable γ. Noting the fact that g_n and d_n $(n = 1, \cdots, N_I)$ are independent, one obtains the CF of $\mathscr{X}$ by

$$\phi_{\mathscr{X}}(j\omega) = \prod_{n=1}^{N_I}\phi_{I_n}(j\omega). \tag{5.39}$$

Since d_n is independent of g_n and takes values from $\{+1,-1\}$ with equal probability, the CF of I_n conditioned on g_n, is given by

$$\phi_{I_n|g_n}(j\omega) = \frac{e^{j\omega\sqrt{P_n}g_n}}{2} + \frac{e^{-j\omega\sqrt{P_n}g_n}}{2} = \cos(\sqrt{P_n}g_n\omega). \tag{5.40}$$

Averaging (5.40) over g_n and combining with [6, eq. (3.896.2)], the CF of I_n becomes

$$\begin{aligned}\phi_{I_n}(j\omega) &= \frac{1}{\sqrt{\pi}}\int_{-\infty}^{\infty}\cos(\sqrt{P_n}g_n\omega)e^{-g_n^2}dg_n \\ &= \exp\left(-\frac{P_n\omega^2}{4}\right).\end{aligned} \tag{5.41}$$

Substituting (5.41) into (5.39), one can obtain the CF of $\mathscr{X}$ by

$$\phi_{\mathscr{X}}(j\omega) = \prod_{n=1}^{N_I}\phi_{I_n}(j\omega) = \exp\left(-\sum_{n=1}^{N_I}\frac{P_n\omega^2}{4}\right) = \exp\left(-\frac{P_I\omega^2}{4}\right) \tag{5.42}$$

where $P_I = \sum_{n=1}^{N_I} P_n$ is the total interference power, as defined previously. Note that the interference term $\mathscr{X}$ is actually a Gaussian RV with zero mean and variance $P_I/2$ [35], and is determined by only the total interfering power and is independent of the number of interfering users N_I and the individual interfering user powers.

Since n_0 conditioned on $\mathbf{c_0}$ is Gaussian with zero mean and variance $\sigma_{n_0}^2$, the CF of n_0 is given by [35]

$$\phi_{n_0}(j\omega) = \exp\left(-\frac{\omega^2}{2}\times\frac{N_0(\mathbf{c_0}^H\mathbf{c_0})}{2(\mathbf{c_0}^H\Sigma\mathbf{c_0})}\right). \tag{5.43}$$

Then the CF of Y conditioned on $\mathbf{c_0}$ is given by

$$\begin{aligned}\phi_{Y|\mathbf{c_0}}(j\omega) &= \exp\left(-\frac{\omega^2}{2}\left(\frac{P_I}{2}+\frac{N_0(\mathbf{c_0}^H\mathbf{c_0})}{2(\mathbf{c_0}^H\Sigma\mathbf{c_0})}\right)\right) \\ &= \exp\left(-\frac{\omega^2\sigma_Y^2}{2}\right)\end{aligned} \tag{5.44}$$

where $\sigma_Y^2 = P_I/2 + N_0(\mathbf{c_0}^H\mathbf{c_0})/(2(\mathbf{c_0}^H\Sigma\mathbf{c_0}))$. Again, the random variable Y conditioned on $\mathbf{c_0}$ is a Gaussian RV with zero mean and variance σ_Y^2 [35].

Thus, the conditional error probability $P_{e|\mathbf{c_0}}$ in (5.37) can be calculated by

$$\begin{aligned} P_{e|\mathbf{c_0}} &= \Pr\left(\frac{\sqrt{P_0}(\mathbf{c_0}^H\mathbf{c_0})}{\sqrt{\mathbf{c_0}^H\sum\mathbf{c_0}}}+Y<0|\mathbf{c_0}\right) \\ &= \Pr\left(Y<-\frac{\sqrt{P_0}(\mathbf{c_0}^H\mathbf{c_0})}{\sqrt{\mathbf{c_0}^H\sum\mathbf{c_0}}}|\mathbf{c_0}\right) \\ &= Q\left(\sqrt{2\gamma_{BER}}\right) \end{aligned} \tag{5.45}$$

where $Q(x)=(1/\sqrt{2\pi})\int_x^\infty e^{-t^2/2}dt$ is the Q function, and γ_{BER} is given by

$$\gamma_{BER} = \frac{P_0(\mathbf{c_0}^H\mathbf{c_0})^2}{P_I(\mathbf{c_0}^H\sum\mathbf{c_0})+N_0(\mathbf{c_0}^H\mathbf{c_0})}. \tag{5.46}$$

Averaging (5.45) over γ_{BER}, the average BER of coherent BPSK using MRC in the presence of interferers and correlated Rayleigh fading is given by

$$\begin{aligned} P_e &= \int_0^\infty Q(\sqrt{2t})f_{\gamma_{BER}}(t)dt \\ &= \frac{1}{2\sqrt{\pi}}\int_0^\infty t^{-1/2}e^{-t}F_{\gamma_{BER}}(t)dt \end{aligned} \tag{5.47}$$

where $f_{\gamma_{BER}}(t)$ and $F_{\gamma_{BER}}(t)$ are the PDF and CDF of γ_{BER}, respectively. If the PDF or the CDF of γ_{BER} is known, the BER of coherent BPSK can be obtained using (5.47).

Rewrite γ_{BER} in (5.46) as

$$\gamma_{BER}=\frac{P_0u^2}{P_Iw+N_0u} \tag{5.48}$$

where $u=\mathbf{v}^H\Lambda\mathbf{v}$, $w=\mathbf{v}^H\Lambda^2\mathbf{v}$, $\mathbf{v}=\Lambda^{-1/2}U^H\mathbf{c_0}$, and Λ is the diagonal matrix composed of the eigenvalues of the correlation matrix $\sum$, λ_i $(i=1,\cdots,N)$, as defined in Section 5.3. Then, the CDF of γ_{BER} is given by

$$\begin{aligned} F_{\gamma_{BER}}(y) &= \Pr(\gamma_{BER}\le y) \\ &= \Pr\left(\frac{P_0u^2}{P_Iw+N_0u}\le y\right) \\ &= \Pr\left(\frac{P_0}{P_Iy}u^2-\frac{N_0}{P_I}u\le w\right) \\ &= \Pr\left(\frac{\Gamma_I}{y}u^2-\frac{\Gamma_I}{\Gamma_0}u\le w\right) \end{aligned} \tag{5.49}$$

where $\Gamma_0 = P_0/N_0$ is the average power SNR and $\Gamma_I = P_0/P_I$ is the average power SIR as defined in Section 5.3. In the following, the CDF of γ_{BER} for the two cases that the correlation matrix has different eigenvalues and that the correlation matrix is equi-correlated will be studied respectively.

5.4.1 Case I: Correlation Matrix With Different Eigenvalues

Substituting the joint PDF of u and w in (5.16) into (5.49) and combining with (C.6) in Appendix C, the CDF of γ_{BER} becomes

$$\begin{aligned} F_{\gamma_{BER}}(y) &= \sum_{i,j\in\{1,\cdots,N\},\, i<j} \frac{(\lambda_i\lambda_j)^{N-3}}{(\lambda_i-\lambda_j)\prod_{l=1,\, l\neq i,j}^{N}(\lambda_i-\lambda_l)(\lambda_j-\lambda_l)} \times \\ &\quad \left[\int_0^{\left(\frac{\lambda_j}{\Gamma_I}+\frac{1}{\Gamma_0}\right)y} du \int_{\lambda_j u}^{\lambda_i u} e^{\frac{w}{\lambda_i\lambda_j}-u\left(\frac{1}{\lambda_i}+\frac{1}{\lambda_j}\right)} dw + \right. \\ &\quad \left. \int_{\left(\frac{\lambda_j}{\Gamma_I}+\frac{1}{\Gamma_0}\right)y}^{\left(\frac{\lambda_i}{\Gamma_I}+\frac{1}{\Gamma_0}\right)y} du \int_{\frac{\Gamma_I u^2}{y}-\frac{\Gamma_I u}{\Gamma_0}}^{\lambda_i u} e^{\frac{w}{\lambda_i\lambda_j}-u\left(\frac{1}{\lambda_i}+\frac{1}{\lambda_j}\right)} dw \right] \\ &= 1 - \sum_{i,j\in\{1,\cdots,N\},\, i<j} \frac{(\lambda_i\lambda_j)^{N-2}\left(\lambda_i e^{-(y/\Gamma_I+y/(\lambda_i\Gamma_0))} - \lambda_j e^{-\left(y/\Gamma_I+y/(\lambda_j\Gamma_0)\right)}\right)}{(\lambda_i-\lambda_j)\prod_{l=1,\, l\neq i,j}^{N}(\lambda_i-\lambda_l)(\lambda_j-\lambda_l)} \\ &\quad - \sum_{i,j\in\{1,\cdots,N\},\, i<j} \frac{(\lambda_i\lambda_j)^{N-2}}{(\lambda_i-\lambda_j)\prod_{l=1,\, l\neq i,j}^{N}(\lambda_i-\lambda_l)(\lambda_j-\lambda_l)} \int_{\left(\frac{1}{\Gamma_0}+\frac{\lambda_j}{\Gamma_I}\right)y}^{\left(\frac{1}{\Gamma_0}+\frac{\lambda_i}{\Gamma_I}\right)y} \\ &\quad \exp\left(\frac{\Gamma_I u^2}{\lambda_i\lambda_j y} - u\left(\frac{\Gamma_I}{\lambda_i\lambda_j\Gamma_0}+\frac{1}{\lambda_i}+\frac{1}{\lambda_j}\right)\right) du. \end{aligned} \tag{5.50}$$

Substituting (5.50) into (5.47), the average BER of BPSK in correlated Rayleigh fading and CCI is derived as

$$\begin{aligned} P_e &= \frac{1}{2} - \frac{1}{2} \sum_{i,j\in\{1,\cdots,N\},\, i<j} \frac{(\lambda_i\lambda_j)^{N-2}}{(\lambda_i-\lambda_j)\prod_{l=1,\, l\neq i,j}^{N}(\lambda_i-\lambda_l)(\lambda_j-\lambda_l)} \left(\frac{\lambda_i}{\sqrt{1+\frac{1}{\Gamma_I}+\frac{1}{\lambda_i\Gamma_0}}} \right. \\ &\quad \left. - \frac{\lambda_j}{\sqrt{1+\frac{1}{\Gamma_I}+\frac{1}{\lambda_j\Gamma_0}}} \right) - \frac{1}{2\sqrt{\pi}} \sum_{i,j\in\{1,\cdots,N\},\, i<j} \frac{(\lambda_i\lambda_j)^{N-2}}{(\lambda_i-\lambda_j)\prod_{l=1,\, l\neq i,j}^{N}(\lambda_i-\lambda_l)(\lambda_j-\lambda_l)} \\ &\quad \int_0^{\infty} dy \int_{\left(\frac{1}{\Gamma_0}+\frac{\lambda_j}{\Gamma_I}\right)y}^{\left(\frac{1}{\Gamma_0}+\frac{\lambda_i}{\Gamma_I}\right)y} y^{-\frac{1}{2}} \exp\left(\frac{\Gamma_I u^2}{\lambda_i\lambda_j y} - u\left(\frac{\Gamma_I}{\lambda_i\lambda_j\Gamma_0}+\frac{1}{\lambda_i}+\frac{1}{\lambda_j}\right) - y\right) du. \end{aligned} \tag{5.51}$$

Letting $u = yx$, (5.51) can be further simplified in closed form as

$$P_e = \frac{1}{2} - \frac{1}{2} \sum_{i,j \in \{1,\cdots,N\},\, i<j} \frac{(\lambda_i \lambda_j)^{N-2}}{(\lambda_i - \lambda_j) \prod_{l=1,\, l \neq i,j}^{N} (\lambda_i - \lambda_l)(\lambda_j - \lambda_l)} \left(\frac{\lambda_i}{\sqrt{1 + \frac{1}{\Gamma_I} + \frac{1}{\lambda_i \Gamma_0}}} - \frac{\lambda_j}{\sqrt{1 + \frac{1}{\Gamma_I} + \frac{1}{\lambda_j \Gamma_0}}} \right) - \frac{1}{4} \sum_{i,j \in \{1,\cdots,N\},\, i<j} \frac{(\lambda_i \lambda_j)^{N-2}}{(\lambda_i - \lambda_j) \prod_{l=1,\, l \neq i,j}^{N} (\lambda_i - \lambda_l)(\lambda_j - \lambda_l)} \int_{C_3^j}^{C_4^i} \frac{1}{(1 + C_2^{i,j} x - C_1^{i,j} x^2)^{3/2}} dx \tag{5.52}$$

where $C_1^{i,j} = \Gamma_I/(\lambda_i \lambda_j)$, $C_2^{i,j} = \left(1/\lambda_i + 1/\lambda_j + \Gamma_I/(\lambda_i \lambda_j \Gamma_0)\right)$, $C_3^j = (1/\Gamma_0 + \lambda_j/\Gamma_I)$, and $C_4^i = (1/\Gamma_0 + \lambda_i/\Gamma_I)$, and the integration term $\int_{C_3^j}^{C_4^i} 1/(1 + C_2^{i,j} x - C_1^{i,j} x^2)^{3/2} dx$ can be calculated by [6, eq. (2.264.5)]

$$\int \frac{dx}{\sqrt{R^3}} = \int \frac{dx}{\sqrt{(a + bx + cx^2)^3}} = \frac{2(2cx + b)}{\Delta \sqrt{a + bx + cx^2}} \tag{5.53}$$

where $\Delta = 4ac - b^2$. Eq. (5.52) is a new closed-form expression for the BER of coherent BPSK using MRC in CCI and correlated Rayleigh fading for the case when the correlation matrix has different eigenvalues.

When $\Gamma_0 = \infty$, namely the noise is negligible, (5.52) becomes

$$P_e = \frac{1}{2} - \frac{1}{2} \sqrt{\frac{\Gamma_I}{1 + \Gamma_I}} - \frac{1}{4} \sum_{i,j \in \{1,\cdots,N\},\, i<j} \frac{(\lambda_i \lambda_j)^{N-2}}{(\lambda_i - \lambda_j) \prod_{l=1,\, l \neq i,j}^{N} (\lambda_i - \lambda_l)(\lambda_j - \lambda_l)} \int_{\frac{\lambda_j}{\Gamma_I}}^{\frac{\lambda_i}{\Gamma_I}} \frac{1}{\left(1 + \left(\frac{1}{\lambda_i} + \frac{1}{\lambda_j}\right) x - \frac{\Gamma_I}{\lambda_i \lambda_j} x^2\right)^{3/2}} dx. \tag{5.54}$$

When $\Gamma_I = \infty$, namely the interference is negligible, (5.52) becomes the average BER for coherent BPSK using MRC in additive white Gaussian noise and correlated Rayleigh fading, namely,

$$P_e = \frac{1}{2} - \frac{1}{2} \sum_{i,j \in \{1,\cdots,N\},\, i<j} \frac{(\lambda_i \lambda_j)^{N-2}}{(\lambda_i - \lambda_j) \prod_{l=1,\, l \neq i,j}^{N} (\lambda_i - \lambda_l)(\lambda_j - \lambda_l)} \times \left(\lambda_i \sqrt{\frac{\lambda_i \Gamma_0}{1 + \lambda_i \Gamma_0}} - \lambda_j \sqrt{\frac{\lambda_j \Gamma_0}{1 + \lambda_j \Gamma_0}} \right). \tag{5.55}$$

Eq. (5.55) is a new closed-form expression for the average BER of coherent BPSK using MRC in correlated Rayleigh fading valid for the case when the correlation matrix has different eigenvalues.

5.4.2 Case II: Equi-Correlated Correlation Matrix

Substituting (5.19) into (5.49), the CDF of γ_{BER} is given by

$$\begin{aligned} F_{\gamma_{BER}}(y) &= \frac{1}{(N-2)!\lambda_1\lambda_2^{N-1}(\lambda_1-\lambda_2)^{N-1}}\left[\int_0^{\left(\frac{\lambda_2}{\Gamma_I}+\frac{1}{\Gamma_0}\right)y} du\int_{\lambda_2 u}^{\lambda_1 u} e^{\frac{w}{\lambda_1\lambda_2}-\left(\frac{1}{\lambda_1}+\frac{1}{\lambda_2}\right)u}\times\right. \\ &\left.(\lambda_1 u-w)^{N-2}dw+\int_{\left(\frac{\lambda_2}{\Gamma_I}+\frac{1}{\Gamma_0}\right)y}^{\left(\frac{\lambda_1}{\Gamma_I}+\frac{1}{\Gamma_0}\right)y} du\int_{\frac{\Gamma_I u^2}{y}-\frac{\Gamma_I u}{\Gamma_0}}^{\lambda_1 u} e^{\frac{w}{\lambda_1\lambda_2}-\left(\frac{1}{\lambda_1}+\frac{1}{\lambda_2}\right)u}(\lambda_1 u-w)^{N-2}dw\right] \\ &= 1-\left(\frac{\lambda_1}{\lambda_1-\lambda_2}\right)^{N-1}e^{-\left(\frac{1}{\Gamma_I}+\frac{1}{\Gamma_0\lambda_1}\right)y}+\frac{\lambda_2}{\lambda_1}\sum_{q=0}^{N-2}\sum_{l=0}^{q}\frac{1}{l!}\left(\frac{\lambda_1}{\lambda_1-\lambda_2}\right)^{N-1-q}\left(\frac{y}{\Gamma_I}+\frac{y}{\Gamma_0\lambda_2}\right)^{l} \\ &\times e^{-\left(\frac{1}{\Gamma_I}+\frac{1}{\Gamma_0\lambda_2}\right)y}-\frac{\lambda_1^{N-2}}{(\lambda_1-\lambda_2)^{N-1}}\sum_{q=0}^{N-2}\frac{1}{q!}\int_{\left(\frac{1}{\Gamma_0}+\frac{\lambda_2}{\Gamma_I}\right)y}^{\left(\frac{1}{\Gamma_0}+\frac{\lambda_1}{\Gamma_I}\right)y}\left(\frac{u}{\lambda_2}+\frac{\Gamma_I u}{\lambda_1\lambda_2\Gamma_0}-\frac{\Gamma_I u^2}{\lambda_1\lambda_2 y}\right)^{q} \\ &\times\exp\left(\frac{\Gamma_I u^2}{\lambda_1\lambda_2 y}-u\left(\frac{1}{\lambda_1}+\frac{1}{\lambda_2}+\frac{\Gamma_I}{\lambda_1\lambda_2\Gamma_0}\right)\right)du. \end{aligned} \tag{5.56}$$

Substituting (5.56) into (5.47) and combining with [6, eqs. (3.381.4), (8.339.2)], the average BER of coherent BPSK in equi-correlated Rayleigh fading and CCI is derived as

$$\begin{aligned} P_e &= \frac{1}{2}-\left(\frac{\lambda_1}{\lambda_1-\lambda_2}\right)^{N-1}\frac{1}{2\sqrt{1+\frac{1}{\Gamma_I}+\frac{1}{\Gamma_0\lambda_1}}}+\frac{\lambda_2}{\lambda_1}\sum_{q=0}^{N-2}\sum_{l=0}^{q}\frac{1}{l!}\left(\frac{\lambda_1}{\lambda_1-\lambda_2}\right)^{N-1-q} \\ &\times\left(\frac{1}{\Gamma_I}+\frac{1}{\Gamma_0\lambda_2}\right)^{l}\frac{(2l-1)!!}{2^{l+1}\left(1+\frac{1}{\Gamma_I}+\frac{1}{\Gamma_0\lambda_2}\right)^{l+1/2}}-\frac{\lambda_1^{N-2}}{2\sqrt{\pi}(\lambda_1-\lambda_2)^{N-1}}\sum_{q=0}^{N-2}\frac{1}{q!} \\ &\times\int_0^{\infty}dy\int_{\left(\frac{1}{\Gamma_0}+\frac{\lambda_2}{\Gamma_I}\right)y}^{\left(\frac{1}{\Gamma_0}+\frac{\lambda_1}{\Gamma_I}\right)y}y^{-\frac{1}{2}}\left(\frac{u}{\lambda_2}+\frac{\Gamma_I u}{\lambda_1\lambda_2\Gamma_0}-\frac{\Gamma_I u^2}{\lambda_1\lambda_2 y}\right)^{q} \\ &\times\exp\left(\frac{\Gamma_I u^2}{\lambda_1\lambda_2 y}-u\left(\frac{1}{\lambda_1}+\frac{1}{\lambda_2}+\frac{\Gamma_I}{\lambda_1\lambda_2\Gamma_0}\right)-y\right)du \end{aligned} \tag{5.57}$$

where $(2l-1)!!=1\cdot 3\cdot\cdots\cdot(2l-1)$ [6].

Similarly, letting $u = yx$, eq. (5.57) can be further simplified in closed form as

$$P_e = \frac{1}{2} - \left(\frac{\lambda_1}{\lambda_1-\lambda_2}\right)^{N-1} \frac{1}{2\sqrt{1+\frac{1}{\Gamma_I}+\frac{1}{\Gamma_0\lambda_1}}} + \frac{\lambda_2}{\lambda_1}\sum_{q=0}^{N-2}\sum_{l=0}^{q}\frac{1}{l!}\left(\frac{\lambda_1}{\lambda_1-\lambda_2}\right)^{N-1-q} \times \left(\frac{1}{\Gamma_I}+\frac{1}{\Gamma_0\lambda_2}\right)^{l} \frac{(2l-1)!!}{2^{l+1}\left(1+\frac{1}{\Gamma_I}+\frac{1}{\Gamma_0\lambda_2}\right)^{l+1/2}} - \frac{\lambda_1^{N-2}}{4(\lambda_1-\lambda_2)^{N-1}} \times \sum_{q=0}^{N-2}\frac{(2q+1)!!}{q!2^q}\int_{D_3}^{D_4}\frac{(D_5x-D_1x^2)^q}{(1+D_2x-D_1x^2)^{q+3/2}}dx \tag{5.58}$$

where $D_1 = \Gamma_I/(\lambda_1\lambda_2), D_2 = (1/\lambda_1+1/\lambda_2+D_1/\Gamma_0), D_3 = (1/\Gamma_0+\lambda_2/\Gamma_I), D_4 = (1/\Gamma_0+\lambda_1/\Gamma_I)$, and $D_5 = (1/\lambda_2+D_1/\Gamma_0)$. The integration term $\int_{D_3}^{D_4}(D_5x-D_1x^2)^q/(1+D_2x-D_1x^2)^{q+3/2}dx$ can be iteratively calculated in closed form by [6, eqs. (2.263) and (2.264)]. Eq. (5.58) is a new closed-form expression for BER of coherent BPSK using MRC in CCI and equi-correlated Rayleigh fading.

When $\Gamma_0 = \infty$, namely the noise is negligible, (5.58) becomes

$$P_e = \frac{1}{2} - \frac{1}{2}\left(\frac{\lambda_1}{\lambda_1-\lambda_2}\right)^{N-1}\sqrt{\frac{\Gamma_I}{1+\Gamma_I}} + \frac{\lambda_2}{\lambda_1}\sum_{q=0}^{N-2}\sum_{l=0}^{q}\frac{1}{l!}\left(\frac{\lambda_1}{\lambda_1-\lambda_2}\right)^{N-1-q} \times \frac{(2l-1)!!\sqrt{\Gamma_I}}{2^{l+1}(1+\Gamma_I)^{l+1/2}} - \frac{\lambda_1^{N-2}}{4(\lambda_1-\lambda_2)^{N-1}}\sum_{q=0}^{N-2}\frac{(2q+1)!!}{q!2^q} \times \int_{\frac{\lambda_2}{\Gamma_I}}^{\frac{\lambda_1}{\Gamma_I}} \frac{\left(\frac{x}{\lambda_2}-\frac{\Gamma_I x^2}{\lambda_1\lambda_2}\right)^q}{\left(1+\frac{x}{\lambda_1}+\frac{x}{\lambda_2}-\frac{\Gamma_I x^2}{\lambda_1\lambda_2}\right)^{q+3/2}}dx. \tag{5.59}$$

When $\Gamma_I = \infty$, (5.58) becomes the average BER for coherent BPSK using MRC in additive Gaussian noise and equi-correlated Rayleigh fading given by

$$P_e = \frac{1}{2} - \frac{1}{2}\left(\frac{\lambda_1}{\lambda_1-\lambda_2}\right)^{N-1}\sqrt{\frac{\Gamma_0\lambda_1}{1+\Gamma_0\lambda_1}} + \frac{\lambda_2}{\lambda_1}\sum_{q=0}^{N-2}\sum_{l=0}^{q}\frac{1}{l!}\left(\frac{\lambda_1}{\lambda_1-\lambda_2}\right)^{N-1-q} \times \frac{(2l-1)!!\sqrt{\Gamma_0\lambda_2}}{2^{l+1}(1+\Gamma_0\lambda_2)^{l+1/2}}. \tag{5.60}$$

Eq. (5.60) is a new closed-form expression for BER of coherent BPSK using MRC in equi-correlated Rayleigh fading.

5.4.3 Numerical Results

In this section, some numerical examples of the average BER of coherent BPSK in CCI and correlated Rayleigh fading are given. In our examples, we assume that the channel gain vector $\mathbf{c_n} = [x_{n,1} + jy_{n,1} \cdots x_{n,N} + jy_{n,N}]^T$ $(n = 0, \cdots, N_I)$ satisfies $\mathbb{E}[x_{n,i}x_{n,j}] = \mathbb{E}[y_{n,i}y_{n,j}]$ and $\mathbb{E}[x_{n,i}y_{n,j}] = \mathbb{E}[y_{n,i}x_{n,j}] = 0$ $(i, j = 1, \cdots, N)$, as used previously. The average power SIR $\Gamma_I = P_0/P_I$, and the average power SNR $\Gamma_0 = P_0/N_0$, as defined previously. Since the average BER depends only on the total interference power P_I, and is independent of the number of interfering users, $N_I = 6$ interfering users with equal powers are used for the average BER examples.

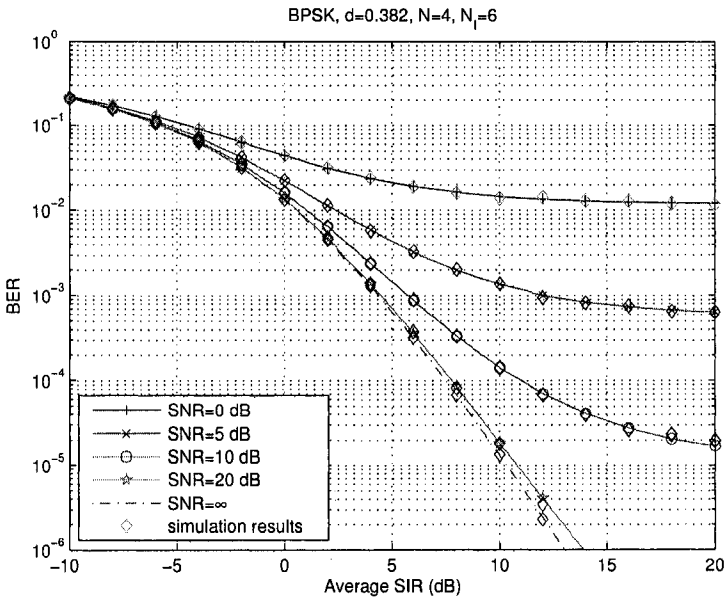

Fig. 5.5. The BER versus the average power SIR of BPSK using MRC diversity with $N = 4$, $d = 0.382$, and $N_I = 6$ equal-power interferers for different values of average power SNR.

Fig. 5.5 shows the average BER versus the average power SIR, Γ_I, of coherent BPSK using MRC for the channel model from [18] with $\Delta = \pi$, $N = 4$, for normalized spacing between any two adjacent antenna elements, $d = 0.382$. Different values of average power

SNR are considered, among which average power SNR= ∞ corresponds to the CCI-limited case. It is seen that the analytical results and the simulation results denoted by the diamond markers are in excellent agreement. Observe that an error rate floor appears for a fixed value of SNR when the average power SIR is large. This is because the average BER at large values of SIR is mainly affected by the fixed value of average power SNR when the noise dominates the cochannel interference. As expected, the error rate floor decreases with increasing average power SNR.

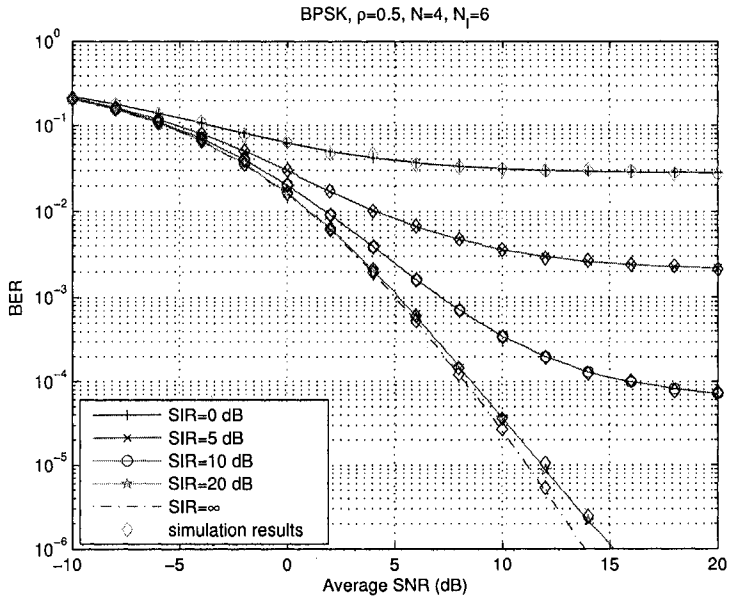

Fig. 5.6. The BER versus the average power SNR of BPSK using MRC diversity in equi-correlated Rayleigh fading with $N = 4$, $\rho = 0.5$, and $N_I = 6$ equal-power interferers for different values of average power SIR.

Fig. 5.6 shows the average BER as a function of the average power SNR of BPSK using MRC in equi-correlated Rayleigh fading with $N = 4$ receiver antennas and correlation coefficient $\rho = 0.5$ for different values of average power SIR, where average power SIR= ∞ corresponds to the noise-limited case. In this figure, one sees that when the interference dominates the noise, an error rate floor is established by the value of the SIR. The floor can be reduced by increasing the SIR, as expected.

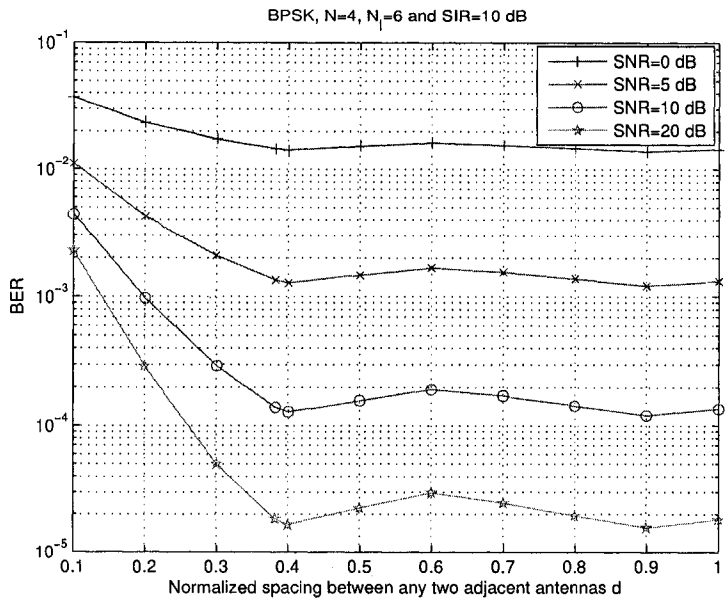

Fig. 5.7. The BER versus the normalized spacing between two adjacent antennas, d, of BPSK using MRC diversity with $N = 4$, $N_I = 6$ equal-power interferers, and average power SIR=10 dB for different values of average power SNR.

The effect of the normalized spacing between two adjacent antennas, d, on the average BER of BPSK is examined in Fig. 5.7. The channel model from [18] with $\Delta = \pi$ is considered for $N_I = 6$ equal-power interferers with average power SIR=10 dB. It is seen that the BERs when $d = 0.382$ and 0.4 are very close to the globally minimum BER at $d = 0.9$. Combining with the result from Fig. 5.3, $d = 0.382$ or 0.4 is an optimal choice to achieve a good compromise between the system performance and space limitations.

Fig. 5.8 shows the average BER versus the number of antennas, N, for BPSK with MRC when the total length of the antenna array is fixed to one-wavelength. Different values of average power SNR are considered. From this figure, one can see that the BER decreases with N. However the incremental benefit from increasing N decreases, especially when the average power SNR is large. Fig. 5.8 indicates a suitable number of antennas for the system design. For example, when SNR=20 dB, one may set $N = 6$ or 7 to achieve a good compromise between system performance and system cost for an antenna array of length

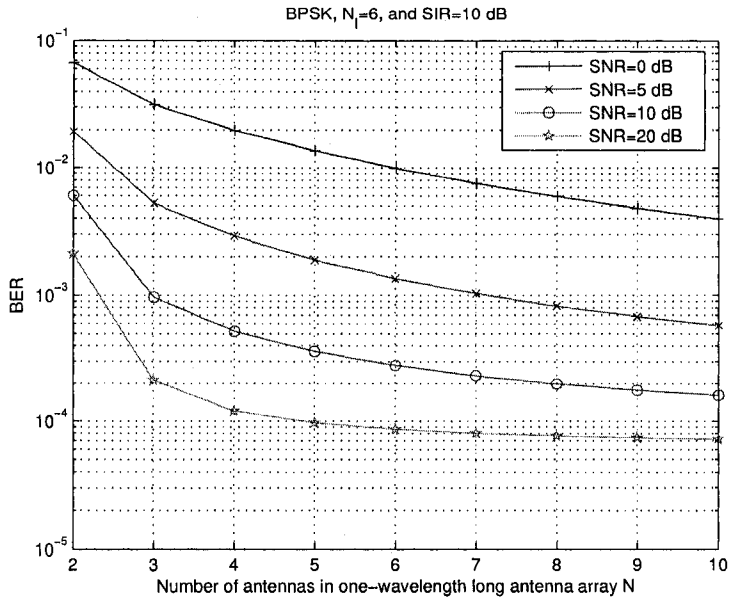

Fig. 5.8. The BER versus the total number of antennas, N, of BPSK using MRC diversity for a one-wavelength antenna array, with $N_I = 6$ equal-power interferers, and average power SIR=10 dB for different values of average power SNR.

one wavelength.

Fig. 5.9 shows the average BER versus the correlation coefficient, ρ, for coherent BPSK in equi-correlated Rayleigh fading with the average power SNR=10 dB for different values of average power SIR. It is seen that the BER generally increases with correlation coefficient ρ, as expected. Further, the performance degrades more significantly at large values of correlation coefficient ρ.

5.5 BER of BPSK with Imperfect Channel Estimation

In the following, we examine the effect of imperfect channel estimation on the BER performance. First we describe the channel estimation model. Then two cases that the correlation matrix has different eigenvalues and that the correlation matrix is equi-correlated, are studied and presented with some numerical results.

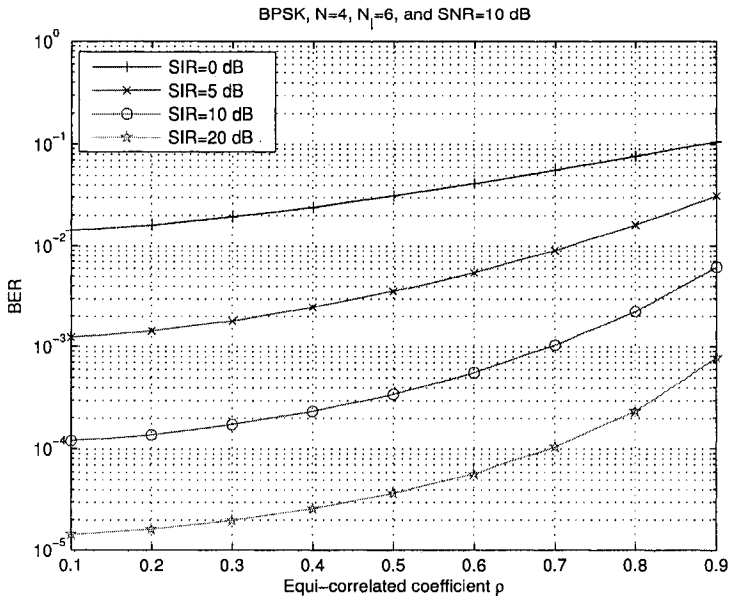

Fig. 5.9. The BER versus the correlation coefficient, ρ, of BPSK using MRC in equi-correlated Rayleigh fading with $N = 4$ and $N_I = 6$ equal-power interferers for different values of average power SIR.

5.5.1 Channel Estimation Model

Let $\tilde{\mathbf{c_0}}$ denote the estimate of the branch gain vector for the desired user $\mathbf{c_0}$, assumed to be zero-mean complex Gaussian with covariance matrix $\Sigma_{\tilde{\mathbf{c_0}}}$. Then the output after the MRC combiner is obtained by replacing $\mathbf{w_0}$ in (5.2) with $\tilde{\mathbf{c_0}}$

$$r = \tilde{\mathbf{c_0}}^H \mathbf{r} = \sqrt{P_0}(\tilde{\mathbf{c_0}}^H \mathbf{c_0}) d_0 + \sum_{n=1}^{N_I} \sqrt{P_n}(\tilde{\mathbf{c_0}}^H \mathbf{c_n}) d_n + (\tilde{\mathbf{c_0}}^H \mathbf{z_0}). \tag{5.61}$$

We assume that even in the presence of interferers, the Gaussian approximation of the channel estimation error is still valid as discussed in [96] and that the relationship between the branch gain vector $\mathbf{c_0}$ and its estimate $\tilde{\mathbf{c_0}}$ satisfies [92], [99]

$$\mathbf{c_0} = \alpha \tilde{\mathbf{c_0}} + \mathbf{e} \tag{5.62}$$

where $\tilde{\mathbf{c_0}}$ and $\mathbf{e}$ are independent complex Gaussian vectors with zero mean and covariance matrices $\Sigma_{\tilde{\mathbf{c_0}}}$ and $\Sigma_{\mathbf{e}}$, respectively. α is a complex number representing the normalized

correlation between the elements of $\mathbf{c_0}$ and $\tilde{\mathbf{c}}_0$. Note that the analysis in this paper can be easily extended to the situation where the covariance matrices Σ and $\Sigma_{\tilde{c}_0}$ satisfy $\Sigma = a\Sigma_{\tilde{c}_0} + bI$ for non-negative real values of a and b. For simplicity, we assume here that the branch gain vector $\mathbf{c_0}$ and its estimate $\tilde{\mathbf{c}}_0$ have the same covariance matrix, namely, $\Sigma_{\tilde{c}_0} = \Sigma$. Then, the covariance matrix of $\mathbf{e}$ is given by

$$\Sigma_{\mathbf{e}} = (1 - |\alpha|^2)\Sigma, \qquad |\alpha| \leq 1. \tag{5.63}$$

From (5.62) and (5.63), one can see that $|\alpha| = 1$ corresponds to the case that the channel estimation error is a phase error on the channel gain, and there is no Gaussian error, namely, $\mathbf{c_0} = e^{j\theta}\tilde{\mathbf{c}}_0$, where θ is a phase difference between $\mathbf{c_0}$ and $\tilde{\mathbf{c}}_0$. Specially, $\alpha = 1$ corresponds to perfect channel estimation.

5.5.2 Average BER of BPSK

At the receiver, the decision variable after the MRC combiner is given by

$$D = Re\{r\} = \sqrt{P_0}Re\{(\tilde{\mathbf{c}}_0^H \mathbf{c_0})\}d_0 + \sum_{n=1}^{N_I} \sqrt{P_n}Re\{(\tilde{\mathbf{c}}_0^H \mathbf{c_n})\}d_n + Re\{(\tilde{\mathbf{c}}_0^H \mathbf{z_0})\}. \tag{5.64}$$

Without loss of generality, assume that $d_0 = +1$ is transmitted. Since $\mathbf{c_n}$ $(n = 1, \cdots, N_I)$ and $\mathbf{z_0}$ are independent zero-mean Gaussian distributed, and independent of $\mathbf{c_0}$ and $\tilde{\mathbf{c}}_0$, the average BER for the desired user conditioned on $\mathbf{c_0}$, $\tilde{\mathbf{c}}_0$, and the interfering information bits d_n $(n = 1, \cdots, N_I)$ denoted by $D_{N_I} = \{d_1, d_2, \cdots, d_{N_I}\}$, is given by

$$\begin{aligned} P_{e|\mathbf{c_0},\tilde{\mathbf{c}}_0,D_{N_I}} &= \Pr(D < 0 | \mathbf{c_0}, \tilde{\mathbf{c}}_0, D_{N_I}) \\ &= \Pr\left(\sqrt{P_0}Re\{(\tilde{\mathbf{c}}_0^H \mathbf{c_0})\} + \sum_{n=1}^{N_I} \sqrt{P_n}Re\{(\tilde{\mathbf{c}}_0^H \mathbf{c_n})\}d_n + Re\{(\tilde{\mathbf{c}}_0^H \mathbf{z_0})\} < 0 \right) \\ &= Q\left(\frac{\sqrt{2P_0}Re\{\tilde{\mathbf{c}}_0^H \mathbf{c_0}\}}{\sqrt{P_I(\tilde{\mathbf{c}}_0^H \Sigma \tilde{\mathbf{c}}_0) + N_0(\tilde{\mathbf{c}}_0^H \tilde{\mathbf{c}}_0)}} \right) \end{aligned} \tag{5.65}$$

where $P_I = \sum_{n=1}^{N_I} P_n$ is the total interference power, as defined previously. From (5.65), one can see that the conditional BER is independent of the interfering information bits

d_n $(n = 1, \cdots, N_I)$ as well as the individual interference powers, P_n $(n = 1, \cdots, N_I)$, and only depends on the total interference power P_I.

Substituting (5.62) into (5.65), the conditional BER becomes

$$P_{e|\tilde{\mathbf{c}}_0,\mathbf{e}} = Q\left(\frac{\sqrt{2P_0}(Re\{\alpha\}(\tilde{\mathbf{c}}_0{}^H\tilde{\mathbf{c}}_0)+Re\{\tilde{\mathbf{c}}_0{}^H\mathbf{e}\})}{\sqrt{N_0(\tilde{\mathbf{c}}_0{}^H\tilde{\mathbf{c}}_0)+P_I(\tilde{\mathbf{c}}_0{}^H\Sigma\tilde{\mathbf{c}}_0)}}\right). \tag{5.66}$$

Since $\mathbf{e}$ is a zero-mean complex Gaussian vector with covariance matrix $(1-|\alpha|^2)\Sigma$, and is independent of $\tilde{\mathbf{c}}_0$, averaging (5.66) over $\mathbf{e}$ and combining with [91, eq. (18)], one obtains

$$\begin{aligned} P_{e|\tilde{\mathbf{c}}_0} &= \mathbb{E}_{\mathbf{e}}(P_{e|\tilde{\mathbf{c}}_0,\mathbf{e}}) \\ &= Q\left(sign\{Re\{\alpha\}\}\sqrt{\frac{2(Re\{\alpha\})^2P_0(\tilde{\mathbf{c}}_0{}^H\tilde{\mathbf{c}}_0)^2}{N_0(\tilde{\mathbf{c}}_0{}^H\tilde{\mathbf{c}}_0)+(P_I+P_0(1-|\alpha|^2))(\tilde{\mathbf{c}}_0{}^H\Sigma\tilde{\mathbf{c}}_0)}}\right) \\ &= Q\left(\hat{\beta}\sqrt{2\gamma_{ICE}}\right) \end{aligned} \tag{5.67}$$

where $\beta = Re\{\alpha\}$, $\hat{\beta} = sign\{\beta\}$ denotes the signum function of the real number β, and γ_{ICE} is given by

$$\gamma_{ICE} = \frac{\beta^2P_0(\tilde{\mathbf{c}}_0{}^H\tilde{\mathbf{c}}_0)^2}{N_0(\tilde{\mathbf{c}}_0{}^H\tilde{\mathbf{c}}_0)+(P_I+P_0(1-|\alpha|^2))(\tilde{\mathbf{c}}_0{}^H\Sigma\tilde{\mathbf{c}}_0)}. \tag{5.68}$$

Let $\tilde{u} = \tilde{\mathbf{v}}^H\Lambda\tilde{\mathbf{v}}$, and $\tilde{w} = \tilde{\mathbf{v}}^H\Lambda^2\tilde{\mathbf{v}}$, where Λ is the diagonal matrix composed of the eigenvalues of covariance matrix Σ, as defined in Section 5.3, and $\tilde{\mathbf{v}} = \Lambda^{-1/2}U^H\tilde{\mathbf{c}}_0$ is a complex Gaussian vector with zero mean and unit variance I. Then (5.68) becomes

$$\begin{aligned} \gamma_{ICE} &= \frac{\beta^2P_0\tilde{u}^2}{N_0\tilde{u}+(P_I+P_0(1-|\alpha|^2))\tilde{w}} \\ &= \frac{P_0'\tilde{u}^2}{N_0\tilde{u}+P_I'\tilde{w}} \end{aligned} \tag{5.69}$$

where $P_0' = \beta^2P_0$, and $P_I' = P_I+(1-|\alpha|^2)P_0$.

Averaging (5.67) over γ_{ICE}, the BER of BPSK is given by

$$\begin{aligned} P_e &= \int_0^\infty Q(\hat{\beta}\sqrt{2t})f_{\gamma_{ICE}}(t)dt \\ &= Q(\hat{\beta}\times\infty)+\frac{\hat{\beta}}{2\sqrt{\pi}}\int_0^\infty t^{-1/2}e^{-t}F_{\gamma_{ICE}}(t)dt \\ &= \begin{cases} \frac{1}{2\sqrt{\pi}}\int_0^\infty t^{-1/2}e^{-t}F_{\gamma_{ICE}}(t)dt & , \quad \hat{\beta}=+1 \\ 1-\frac{1}{2\sqrt{\pi}}\int_0^\infty t^{-1/2}e^{-t}F_{\gamma_{ICE}}(t)dt & , \quad \hat{\beta}=-1 \end{cases} \end{aligned} \tag{5.70}$$

where the functions $f_{\gamma_{ICE}}(\cdot)$ and $F_{\gamma_{ICE}}(\cdot)$ represent the PDF and the CDF of the random variable γ_{ICE}, respectively.

Since (5.69) has a similar expression as (5.48), one can use the results in Section 5.4 to calculate the CDF of γ_{ICE} in (5.69) by replacing P_0 and P_I in Section 5.4 with $P_0^{'}$ and $P_I^{'}$ for the two cases that the correlation matrix has different eigenvalues and that the correlation matrix is equi-correlated.

5.5.3 Case I: Correlation Matrix With Different Eigenvalues

Assume all of the eigenvalues λ_i are not equal, and satisfy $\lambda_1 > \lambda_2 > \cdots > \lambda_N > 0$. The CDF of γ_{ICE} can be obtained from (5.50)

$$\begin{aligned} F_{\gamma_{ICE}}(y) &= 1-\exp\left(-\frac{y(1-|\alpha|^2+1/\Gamma_I)}{\beta^2}\right)\times \\ &\sum_{i,j\in\{1,\cdots,N\},\, i<j} \frac{(\lambda_i\lambda_j)^{N-2}\left(\lambda_i e^{-y/(\lambda_i\beta^2\Gamma_0)}-\lambda_j e^{-y/(\lambda_j\beta^2\Gamma_0)}\right)}{(\lambda_i-\lambda_j)\prod_{l=1,\, l\neq i,j}^{N}(\lambda_i-\lambda_l)(\lambda_j-\lambda_l)} - \\ &\sum_{i,j\in\{1,\cdots,N\},\, i<j} \frac{(\lambda_i\lambda_j)^{N-2}}{(\lambda_i-\lambda_j)\prod_{l=1,\, l\neq i,j}^{N}(\lambda_i-\lambda_l)(\lambda_j-\lambda_l)}\times \\ &\int_{\left(\frac{1}{\Gamma_0}+\frac{\lambda_j}{\Gamma_I}+\lambda_j(1-|\alpha|^2)\right)\frac{y}{\beta^2}}^{\left(\frac{1}{\Gamma_0}+\frac{\lambda_i}{\Gamma_I}+\lambda_i(1-|\alpha|^2)\right)\frac{y}{\beta^2}} \exp\left(\frac{\beta^2\Gamma_I u^2}{\lambda_i\lambda_j y(1+(1-|\alpha|^2)\Gamma_I)}-\right. \\ &\left. u\left(\frac{\Gamma_I}{\lambda_i\lambda_j\Gamma_0(1+(1-|\alpha|^2)\Gamma_I)}+\frac{1}{\lambda_i}+\frac{1}{\lambda_j}\right)\right)du \end{aligned} \tag{5.71}$$

where $\Gamma_0 = P_0/N_0$ is the average power SNR, and $\Gamma_I = P_0/P_I$ is the average power SIR as defined previously.

Substituting (5.71) into (5.70), the average BER of BPSK in correlated Rayleigh fading

and cochannel interference is derived as

$$
\begin{aligned}
P_e &= \frac{1}{2} - \frac{\hat{\beta}}{2} \sum_{i,j\in\{1,\cdots,N\},\, i<j} \frac{(\lambda_i\lambda_j)^{N-2}}{(\lambda_i-\lambda_j)\prod_{l=1,\, l\neq i,j}^{N}(\lambda_i-\lambda_l)(\lambda_j-\lambda_l)} \\
&\times \left(\frac{\lambda_i}{\sqrt{1+\frac{1}{\beta^2\Gamma_I}+\frac{1}{\lambda_i\beta^2\Gamma_0}+\frac{1-|\alpha|^2}{\beta^2}}} - \frac{\lambda_j}{\sqrt{1+\frac{1}{\beta^2\Gamma_I}+\frac{1}{\lambda_j\beta^2\Gamma_0}+\frac{1-|\alpha|^2}{\beta^2}}} \right) \\
&- \frac{\hat{\beta}}{2\sqrt{\pi}} \sum_{i,j\in\{1,\cdots,N\},\, i<j} \frac{(\lambda_i\lambda_j)^{N-2}}{(\lambda_i-\lambda_j)\prod_{l=1,\, l\neq i,j}^{N}(\lambda_i-\lambda_l)(\lambda_j-\lambda_l)} \\
&\int_0^{\infty} dy \int_{\left(\frac{1}{\Gamma_0}+\frac{\lambda_j}{\Gamma_I}+\lambda_j(1-|\alpha|^2)\right)\frac{y}{\beta^2}}^{\left(\frac{1}{\Gamma_0}+\frac{\lambda_i}{\Gamma_I}+\lambda_i(1-|\alpha|^2)\right)\frac{y}{\beta^2}} y^{-\frac{1}{2}} \exp\left(\frac{\beta^2\Gamma_I u^2}{\lambda_i\lambda_j(1+(1-|\alpha|^2)\Gamma_I)y} - \right. \\
&\left. u\left(\frac{\Gamma_I}{\lambda_i\lambda_j\Gamma_0(1+(1-|\alpha|^2)\Gamma_I)} + \frac{1}{\lambda_i} + \frac{1}{\lambda_j} \right) - y \right) du. \qquad (5.72)
\end{aligned}
$$

Using [98, eq. (3)], (5.72) is further simplified in closed-form as

$$
\begin{aligned}
P_e &= \frac{1}{2} - \frac{\hat{\beta}}{2} \sum_{i,j\in\{1,\cdots,N\},\, i<j} \frac{(\lambda_i\lambda_j)^{N-2}}{(\lambda_i-\lambda_j)\prod_{l=1,\, l\neq i,j}^{N}(\lambda_i-\lambda_l)(\lambda_j-\lambda_l)} \\
&\times \left(\frac{\lambda_i}{\sqrt{1+\frac{1}{\beta^2\Gamma_I}+\frac{1}{\lambda_i\beta^2\Gamma_0}+\frac{1-|\alpha|^2}{\beta^2}}} - \frac{\lambda_j}{\sqrt{1+\frac{1}{\beta^2\Gamma_I}+\frac{1}{\lambda_j\beta^2\Gamma_0}+\frac{1-|\alpha|^2}{\beta^2}}} \right) \\
&- \frac{\hat{\beta}}{4} \sum_{i,j\in\{1,\cdots,N\},\, i<j} \frac{(\lambda_i\lambda_j)^{N-2}}{(\lambda_i-\lambda_j)\prod_{l=1,\, l\neq i,j}^{N}(\lambda_i-\lambda_l)(\lambda_j-\lambda_l)} \\
&\times \int_{E_3^j}^{E_4^i} \frac{1}{(1+E_2^{i,j}x-E_1^{i,j}x^2)^{3/2}} dx \qquad (5.73)
\end{aligned}
$$

where $E_1^{i,j} = \beta^2\Gamma_I/[\lambda_i\lambda_j(1+(1-|\alpha|^2)\Gamma_I)]$, $E_2^{i,j} = 1/\lambda_i + 1/\lambda_j + \Gamma_I/(\lambda_i\lambda_j\Gamma_0(1+(1-|\alpha|^2)\Gamma_I))$, $E_3^j = \left(1/\Gamma_0 + \lambda_j/\Gamma_I + \lambda_j(1-|\alpha|^2)\right)/\beta^2$, and $E_4^i = \left(1/\Gamma_0 + \lambda_i/\Gamma_I + \lambda_i(1-|\alpha|^2)\right)/\beta^2$. When $\alpha = 1$, (5.73) becomes (5.52) corresponding to the case of perfect channel estimation.

When $\Gamma_0 = \infty$, namely the noise is negligible, (5.73) becomes

$$\begin{aligned} P_e &= \frac{1}{2} - \frac{\hat{\beta}}{2}\sqrt{\frac{\beta^2\Gamma_I}{1+(\beta^2+1-|\alpha|^2)\Gamma_I}} - \frac{\hat{\beta}}{4}\sum_{i,j\in\{1,\cdots,N\},\, i<j} \\ &\quad \frac{(\lambda_i\lambda_j)^{N-2}}{(\lambda_i-\lambda_j)\prod_{l=1,\, l\neq i,j}^{N}(\lambda_i-\lambda_l)(\lambda_j-\lambda_l)} \\ &\quad \times \int_{F_3^j}^{F_4^i}\left(1+\left(\frac{1}{\lambda_i}+\frac{1}{\lambda_j}\right)x - E_1^{i,j}x^2\right)^{-3/2} dx \end{aligned} \tag{5.74}$$

where $F_3^j = \lambda_j\left(1/\Gamma_I + 1 - |\alpha|^2\right)/\beta^2$ and $F_4^i = \lambda_i\left(1/\Gamma_I + 1 - |\alpha|^2\right)/\beta^2$.

When $\Gamma_I = \infty$, namely the interference is negligible, (5.73) becomes the average BER for coherent BPSK using MRC in AWGN and correlated Rayleigh fading

$$\begin{aligned} P_e &= \frac{1}{2} - \frac{\hat{\beta}}{2}\sum_{i,j\in\{1,\cdots,N\},\, i<j} \frac{(\lambda_i\lambda_j)^{N-2}}{(\lambda_i-\lambda_j)\prod_{l=1,\, l\neq i,j}^{N}(\lambda_i-\lambda_l)(\lambda_j-\lambda_l)} \\ &\quad \times\left(\frac{\lambda_i}{\sqrt{1+\frac{1}{\lambda_i\beta^2\Gamma_0}+\frac{1-|\alpha|^2}{\beta^2}}} - \frac{\lambda_j}{\sqrt{1+\frac{1}{\lambda_j\beta^2\Gamma_0}+\frac{1-|\alpha|^2}{\beta^2}}}\right) \\ &\quad -\frac{\hat{\beta}}{4}\sum_{i,j\in\{1,\cdots,N\},\, i<j} \frac{(\lambda_i\lambda_j)^{N-2}}{(\lambda_i-\lambda_j)\prod_{l=1,\, l\neq i,j}^{N}(\lambda_i-\lambda_l)(\lambda_j-\lambda_l)} \\ &\quad \times\int_{G_3^j}^{G_4^i}\frac{1}{\left(1+G_2^{i,j}x - G_1^{i,j}x^2\right)^{3/2}}dx \end{aligned} \tag{5.75}$$

where $G_1^{i,j} = \beta^2/(\lambda_i\lambda_j(1-|\alpha|^2))$, $G_2^{i,j} = 1/(\lambda_i\lambda_j\Gamma_0(1-|\alpha|^2)) + 1/\lambda_i + 1/\lambda_j$, and $G_3^j = \left(1/\Gamma_0 + \lambda_j(1-|\alpha|^2)\right)/\beta^2$, and $G_4^i = \left(1/\Gamma_0 + \lambda_i(1-|\alpha|^2)\right)/\beta^2$.

5.5.4 Case II: Equi-Correlated Correlation Matrix

When all of the users experience equi-correlated Rayleigh fading with correlation coefficient ρ $(0 < \rho < 1)$, the CDF of γ_{ICE} is derived from (5.56)

$$F_{\gamma_{ICE}}(y) = 1 - \left(\frac{\lambda_1}{\lambda_1-\lambda_2}\right)^{N-1} e^{-\left(\frac{1}{\Gamma_I}+\frac{1}{\Gamma_0\lambda_1}+1-|\alpha|^2\right)\frac{y}{\beta^2}} + \frac{\lambda_2}{\lambda_1}\sum_{q=0}^{N-2}\sum_{l=0}^{q}\frac{1}{l!}\left(\frac{\lambda_1}{\lambda_1-\lambda_2}\right)^{N-1-q}$$
$$\times\left(\frac{y}{\beta^2}\right)^{l}\left(\frac{1}{\Gamma_I}+\frac{1}{\Gamma_0\lambda_2}+1-|\alpha|^2\right)^{l} e^{-\left(\frac{1}{\Gamma_I}+\frac{1}{\Gamma_0\lambda_2}+1-|\alpha|^2\right)\frac{y}{\beta^2}} - \frac{\lambda_1^{N-2}}{(\lambda_1-\lambda_2)^{N-1}}\sum_{q=0}^{N-2}\frac{1}{q!}$$
$$\times\int_{\left(\frac{1}{\Gamma_0}+\frac{\lambda_2}{\Gamma_I}+\lambda_2(1-|\alpha|^2)\right)\frac{y}{\beta^2}}^{\left(\frac{1}{\Gamma_0}+\frac{\lambda_1}{\Gamma_I}+\lambda_1(1-|\alpha|^2)\right)\frac{y}{\beta^2}}\left(\frac{u}{\lambda_2}+\frac{\Gamma_I u}{\lambda_1\lambda_2\Gamma_0(1+(1-|\alpha|^2)\Gamma_I)}-\frac{\beta^2\Gamma_I u^2}{\lambda_1\lambda_2 y(1+(1-|\alpha|^2)\Gamma_I)}\right)^{q}$$
$$\times\exp\left(\frac{\Gamma_I\beta^2u^2}{\lambda_1\lambda_2 y(1+(1-|\alpha|^2)\Gamma_I)}-u\left(\frac{1}{\lambda_1}+\frac{1}{\lambda_2}+\frac{\Gamma_I}{\lambda_1\lambda_2\Gamma_0(1+(1-|\alpha|^2)\Gamma_I)}\right)\right)du. \tag{5.76}$$

Substituting (5.76) into (5.70) and combining with [6, eqs. (3.381.4) and (8.339.2)], the average BER of coherent BPSK in equi-correlated Rayleigh fading and CCI is derived as

$$P_e = \frac{1}{2}-\frac{\hat{\beta}}{2}\left(\frac{\lambda_1}{\lambda_1-\lambda_2}\right)^{N-1}\frac{1}{\sqrt{1+\frac{1}{\beta^2\Gamma_I}+\frac{1}{\beta^2\Gamma_0\lambda_1}+\frac{1-|\alpha|^2}{\beta^2}}}+\frac{\hat{\beta}\lambda_2}{\lambda_1}\sum_{q=0}^{N-2}\sum_{l=0}^{q}\frac{(2l-1)!!}{l!2^{l+1}}$$
$$\times\left(\frac{\lambda_1}{\lambda_1-\lambda_2}\right)^{N-1-q}\frac{\sqrt{\beta^2\Gamma_0\Gamma_I\lambda_2}(\lambda_2\Gamma_0+(1-|\alpha|^2)\Gamma_0\Gamma_I\lambda_2+\Gamma_I)^{l}}{(\beta^2\Gamma_0\Gamma_I\lambda_2+\Gamma_0\lambda_2+\Gamma_0\Gamma_I\lambda_2(1-|\alpha|^2)+\Gamma_I)^{l+1/2}}$$
$$-\frac{\hat{\beta}\lambda_1^{N-2}}{2\sqrt{\pi}(\lambda_1-\lambda_2)^{N-1}}\sum_{q=0}^{N-2}\frac{1}{q!}\int_0^{\infty}dy\int_{\left(\frac{1}{\Gamma_0}+\frac{\lambda_2}{\Gamma_I}+\lambda_2(1-|\alpha|^2)\right)\frac{y}{\beta^2}}^{\left(\frac{1}{\Gamma_0}+\frac{\lambda_1}{\Gamma_I}+\lambda_1(1-|\alpha|^2)\right)\frac{y}{\beta^2}}y^{-\frac{1}{2}}$$
$$\times\left(\frac{u}{\lambda_2}+\frac{\Gamma_I u}{\lambda_1\lambda_2\Gamma_0(1+(1-|\alpha|^2)\Gamma_I)}-\frac{\beta^2\Gamma_I u^2}{\lambda_1\lambda_2 y(1+(1-|\alpha|^2)\Gamma_I)}\right)^{q}$$
$$\times\exp\left(\frac{\beta^2\Gamma_I u^2}{\lambda_1\lambda_2 y(1+(1-|\alpha|^2)\Gamma_I)}-u\left(\frac{1}{\lambda_1}+\frac{1}{\lambda_2}+\frac{\Gamma_I}{\lambda_1\lambda_2\Gamma_0(1+(1-|\alpha|^2)\Gamma_I)}\right)-y\right)du \tag{5.77}$$

where $(2l-1)!! = 1\cdot 3\cdot\cdots\cdot(2l-1)$ [6].

Eq. (5.77) is further simplified in closed-form as

$$P_e = \frac{1}{2} - \frac{\hat{\beta}}{2}\left(\frac{\lambda_1}{\lambda_1-\lambda_2}\right)^{N-1} \frac{1}{\sqrt{1+\frac{1}{\beta^2\Gamma_I}+\frac{1}{\beta^2\Gamma_0\lambda_1}+\frac{1-|\alpha|^2}{\beta^2}}} + \frac{\hat{\beta}\lambda_2}{\lambda_1}\sum_{q=0}^{N-2}\sum_{l=0}^{q}\frac{(2l-1)!!}{l!2^{l+1}}$$
$$\times\left(\frac{\lambda_1}{\lambda_1-\lambda_2}\right)^{N-1-q} \frac{\sqrt{\beta^2\Gamma_0\Gamma_I\lambda_2}(\lambda_2\Gamma_0+(1-|\alpha|^2)\Gamma_0\Gamma_I\lambda_2+\Gamma_I)^l}{(\beta^2\Gamma_0\Gamma_I\lambda_2+\Gamma_0\lambda_2+\Gamma_0\Gamma_I\lambda_2(1-|\alpha|^2)+\Gamma_I)^{l+1/2}} -$$
$$\frac{\hat{\beta}\lambda_1^{N-2}}{4(\lambda_1-\lambda_2)^{N-1}}\sum_{q=0}^{N-2}\frac{(2q+1)!!}{q!2^q}\int_{H_3}^{H_4}\frac{(H_5x-H_1x^2)^q}{(1+H_2x-H_1x^2)^{q+3/2}}dx \tag{5.78}$$

where $H_1 = \beta^2\Gamma_I/(\lambda_1\lambda_2(1+(1-|\alpha|^2)\Gamma_I))$, $H_2 = 1/\lambda_1 + 1/\lambda_2 + \Gamma_I/(\lambda_1\lambda_2\Gamma_0(1+(1-|\alpha|^2)\Gamma_I))$, $H_3 = \left(1/\Gamma_0 + \lambda_2/\Gamma_I + \lambda_2(1-|\alpha|^2)\right)/\beta^2$, $H_4 = \left(1/\Gamma_0 + \lambda_1/\Gamma_I + \lambda_1(1-|\alpha|^2)\right)/\beta^2$, $H_5 = (H_2 - 1/\lambda_1)$. Similarly, when $\alpha = 1$, (5.78) becomes (5.58) for the case of perfect channel estimation.

When $\Gamma_0 = \infty$, namely the noise is negligible, (5.78) becomes

$$P_e = \frac{1}{2} - \frac{\hat{\beta}}{2}\left(\frac{\lambda_1}{\lambda_1-\lambda_2}\right)^{N-1} \frac{1}{\sqrt{1+\frac{1}{\beta^2\Gamma_I}+\frac{1-|\alpha|^2}{\beta^2}}} + \frac{\hat{\beta}\lambda_2}{\lambda_1}\sum_{q=0}^{N-2}\sum_{l=0}^{q}\frac{(2l-1)!!}{l!2^{l+1}}$$
$$\left(\frac{\lambda_1}{\lambda_1-\lambda_2}\right)^{N-1-q} \frac{\sqrt{\beta^2\Gamma_I}(1+(1-|\alpha|^2)\Gamma_I)^l}{(1+\beta^2\Gamma_I+\Gamma_I(1-|\alpha|^2))^{l+1/2}} -$$
$$\frac{\hat{\beta}\lambda_1^{N-2}}{4(\lambda_1-\lambda_2)^{N-1}}\sum_{q=0}^{N-2}\frac{(2q+1)!!}{q!2^q}\int_{I_3}^{I_4}\frac{(x/\lambda_2-H_1x^2)^q}{\left(1+\left(\frac{1}{\lambda_1}+\frac{1}{\lambda_2}\right)x-H_1x^2\right)^{q+3/2}}dx \tag{5.79}$$

where $I_3 = \lambda_2\left(1/\Gamma_I + 1 - |\alpha|^2\right)/\beta^2$ and $I_4 = \lambda_1\left(1/\Gamma_I + 1 - |\alpha|^2\right)/\beta^2$.

When $\Gamma_I = \infty$, (5.78) becomes the average BER for coherent BPSK using MRC in additive Gaussian noise and equi-correlated Rayleigh fading given by

$$P_e = \frac{1}{2} - \frac{\hat{\beta}}{2}\left(\frac{\lambda_1}{\lambda_1-\lambda_2}\right)^{N-1} \frac{1}{\sqrt{1+\frac{1}{\beta^2\Gamma_0\lambda_1}+\frac{1-|\alpha|^2}{\beta^2}}} + \frac{\hat{\beta}\lambda_2}{\lambda_1}\sum_{q=0}^{N-2}\sum_{l=0}^{q}\frac{(2l-1)!!}{l!2^{l+1}}$$
$$\left(\frac{\lambda_1}{\lambda_1-\lambda_2}\right)^{N-1-q} \frac{\sqrt{\beta^2\Gamma_0\lambda_2}((1-|\alpha|^2)\Gamma_0\lambda_2+1)^l}{(\beta^2\Gamma_0\lambda_2+\Gamma_0\lambda_2(1-|\alpha|^2)+1)^{l+1/2}} -$$
$$\frac{\hat{\beta}\lambda_1^{N-2}}{4(\lambda_1-\lambda_2)^{N-1}}\sum_{q=0}^{N-2}\frac{(2q+1)!!}{q!2^q}\int_{J_3}^{J_4}\frac{(J_5x-J_1x^2)^q}{(1+J_2x-J_1x^2)^{q+3/2}}dx \tag{5.80}$$

where $J_1 = \beta^2/(\lambda_1\lambda_2(1-|\alpha|^2))$, $J_2 = 1/\lambda_1 + 1/\lambda_2 + 1/(\lambda_1\lambda_2\Gamma_0(1-|\alpha|^2))$, $J_3 = (1/\Gamma_0 + \lambda_2(1-|\alpha|^2))/\beta^2$, $J_4 = (1/\Gamma_0 + \lambda_1(1-|\alpha|^2))/\beta^2$, and $J_5 = (J_2 - 1/\lambda_1)$.

5.5.5 Numerical Results

In this section, some numerical examples of the average BER of coherent BPSK using MRC with imperfect MMSE channel estimation in CCI and correlated Rayleigh fading are given. Noting that the average BER depends only on the total interference power P_I, and is independent of the number of interfering users, the examples use $N_I = 6$ equal-power interfering users for the average BER examples.

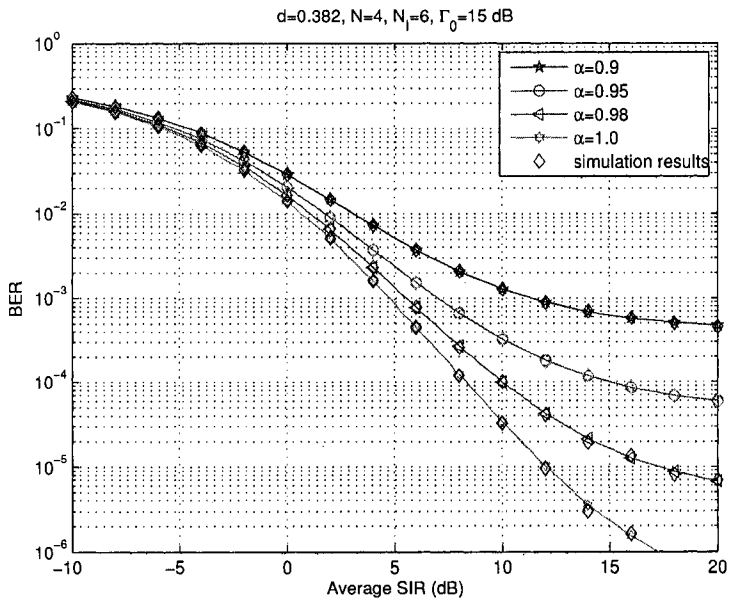

Fig. 5.10. The BER versus the average power SIR of BPSK using MRC diversity with $N = 4$, $d = 0.382$, $\Gamma_0 = 15$ dB, and $N_I = 6$ equal-power interferers for different real values of α.

Fig. 5.10 shows the average BER versus the average power SIR, Γ_I, of coherent BPSK using MRC for the channel model from [18] with $\Delta = \pi$, $N = 4$, and $\Gamma_0 = 15$ dB, for normalized spacing between any two adjacent antenna elements, $d = 0.382$. Different real

values of α are considered, among which $\alpha = 1.0$ corresponds to the perfect channel estimation case. It is seen that the analytical results and the simulation results denoted by the diamond markers are in excellent agreement. In a combined CCI plus AWGN environment, an error rate floor must occur for large values of SIR due to the AWGN. However, the channel estimation error also contributes to the error floor. Observe that the error rate floor with imperfect channel estimation is much greater than that for the case with perfect channel estimation. As expected, the error rate floor decreases as the magnitude of α increases.

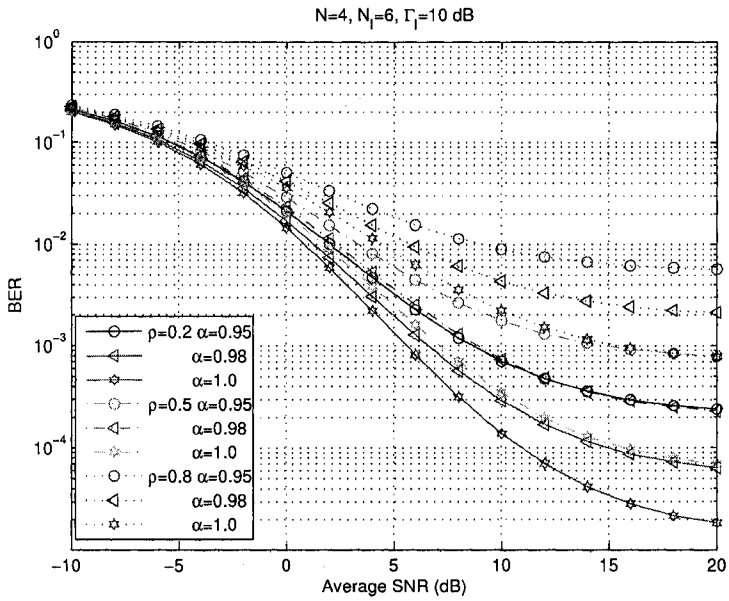

Fig. 5.11. The BER versus the average power SNR of BPSK using MRC diversity in equi-correlated Rayleigh fading with $N = 4$, $\Gamma_I = 10$ dB, and $N_I = 6$ equal-power interferers for different values of α and ρ.

Fig. 5.11 shows the average BER as a function of the average power SNR, Γ_0, of BPSK using MRC in equi-correlated Rayleigh fading with $N = 4$ receiver antennas, and $\Gamma_I = 10$ dB, for different values of α and correlation coefficient ρ. In this figure, one sees that the error rate floor can be reduced by increasing the magnitude of α or decreasing ρ, as expected.

Fig. 5.12 shows the average BER versus the number of antennas, N, for BPSK with

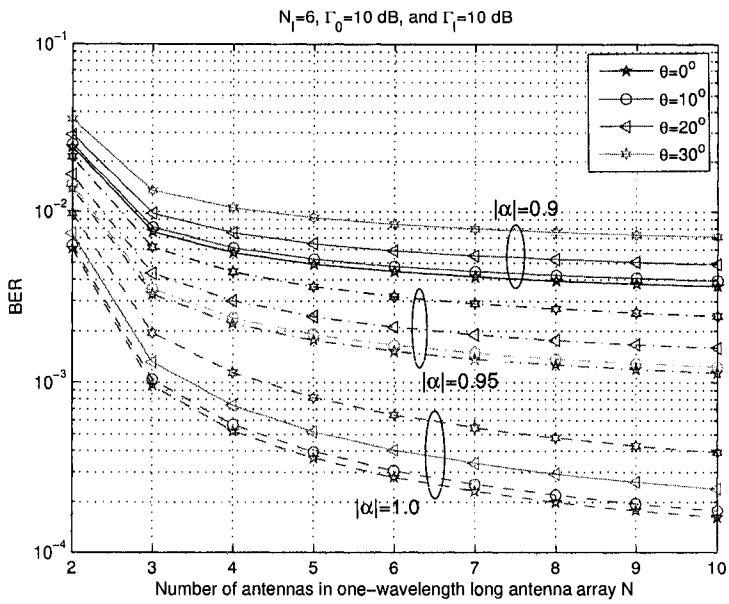

Fig. 5.12. The BER versus the total number of antennas, N, of BPSK using MRC diversity for a one-wavelength antenna array, with $N_I = 6$ equal-power interferers, $\Gamma_0 = 10$ dB, and $\Gamma_I = 10$ dB for different complex values of α.

MRC using the channel model from [18] when the total length of the antenna array is fixed at one-wavelength. Different complex values of α, where $\alpha = |\alpha|e^{j\theta}$, are considered. From this figure, one can see that the BER decreases with N. However the incremental benefit from increasing N decreases, especially when $|\alpha|$ is small. In addition, for a fixed value of $|\alpha|$, the BER increases with θ. Further, the degradation of BER from increasing θ increases with θ, as well.

5.6 Summary

In this chapter, explicit expressions for the outage probability of MRC output and closed-form expressions for the average BER of a coherent BPSK system with CCI and thermal noise in correlated Rayleigh fading were derived through the CDF of the MRC output SINR. Correlation matrices with different eigenvalues and with equi-correlated coefficients

were studied respectively. Further, closed-form expressions for the average BER of a coherent BPSK system with imperfect channel estimation in the presence of CCI and correlated Rayleigh fading were obtained. The effect of channel estimation error on the BER performance was examined for a special channel estimator. In contrast to previous results, these expressions do not require iterative numerical procedures for evaluation, although some well-behaved numerical integrations are required in the general cases for outage probability. The effects of average power SIR and average power SNR on the performances were examined through the numerical examples. In addition, new closed-form results for the BER of coherent BPSK in AWGN and correlated Rayleigh fading were also presented.

Chapter 6

Maximum Effective Number of MRC Receiver Antennas in Cochannel Interference and Correlated Ricean Fading

6.1 Introduction

Wireless antenna systems using multiple antennas at the receiver and/or the transmitter have attracted significant interest in recent years. Fundamental works [8], [9] show that the capacity of multiple antenna systems in independent Rayleigh fading grows linearly with the minimum number of transmitter antennas and receiver antennas. However, in practice, the assumption of independent fading can often be violated due to either insufficient spacing of antennas or the absence of a rich scattering environment around the transmitter and/or the receiver. In such situations, the correlation among the antennas influences the system capacity greatly [100], [101]. Several works suggest that there are fundamental physical limits to the capacity growth for fixed-size multiple antenna systems, independent of the number of antennas [11, 102–108]. These works touch on an interesting and practical ques-

tion; that is, from the viewpoint of system design, given a multiple antenna system with size constraints, how many antennas are needed to achieve a good compromise between system performance and system cost. All of the previous works except [104] [105] assume noise-limited environments. However, in cellular systems, cochannel interference is an important factor and cannot be ignored. Therefore, it is interesting to study the performance limits of a fixed-size multiple antenna system in the presence of interference. The study gives invaluable insights into the theory and practice of multiple antenna systems for CCI environments. For example, an important question is, how many antennas can be used in a given space (area or volume) before diminishing returns vitiate any worthwhile additional benefits to be achieved by adding additional antennas.

In this chapter, we examine how many receiver antennas should be employed in a given region of space in a receiver diversity system; in particular, we seek the performance limits and the optimal number of antennas. Our focus here is on the performance of economical MRC receiver diversity systems operating with a fixed-size antenna array in correlated Rayleigh and Ricean fading corrupted by cochannel interference. We do not consider the application of adaptive antenna arrays and interference nulling receivers, for which the reader is referred to references [18, 109, 110]. To illustrate this research topic clearly, we first consider the CCI-limited case. To conduct the investigations, we must find performance measures that will both be analytically tractable and meaningful practically. In order to test the consistency of the results and obtain broad perspectives, we employ four different measures, the long term output signal-power-to-interference-power ratio (SIRP), the long term signal amplitude to the square root of the interference power ratio (SAPR), the average instantaneous output signal-to-interference ratio (AISIR), and the average bit error rate. The use of SIRP and SAPR measures is motivated by analytical tractability, which permits obtaining analytical solutions for the present problems. The AISIR and the average BER measures are of greater interest in wireless system study and design, but do not lend themselves to tractable analytical solutions for the problems examined in our work, especially when the number of cochannel interferers in Ricean fading is large. Results in the sequel indicate that the tractable alternative measures can be used with small inaccuracy

in place of the clearly-motivated metrics to find the optimal number of antennas. Examples of linear antenna arrays [26] and circular antenna arrays [111] show that, in general, the four performance criteria when used to study the choice of the number of antennas for correlated Ricean fading have similar behaviors under the assumptions that the fadings of the desired user signal and the interfering signals have the same covariance matrix, and that the thermal noise is negligible. This means that one can use the easily obtained SIRP and SAPR measures to determine the optimal number of antennas for a fixed-size MRC diversity system, or as an excellent starting point for a search for the optimal number. Alternatively, the optimal number of antennas in the SIRP or SAPR sense can be used to achieve good BER and SIR performance at the same time, while being somewhat suboptimal in the average BER sense. Importantly, the results show that the performance of a fixed-size antenna array containing the maximum number of independent antennas in CCI-limited correlated Ricean fading cannot be significantly improved by adding more than one additional antenna [112], [113].

Then we extend our CCI-limited theory to a more practical system model in the presence of noise. We investigate the effect of noise on the determination of the maximum number of receiver antennas that can be usefully deployed in a MRC receiver diversity system with a fixed-size antenna array operating in correlated Ricean fading corrupted by CCI. Similar to the CCI-limited case, four different measures, the long term output signal-power-to-interference-plus-noise-power ratio (SINRP), the long term signal amplitude to the square root of interference plus noise power ratio (SAINPR), the average instantaneous output signal-to-interference-plus-noise ratio (AISINR), and the average BER are evaluated here. Examples in the sequel of linear antenna arrays and circular antenna arrays indicate that, in general, the four performance criteria have similar behaviors when used to study the choice of the number of antennas under the assumptions that the fadings of the desired user signal and the interfering signals have the same covariance matrix. This means that one can use the easily obtained SINRP and SAINPR measures to determine the maximum effective number of antennas for a fixed-size MRC diversity system, or as an excellent starting point for a search for the maximum effective number. Importantly, the results show that the previ-

ous design rule discovered for the case of CCI-limited environments that the performance of a fixed-size antenna array containing the maximum number of independent antennas cannot be significantly improved by adding more than one additional antenna, still applies for moderate and large values of interference-power-to-noise-power ratio (INRP). Further, for Rayleigh fading, the performance limits in the presence of noise when the number of antennas grows without bound are the same as the limits derived for the case of CCI-limited operation in Rayleigh fading without noise [112], [113].

The remainder of this chapter is organized as follows. The system model is described in Section 6.2. In Section 6.3, the long-term MRC output measures are presented. The average BER of coherent BPSK in the presence of arbitrary number of interfering users and arbitrarily correlated Ricean fading is analyzed in Section 6.4. Numerical results and discussion are given in Section 6.5. Finally, we give our conclusions in Section 6.6.

6.2 System Model

Assume that there are N antennas and N_I cochannel interfering user signals at the receiver with a fixed-size antenna array. Assume that the desired user signal and the interfering user signals are independent and experience slow and flat Ricean fadings. However, the fadings for each user at the N receiver antennas are correlated. Then, the received signal vector, $\mathbf{r}$, of length N consisting of components from the desired user and the N_I interfering users, has a baseband model representation given by

$$\mathbf{r} = \sqrt{P_0}\mathbf{c_0}d_0 + \sum_{n=1}^{N_I} \sqrt{P_n}\mathbf{c_n}d_n + \mathbf{z_0} \tag{6.1}$$

where P_n $(n = 0, 1, \cdots, N_I)$ represents the transmitter power of the nth user signal, and the index 0 corresponds to the desired user signal. The symbol d_n, denotes the information bit of the nth user signal, and has zero mean and unit variance. The complex vector $\mathbf{c_n}$ of length N represents the channel gains experienced by the nth user signal. Further, the fadings for each user are assumed to be correlated Ricean fadings with mean vector $\mu_{\mathbf{c_n}}$ and covariance matrix $\Sigma_{\mathbf{c_n}} = \mathbb{E}\{(\mathbf{c_n} - \mu_{\mathbf{c_n}})(\mathbf{c_n} - \mu_{\mathbf{c_n}})^H\}$. In this work, we assume that

all of the interfering signals have the same mean vector $\mu_{\mathbf{c_n}} = \mu_{\mathbf{c_I}}$ and covariance matrix $\Sigma_{\mathbf{c_n}} = \Sigma_{\mathbf{c_I}}$ $(n = 1, \cdots, N_I)$. The noise vector $\mathbf{z_0}$ is complex white (both temporally and spatially) Gaussian with zero mean and variance matrix $N_0 I$, where I is a $N \times N$ identity matrix. Then the output signal after the MRC combiner is given by

$$r = \mathbf{c_0}^H \mathbf{r} = \sqrt{P_0}(\mathbf{c_0}^H \mathbf{c_0}) d_0 + \sum_{n=1}^{N_I} \sqrt{P_n}(\mathbf{c_0}^H \mathbf{c_n}) d_n + (\mathbf{c_0}^H \mathbf{z_0}). \tag{6.2}$$

In this study, uniform linear arrays and uniform circular arrays with a two-dimensional (2D) omnidirectional scattering channel model and a three-dimensional (3D) omnidirectional scattering channel model are examined in the examples. In a 2D omnidirectional scattering environment, the correlation between two antennas is $J_0(2\pi l/\lambda_w)$ [26], where l is the distance between the two antennas, λ_w is the wavelength, and $J_0(\cdot)$ is the zeroth-order Bessel function of the first kind [26], [18]. For the case of 3D omnidirectional scattering environments, the correlation between two antennas is $sinc(2\pi l/\lambda_w)$, where $sinc(x) = sin(x)/x$, l is the distance between the two antennas and λ_w is the wavelength [114], [115].

6.3 Output Measures

In this section, we study three simple long-term MRC output measures. First we consider the CCI-limited case. Then we extend the results to include the effect of noise.

6.3.1 CCI-Limited Output Measures

SIRP

The long term output signal-power-to-interference-power ratio or SIRP is defined as the ratio of the average received desired signal power to the average received interfering signal power at the MRC combiner output given by

$$\gamma_{SIRP} = \frac{\mathbb{E}\{P_0 |\mathbf{c_0}^H \mathbf{c_0}|^2 d_0^2\}}{\mathbb{E}\{|\sum_{n=1}^{N_I} \sqrt{P_n}(\mathbf{c_0}^H \mathbf{c_n}) d_n|^2\}}. \tag{6.3}$$

Note that the expectations in (6.3) are over the data symbols, d_n, as well as the fading gains, $\mathbf{c_n}$. In the case where the data symbols and the fading gains are uncorrelated and all of the data symbols are uncorrelated with zero mean and unit variance, (6.3) becomes

$$\gamma_{SIRP} = \frac{P_0 \mathbb{E}\{|\mathbf{c_0}^H \mathbf{c_0}|^2\}}{\sum_{n=1}^{N_I} P_n \mathbb{E}\{|\mathbf{c_0}^H \mathbf{c_n}|^2\}} = \frac{\mathbb{E}\{(\mathbf{c_0}^H \mathbf{c_0})^2\}}{\sum_{n=1}^{N_I} \frac{1}{\Gamma_I^n} \mathbb{E}\{|\mathbf{c_0}^H \mathbf{c_n}|^2\}} \tag{6.4}$$

where $\Gamma_I^n = P_0/P_n$ $(n = 1, \cdots, N_I)$ is the ratio of the desired user transmitter signal power to the nth interfering user transmitter signal power, as defined in Chapter 5.

The long term SIRP in (6.4) can be calculated by

$$\gamma_{SIRP} = \frac{tr(\Sigma_{\mathbf{c_0}}^2) + 2(\mu_{\mathbf{c_0}}{}^H \Sigma_{\mathbf{c_0}} \mu_{\mathbf{c_0}}) + tr^2(R_{\mathbf{c_0}})}{\sum_{n=1}^{N_I} \frac{1}{\Gamma_I^n} tr(R_{\mathbf{c_0}} R_{\mathbf{c_n}})} \tag{6.5}$$

where $R_{\mathbf{c_n}} = \mathbb{E}\{\mathbf{c_n}\mathbf{c_n}^H\}$, is the correlation matrix of the fading vector for the nth user signal $\mathbf{c_n}$ $(n = 0, 1, \cdots, N_I)$, and $tr(\cdot)$ denotes the trace of a matrix. The detailed derivation of (6.5) from (6.4) is given in Appendix D.1. From (6.5), one can see that the SIRP depends only on the user signal powers and the statistics of the user channel fadings, that is, the covariance matrices $\Sigma_{\mathbf{c_n}}$ and the mean vectors $\mu_{\mathbf{c_n}}$ $(n = 0, \cdots, N_I)$.

Since we assume that $\Sigma_{\mathbf{c_n}} = \Sigma_{\mathbf{c_I}}$ and $\mu_{\mathbf{c_n}} = \mu_{\mathbf{c_I}}$ for the interfering user signals, (6.5) becomes

$$\gamma_{SIRP} = \frac{\Gamma_I [tr(\Sigma_{\mathbf{c_0}}^2) + 2(\mu_{\mathbf{c_0}}{}^H \Sigma_{\mathbf{c_0}} \mu_{\mathbf{c_0}}) + tr^2(R_{\mathbf{c_0}})]}{tr(R_{\mathbf{c_0}} R_{\mathbf{c_I}})} \tag{6.6}$$

where $R_{\mathbf{c_I}}$ is the correlation matrix for the interfering signals, and $\Gamma_I = P_0/P_I$ is the ratio of the desired user signal power to the total interference power with $P_I = \sum_{n=1}^{N_I} P_n$, as defined previously.

When $R_{\mathbf{c_0}} = R_{\mathbf{c_I}} = R_0$ and $\Sigma_{\mathbf{c_0}} = \Sigma_{\mathbf{c_I}} = \Sigma_0$, namely, all of the user signals have the same fading statistics, (6.6) becomes

$$\begin{aligned} \gamma_{SIRP} &= \frac{\Gamma_I [tr(R_0^2) - (\mu_{\mathbf{c_0}}{}^H \mu_{\mathbf{c_0}})^2 + tr^2(R_0)]}{tr(R_0^2)} \\ &= \Gamma_I \left(1 - \frac{(\mu_{\mathbf{c_0}}{}^H \mu_{\mathbf{c_0}})^2}{tr(R_0^2)} + \frac{tr^2(R_0)}{tr(R_0^2)}\right). \end{aligned} \tag{6.7}$$

When the channel experiences Rayleigh fading with $\mu_{\mathbf{c_n}} = \mathbf{0}$ $(n = 0, \cdots, N_I)$, (6.7) can be further simplified to

$$\gamma_{SIRP} = \Gamma_I \left(1 + \frac{tr^2(\Sigma_0)}{tr(\Sigma_0^2)}\right) = \Gamma_I \left(1 + \frac{tr^2(\Lambda_0)}{tr(\Lambda_0{}^2)}\right) \tag{6.8}$$

where Λ_0 is the diagonal matrix composed of the eigenvalues of Σ_0 with $\Sigma_0 = Q\Lambda_0 Q^H$, as is defined in Appendix D. For correlated Rayleigh fading, one can see that the SIRP only depends on the eigenvalues of the correlation matrix Σ_0 and the SIR power ratio Γ_I.

SAPR

Another useful and interesting measure is called here the long term average signal amplitude to the square root of interference power ratio or SAPR defined by

$$\gamma_{SAPR} = \frac{\mathbb{E}\{|\sqrt{P_0}(\mathbf{c_0}{}^H\mathbf{c_0})d_0|\}}{\sqrt{\mathbb{E}\{|\sum_{n=1}^{N_I}\sqrt{P_n}(\mathbf{c_0}{}^H\mathbf{c_n})d_n|^2\}}} = \frac{\mathbb{E}\{\mathbf{c_0}{}^H\mathbf{c_0}\}}{\sqrt{\sum_{n=1}^{N_I}\frac{1}{\Gamma_I^n}\mathbb{E}\{|\mathbf{c_0}{}^H\mathbf{c_n}|^2\}}}. \tag{6.9}$$

The use of the SAPR measure is motivated by the fact that in a BPSK system disturbed by additive Gaussian noise, the probability of error is given by $Q(A/\sigma)$ where A is the signal amplitude, σ is the square root of the noise power and $Q(x) = \int_x^\infty e^{-t^2/2}dt/\sqrt{2\pi}$; that is, the argument of the Q-function is the SAPR.

From Appendix D.1, we have that $\mathbb{E}\{u\} = \mathbb{E}\{\mathbf{c_0}{}^H\mathbf{c_0}\} = tr(R_{\mathbf{c_0}})$ and $\mathbb{E}\{|\mathbf{c_0}{}^H\mathbf{c_n}|^2\} = tr(R_{\mathbf{c_0}}R_{\mathbf{c_I}})$. Thus the SAPR in (6.9) becomes

$$\gamma_{SAPR} = \frac{tr(R_{\mathbf{c_0}})}{\sqrt{\sum_{n=1}^{N_I}\frac{1}{\Gamma_I^n}tr(R_{\mathbf{c_0}}R_{\mathbf{c_I}})}} = \sqrt{\frac{\Gamma_I tr^2(R_{\mathbf{c_0}})}{tr(R_{\mathbf{c_0}}R_{\mathbf{c_I}})}}. \tag{6.10}$$

Compared with the SIRP in (6.6), the expression for γ_{SAPR} in (6.10) is simpler. When $R_{\mathbf{c_0}} = R_{\mathbf{c_I}} = R_0$, (6.10) becomes

$$\gamma_{SAPR} = \sqrt{\Gamma_I \frac{tr^2(R_0)}{tr(R_0^2)}}. \tag{6.11}$$

Comparing the expression for the SAPR in (6.11) with the expression for the SIRP in (6.8), one sees that they are very similar in the case of Rayleigh fading; we will see in the sequel that these two measures give consistent results.

AISIR

The instantaneous output signal-to-interference ratio or SIR is defined by

$$\gamma_{SIR} = \frac{P_0|\mathbf{c_0}^H\mathbf{c_0}|^2}{\sum_{n=1}^{N_I} P_n|\mathbf{c_0}^H\mathbf{c_n}|^2} = \frac{|\mathbf{c_0}^H\mathbf{c_0}|^2}{\sum_{n=1}^{N_I} \frac{1}{\Gamma_I^n}|\mathbf{c_0}^H\mathbf{c_n}|^2}. \tag{6.12}$$

The average instantaneous output SIR or AISIR is calculated by averaging (6.12) over $\mathbf{c_n}$ $(n = 0, \cdots, N_I)$ to give

$$\gamma_{AISIR} = \mathbb{E}\{\gamma_{SIR}\} = \mathbb{E}\left\{\frac{|\mathbf{c_0}^H\mathbf{c_0}|^2}{\sum_{n=1}^{N_I} \frac{1}{\Gamma_I^n}|\mathbf{c_0}^H\mathbf{c_n}|^2}\right\}. \tag{6.13}$$

From (6.13), the AISIR measure is an expectation averaging over all of the user fadings. Owing to the correlation between the numerator and the denominator in the expression for γ_{SIR}, we were unable to derive an analytical result for the AISIR in generally correlated Ricean fading. In the sequel, we will use Monte Carlo simulation to assess the AISIR when both the desired user and the CCI are subjected to correlated Rayleigh and Ricean fading.

Limits of SIRP and SAPR in Correlated Rayleigh Fading

In this subsection, we will show that the SIRP and the SAPR reach a limit asymptotically as the number of antennas N increases without bound for the fixed-length uniform linear antenna array and the fixed-radius uniform circular antenna array when both the desired user signal and the interfering signals experience correlated Rayleigh fading with the same covariance matrix $\sum_0$.

We consider linear antenna arrays first. Assume that the antennas are uniformly placed in a linear array with length L. Further assume that the correlation between the ith antenna and the jth antenna, $\rho_{i,j} = \psi(|i-j|d)$, where d is the distance between two adjacent antennas, and $\psi(\cdot)$ represents a correlation function. Then, the limits of the SIRP and the SAPR for a linear antenna array are given, respectively, by

$$\lim_{N\to\infty} \gamma_{SIRP} = \Gamma_I\left(1 + \frac{L^2}{2\int_0^L (L-x)\psi^2(x)dx}\right) \tag{6.14}$$

and

$$\lim_{N\to\infty} \gamma_{SAPR} = L\sqrt{\frac{\Gamma_I}{2\int_0^L (L-x)\psi^2(x)dx}}. \tag{6.15}$$

The detailed derivations of (6.14) and (6.15) are given in Appendix D.2. Eqs. (6.14) and (6.15) indicate that there exist limits for the SIRP and the SAPR for linear antenna arrays, and hence the performance improves little by adding more antennas when N is large enough. Examples discussed in the sequel indicate that little performance enhancement is achieved by using more than the maximum number of independent antennas that can be accommodated in a region of space.

For example, for a linear antenna array in 2D omnidirectional scattering, the limits of the SIRP and the SAPR are given, respectively, by

$$\begin{aligned} \lim_{N\to\infty} \gamma_{SIRP} &= \Gamma_I \left(1 + \frac{L^2/2}{\int_0^L (L-x) J_0^2(2\pi x/\lambda_w)dx}\right) \\ &= \Gamma_I \left(1 + \frac{L_0^2/2}{\int_0^{L_0} (L_0-x) J_0^2(2\pi x)dx}\right) \end{aligned} \tag{6.16}$$

and

$$\begin{aligned} \lim_{N\to\infty} \gamma_{SAPR} &= L\sqrt{\frac{\Gamma_I}{2\int_0^L (L-x) J_0^2(2\pi x/\lambda_w)dx}} \\ &= L_0\sqrt{\frac{\Gamma_I}{2\int_0^{L_0} (L_0-x) J_0^2(2\pi x)dx}} \end{aligned} \tag{6.17}$$

where L_0 is the ratio of the array length L to the wavelength λ_w.

Similar results can be derived for circular antenna arrays with a fixed radius L. Assume that the correlation between the ith antenna and the jth antenna, $\rho_{i,j} = \psi(d_{i,j}) = \varphi(|i-j|\theta)$, where $d_{ij} = L\sqrt{2-2\cos(|i-j|\theta)}$ is the distance between the ith and the jth antennas, θ is the angle between two adjacent antennas, and $\psi(\cdot)$ represents a correlation function. Then the limits of the SIRP and the SAPR for a circular antenna array are given, respectively, by

$$\lim_{N\to\infty} \gamma_{SIRP} = \Gamma_I \left(1 + \frac{2\pi^2}{\int_0^{2\pi} (2\pi-\theta)\varphi^2(\theta)d\theta}\right) \tag{6.18}$$

and

$$\lim_{N\to\infty} \gamma_{SAPR} = \pi\sqrt{\frac{2\Gamma_I}{\int_0^{2\pi} (2\pi-\theta)\varphi^2(\theta)d\theta}}. \tag{6.19}$$

For example, the limits of the SIRP and the SAPR for a circular antenna array in 3D omnidirectional scattering are given by

$$\lim_{N\to\infty} \gamma_{SIRP} = \Gamma_I \left(1 + \frac{2\pi^2}{\int_0^{2\pi} (2\pi - \theta) sinc^2(2\pi L_0 \sqrt{2 - 2\cos\theta}) d\theta} \right) \tag{6.20}$$

and

$$\lim_{N\to\infty} \gamma_{SAPR} = \pi \sqrt{\frac{2\Gamma_I}{\int_0^{2\pi} (2\pi - \theta) sinc^2(2\pi L_0 \sqrt{2 - 2\cos\theta}) d\theta}}. \tag{6.21}$$

We will see in the sequel that the SIRP and the SAPR approach their limiting values very quickly as N increases beyond the maximum number of independent antennas.

6.3.2 The Effect of Noise

Now let us consider the effect of noise on the long-term MRC output measures.

SINRP

The long term output signal-power-to-interference-plus-noise-power ratio or SINRP is defined as the ratio of the average received desired signal power to the average received interference-power-plus-noise-power at the combiner output given by

$$\begin{aligned} \gamma_{SINRP} &= \frac{\mathbb{E}\{P_0 |\mathbf{c_0}^H \mathbf{c_0}|^2 d_0^2\}}{\mathbb{E}\{|\sum_{n=1}^{N_I} \sqrt{P_n} (\mathbf{c_0}^H \mathbf{c_n}) d_n + (\mathbf{c_0}^H \mathbf{z_0})|^2\}} \\ &= \frac{P_0 \mathbb{E}\{(\mathbf{c_0}^H \mathbf{c_0})^2\}}{\sum_{n=1}^{N_I} P_n \mathbb{E}\{|\mathbf{c_0}^H \mathbf{c_n}|^2\} + \mathbb{E}\{|\mathbf{c_0}^H \mathbf{z_0}|^2\}}. \end{aligned} \tag{6.22}$$

The long term SINRP of the MRC system in correlated Ricean fading can be derived from Appendix D as

$$\gamma_{SINRP} = \frac{tr(\Sigma_{\mathbf{c_0}}^2) + 2(\mu_{\mathbf{c_0}}{}^H \Sigma_{\mathbf{c_0}} \mu_{\mathbf{c_0}}) + tr^2(R_{\mathbf{c_0}})}{\sum_{n=1}^{N_I} \frac{1}{\Gamma_I} tr(R_{\mathbf{c_0}} R_{\mathbf{c_n}}) + \frac{1}{\Gamma_0} tr(R_{\mathbf{c_0}})} \tag{6.23}$$

where $\Gamma_0 = P_0/N_0$, denotes the ratio of the desired signal power to the noise power as defined previously. Since we assume that $\Sigma_{\mathbf{c_n}} = \Sigma_{\mathbf{c_I}}$ and $\mu_{\mathbf{c_n}} = \mu_{\mathbf{c_I}}$ for the interfering user

signals, (6.23) becomes

$$\gamma_{SINRP} = \frac{tr(\Sigma_{\mathbf{c}_0}^2) + 2(\mu_{\mathbf{c}_0}{}^H \Sigma_{\mathbf{c}_0} \mu_{\mathbf{c}_0}) + tr^2(R_{\mathbf{c}_0})}{\frac{1}{\Gamma_I} tr(R_{\mathbf{c}_0} R_{\mathbf{c}_I}) + \frac{1}{\Gamma_0} tr(R_{\mathbf{c}_0})} \tag{6.24}$$

where $R_{\mathbf{c}_I}$ is the correlation matrix for the interfering signals, and $\Gamma_I = P_0/P_I$ is the ratio of the desired user signal power to the total interfering power as defined previously.

When $R_{\mathbf{c}_0} = R_{\mathbf{c}_I} = R_0$ and $\Sigma_{\mathbf{c}_0} = \Sigma_{\mathbf{c}_I} = \Sigma_0$, namely, all of the user signals have the same fading statistics, (6.24) becomes

$$\gamma_{SINRP} = \frac{tr(R_0^2) - (\mu_{\mathbf{c}_0}{}^H \mu_{\mathbf{c}_0})^2 + tr^2(R_0)}{\frac{1}{\Gamma_I} tr(R_0^2) + \frac{1}{\Gamma_0} tr(R_0)}. \tag{6.25}$$

When the channel experiences Rayleigh fading with $\mu_{\mathbf{c}_n} = \mathbf{0}$ $(n = 0, \cdots, N_I)$, (6.25) can be further simplified to

$$\gamma_{SINRP} = \frac{tr(\Sigma_0^2) + tr^2(\Sigma_0)}{\frac{1}{\Gamma_I} tr(\Sigma_0^2) + \frac{1}{\Gamma_0} tr(\Sigma_0)} = \frac{tr(\Lambda_0^2) + tr^2(\Lambda_0)}{\frac{1}{\Gamma_I} tr(\Lambda_0^2) + \frac{1}{\Gamma_0} tr(\Lambda_0)} \tag{6.26}$$

where Λ_0 is the diagonal matrix composed of the eigenvalues of Σ_0, as defined in Appendix D. For correlated Rayleigh fading, one can see that the SINRP only depends on the eigenvalues of the correlation matrix Σ_0, the average power SIR Γ_I, and the average power SNR Γ_0.

SAINPR

The long term average signal amplitude to the square root of interference power plus noise power ratio or SAINPR is defined by

$$\begin{aligned} \gamma_{SAINPR} &= \frac{\mathbb{E}\{|\sqrt{P_0}(\mathbf{c}_0{}^H \mathbf{c}_0) d_0|\}}{\sqrt{\mathbb{E}\{|\sum_{n=1}^{N_I} \sqrt{P_n}(\mathbf{c}_0{}^H \mathbf{c}_n) d_n + (\mathbf{c}_0{}^H \mathbf{z}_0)|^2\}}} \\ &= \frac{\sqrt{P_0}\mathbb{E}\{\mathbf{c}_0{}^H \mathbf{c}_0\}}{\sqrt{\sum_{n=1}^{N_I} P_n \mathbb{E}\{|\mathbf{c}_0{}^H \mathbf{c}_n|^2\} + \mathbb{E}\{|\mathbf{c}_0{}^H \mathbf{z}_0|^2\}}}. \end{aligned} \tag{6.27}$$

The SAINPR in (6.27) can be calculated by

$$\gamma_{SAINPR} = \sqrt{\frac{tr^2(R_{\mathbf{c}_0})}{\sum_{n=1}^{N_I} \frac{1}{\Gamma_I} tr(R_{\mathbf{c}_0} R_{\mathbf{c}_I}) + \frac{1}{\Gamma_0} tr(R_{\mathbf{c}_0})}}. \tag{6.28}$$

When $R_{\mathbf{c_0}} = R_{\mathbf{c_I}} = R_0$, (6.28) becomes

$$\gamma_{SAINPR} = \sqrt{\frac{tr^2(R_0)}{\frac{1}{\Gamma_I} tr(R_0^2) + \frac{1}{\Gamma_0} tr(R_0)}}. \tag{6.29}$$

Comparing the expression for the SAINPR in (6.29) with the expression for the SINRP in (6.26), one sees that they are very similar in the case of Rayleigh fading.

AISINR

The instantaneous output signal-to-interference-plus-noise ratio or SINR is given by

$$\gamma_{SINR} = \frac{P_0 |\mathbf{c_0}^H \mathbf{c_0}|^2}{\sum_{n=1}^{N_I} P_n |\mathbf{c_0}^H \mathbf{c_n}|^2 + |\mathbf{c_0}^H \mathbf{z_0}|^2}. \tag{6.30}$$

Averaging (6.30) over $\mathbf{c_n}$ $(n = 0, \cdots, N_I)$ gives the average instantaneous output SINR or AISINR as

$$\gamma_{AISINR} = \mathbb{E}\{\gamma_{SINR}\} = \mathbb{E}\left\{ \frac{P_0 |\mathbf{c_0}^H \mathbf{c_0}|^2}{\sum_{n=1}^{N_I} P_n |\mathbf{c_0}^H \mathbf{c_n}|^2 + |\mathbf{c_0}^H \mathbf{z_0}|^2} \right\}. \tag{6.31}$$

From (6.31), the AISINR measure is an expectation averaging over all of the user fadings. Owing to the correlation between the numerator and the denominator in the expression for γ_{SINR}, we were unable to derive an analytical result for the AISINR in generally correlated Ricean fading. In the sequel, we will use Monte Carlo simulation to assess the AISINR when both the desired user and the CCI are subjected to correlated Ricean fading.

Limits of SINRP and SAINPR in Correlated Rayleigh Fading

In Section 6.3.1, it was shown that the SIRP and the SAPR attain limits asymptotically as the number of correlated antennas grows without bound. These results were derived there, however, under a noiseless assumption. It may not be clear whether the limits exist, or if the limits exist whether the limits are the same for the noiseless case and when noise is present. In this part, we will show that when additive noise is present, the SINRP and the SAINPR reach a limit asymptotically as the number of antennas N increases without bound for the fixed-length linear antenna array and the fixed-radius circular antenna array when both the

desired user signal and the interfering signals experience correlated Rayleigh fading with the same covariance matrix Σ_0.

We consider linear antenna arrays first. Assume that the antennas are uniformly placed in a linear array with length L. Then, the SINRP in (6.26) can be rewritten as

$$\gamma_{SINRP} = \frac{(L+d)^2 + d(L+d) + 2d\sum_{i=1}^{L/d} d\psi^2(id) + 2\sum_{i=1}^{L/d}(L-id)\psi^2(id)d}{d(L+d)(\frac{1}{\Gamma_I}+\frac{1}{\Gamma_0}) + \frac{2d}{\Gamma_I}\sum_{i=1}^{L/d} d\psi^2(id) + \frac{2}{\Gamma_I}\sum_{i=1}^{L/d}(L-id)\psi^2(id)d} \tag{6.32}$$

where $L = (N-1)d$. When $N \to \infty$, and $d \to 0$, the limit of γ_{SINRP} for a linear antenna array is given by

$$\lim_{N\to\infty} \gamma_{SINRP} = \Gamma_I \left(1 + \frac{L^2}{2\int_0^L (L-x)\psi^2(x)dx}\right). \tag{6.33}$$

Similarly, the limit of γ_{SAINPR} for a linear antenna array is given by

$$\lim_{N\to\infty} \gamma_{SAINPR} = L\sqrt{\frac{\Gamma_I}{2\int_0^L (L-x)\psi^2(x)dx}}. \tag{6.34}$$

Note that the limits of the long term SINRP and SAINPR in (6.33) and (6.34) are independent of the noise power, and are the same as the limits of γ_{SIRP} and γ_{SAPR} for fixed-length linear antenna arrays in CCI-limited Rayleigh fading given in (6.14) and (6.15) in Section 6.3.1. That is, the effect of noise on the SINRP and the SAINPR in Rayleigh fading can be ignored when the number of antennas N is large enough.

Similar results can be derived for circular antenna arrays with a fixed radius L. The limits of the SINRP and the SAINPR for a circular antenna array are given, respectively, by

$$\lim_{N\to\infty} \gamma_{SINRP} = \Gamma_I \left(1 + \frac{2\pi^2}{\int_0^{2\pi}(2\pi-\theta)\varphi^2(\theta)d\theta}\right) \tag{6.35}$$

and

$$\lim_{N\to\infty} \gamma_{SAINPR} = \pi\sqrt{\frac{2\Gamma_I}{\int_0^{2\pi}(2\pi-\theta)\varphi^2(\theta)d\theta}}. \tag{6.36}$$

Again, the limits of the long term SINRP and SAINPR for fixed-radius circular antenna arrays in (6.35) and (6.36) are the same as the limits of γ_{SIRP} and γ_{SAPR} derived for fixed-radius circular antenna arrays in CCI-limited Rayleigh fading given in (6.18) and (6.19) in Section 6.3.1.

6.4 Average BER of BPSK in Correlated Ricean Fading

In this section, we assume that all of the user signals are BPSK modulated, namely, the information bit of the nth user signal, d_n $(n = 0, \cdots, N_I)$, takes values from $\{+1, -1\}$ with equal probabilities. Further, we assume that both the covariance matrix of the desired signal, $\Sigma_{\mathbf{c_0}}$, and that of the interfering signals, $\Sigma_{\mathbf{c_I}}$, have the same eigenvector matrix Q, namely, the covariance matrices satisfy $\Sigma_{\mathbf{c_0}} = Q\Lambda_0 Q^H$ and $\Sigma_{\mathbf{c_I}} = Q\Lambda_I Q^H$, where $QQ^H = Q^H Q = I$, and Λ_0 and Λ_I are the diagonal matrices composed of the eigenvalues of the corresponding covariance matrices. Then the decision variable after the MRC combiner is given by

$$D = Re\{r\} = \sqrt{P_0}(\mathbf{c_0}^H \mathbf{c_0})d_0 + \sum_{n=1}^{N_I} \sqrt{P_n} Re\{(\mathbf{c_0}^H \mathbf{c_n})\} d_n + Re\{\mathbf{c_0}^H \mathbf{z_0}\} \tag{6.37}$$

where $Re\{z\}$ denotes the real part operation on the complex number z. Without loss of generality, assume that $d_0 = +1$ is transmitted, then the average BER conditioned on $\mathbf{c_0}$ and the data set $D_{N_I} = \{d_1, \cdots, d_{N_I}\}$ for the desired user, is given by

$$\begin{aligned} P_{e|\mathbf{c_0}, D_{N_I}} &= \Pr(D < 0 | d_0 = +1, \mathbf{c_0}, D_{N_I}) \\ &= \Pr\left((\mathbf{c_0}^H \mathbf{c_0}) + \sum_{n=1}^{N_I} \frac{d_n}{\sqrt{\Gamma_I^n}} Re\{(\mathbf{c_0}^H \mathbf{c_n})\} + \frac{1}{\sqrt{P_0}} Re\{\mathbf{c_0}^H \mathbf{z_0}\} < 0 \right). \end{aligned} \tag{6.38}$$

One can show that $Y = (\mathbf{c_0}^H \mathbf{c_0}) + \sum_{n=1}^{N_I} d_n Re\{(\mathbf{c_0}^H \mathbf{c_n})\}/\sqrt{\Gamma_I^n} + Re\{\mathbf{c_0}^H \mathbf{z_0}\}/\sqrt{P_0}$ conditioned on $\mathbf{c_0}$ and D_{N_I}, is a Gaussian RV with mean $\mu_Y = (\mathbf{c_0}^H \mathbf{c_0}) + \sum_{n=1}^{N_I} d_n Re\{\mathbf{c_0}^H \mu_{\mathbf{c_I}}\}/\sqrt{\Gamma_I^n}$ and variance $\sigma_Y^2 = (\mathbf{c_0}^H \Sigma_{\mathbf{c_I}} \mathbf{c_0})/(2\Gamma_I) + (\mathbf{c_0}^H \mathbf{c_0})/(2\Gamma_0)$. Then the MGF of Y conditioned on $\mathbf{c_0}$ and D_{N_I} is given by [35]

$$\begin{aligned} \phi_{Y|\mathbf{c_0}, D_{N_I}}(s) &= \mathbb{E}_{Y|\mathbf{c_0}, D_{N_I}}\{e^{sY}\} = e^{s\mu_Y + (s^2\sigma_Y^2)/2} \\ &= \exp\left(s(\mathbf{c_0}^H \mathbf{c_0}) + sb(\mathbf{c_0}^H \mu_{\mathbf{c_I}} + \mu_{\mathbf{c_I}}{}^H \mathbf{c_0}) + s^2 a_1 (\mathbf{c_0}^H \textstyle\sum_{\mathbf{c_I}} \mathbf{c_0}) + s^2 a_2 (\mathbf{c_0}^H \mathbf{c_0}) \right) \end{aligned} \tag{6.39}$$

where $a_1 = 1/(4\Gamma_I)$, $a_2 = 1/(4\Gamma_0)$, and $b = \sum_{n=1}^{N_I} d_n/(2\sqrt{\Gamma_I^n})$. Note that the random variable b is a function of the data set D_{N_I}; therefore, the MGF of Y conditioned on D_{N_I} is

equivalent to the MGF of Y conditioned on b. Substituting $\mathbf{v_0} = \Lambda_0^{-1/2} Q^H \mathbf{c_0}$ into (6.39), the conditional MGF of Y becomes

$$\begin{aligned}
\phi_{Y|\mathbf{c_0},D_{N_I}}(s) &= \phi_{Y|\mathbf{c_0},b}(s) \\
&= \exp\left((s+a_2s^2)(\mathbf{v_0}^H\Lambda_0\mathbf{v_0}) + sb(\mathbf{v_0}^H\mu_\mathbf{I} + \mu_\mathbf{I}^H\mathbf{v_0}) + a_1s^2(\mathbf{v_0}^H\Lambda_0\Lambda_I\mathbf{v_0})\right) \\
&= \prod_{i=1}^{N} \exp\left((s\lambda_0^i + a_1s^2\lambda_0^i\lambda_I^i + a_2s^2\lambda_0^i)|v_0^i|^2 + bs(\mu_I^i(v_0^i)^H + (\mu_I^i)^H v_0^i)\right)
\end{aligned} \tag{6.40}$$

where $\mu_\mathbf{I} = \Lambda_0^{1/2} Q^H \mu_{\mathbf{c_I}}$, v_0^i and μ_I^i denote the ith elements of the vectors $\mathbf{v_0}$ and $\mu_\mathbf{I}$ respectively, and λ_0^i and λ_I^i denote the eigenvalues of the covariance matrix $\Sigma_{\mathbf{c_0}}$ and $\Sigma_{\mathbf{c_I}}$, respectively.

Averaging $\phi_{Y|\mathbf{c_0},b}(s)$ over $\mathbf{c_0}$, namely, over $\mathbf{v_0}$, and setting $s = j\omega$, the CF of Y conditioned on b is obtained as

$$\begin{aligned}
\phi_{Y|b}(j\omega) &= \prod_{i=1}^{N} \frac{1}{1 - j\omega\lambda_0^i + \omega^2(a_1\lambda_0^i\lambda_I^i + a_2\lambda_0^i)} \times \\
&\exp\left(\sum_{i=1}^{N} \frac{|\mu_0^i|^2(j\omega\lambda_0^i - \omega^2(a_1\lambda_0^i\lambda_I^i + a_2\lambda_0^i)) - b^2\omega^2|\mu_I^i|^2 + j\omega 2bRe\{\mu_0^i(\mu_I^i)^H\}}{1 - j\omega\lambda_0^i + \omega^2(a_1\lambda_0^i\lambda_I^i + a_2\lambda_0^i)}\right).
\end{aligned} \tag{6.41}$$

The detailed derivation of (6.41) from (6.40) is given in Appendix D.3. Then the average BER conditioned on b can be calculated according to [116, eq. (9)]

$$\begin{aligned}
P_{e|b} &= \Pr\{Y < 0|b\} \\
&= \frac{1}{2} - \frac{1}{\pi}\int_0^\infty \frac{Im\{\phi_{Y|b}(j\omega)\}}{\omega} d\omega
\end{aligned} \tag{6.42}$$

where $Im\{z\}$ denotes the imaginary part operation on the complex number z. Averaging (6.42) on b for the whole data set D_{N_I}, the average BER of BPSK in the presence of CCI and noise over correlated Ricean fading is given by

$$P_e = \sum_b P_{e|b} \times \Pr\left(b = \frac{1}{2}\sum_{n=1}^{N_I} \frac{d_n}{\sqrt{\Gamma_I^n}}\right) \tag{6.43}$$

where $\Pr(b = \sum_{n=1}^{N_I} d_n/(2\sqrt{\Gamma_I^n})$ is the probability for $b = \sum_{n=1}^{N_I} d_n/(2\sqrt{\Gamma_I^n})$ over the whole data set D_{N_I}.

When all of the interfering users have the same transmitter power, namely, $\Gamma_I^n = N_I\Gamma_I$, the probability mass function of the random variable b is given by [113, eq. (29)]

$$\Pr\left(b = \frac{(2k - N_I)}{2\sqrt{N_I\Gamma_I}}\right) = \frac{C_{N_I}^k}{2^{N_I}}, \qquad k = 0, 1, \cdots, N_I. \tag{6.44}$$

Then the average BER for equal-power cochannel interferers and AWGN becomes

$$P_e = \sum_{k=0}^{N_I} \frac{C_{N_I}^k}{2^{N_I}} \times P_{e|b=\frac{(2k-N_I)}{2\sqrt{N_I\Gamma_I}}}. \tag{6.45}$$

Particularly, when the fading is Rayleigh, namely, $\mu_{\mathbf{c_n}} = \mathbf{0}$ $(n = 0, \cdots, N_I)$, the conditional CF of Y in (6.41) can be further simplified to

$$\phi_{Y|b}(j\omega) = \prod_{i=1}^{N} \frac{1}{1 - j\omega\lambda_0^i + \omega^2(\lambda_0^i\lambda_I^i/\Gamma_I + \lambda_0^i/\Gamma_0)/4}. \tag{6.46}$$

Since (6.46) is independent of b and the number of interfering users, the average BER in correlated Rayleigh fading becomes

$$P_e = \frac{1}{2} - \frac{1}{\pi}\int_0^\infty \frac{1}{\omega} Im\left\{\prod_{i=1}^{N} \frac{1}{1 - j\omega\lambda_0^i + \omega^2(\lambda_0^i\lambda_I^i/\Gamma_I + \lambda_0^i/\Gamma_0)/4}\right\} d\omega. \tag{6.47}$$

When the AWGN is ignorable, $\Gamma_0 = \infty$, namely, $a_2 = 0$ in (6.41). Then the CF of Y in CCI-limited correlated Ricean fading is obtained from (6.41) as

$$\begin{aligned}\phi_{Y|b}(j\omega) = & \prod_{i=1}^{N} \frac{1}{1 - j\omega\lambda_0^i + \omega^2 a_1\lambda_0^i\lambda_I^i} \times \\ & \exp\left(\sum_{i=1}^{N} \frac{|\mu_0^i|^2(j\omega\lambda_0^i - \omega^2 a_1\lambda_0^i\lambda_I^i) - b^2\omega^2|\mu_I^i|^2 + j\omega 2bRe\{\mu_0^i(\mu_I^i)^H\}}{1 - j\omega\lambda_0^i + \omega^2 a_1\lambda_0^i\lambda_I^i}\right).\end{aligned} \tag{6.48}$$

When the fading is Rayleigh,the conditional CF of Y in (6.48) can be further simplified to

$$\phi_{Y|b}(j\omega) = \prod_{i=1}^{N} \frac{1}{1 - j\omega\lambda_0^i + \omega^2\lambda_0^i\lambda_I^i/(4\Gamma_I)}. \tag{6.49}$$

Since (6.49) is independent of b and the number of interfering users, the average BER in correlated Rayleigh fading becomes

$$P_e = \frac{1}{2} - \frac{1}{\pi}\int_0^\infty \frac{1}{\omega} Im\left\{\prod_{i=1}^{N} \frac{1}{1 - j\omega\lambda_0^i + \omega^2\lambda_0^i\lambda_I^i/(4\Gamma_I)}\right\} d\omega. \tag{6.50}$$

Eq. (6.50) can be further derived in closed form as follows. The MGF of Y in CCI-limited Rayleigh fading is obtained from (6.49) as

$$\begin{aligned}\phi_Y(s) &= \prod_{i=1}^{N} \frac{1}{(1 - v_i s)(1 + w_i s)} \\ &= \left[\prod_{i=1}^{N} \frac{1}{1 - v_i s}\right] \times \left[\prod_{j=1}^{N} \frac{1}{1 + w_j s}\right]\end{aligned} \tag{6.51}$$

where $v_i = \left(\lambda_0^i + \sqrt{(\lambda_0^i)^2 + \lambda_0^i\lambda_I^i/\Gamma_I}\right)/2$ and $w_i = \left(-\lambda_0^i + \sqrt{(\lambda_0^i)^2 + \lambda_0^i\lambda_I^i/\Gamma_I}\right)/2$. Assuming that there are P_v different non-zero values of v_i and P_w different non-zero values of w_i, namely, $\sum_{i=1}^{P_v} tv_i = N$, and $\sum_{i=1}^{P_w} tw_i = N$, (6.51) becomes

$$\phi_Y(s) = \left[\prod_{i=1}^{P_v} \frac{1}{(1 - v_i s)^{tv_i}}\right] \times \left[\prod_{j=1}^{P_w} \frac{1}{(1 + w_j s)^{tw_j}}\right]. \tag{6.52}$$

Using [77, eq. (11)], one has

$$\prod_{i=1}^{P_v} \frac{1}{(1 - v_i s)^{tv_i}} = \sum_{i=1}^{P_v} \sum_{l_v=1}^{tv_i} \frac{\alpha_{i,l_v}}{\left(s - \frac{1}{v_i}\right)^{l_v}} \tag{6.53}$$

and

$$\prod_{j=1}^{P_w} \frac{1}{(1 + w_j s)^{tw_j}} = \sum_{j=1}^{P_w} \sum_{l_w=1}^{tw_j} \frac{\beta_{j,l_w}}{\left(s + \frac{1}{w_j}\right)^{l_w}} \tag{6.54}$$

where α_{i,l_v} and β_{j,l_w} are respectively given by

$$\alpha_{i,l_v} = \left(-\frac{1}{v_i}\right)^{tv_i} \sum_{\tau(i,l_v)} \prod_{k=1;k\neq i}^{P_v} C_{tv_k+q_k-1}^{q_k} \frac{(v_k)^{q_k}}{\left(1 - \frac{v_k}{v_i}\right)^{tv_k+q_k}} \tag{6.55}$$

and

$$\beta_{j,l_w} = \frac{1}{w_j{}^{tw_j}} \sum_{\tau(j,l_w)} \prod_{k=1;k\neq j}^{P_w} C_{tw_k+q_k-1}^{q_k} \frac{(-w_k)^{q_k}}{\left(1 - \frac{w_k}{w_j}\right)^{tw_k+q_k}} \tag{6.56}$$

where $\tau(i,l_v)=\{(q_1,\cdots,q_{P_v}): q_k\in\mathbb{N}_0,\ q_i=0,\sum_{k=1}^{P_v}q_k=tv_i-l_v\}$ and $\tau(j,l_w)=\{(q_1,\cdots,q_{P_w}): q_k\in\mathbb{N}_0,\ q_j=0,\sum_{k=1}^{P_w}q_k=tw_j-l_w\}$.

Then (6.52) becomes

$$\begin{aligned}\phi_Y(s) &= \left(\sum_{i=1}^{P_v}\sum_{l_v=1}^{tv_i}\frac{\alpha_{i,l_v}}{\left(s-\frac{1}{v_i}\right)^{l_v}}\right)\times\left(\sum_{j=1}^{P_w}\sum_{l_w=1}^{tw_j}\frac{\beta_{j,l_w}}{\left(s+\frac{1}{w_j}\right)^{l_w}}\right)\\ &= \sum_{i=1}^{P_v}\sum_{l_v=1}^{tv_i}\sum_{j=1}^{P_w}\sum_{l_w=1}^{tw_j}\frac{(\alpha_{i,l_v})(\beta_{j,l_w})}{\left(s-\frac{1}{v_i}\right)^{l_v}\left(s+\frac{1}{w_j}\right)^{l_w}}.\end{aligned}\tag{6.57}$$

Taking the inverse Laplace transform on (6.57), the PDF of Y can be calculated by

$$f_Y(t)=\sum_{i=1}^{P_v}\sum_{l_v=1}^{tv_i}\sum_{j=1}^{P_w}\sum_{l_w=1}^{tw_j}(\alpha_{i,l_v})(\beta_{j,l_w})[x_{i,l_v}(t)*y_{j,l_w}(t)]\tag{6.58}$$

where $x_{i,l_v}(t)$ and $y_{j,l_w}(t)$ are given by

$$x_{i,l_v}(t)=\frac{(-1)^{l_v}}{(l_v-1)!}t^{l_v-1}e^{-t/v_i},\qquad t\geq 0\tag{6.59}$$

and

$$y_{j,l_w}(t)=\frac{(-1)^{l_w-1}}{(l_w-1)!}t^{l_w-1}e^{t/w_j},\qquad t\leq 0.\tag{6.60}$$

Then the BER of BPSK in (6.38) can be calculated as

$$\begin{aligned}P_e &= \int_{-\infty}^{0}f_Y(t)dt\\ &= \sum_{i=1}^{P_v}\sum_{l_v=1}^{tv_i}\sum_{j=1}^{P_w}\sum_{l_w=1}^{tw_j}(\alpha_{i,l_v})(\beta_{j,l_w})\frac{(-1)^{l_v}w_j^{l_w}}{\left(\frac{1}{v_i}+\frac{1}{w_j}\right)^{l_v}}\times\sum_{q=0}^{l_w-1}C_{l_v+q-1}^{q}\frac{1}{\left(1+\frac{w_j}{v_i}\right)^{q}}.\end{aligned}\tag{6.61}$$

Eq. (6.61) is a closed-form expression for the BER of BPSK using MRC in CCI and correlated Rayleigh fading. When all of v_i and w_j are not equal, (6.61) can be further simplified as

$$P_e = \sum_{i=1}^{N}\sum_{j=1}^{N}\frac{v_i^{N-1}w_j^{N}}{(v_i+w_j)}\times\frac{1}{\prod_{k=1;k\neq i}^{N}(v_i-v_k)}\times\frac{1}{\prod_{k=1;k\neq j}^{N}(w_j-w_k)}.\tag{6.62}$$

Observe that the BER in (6.61) and (6.62) depends, through the v_i, w_j, α_{i,l_v} and β_{j,l_w}, only on the eigenvalues of the correlation matrix and not on the elements of the correlation matrix. This is a consequence of the fact that the same MRC diversity structure with the same

branch weights is an optimal, maximum likelihood (ML) structure, both for independent branches and for correlated branches [117].

6.5 Numerical Results

In this section, some examples using linear antenna arrays and circular antenna arrays with a 2D omnidirectional scattering channel model and a 3D omnidirectional scattering channel model are given. We assume that the antennas are uniformly placed in a fixed-length linear antenna array or a fixed-radius circular antenna array. The length of the linear antenna array is assumed the minimum required to accommodate T independent antennas. That is, the ratio of the linear antenna array length to the wavelength, L_0, is only determined by the number of independent antennas T. Observe from Fig 6.1 that for the 3D case, one can neatly place the antennas at the zero-crossings of the correlation function, which are uniformly spaced, and the antennas will be independent. In contrast, for the 2D case, the zero-crossings of the correlation function are not uniformly spaced. Motivated by practical considerations, we space the T antennas uniformly across the total length of the array. The correlation between the T antennas, while not zero, is extremely small, so small that the antennas are virtually independent. The independent and virtually independent antennas will be referred to as the "primary" antennas, as shown in Fig. 6.2, where the diagrams of uniform linear antenna array and uniform circular antenna array are given. The normalized array length L_0 for the 2D channel model is determined by the $(T-1)$ zero-crossing of $J_0(2\pi x)$ [6, eq. (8.548)] and $L_0 = (T-1)/2$ for the 3D channel model. For the case of circular antenna arrays, we assume that the normalized radius, L_0, is determined by the minimum distance between two adjacent primary antennas, namely, $L_0 = 0.382/\sqrt{2-2cos(2\pi/T)}$ for the 2D channel model, and $L_0 = 0.5/\sqrt{2-2cos(2\pi/T)}$ for the 3D channel model. Further, we assume that the channel gains $c_{n,p} = x_{n,p} + jy_{n,p} + \mu_{c_n,p}$ $(n = 0,\cdots,N_I, p = 1,\cdots,N)$ at the receiver satisfy $\mathbb{E}[x_{n,p}x_{n,q}] = \mathbb{E}[y_{n,p}y_{n,q}]$, and $\mathbb{E}[x_{n,p}y_{n,q}] = \mathbb{E}[y_{n,p}x_{n,q}] = 0$ $(p,q = 1,\cdots,N)$. For our examples, we assume that the covariance matrix for the desired user signal and that of the

interfering signals are equal, that is, $\Sigma_{c_I} = \Sigma_{c_0}$, and all of the interfering signals in correlated Ricean fading have the same average power.

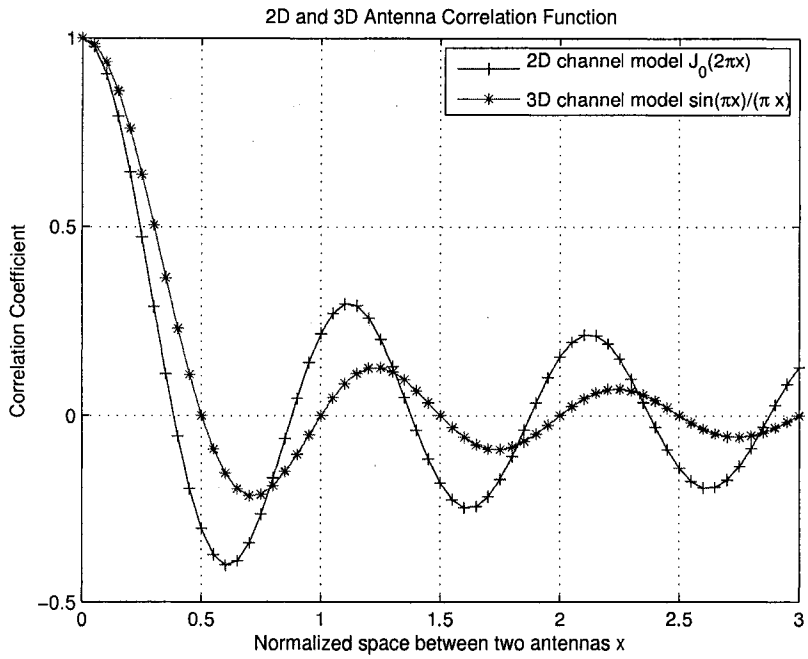

Fig. 6.1. The correlation coefficient of two antennas versus the normalized antenna spacing.

6.5.1 CCI-Limited Case

Let us first consider the CCI-limited case. Fig. 6.3 shows the SIRP, the SAPR, the AISIR, and the average BER versus the number of antennas, N, in correlated Rayleigh fading with $N_I = 2$ equal-power interferers and $\Gamma_I = 5$ dB for a linear antenna array using the channel model in [18] with $\Delta = \pi$. Different numbers of primary antennas T are considered. In Figs. 6.3(a) to 6.3(c), one can see that for all the values of T except $T = 2$, the values of γ_{SIRP}, γ_{SAPR} and γ_{AISIR} reach the maximum at $N = T + 1$ and the curves become flat or even deteriorate when N is larger than $T + 1$, which indicates that adding more antennas cannot always increase the values of γ_{SIRP}, γ_{SAPR} and γ_{AISIR}; namely, there exists a saturation point

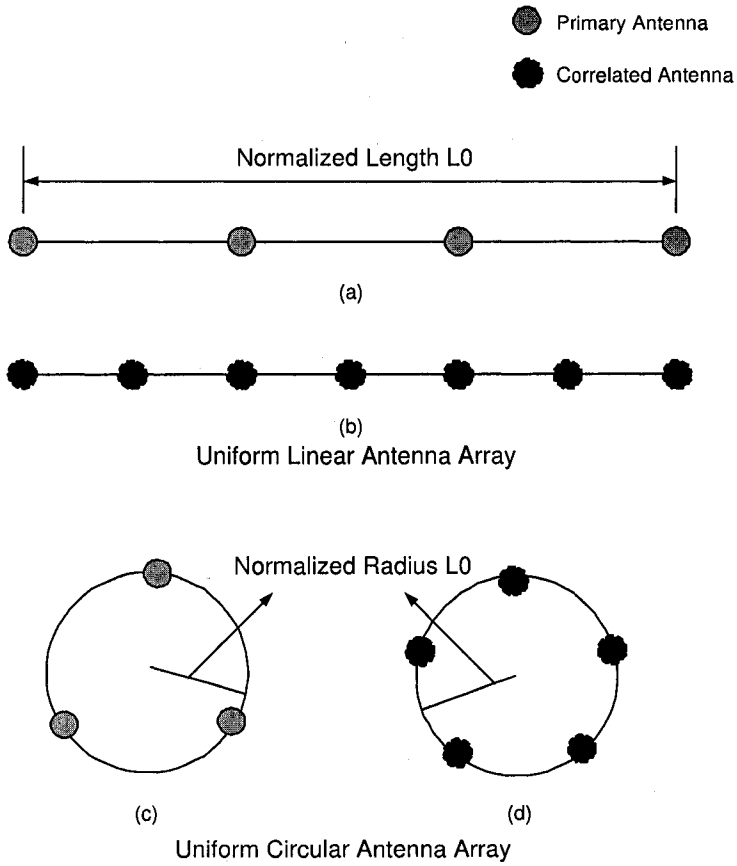

Fig. 6.2. The diagram of uniform linear antenna array and uniform circular antenna array.

at $N = T + 1$, beyond which little benefit can be achieved from adding more antennas. Similar observations can be drawn from Fig. 6.3(d). In Fig. 6.3(d), the diamond markers denote the BERs obtained using Monte Carlo simulation. It is seen that the analytical results are in excellent agreement with the simulation results. Importantly and usefully, for all of the values of T, the average BER becomes best at $N = T + 1$. In addition, the SIRP and the SAPR are very close to the corresponding limits denoted by the dashed curves in Figs. 6.3(a) and 6.3(b), when $N > 10$.

Fig. 6.4 shows the SIRP, the SAPR, the AISIR, and the average BER versus N with $N_I = 2$ equal-power interferers and $\Gamma_I = 5$ dB for a linear antenna array in correlated Rayleigh fading. A 3D channel model is considered for different numbers of primary antennas T.

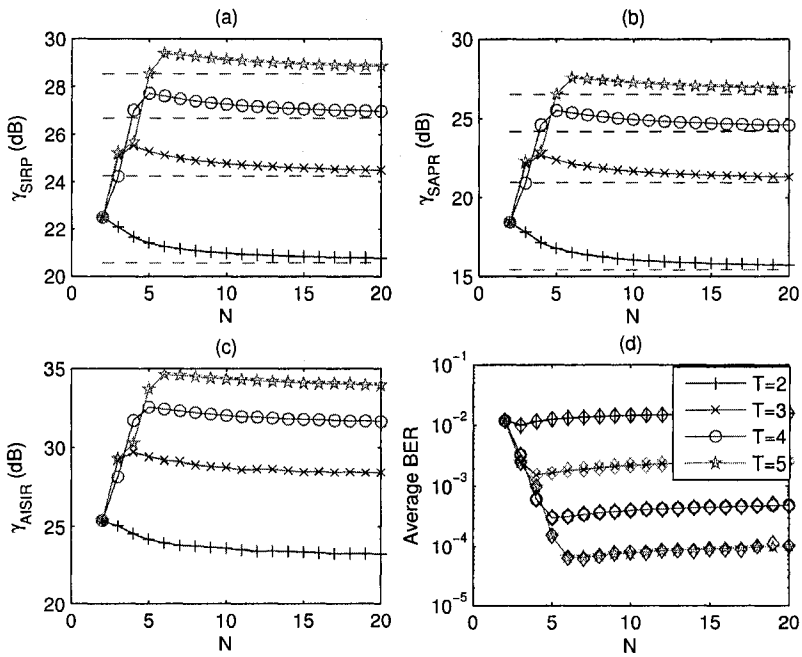

Fig. 6.3. The γ_{SIRP}, the γ_{SAPR}, the γ_{AISIR}, and the average BER of a linear antenna array versus the number of antennas, N, in correlated Rayleigh fading described by the 2D omnidirectional scattering model with $N_I = 2$ equal-power interferers and $\Gamma_I = 5$ dB for different values of T.

Observe that except for the case of $T = 2$, γ_{SIRP} and γ_{SAPR} indicate an optimal number of antennas at $N = T + 1$ for the system design that is the same as the number indicated by the AISIR and the average BER performance measures.

The case that both the desired user signal and the interfering user signals experience correlated Ricean fading is presented in Figs. 6.5 and 6.6, where all of the branches of the nth user signal have the same LOS component denoted by $\sqrt{\mathbb{K}_n}e^{j\theta_n}$ $(n = 0, \cdots, N_I)$, where $\mathbb{K}_n = |\mu_{c_n}^i|^2/var(c_n^i)$ and θ_n is the phase of the LOS component. In the examples, the LOS component for the desired user signal is $\mathbb{K}_0 = 10$ dB and $\theta_0 = \pi/4$, and the LOS component for each of the interfering user signals is $\mathbb{K}_I = 3$ dB and $\theta_I = \pi/6$. The 2D and 3D channel model with $\Gamma_I = 0$ dB and $N_I = 2$ equal-power interfering signals are used for

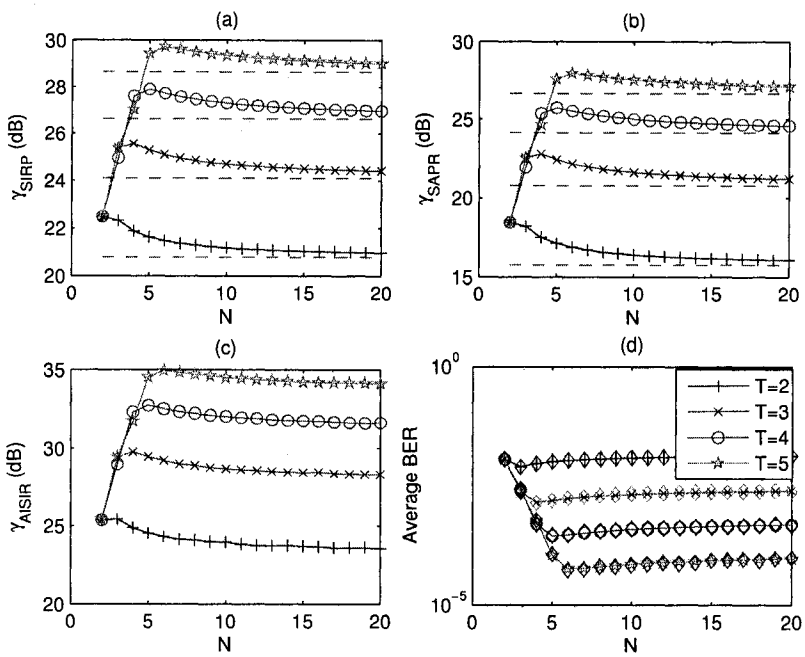

Fig. 6.4. The γ_{SIRP}, the γ_{SAPR}, the γ_{AISIR}, and the average BER of a linear antenna array versus the number of antennas, N, in correlated Rayleigh fading described by the 3D omnidirectional scattering model with $N_I = 2$ equal-power interferers and $\Gamma_I = 5$ dB for different values of T.

different values of T in Fig. 6.5 and Fig. 6.6, respectively. The diamond markers in Fig. 6.5(d) and 6.6(d) denote the BERs obtained using Monte Carlo simulation. It is seen that the theoretical results are in good agreement with the simulation results. Observe in Fig. 6.5 that all of the four measures improve little, or even become worse, when N is larger than T. This means that the saturation point of N predicted by the SIRP and the SAPR indicates a threshold in the number of antennas beyond which the AISIR and the BER performance gain little by adding more antennas. Furthermore, the performance for $T = 4$ becomes best at $N = 3$, although the performance at $N = 4$ is close to the best performance. Similar observations are made from Fig. 6.6, where all of the four measures improve little, or even become worse, when N is larger than T.

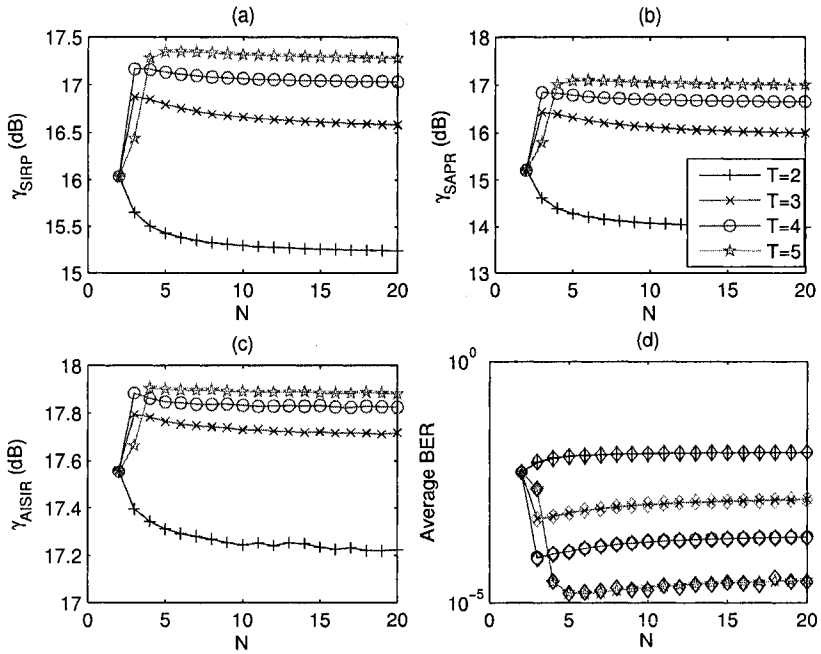

Fig. 6.5. The γ_{SIRP}, the γ_{SAPR}, the γ_{AISIR}, and the average BER of a linear antenna array versus the number of antennas, N, in correlated Ricean fading described by the 2D omnidirectional scattering model with $N_I = 2$ equal-power interferers and $\Gamma_I = 0$ dB for different values of T.

Fig. 6.7 examines the effect of the number of equal-power interfering signals on the average BER for a fixed value of $\Gamma_I = 0$ dB. A linear antenna array with a 2D scattering model with $T = 6$, $\mathbb{K}_0 = 10$ dB, $\theta_0 = \pi/4$, $\mathbb{K}_I = 3$ dB and $\theta_I = \pi/6$ is used here. It is seen that the BERs at $N = 6$ are very close to the minimum BERs at $N = 7$. Further the BER increases with the number of interferers although there is no difference for the γ_{SIRP} measure. Significantly, from the viewpoint of system design, the SIRP measure indicates that $N = 6$ is a good choice to achieve a good compromise between the BER performance and the system cost for all values of N_I examined.

The performance of circular antenna arrays with a fixed radius in correlated Ricean fading using a 3D channel model is presented in Fig. 6.8 and using a 2D channel model

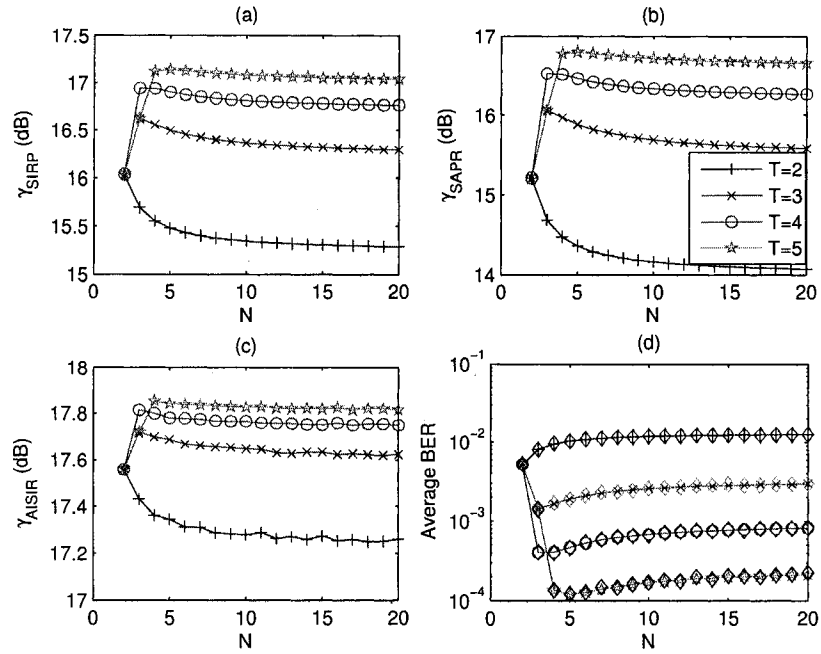

Fig. 6.6. The γ_{SIRP}, the γ_{SAPR}, the γ_{AISIR}, and the average BER of a linear antenna array versus the number of antennas, N, in correlated Ricean fading described by the 3D omnidirectional scattering model with $N_I = 2$ equal-power interferers and $\Gamma_I = 0$ dB for different values of T.

in Fig. 6.9, respectively. In both of the figures, the desired user signal with $\mathbb{K}_0 = 10$ dB and $\theta_0 = 0$ is disturbed by $N_I = 4$ equal-power interferers with $\mathbb{K}_I = 2$ dB and $\theta_I = 0$. The average SIR power ratio Γ_I is 0 dB for different values of T. It is seen that the SIRP and the SAPR indicate a saturation point of the number of antennas around $N = T + 1$, beyond which, the average BER and the AISIR become very flat.

Fig. 6.10 shows the SIRP and the average BER versus the number of antennas N for a circular antenna array in correlated Rayleigh fading using a 3D channel model with $\Gamma_I = 5$ dB and $N_I = 7$ interferers. The dashed curves in Fig. 6.10(a) represent the limits of the SIRP for different values of T. It is seen that the SIRP is very close to the corresponding limit for $N > 8$. In addition, the SIRP indicates a saturation point around $N = T + 3$, beyond

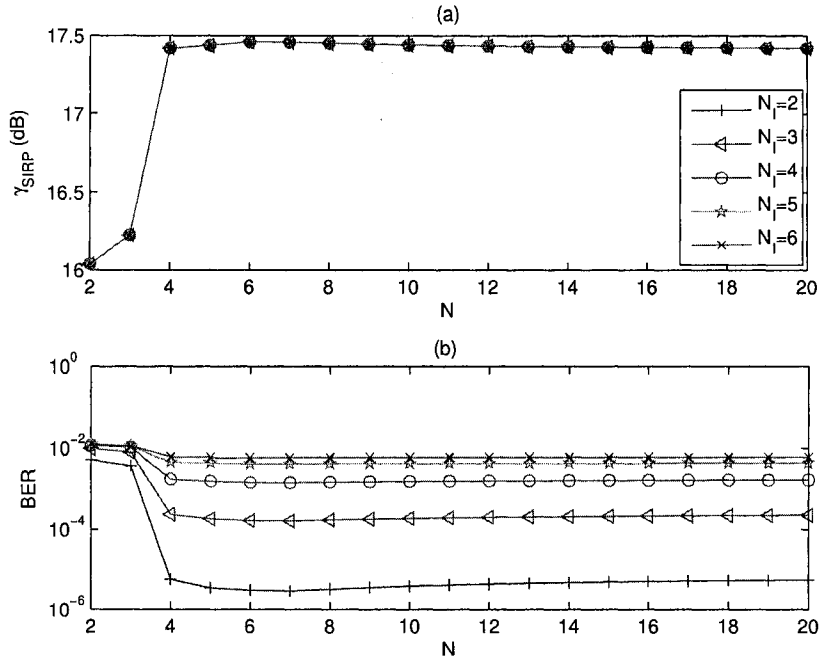

Fig. 6.7. The γ_{SIRP} and the average BER of a linear antenna array versus the number of antennas, N, in correlated Ricean fading described by the 2D omnidirectional scattering model with $T = 6$ and $\Gamma_I = 0$ dB for different values of N_I.

which, the average BER decreases little by adding more antennas.

The effect of the LOS component in the Ricean fading on the BER performance is examined in Fig. 6.11, where different values of $\mathbb{K}_I$ for the interfering signals are considered for a circular antenna array using a 2D scattering model with $T = 5$, $N_I = 5$ equal-power interferers, $\Gamma_I = 3$ dB, $\mathbb{K}_0 = 10$ dB, $\theta_0 = 0$, and $\theta_I = 0$. Observe that the two performance measures improve with decreasing $\mathbb{K}_I$. Further, the performance measures becomes flat after $N = 6$, and the performance at $N = 5$ nearly equals that at $N = 6$.

The examples indicate that addition of more than one antenna beyond the number of independent antennas is not always worthwhile. This rule of thumb appears to be widely applicable, and is intuitive. If one considers the antennas as sampling points of the spatial signal field shown in Fig. 6.12, one expects from a sampling theorem viewpoint that using

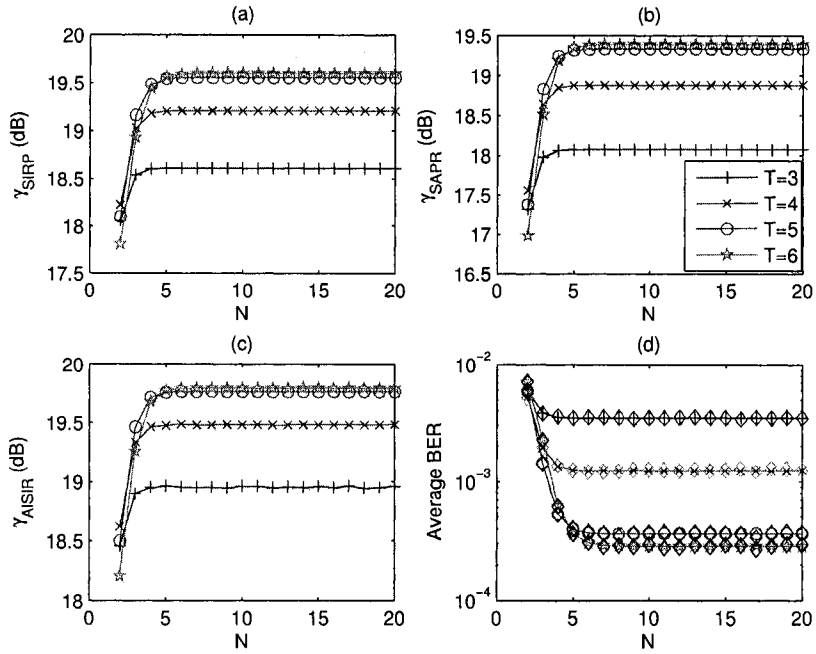

Fig. 6.8. The γ_{SIRP}, the γ_{SAPR}, the γ_{AISIR}, and the average BER of a circular antenna array versus the number of antennas, N, in correlated Ricean fading described by the 3D omnidirectional scattering model with $N_I = 4$ equal-power interferers and $\Gamma_I = 0$ dB for different values of T.

more than the maximum number of independent antennas should be unnecessary.

6.5.2 The Effect of Noise

In this part, the effect of noise on the maximum effective number of antennas is investigated. Fig. 6.13 shows the SINRP, the SAINPR, the AISINR, and the average BER versus the number of antennas, N, in correlated Ricean fading with $N_I = 2$ equal-power interferers, $\Gamma_I = 0$ dB, and $\Gamma_0 = 5$ dB for a linear antenna array using the channel model in [18] with $\Delta = \pi$. All of the branches of the nth user signal have the same LOS component $\sqrt{\mathbb{K}_n}e^{j\theta_n}$ $(n = 0, \cdots, N_I)$. In the example, the LOS component for the desired user signal is $\mathbb{K}_0 = 10$ dB and $\theta_0 = \pi/4$, and the LOS component for each of the interfering user

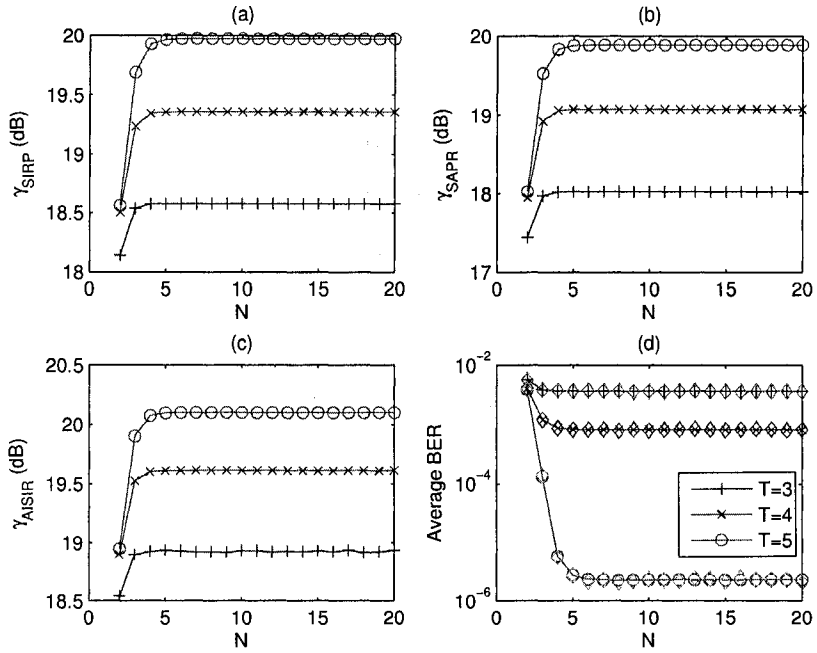

Fig. 6.9. The γ_{SIRP}, the γ_{SAPR}, the γ_{AISIR}, and the average BER of a circular antenna array versus the number of antennas, N, in correlated Ricean fading described by the 2D omnidirectional scattering model with $N_I = 4$ equal-power interferers and $\Gamma_I = 0$ dB for different values of T.

signals is $\mathbb{K}_I = 3$ dB and $\theta_I = \pi/6$. Different numbers of primary antennas T are considered. In Fig. 6.13(d), the diamond markers denote the BERs obtained using Monte Carlo simulation. It is seen that the analytical results are in excellent agreement with the simulation results. Further, one can see that for all the values of T except $T = 2$, the curves of the γ_{SINRP}, the γ_{SAINPR}, the γ_{AISINR}, and the average BER behavior similarly with N, and become flat when N is large enough, which indicates that adding more antennas cannot always increase the system performance usefully.

Similar observations can be drawn from Fig. 6.14, where a fixed-radius circular antenna array in correlated Ricean fading using a 3D channel model with $\Gamma_I = 0$ dB and $\Gamma_0 = 5$ dB is considered for different values of T. Here, the desired user signal with $\mathbb{K}_0 = 10$ dB and

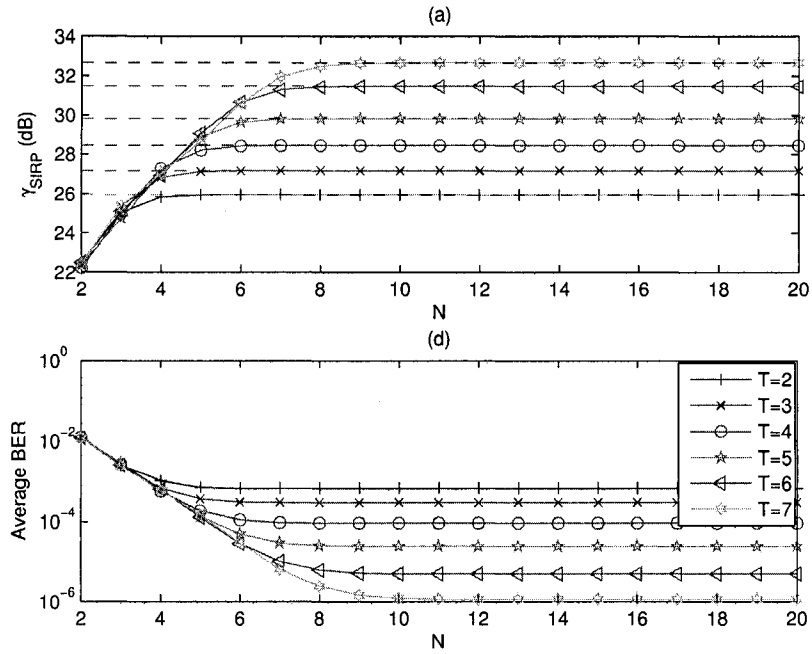

Fig. 6.10. The γ_{SIRP} and the average BER of a circular antenna array versus the number of antennas, N, in correlated Rayleigh fading described by the 3D omnidirectional scattering model with $N_I = 7$ equal-power interferers and $\Gamma_I = 5$ dB for different values of T.

$\theta_0 = 0$ is disturbed by $N_I = 4$ equal-power interferers with $\mathbb{K}_I = 2$ dB and $\theta_I = 0$. It is seen that the SINRP and the SAINPR indicate a saturation point of the number of antennas beyond which, the average BER and the AISINR improve very little. Comparing Fig. 6.13 and Fig. 6.14 with Fig. 6.5 and Fig. 6.8, respectively, where the noise is ignored, one can see that the saturation point of the number of antennas when noise is present in addition to CCI is no longer closest to T or $T + 1$, but rather shifts to larger values.

To further investigate the effect of noise on the maximum effective number of antennas, the SINRP, the SAINPR, the AISINR, and the average BER versus the number of antennas, N, in correlated Ricean fading with $T = 5, N_I = 2$ equal-power interferers and $\Gamma_I = 0$ dB is considered in Fig. 6.15. The channel model in Fig. 6.13 is used for different values of SNR

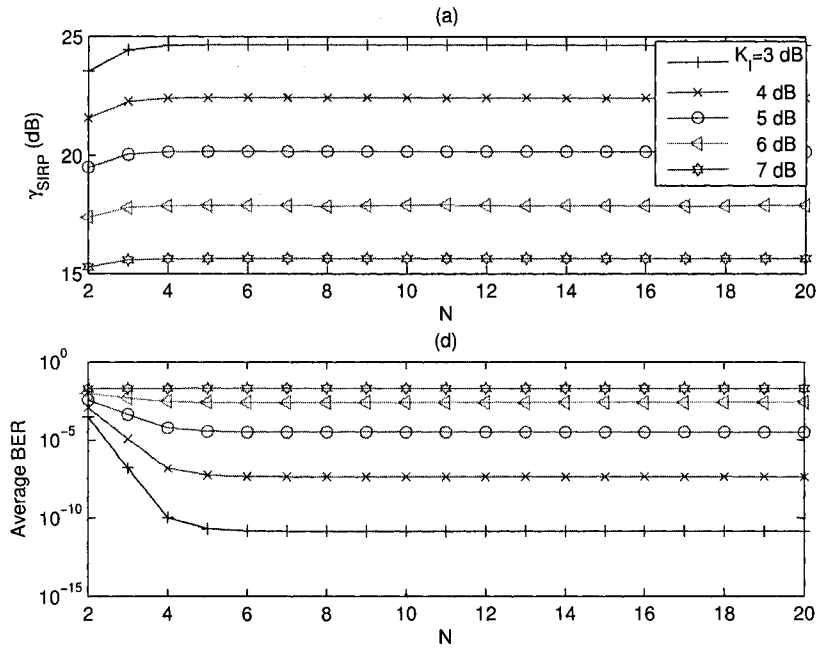

Fig. 6.11. The γ_{SIRP} and the average BER of a circular antenna array versus the number of antennas, N, in correlated Ricean fading described by the 2D omnidirectional scattering model with $T = 5$, $N_I = 5$ equal-power interferers and $\Gamma_I = 3$ dB for different values of $\mathbb{K}_I$.

power ratio Γ_0 with $\Gamma_0 = \infty$ corresponding to the CCI-limited case. It is seen that the system performances improve with increasing Γ_0, as expected. Further, the curves converge when Γ_0 becomes large. For example, the performances with $\Gamma_0 = 10$ dB and $\Gamma_0 = 15$ dB are very close to the performance with $\Gamma_0 = \infty$, the CCI-limited case. In other words, one can still apply the design rule for the CCI-limited case to determine the maximum effective number of antennas for a fixed-size antenna array when the SNR power ratio Γ_0 is large enough, say 5 dB or greater.

Fig. 6.16 shows the SINRP and the average BER versus the number of antennas N for a circular antenna array in correlated Rayleigh fading using a 3D channel model with $T = 4$ and $N_I = 7$ interferers. Different values of the interference power to noise power

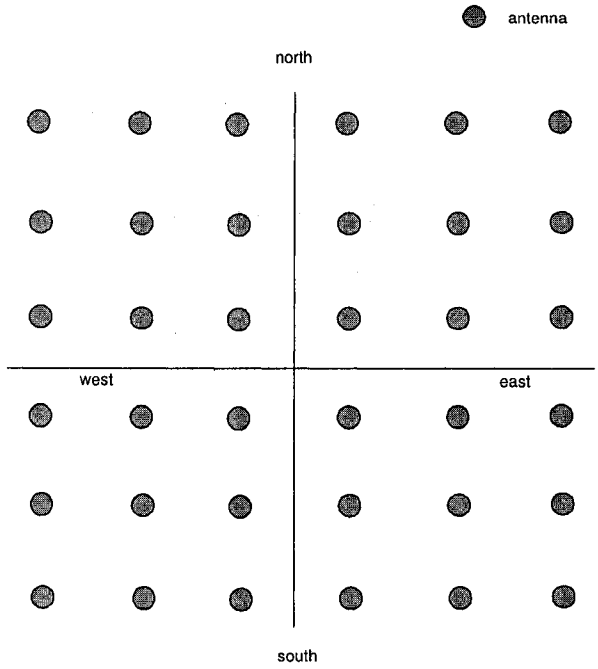

Fig. 6.12. The diagram of CCI-sampling space

ratio $\Gamma_{INRP} = P_I/N_0$ are considered. The dash-dot curves in Fig. 6.16(a) represent the limits of the SINRP for different values of Γ_I. It is seen that the SINRP is very close to the corresponding limit when Γ_{INRP} is equal to or larger than 10 dB for $N > 8$.

6.6 Summary

In this chapter, the performances of MRC receiver diversity systems with a fixed-length linear antenna array and a fixed-radius circular antenna array were analyzed. For the case of CCI-limited environment, examples show that, in general, the long term output SIRP, the long term SAPR, the average instantaneous output SIR, and the average BER versus the number of antennas for a fixed-size antenna array have similar behaviors in correlated Ricean fading. The optimal number of antennas predicted by the SIRP or the SAPR can be used, or as an excellent starting search point, to achieve a good compromise between the system performance, such as the AISIR and the average BER, and system cost. A

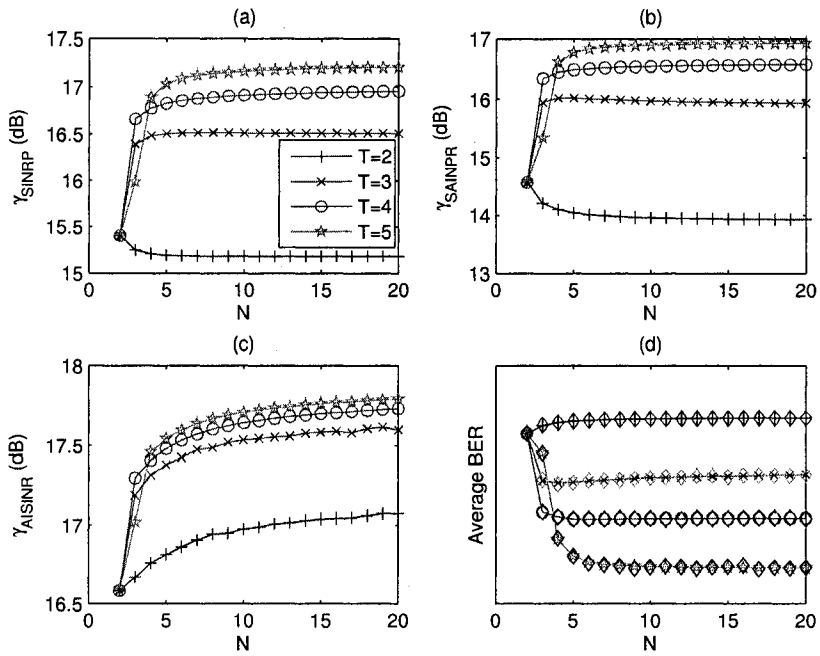

Fig. 6.13. The γ_{SINRP}, the γ_{SAINPR}, the γ_{AISINR}, and the average BER of a linear antenna array versus the number of antennas, N, in correlated Ricean fading described by the 2D omnidirectional scattering model with $N_I = 2$ equal-power interferers, $\Gamma_I = 0$ dB, and $\Gamma_0 = 5$ dB for different values of T.

widely applicable general rule of thumb emerges which is that the performance of a fixed-size antenna array containing the maximum number of independent antennas cannot be significantly improved by adding more than one additional antenna. Special cases where particular performance gains can be achieved by adding additional correlated antennas were also discussed. When the noise is present, the results show that the design rule for the CCI-limited case, still applies for moderate and large values of interference-to-noise power ratio. In addition, for Rayleigh fading, the limits of the long term SINRP and the SAINPR in the presence of noise are the same as the limits for the CCI-limited case.

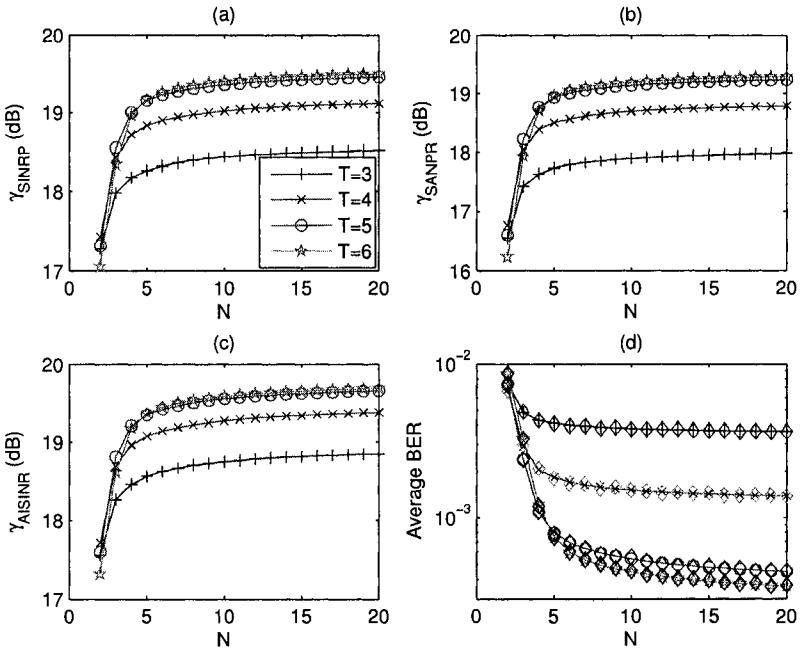

Fig. 6.14. The γ_{SINRP}, the γ_{SAINPR}, the γ_{AISINR}, and the average BER of a circular antenna array versus the number of antennas, N, in correlated Ricean fading described by the 3D omnidirectional scattering model with $N_I = 4$ equal-power interferers, $\Gamma_I = 0$ dB, and $\Gamma_0 = 5$ dB for different values of T.

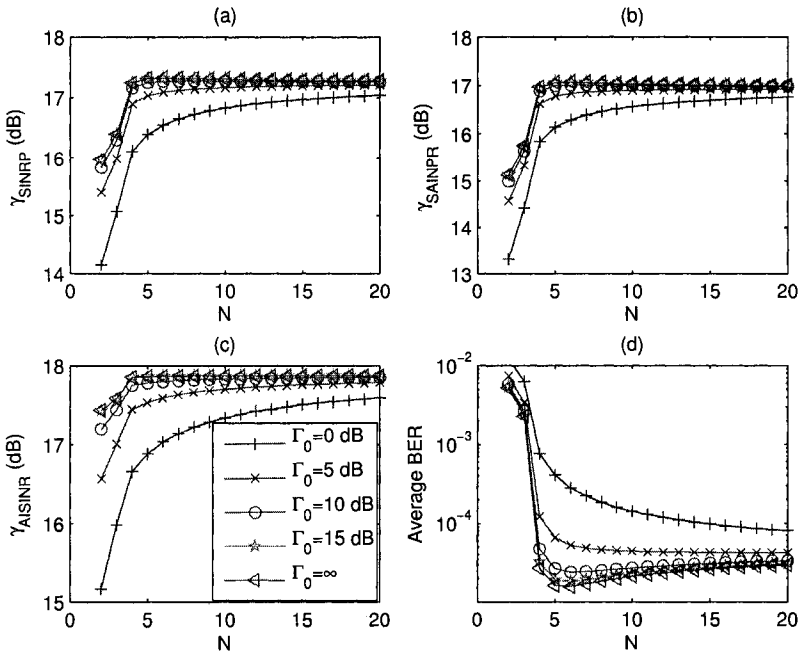

Fig. 6.15. The γ_{SINRP}, the γ_{SAINPR}, the γ_{AISINR}, and the average BER of a linear antenna array versus the number of antennas, N, in correlated Ricean fading described by the 2D omnidirectional scattering model with $T = 5$, $N_I = 2$ equal-power interferers, $\Gamma_I = 0$ dB for different values of Γ_0.

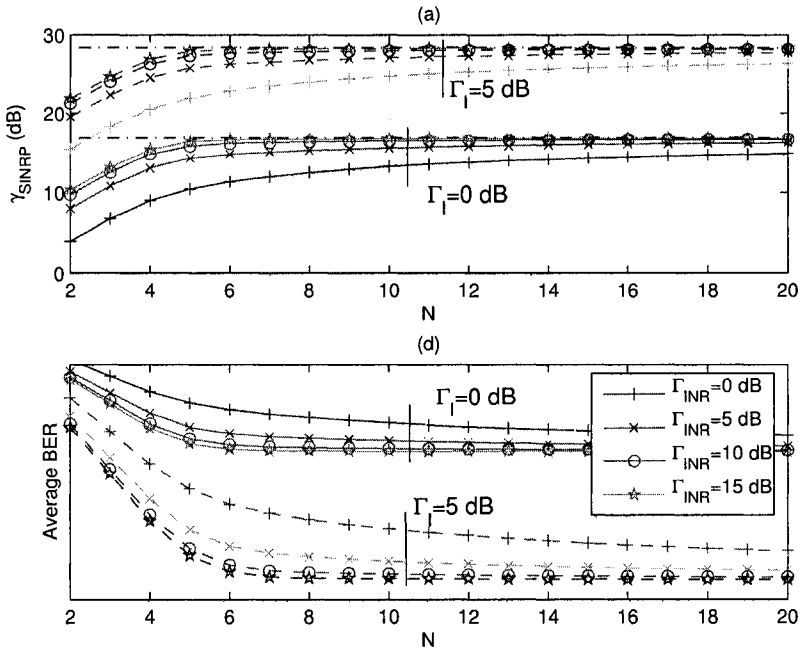

Fig. 6.16. The γ_{SINRP} and the average BER of a circular antenna array versus the number of antennas, N, in correlated Rayleigh fading described by the 3D omnidirectional scattering model with $T = 4$ and $N_I = 7$ equal-power interferers for different values of the INRP ratio $\Gamma_{INRP} = P_I/N_0$.

Chapter 7

Conclusions and Suggestions for Future Work

In this chapter, we first summarize the major contributions of this thesis and then suggest several topics for future research.

7.1 Conclusions

1. An exact and unified analysis framework for T-HS/MRC over generalized fading channels was developed using the total probability theorem and MGF method. This theory allows various fading models and different modulation schemes.

2. The previous published analytical results on T-HS/MRC were shown to be inaccurate.

3. Explicit expressions for the average SER and outage probability of T-HS/MRC in i.i.d. diversity branches and i.n.d. diversity branches were obtained.

4. Closed-form expressions for SER and outage probability of T-HS/MRC in i.i.d. and i.n.d. Rayleigh fadings were obtained.

5. The performances of SC, H-S/MRC and T-HS/MRC in correlated Nakagami-m fading with a special correlation structure were analyzed when the fading parameter m is a positive integer. This correlation structure is more general than equal correlation and includes equal correlation as a special case.

6. New representations of Rayleigh fading amplitudes and Nakagami-m fading amplitudes with the special correlation structure were provided by linearly combining a set of independent Gaussian RVs. These representations greatly simplify the performance analyses of SC, H-S/MRC, and T-HS/MRC in correlated Nakagami-m fading.

7. An approximate SER analysis of H-S/MRC and T-HS/MRC in arbitrarily correlated Nakagami-m fading with positive integer values of fading parameter m was proposed using a Green's matrix method. Various correlation models in diversity systems were used to examine the efficiency of this approximate analysis.

8. The exact SER of T-HS/MRC in correlated Nakagami-m fading when the inverse of the covariance matrix is tridiagonal, was obtained.

9. The outage probabilities of MRC diversity systems with an arbitrary number of antennas in the presence of an arbitrary number of cochannel interferers and noise were derived when the branch gains of the desired user signal and interfering signals experience Rayleigh fading and have the same correlation matrix. Two cases that the correlation matrix has different eigenvalues and that the correlation matrix is equally correlated are considered. The results apply for both equal-power and unequal-power cochannel interferers.

10. Closed-form outage probabilities of MRC in CCI-limited Rayleigh fading were obtained for the two correlation structures.

11. Closed-form SERs of BPSK modulated cellular systems using MRC in the presence of CCI and correlated Rayleigh fading were derived for both the equi-correlated covariance matrix and the covariance matrix with different eigenvalues.

12. Closed-form BERs of BPSK using MRC with a special channel estimator were obtained in the presence of CCI and correlated Rayleigh fading. The effect of imperfect channel estimation on the BER performance was examined.

13. The question of how many receiver antennas to employ in a diversity system operating in CCI and fading was investigated. Three long-term output measures and the average BER of a MRC diversity system with CCI and noise in arbitrarily correlated Ricean fading were analyzed.

14. For the CCI-limited case, a widely applicable general rule of thumb that the performance of a fixed-size antenna array containing the maximum number of independent antennas cannot be significantly improved by adding more than one additional antenna was developed.

15. Some special cases where particular gains can be achieved by adding additional correlated antennas were discussed.

16. When noise is present, results show that the rule for the CCI-limited case still applies when the interference dominates the noise.

17. It was shown that the long-term SINRP and SAINPR reach a limit asymptotically as the number of antennas increases without bound for the fixed-length uniform linear antenna array and the fixed-radius uniform circular antenna array when both the desired user signal and the interfering signals experience correlated Rayleigh fading with the same correlation matrix. Further, the asymptotic limits are unchanged when noise is neglected.

18. A closed-form BER expression for BPSK using MRC in CCI and arbitrarily correlated Rayleigh fading was obtained.

7.2 Future Work

1. In Chapter 3, we studied the performance of generalized selection combining in correlated Nakagami-*m* fading with a special correlation structure. However, an exact performance analysis of SC, EGC, H-S/MRC and T-HS/MRC in arbitrarily correlated fadings is still an open problem. Further, the performance of diversity systems with unequal power branch signals over correlated fading channels has not been solved.

2. In general, diversity techniques rely, to a large extent, on accurate channel estimation. In Chapters 2, 3 and 4, perfect channel estimation for H-S/MRC and T-HS/MRC systems are assumed. However, in practice, these estimates are obtained in the presence of noise and time delay. In the literature, the performance of H-S/MRC in i.i.d. Rayleigh fading with channel estimation error was analyzed in [118], [119]. It is of interest to study the effects of channel estimation error on the performance of H-S/MRC and T-HS/MRC in correlated fading channels.

3. In this thesis, we consider the performance of H-S/MRC and T-HS/MRC in slow and flat fading. However, in wideband systems, such as an UWB system, the fading is frequency-selective. Therefore, it is useful to extend the results and analyze the performance of a wideband receiver with H-S/MRC and T-HS/MRC in frequency-selective and correlated fading channels.

4. In Chapter 5, we assumed that the fadings of the desired user signal and the interfering user signals were Rayleigh distributed and had the same correlation matrix. Two correlation structures were studied. The results may be extended to study the outage probability of MRC with CCI in arbitrarily correlated fading channels. Further a more general case that the desired user signal and the interfering user signals experience different fadings with different correlation matrices may be considered in future work.

5. In Chapter 6, we studied the maximum number of antennas that can be usefully

employed in a MRC receiver diversity system over correlated Ricean fading. The case of Nakagami-*m* fading may be considered. Further, it is of interest to study the case of various antenna arrays in addition to uniform linear antenna arrays and circular antenna arrays.

6. In Chapter 6, MRC receiver diversity systems were studied. It is of interest to investigate the maximum effective number of antennas at the both of the transmitter end and the receiver end for MIMO systems. One can first consider the case that the transmitter has no knowledge of the channel status but the receiver has perfect knowledge of the channel information, and the total transmit power is constrained and divided equally among the transmitter antennas. Different correlation models can be examined. For example, only the fadings at the transmitter end, or at the receiver end, are correlated. That is, only the elements in each column or each row of the MIMO fading channel matrix, are correlated with the same correlation matrix, and all of the columns or the rows are independent. A more general case that the correlation of the MIMO fading channel is arbitrary may be also studied.

Appendix A

A Useful Expression for the Product $\prod_{i=1}^{N}(1-c_i)$

In this appendix, we derive a useful expression for the product $\prod_{i=1}^{N}(1-c_i)$, namely

$$\prod_{i=1}^{N}(1-c_i) = 1+\sum_{p=1}^{N}(-1)^p \sum_{v\in S_{(\{1,\cdots,N\},p)}} \prod_{q=1}^{p} c_{v(q)} \tag{A.1}$$

where $S_{(\{1,\cdots,N\},p)}$ denotes the set of total combinations of the integers $\{1,\cdots,N\}$ taken $p\,(1\le p\le N)$ numbers at a time, and $v=\{v(1),\cdots,v(p)\}\in S_{(\{1,\cdots,N\},p)}$ denotes a specific combination of the integers $\{1,\cdots,N\}$ taken $p\,(1\le p\le N)$ numbers at a time. The following proof of eq. (A.1) is by induction.

Before the induction proof for (A.1), we first state and prove a lemma required for the induction proof of (A.1). The lemma is as follows:

Lemma: For positive integer $p\,(2\le p\le L)$,

$$\sum_{v\in S_{(\{1,\cdots,L+1\},p)}} \prod_{q=1}^{p} c_{v(q)} = \sum_{v\in S_{(\{1,\cdots,L\},p)}} \prod_{q=1}^{p} c_{v(q)} + \sum_{v\in S_{(\{1,\cdots,L\},p-1)}} c_{L+1} \prod_{q=1}^{p-1} c_{v(q)}, \tag{A.2}$$

where the set $S_{(\{1,\cdots,L\},p)}$, v and $c_i\,(1\le i\le N)$ were defined in (A.1).

Lemma Proof: The set of total combinations of the integers $\{1,\cdots,L+1\}$ taken $p\,(2\le p\le L)$ numbers at a time, $S_{(\{1,\cdots,L+1\},p)}$, can be divided into two complementary subsets. One is the set, $S_{(\{1,\cdots,L\},p)}$, the other is the corresponding complementary set of $S_{(\{1,\cdots,L\},p)}$,

denoted by $\bar{S}_{(\{1,\cdots,L\},p)}$. Specifically, the complementary set, $\bar{S}_{(\{1,\cdots,L\},p)}$, is the set of the combinations, in each of which, the integer $L+1$ is taken and the other $p-1$ numbers are taken together from the integers $\{1,\cdots,L\}$ [120, eq. (20)].

Then the left side of (A.2) becomes

$$\sum_{v\in S_{(\{1,\cdots,L+1\},p)}}\prod_{q=1}^{p}c_{v(q)}=\sum_{v\in S_{(\{1,\cdots,L\},p)}}\prod_{q=1}^{p}c_{v(q)}+\sum_{v\in\bar{S}_{(\{1,\cdots,L\},p)}}\prod_{q=1}^{p}c_{v(q)}. \tag{A.3}$$

For each combination in the complementary set, $\bar{S}_{(\{1,\cdots,L\},p)}$, the product, $\prod_{q=1}^{p}c_{v(q)}=c_{L+1}\prod_{q=1}^{p-1}c_{v(q)}$ $(v\in S_{(\{1,\cdots,L\},p-1)})$. Thus, the second term on the right side of (A.3), $\sum_{v\in\bar{S}_{(\{1,\cdots,L\},p)}}\prod_{q=1}^{p}c_{v(q)}$ becomes

$$\sum_{v\in\bar{S}_{(\{1,\cdots,L\},p)}}\prod_{q=1}^{p}c_{v(q)}=\sum_{v\in S_{(\{1,\cdots,L\},p-1)}}c_{L+1}\prod_{q=1}^{p-1}c_{v(q)}. \tag{A.4}$$

Substituting (A.4) into (A.3), (A.3) becomes (A.2).

Now consider the induction proof for the product expression given in (A.1).

Proof: First, when $N=1$ and $p=1$, the set, $S_{(\{1\},1)}=\{[1]\}$, then the right side of (A.1) becomes $1+(-1)c_1$, which equals the left side of (A.1).

When $N=2$, the product $\prod_{i=1}^{2}(1-c_i)$ becomes $1-c_1-c_2+c_1c_2$. The right side of (A.1) becomes $1+\sum_{p=1}^{2}(-1)^p\sum_{v\in S_{(\{1,2\},p)}}\prod_{q=1}^{p}c_{v(q)}$. When $p=1$, the set $S_{(\{1,2\},1)}=\{[1],[2]\}$; when $p=2$, the set $S_{(\{1,2\},2)}=\{[1,2]\}$. Then the right side of (A.1) becomes $1-c_1-c_2+c_1c_2$, which equals the left side of (A.1).

Now assume that when $N=L$, eq. (A.1) is valid. Then when $N=L+1$, the product, $\prod_{i=1}^{L+1}(1-c_i)$ becomes using [121, eq. (1.5)]

$$\begin{aligned}\prod_{i=1}^{L+1}(1-c_i) &= (1-c_{L+1})\prod_{i=1}^{L}(1-c_i)\\ &= (1-c_{L+1})\{1+\sum_{p=1}^{L}(-1)^p\sum_{v\in S_{(\{1,\cdots,L\},p)}}\prod_{q=1}^{p}c_{v(q)}\}\\ &= 1-c_{L+1}+\sum_{p=1}^{L}(-1)^p\sum_{v\in S_{(\{1,\cdots,L\},p)}}\prod_{q=1}^{p}c_{v(q)}+\\ &\quad\sum_{p=1}^{L}(-1)^{p+1}\sum_{v\in S_{(\{1,\cdots,L\},p)}}c_{L+1}\prod_{q=1}^{p}c_{v(q)}\end{aligned}$$

$$
\begin{aligned}
&= 1-\sum_{i=1}^{L} c_i - c_{L+1} + \sum_{p=2}^{L}(-1)^p \sum_{v\in S_{(\{1,\cdots,L\},p)}} \prod_{q=1}^{p} c_{v(q)} + \\
&\quad \sum_{p=1}^{L-1}(-1)^{p+1} \sum_{v\in S_{(\{1,\cdots,L\},p)}} c_{L+1} \prod_{q=1}^{p} c_{v(q)} + (-1)^{L+1} \prod_{i=1}^{L+1} c_i \\
&= 1-\sum_{i=1}^{L+1} c_i + (-1)^{L+1} \prod_{i=1}^{L+1} c_i + \sum_{p=2}^{L}(-1)^p \sum_{v\in S_{(\{1,\cdots,L\},p)}} \prod_{q=1}^{p} c_{v(q)} \\
&\quad + \sum_{p=2}^{L}(-1)^p \sum_{v\in S_{(\{1,\cdots,L\},p-1)}} c_{L+1} \prod_{q=1}^{p-1} c_{v(q)}. \qquad \text{(A.5)}
\end{aligned}
$$

Using the lemma, one can combine the two terms in (A.5) into one term, namely,

$$
\begin{aligned}
&\sum_{p=2}^{L}(-1)^p \sum_{v\in S_{(\{1,\cdots,L\},p)}} \prod_{q=1}^{p} c_{v(q)} + \sum_{p=2}^{L}(-1)^p \sum_{v\in S_{(\{1,\cdots,L\},p-1)}} c_{L+1} \prod_{q=1}^{p-1} c_{v(q)} \\
&= \sum_{p=2}^{L}(-1)^p \sum_{v\in S_{(\{1,\cdots,L+1\},p)}} \prod_{q=1}^{p} c_{v(q)}. \qquad \text{(A.6)}
\end{aligned}
$$

Thus (A.5) becomes

$$
\begin{aligned}
\prod_{i=1}^{L+1}(1-c_i) &= 1-\sum_{i=1}^{L+1} c_i + (-1)^{L+1} \prod_{i=1}^{L+1} c_i + \sum_{p=2}^{L}(-1)^p \sum_{v\in S_{(\{1,\cdots,L+1\},p)}} \prod_{q=1}^{p} c_{v(q)} \\
&= 1+\sum_{p=1}^{L+1}(-1)^p \sum_{v\in S_{(\{1;\cdots,L+1\},p)}} \prod_{q=1}^{p} c_{v(q)}. \qquad \text{(A.7)}
\end{aligned}
$$

Hence, (A.1) is valid for $N = L+1$ when it is valid for $N = L$. Therefore by induction, eq. (A.1) is proved. Eq. (A.1) is used to derive the MGF of $\gamma_{T-HS/MRC}(s)$ for i.n.d. Rayleigh fading in Section 2.4.2.

Appendix B

Joint PDF of the Ordered Random Variables

Let $f_{r_1,\cdots,r_n}(r_1,\cdots,r_n)$ denote the joint PDF of the random variables, $r_1, r_2, \cdots, r_n$. Let $r_{(1)}, r_{(2)}, \cdots, r_{(n)}$ denote the order statistics of r_k $(k = 1, \cdots, n)$ with $r_{(1)} > r_{(2)} > \cdots > r_{(n)}$. Then the joint PDF of the order statistics, $f_{r_{(1)},\cdots,r_{(n)}}(r_{(1)}, r_{(2)}, \cdots, r_{(n)})$, is given by

$$f_{r_{(1)},\cdots,r_{(n)}}(r_{(1)}, r_{(2)}, \cdots, r_{(n)}) = \sum_{e_i \in S_n} f_{r_1,r_2,\cdots,r_n}(r_{(e_i[1])}, r_{(e_i[2])}, \cdots, r_{e_i[n]}) \quad r_{(1)} > r_{(2)} > \cdots > r_{(n)} \quad \text{(B.1)}$$

where $e_i \in S_n$ denotes $e_i = \{e_i[1], \cdots, e_i[n]\}$, one specific permutation of the integers $\{1, \cdots, n\}$.

Proof: The ordered statistics, $r_{(k)}$ $(k = 1, \cdots, n)$, are actually functions of $r_1, \cdots, r_n$ expressed by $r_{(k)} = \overset{\max}{k}\{r_1, \cdots, r_n\}$, where $\overset{\max}{k}\{\cdot\}$ denotes the kth maximal value of the set $\{r_1, \cdots, r_n\}$. The whole space of $r_1, \cdots, r_n$, S, can be divided into $n!$ disjoint sub-spaces, S_{e_i}, each with $S_{e_i} = \{r_{e_i[1]} > r_{e_i[2]} > \cdots > r_{e_i[n]}\}$, where $e_i = \{e_i[1], \cdots, e_i[n]\}$, one specific permutation of the integers $\{1, \cdots, n\}$. Since all of the RVs, $r_1, \cdots, r_n$, are assumed not to be equal, one can show that for each sub-space S_{e_i}, there is one and only one solution to the functions $r_{(k)}$ $(k = 1, \cdots, n)$, namely, $r_{(k)} = r_{e_i[k]}$ $(k = 1, \cdots, n)$. Then, the joint PDF of the

ordered $r_{(1)}, \cdots, r_{(n)}$ can be derived using the Jacobian method [35] as

$$f_{r_{(1)},\cdots,r_{(n)}}(r_{(1)}, r_{(2)}, \cdots, r_{(n)}) = \sum_{e_i \in S_n} \frac{f_{r_1,r_2,\cdots,r_n}(r_{(e_i[1])}, r_{(e_i[2])}, \cdots, r_{(e_i[n])})}{|J_{e_i}(r_1, r_2, \cdots, r_n)|}$$
$$r_{(1)} > r_{(2)} > \cdots > r_{(n)} \qquad \text{(B.2)}$$

where $J_{e_i}(r_1, r_2, \cdots, r_n)$ is the Jacobian of the corresponding sub-space, S_{e_i}, and the absolute value of $J_{e_i}(r_1, r_2, \cdots, r_n)$, $|J_{e_i}(r_1, r_2, \cdots, r_n)| = 1$. Therefore (B.2) becomes (B.1).

Appendix C

Two-Dimensional Inverse Fourier Transform of $\prod_{i=1}^{N} \frac{1}{1+j\lambda_i\omega_1+j\lambda_i^2\omega_2}$

Let $\mathbb{F}(u,w)$ denote the two-dimensional Fourier transform of u and w given by

$$\mathbb{F}_{u,w}(j\omega_1, j\omega_2) = \prod_{i=1}^{N} \frac{1}{1+j\lambda_i\omega_1+j\lambda_i^2\omega_2} \tag{C.1}$$

where all of λ_i $(i = 1, \cdots, N)$ have unequal values.

Using [77, eqs. (10), (11)], (C.1) can be represented by

$$\begin{aligned}
\mathbb{F}_{u,w}(j\omega_1, j\omega_2) &= \frac{1}{\prod_{i=1}^{N}\lambda_i} \sum_{i=1}^{N} \frac{1}{\prod_{k=1,k\neq i}^{N}\left[(\lambda_i-\lambda_k)\left(\frac{1}{\lambda_i\lambda_k}-j\omega_2\right)\right]} \\
&\quad \times \frac{1}{\left(\frac{1}{\lambda_i}+j\lambda_i\omega_2\right)+j\omega_1} \\
&= \frac{1}{\prod_{i=1}^{N}\lambda_i} \sum_{i=1}^{N} \frac{1}{[\prod_{k=1,k\neq i}^{N}(\lambda_i-\lambda_k)]} \\
&\quad \times \frac{1}{\left(\frac{1}{\lambda_i}+j\lambda_i\omega_2\right)+j\omega_1} \times \frac{1}{\prod_{k=1,k\neq i}^{N}\left(\frac{1}{\lambda_i\lambda_k}-j\omega_2\right)} \\
&= \sum_{i=1}^{N}\sum_{k=1,k\neq i}^{N} \frac{(\lambda_i\lambda_k)^{N-3}}{(\lambda_i-\lambda_k)\prod_{q=1,q\neq i,k}^{N}(\lambda_i-\lambda_q)(\lambda_k-\lambda_q)} \\
&\quad \times \frac{1}{\left(\frac{1}{\lambda_i\lambda_k}-j\omega_2\right)\times\left(\frac{1}{\lambda_i}+j\lambda_i\omega_2+j\omega_1\right)}
\end{aligned}$$

$$= \sum_{i,k\in\{1,\cdots,N\},\, i<k} \frac{(\lambda_i\lambda_k)^{N-3}}{\prod_{q=1,q\neq i,k}^{N}(\lambda_i-\lambda_q)(\lambda_k-\lambda_q)} \times \frac{1}{\left(\frac{1}{\lambda_i}+j\lambda_i\omega_2+j\omega_1\right)} \times \frac{1}{\left(\frac{1}{\lambda_k}+j\lambda_k\omega_2+j\omega_1\right)} \tag{C.2}$$

According to the definitions of the two-dimensional Fourier transform and two-dimensional convolution [97], and assuming $\lambda_i > \lambda_j > 0$, we have

$$\mathbb{F}\left\{e^{-\frac{1}{\lambda}u}\delta(w-\lambda u)U(u)\right\} = \frac{1}{\frac{1}{\lambda}+j\lambda\omega_2+j\omega_1} \tag{C.3}$$

and

$$\begin{aligned}
&\mathbb{F}^{-1}\left\{\frac{1}{\left(\frac{1}{\lambda_i}+j\lambda_i\omega_2+j\omega_1\right)}\cdot\frac{1}{\left(\frac{1}{\lambda_k}+j\lambda_k\omega_2+j\omega_1\right)}\right\} \\
&= \left(e^{-\frac{1}{\lambda_i}u}\delta(w-\lambda_i u)U(u)\right) ** \left(e^{-\frac{1}{\lambda_k}u}\delta(w-\lambda_k u)U(u)\right) \\
&= \frac{e^{-\left(\frac{1}{\lambda_i}+\frac{1}{\lambda_k}\right)u+\frac{w}{\lambda_i\lambda_k}}}{\lambda_i-\lambda_k}, \qquad 0\le\lambda_k u\le w\le\lambda_i u
\end{aligned} \tag{C.4}$$

where $\delta(x)$ is Kronecker delta function and $U(x)$ is given by

$$U(x) = \begin{cases} 1, & x\ge 0; \\ 0, & x<0. \end{cases}$$

$\mathbb{F}\{\cdot\}$ and $\mathbb{F}^{-1}\{\cdot\}$ denotes the two-dimensional Fourier transform and inverse Fourier transform, respectively, and $**$ denotes the two-dimensional convolution.

Then, taking the two-dimensional inverse Fourier transform in (C.2) and combining with (C.3) and (C.4), the two-dimensional inverse Fourier transform of (C.1) becomes

$$\begin{aligned}
f_{u,w}(u,w) &= \sum_{i,k\in\{1,\cdots,N\},\, i<k} \frac{(\lambda_i\lambda_k)^{N-3}e^{-\left(\frac{1}{\lambda_i}+\frac{1}{\lambda_k}\right)u+\frac{w}{\lambda_i\lambda_k}}}{(\lambda_i-\lambda_k)\prod_{q=1,\,q\neq i,k}^{N}(\lambda_i-\lambda_q)(\lambda_k-\lambda_q)} \\
&\quad \times\left[U(\lambda_i u-w)-U(\lambda_k u-w)+\delta(\lambda_k u-w)\right], \qquad u\ge 0.
\end{aligned} \tag{C.5}$$

In the following, we prove a equality used in Section 5.3. Assume that λ_i $(i=1,\cdots,N)$ satisfy $\lambda_1 > \lambda_2 > \cdots > \lambda_N > 0$, then

$$\sum_{i,k\in\{1,\cdots,N\},\, i<k} \frac{(\lambda_i\lambda_k)^{N-2}}{\prod_{q=1,\,q\neq i,k}^{N}(\lambda_i-\lambda_q)(\lambda_k-\lambda_q)} = 1. \tag{C.6}$$

Proof: From (C.1) and (C.2), one obtains

$$\prod_{i=1}^{N} \frac{1}{1+j\lambda_i\omega_1+j\lambda_i^2\omega_2} = \sum_{i,k\in\{1,\cdots,N\},\, i<k} \frac{(\lambda_i\lambda_k)^{N-3}}{\prod_{q=1,q\neq i,k}^{N}(\lambda_i-\lambda_q)(\lambda_k-\lambda_q)} \times \frac{1}{\left(\frac{1}{\lambda_i}+j\lambda_i\omega_2+j\omega_1\right)} \times \frac{1}{\left(\frac{1}{\lambda_k}+j\lambda_k\omega_2+j\omega_1\right)}. \quad \text{(C.7)}$$

Let $\omega_1 = 0$ and $\omega_2 = 0$, then the left side of eq. (C.7) equals 1. And the right side of eq. (C.7) becomes

$$\begin{aligned} & \sum_{i,k\in\{1,\cdots,N\},\, i<k} \frac{(\lambda_i\lambda_k)^{N-3}}{\prod_{q=1,q\neq i,k}^{N}(\lambda_i-\lambda_q)(\lambda_k-\lambda_q)} \times \frac{1}{\left(\frac{1}{\lambda_i}\right)} \times \frac{1}{\left(\frac{1}{\lambda_k}\right)} \\ = & \sum_{i,k\in\{1,\cdots,N\},\, i<k} \frac{(\lambda_i\lambda_k)^{N-2}}{\prod_{q=1,\, q\neq i,k}^{N}(\lambda_i-\lambda_q)(\lambda_k-\lambda_q)} \\ = & \ 1. \end{aligned} \quad \text{(C.8)}$$

Thus (C.6) is proved.

Appendix D

Some Derivations for Chapter 6

D.1 Expectation Derivations

In this part, we derive solutions for the expectations in the numerator and the denominator of (6.4). Consider the numerator first. Let the matrix Λ_0 denote a diagonal matrix composed of the eigenvalues of the covariance matrix for the desired user signal fadings $\sum_{\mathbf{c_0}}$, λ_0^i $(i = 1, \cdots, N)$ such that $\sum_{\mathbf{c_0}} = Q\Lambda_0 Q^H$, where Q is the corresponding eigenvector matrix with $Q^H Q = QQ^H = I$, and where I denotes the unit matrix. Further, let $\mathbf{v}_0 = \Lambda_0^{-1/2} Q^H \mathbf{c_0}$, which is a $N \times 1$ complex Gaussian vector with mean vector $\mu_0 = \Lambda_0^{-1/2} Q^H \mu_{\mathbf{c_0}}$ and unit variance matrix I. Let $u = \mathbf{c_0}^H \mathbf{c_0} = \mathbf{v}_0^H \Lambda_0 \mathbf{v}_0 = \sum_{i=1}^N \lambda_0^i |v_0^i|^2$, where v_0^i $(i = 1, \cdots, N)$ are the elements of the vector $\mathbf{v_0}$ and are independent complex Gaussian random variables. Since $|v_0^i|^2$ follows a noncentral chi-square distribution, $\chi_n(s^2, \sigma^2)$ with $n = 2$ degrees of freedom, noncentrality parameter $s^2 = |\mathbb{E}\{v_0^i\}|^2$, and Gaussian variance $\sigma^2 = 1/2$ [4], the

expectation $\mathbb{E}\{u^2\}$ is derived as

$$\begin{aligned}
\mathbb{E}\{u^2\} &= Var\{u\} + (\mathbb{E}\{u\})^2 \\
&= \sum_{i=1}^{N} (\lambda_0^i)^2 Var\{|v_0^i|^2\} + \left(\mathbb{E}\{tr(\mathbf{c_0}^H \mathbf{c_0})\}\right)^2 \\
&= tr\{\Lambda_0^2\} + 2\mu_0{}^H \Lambda_0^2 \mu_0 + \left(tr(\mathbb{E}\{\mathbf{c_0}\mathbf{c_0}^H\})\right)^2 \\
&= tr\{\textstyle\sum_{\mathbf{c_0}}^2\} + 2(\Lambda_0^{-1/2} Q^H \mu_{\mathbf{c_0}})^H \Lambda_0^2 (\Lambda_0^{-1/2} Q^H \mu_{\mathbf{c_0}}) + tr^2(R_{\mathbf{c_0}}) \\
&= tr(\textstyle\sum_{\mathbf{c_0}}^2) + 2(\mu_{\mathbf{c_0}}{}^H \textstyle\sum_{\mathbf{c_0}} \mu_{\mathbf{c_0}}) + tr^2(R_{\mathbf{c_0}})
\end{aligned} \tag{D.1}$$

where $Var\{\cdot\}$ is the variance operator, and $R_{\mathbf{c_0}} = \mathbb{E}\{\mathbf{c_0}\mathbf{c_0}^H\} = \sum_{\mathbf{c_0}} + (\mu_{\mathbf{c_0}}\mu_{\mathbf{c_0}}{}^H)$, is the correlation matrix of $\mathbf{c_0}$, and $tr(\cdot)$ denotes the trace of a matrix and has the property $tr(AB) = tr(BA)$ [122] and $\mathbb{E}\{tr(\cdot)\} = tr(\mathbb{E}\{\cdot\})$ because the trace is a linear operation.

Since $(\mathbf{c_0}^H \mathbf{c_n})$ is a scalar, $(\mathbf{c_0}^H \mathbf{c_n}) = tr(\mathbf{c_0}^H \mathbf{c_n})$. Then, the expectation terms in the sum of the denominator of (6.4) can be rewritten as

$$\begin{aligned}
\mathbb{E}\{|\mathbf{c_0}^H \mathbf{c_n}|^2\} &= \mathbb{E}\{tr(\mathbf{c_0}^H \mathbf{c_n}\mathbf{c_n}^H \mathbf{c_0})\} = \mathbb{E}\{tr(\mathbf{c_0}^H (\mathbf{c_n}\mathbf{c_n}^H)\mathbf{c_0})\} \\
&= \mathbb{E}\{tr((\mathbf{c_0}\mathbf{c_0}^H)(\mathbf{c_n}\mathbf{c_n}^H))\} \\
&= tr(\mathbb{E}\{(\mathbf{c_0}\mathbf{c_0}^H)(\mathbf{c_n}\mathbf{c_n}^H)\}) \\
&= tr(R_{\mathbf{c_0}} R_{\mathbf{c_n}}) \qquad\qquad n = 1, \cdots, N_I
\end{aligned} \tag{D.2}$$

where $R_{\mathbf{c_n}}$ $(n = 1, \cdots, N_I)$ is the fading correlation matrix for the nth interfering user signal, and where $\mathbb{E}\{(\mathbf{c_0}\mathbf{c_0}^H)(\mathbf{c_n}\mathbf{c_n}^H)\} = \mathbb{E}\{\mathbf{c_0}\mathbf{c_0}^H\}\mathbb{E}\{\mathbf{c_n}\mathbf{c_n}^H\}$ because $\mathbf{c_0}$ and $\mathbf{c_n}$ are assumed independent. Substituting (D.1) and (D.2) into (6.4), the SIRP in (6.4) becomes (6.5).

D.2 Limits of SIRP and SAPR in Rayleigh Fading

For linear antenna arrays, since the covariance matrix Σ_0 is a real symmetric toeplitz matrix with element $\Sigma_0^{i,j} = \psi(|i-j|d)$ and $tr(\Sigma_0) = N$, the SIRP in (6.8) becomes

$$\begin{aligned}\gamma_{SIRP} &= \Gamma_I\left(1+\frac{N^2}{\sum_{i=1}^{N}\sum_{j=1}^{N}\psi^2(|i-j|d)}\right)\\ &= \Gamma_I\left(1+\frac{N^2}{N+2\sum_{i=1}^{N-1}(N-i)\psi^2(id)}\right)\\ &= \Gamma_I(1+f(N)).\end{aligned} \tag{D.3}$$

Since the number of antennas N and the array length L satisfy $L=(N-1)d$, one has

$$\begin{aligned}f(N)=f(1+L/d) &= \frac{(d+L)^2}{d^2+Ld+2\sum_{i=1}^{L/d}(L-id+d)\psi^2(id)d}\\ &= \frac{(d+L)^2}{d^2+Ld+2\sum_{i=1}^{L/d}(L-id)\psi^2(id)d+2d\sum_{i=1}^{L/d}\psi^2(id)d}.\end{aligned} \tag{D.4}$$

As N becomes large, $N\to\infty$, and d becomes very close to zero, $d\to 0$. Then the limit of $f(N)$ is given by

$$\lim_{N\to\infty} f(N) = \lim_{d\to 0} f(1+L/d) = \frac{L^2/2}{\int_0^L (L-x)\psi^2(x)dx}. \tag{D.5}$$

Combining (D.5) with (D.3) and (6.11), the limits of SIRP and SAPR for linear antenna arrays in correlated Rayleigh fading are obtained as (6.14) and (6.15), respectively.

Similarly, for circular antenna arrays, the SIRP in (6.8) becomes

$$\gamma_{SIRP} = \Gamma_I\left(1+\frac{N^2}{N+2\sum_{i=1}^{N-1}(N-i)\varphi^2(i\theta)}\right) = \Gamma_I(1+f(N)). \tag{D.6}$$

Since $N = 2\pi/\theta$, one has

$$f(N) = f(2\pi/\theta) = \frac{(2\pi)^2}{2\pi\theta+2\sum_{i=1}^{2\pi/\theta-1}(2\pi-i\theta)\varphi^2(i\theta)\theta}. \tag{D.7}$$

As N becomes large, $N\to\infty$, and θ becomes very close to zero, $\theta\to 0$. Then the limit of $f(N)$ is given by

$$\lim_{N\to\infty} f(N) = \lim_{\theta\to 0} f(2\pi/\theta) = \frac{2\pi^2}{\int_0^{2\pi}(2\pi-\theta)\varphi^2(\theta)d\theta}. \tag{D.8}$$

Combining (D.8) with (D.3) and (6.11), the limits of SIRP and SAPR for circular antenna arrays in correlated Rayleigh fading are obtained as (6.18) and (6.19), respectively.

D.3 CF of Y Conditioned on b

Averaging $\phi_{Y|\mathbf{c_0},\mathbf{b}}(s)$ in (6.40) over $\mathbf{v_0}$, the conditional MGF on b is given by

$$\begin{aligned}\phi_{Y|b}(s) &= \prod_{i=1}^{N}\mathbb{E}_{v_0^i}\left\{\exp\left((s\lambda_0^i+a_1s^2\lambda_0^i\lambda_I^i+a_2s^2\lambda_0^i)|v_0^i|^2+bs(\mu_I^i(v_0^i)^H+(\mu_I^i)^Hv_0^i)\right)\right\}\\ &= \prod_{i=1}^{N}\phi_{v_0^i}. \end{aligned} \tag{D.9}$$

Rewrite $v_0^i = x_0^i + jy_0^i + \mu_0^i$ where $\mu_0^i = \mathbb{E}\{v_0^i\}$, then x_0^i and y_0^i are independent zero-mean Gaussian RVs with variance $1/2$. Then $\phi_{v_0^i}$ can be calculated as

$$\begin{aligned}\phi_{v_0^i} &= \mathbb{E}_{x_0^i}\left\{e^{(s\lambda_0^i+a_1s^2\lambda_0^i\lambda_I^i+a_2s^2\lambda_0^i)(x_0^i)^2+2(Re\{\mu_0^i\}(s\lambda_0^i+a_1s^2\lambda_0^i\lambda_I^i+a_2s^2\lambda_0^i)+bsRe\{\mu_I^i\})x_0^i}\right\}\\ &\quad\times\mathbb{E}_{y_0^i}\left\{e^{(s\lambda_0^i+a_1s^2\lambda_0^i\lambda_I^i+a_2s^2\lambda_0^i)(y_0^i)^2+2(Im\{\mu_0^i\}(s\lambda_0^i+a_1s^2\lambda_0^i\lambda_I^i+a_2s^2\lambda_0^i)+bsIm\{\mu_I^i\})y_0^i}\right\}\\ &\quad\times e^{(s\lambda_0^i+a_1s^2\lambda_0^i\lambda_I^i+a_2s^2\lambda_0^i)|\mu_0^i|^2+2bsRe\{(\mu_0^i)^H\mu_I^i\}}\\ &= \phi_{x_0^i}\times\phi_{y_0^i}\times f_{\mu_I^i,\mu_0^i}\end{aligned} \tag{D.10}$$

where $Im\{z\}$ is the imaginary part operation on the complex number z, and $\phi_{x_0^i}$ and $\phi_{y_0^i}$ are given, respectively, by

$$\begin{aligned}\phi_{x_0^i} &= \frac{1}{\sqrt{1-s\lambda_0^i-a_1s^2\lambda_0^i\lambda_I^i-a_2s^2\lambda_0^i}}\times\\ &\quad\exp\left(\frac{(Re\{\mu_0^i\}(s\lambda_0^i+a_1s^2\lambda_0^i\lambda_I^i+a_2s^2\lambda_0^i)+bsRe\{\mu_I^i\})^2}{1-s\lambda_0^i-a_1s^2\lambda_0^i\lambda_I^i-a_2s^2\lambda_0^i}\right)\end{aligned} \tag{D.11}$$

and

$$\begin{aligned}\phi_{y_0^i} &= \frac{1}{\sqrt{1-s\lambda_0^i-a_1s^2\lambda_0^i\lambda_I^i-a_2s^2\lambda_0^i}}\times\\ &\quad\exp\left(\frac{(Im\{\mu_0^i\}(s\lambda_0^i+a_1s^2\lambda_0^i\lambda_I^i+a_2s^2\lambda_0^i)+bsIm\{\mu_I^i\})^2}{1-s\lambda_0^i-a_1s^2\lambda_0^i\lambda_I^i-a_2s^2\lambda_0^i}\right).\end{aligned} \tag{D.12}$$

Substituting (D.11) and (D.12) into (D.10), $\phi_{v_0^i}$ can be simplified as

$$\phi_{v_0^i} = \frac{1}{1 - s\lambda_0^i - a_1 s^2 \lambda_0^i \lambda_I^i - a_2 s^2 \lambda_0^i} \times \exp\left(\frac{|\mu_0^i|^2 (s\lambda_0^i + a_1 s^2 \lambda_0^i \lambda_I^i + a_2 s^2 \lambda_0^i) + b^2 s^2 |\mu_I^i|^2 + 2bsRe\{\mu_0^i (\mu_I^i)^H\}}{1 - s\lambda_0^i - a_1 s^2 \lambda_0^i \lambda_I^i - a_2 s^2 \lambda_0^i} \right) \tag{D.13}$$

where μ_0^i and μ_I^i are the ith elements of the mean vector $\mu_{\mathbf{0}} = \Lambda_0^{-1/2} Q^H \mu_{\mathbf{c_0}}$ and $\mu_{\mathbf{I}} = \Lambda_0^{1/2} Q^H \mu_{\mathbf{c_I}}$, respectively. Then the conditional CF of Y on b is obtained as (6.41) by substituting (D.13) into (D.9) and setting $s = j\omega$.

References

[1] A. Paulraj, R. Nabar, and D. Gore, *Introduction to Space-Time Wireless Communications*. New York: Cambridge University Press, 2003.

[2] G. L. Stüber, *Principles of Mobile Communication*, 2nd ed. Norwell, MA: Kluwer Academic Publishers, 2001.

[3] M. K. Simon and M.-S. Alouini, *Digital Communications over Fading Channels: A Unified Approach to Performance Analysis*. New York: Wiley, 2002.

[4] J. G. Proakis, *Digital Communications*, 3rd ed. New York: McGraw-Hill, 1995.

[5] M. Nakagami, "The *m*-distribution- a general formula of intensity distribution of rapid fading," in *Statistical Methods in Radio Wave Propagation*, W. G. Hoffman, Oxford: Pergamon Press, 1960, pp. 3–36.

[6] I. S. Gradshteyn and I. M. Ryzhik, Eds., *Table of Integrals, Series, and Products*, 5th ed. New York: Academic Press, 1994.

[7] H. V. MacDonald, "The cellular concept," *Bell System Technical Journal*, vol. 58, pp. 15–41, Jan. 1979.

[8] G. J. Foschini and M. J. Gans, "On limits of wireless communications in a fading environment when using multiple antennas," *Wireless Personal Communications*, vol. 6, pp. 311–335, Mar. 1998.

[9] I. E. Telatar, "Capacity of multi-antenna Gaussian channels," *European Transactions on Telecommunications*, vol. 10, pp. 585–595, Nov.-Dec. 1999.

[10] A. M. D. Turkmani, A. A. Arowojolu, P. A. Jefford, and C. J. Kellett, "An experimental evaluation of the performance of two-branch space and polarization diversity schemes at 1800 MHz," *IEEE Transactions on Vehicular Technology*, vol. VT-44, no. 2, pp. 318–326, May 1995.

[11] N. Chiurtu, B. Rimoldi, and E. Telatar, "Dense multiple antenna systems," in *Information Theory Workshop (ITW'01)*, Cairns, Australia, Sept.2-7 2001, pp. 108–109.

[12] G. L. Turin, F. D. Clapp, T. L. Johnston, S. B. Fine, and D. Lavry, "A statistical model of urban multipath propagation," *IEEE Transactions on Vehicular Technology*, vol. VT-21, no. 1, pp. 1–9, Feb. 1972.

[13] A. S. Bajwa, "UHF wideband statistical model and simulation of mobile radio multipath propagation effects," *IEE Proceedings Part F*, vol. 132, no. 5, pp. 327–333, Aug. 1985.

[14] F. Patenaude, J. H. Lodge, and J. Y. Chouinard, "Temporal correlation analysis of frequency selective fading channels," in *6th Annual International Conference on Wireless Communications (Wireless'94)*, Calgary, Alberta, Canada, July11-13 1994, pp. 134–139.

[15] F. Patenaude, J. Lodge, and J. Y. Chouinard, "Eigen-analysis of wideband fading channel impulse responses," *IEEE Transactions on Vehicular Technology*, vol. 48, no. 2, pp. 593–606, Mar. 1999.

[16] P. Lombardo, G. Fedele, and M. M. Rao, "MRC performance for binary signals in Nakagami fading with general branch correlation," *IEEE Transactions on Communications*, vol. 47, no. 1, pp. 44–52, Jan. 1999.

[17] J. Luo, J. R. Zeidler, and S. Mclaughlin, "Performance analysis of compact antenna arrays with MRC in correlated Nakagami fading channels," *IEEE Transactions on Vehicular Technology*, vol. 50, no. 1, pp. 267–277, Jan. 2001.

[18] J. Salz and J. H. Winters, "Effect of fading correlation on adaptive arrays in digital mobile radio," *IEEE Transactions on Vehicular Technology*, vol. 43, no. 4, pp. 1049–1057, Nov. 1994.

[19] F. Adachi, M. T. Feeney, A. G. Williamson, and J. D. Parsons, "Crosscorrelation between the envelopes of 900 MHz signals received at a mobile radio base station sites," *IEE Proceedings Part F.*, vol. 133, no. 6, pp. 506–512, Oct. 1986.

[20] S. H. Van Wambeck and A. H. Ross, "Performance of diversity receiving systems," *Proceedings of the IRE*, vol. 39, no. 3, pp. 256–264, Mar. 1951.

[21] L. R. Kahn, "Ratio squarer," *Proceedings of the IRE*, vol. 42, Nov. 1954.

[22] D. G. Brennan, "Linear diversity combining techniques," *Proceedings of the IRE*, vol. 47, pp. 1075–1102, June 1959.

[23] M. Z. Win and J. H. Winters, "Analysis of hybrid selection/maximal-ratio combining in Rayleigh fading," *IEEE Transactions on Communications*, vol. 47, no. 12, pp. 1773–1776, Dec. 1999.

[24] M. Z. Win and J. H. Winters, "Virtual branch analysis of symbol error probability for hybrid selection/maximal-ratio combining in Rayleigh fading," *IEEE Transactions on Communications*, vol. 49, no. 11, pp. 1926–1934, Nov. 2001.

[25] M.-S. Alouini and M. K. Simon, "Performance of coherent receivers with hybrid SC/MRC over Nakagami-*m* fading channels," *IEEE Transactions on Vehicular Technology*, vol. 48, no. 4, pp. 1155–1164, July 1999.

[26] W. C. Jakes, Ed., *Microwave Mobile Communications*. New York: John Wiley and Sons, 1974.

[27] R. Price and P. E. Green, "A communication technique for multipath channels," *Proceedings of the IRE*, vol. 46, pp. 555–570, Mar. 1958.

[28] J. S. Lehnert and M. B. Pursley, "Multipath diversity reception of spread spectrum multiple access communications," *IEEE Transactions on Communications*, vol. 35, no. 11, pp. 1189–1198, Nov. 1987.

[29] T. Eng, N. Kong, and L. B. Milstein, "Comparison of diversity combining techniques for Rayleigh-fading channels," *IEEE Transactions on Communications*, vol. 44, no. 9, pp. 1117–1129, Sept. 1996.

[30] A. I. Sulyman and M. Kousa, "Bit error rate performance of a generalized diversity selection combining scheme in Nakagami fading channels," in *Proc. IEEE Wireless Communications and Networking Conference (WCNC'00)*, Chicago, IL, USA, Sept. 23-28 2000, pp. 1080–1085.

[31] J. Foerster, "Channel modeling sub-committee report (final)," *P802.15-02/490r1-SG3a, IEEE P802.15 Wireless Personal Area Networks*, Feb. 2003.

[32] M. K. Simon and M.-S. Alouini, "Performance analysis of generalized selection combining with threshold test per branch (T-GSC)," in *Proc. IEEE Global Telecommunications Conference (GLOBECOM '01)*, Nov. 25-29 2001, vol. 2, pp. 1176–1181.

[33] M. K. Simon and M.-S. Alouini, "Performance analysis of generalized selection combining with threshold test per branch (T-GSC)," *IEEE Transactions on Vehicular Technology*, vol. 51, no. 5, pp. 1018–1029, Sept. 2002.

[34] A. Annamalai, G. Deora, and C. Tellambura, "Unified analysis of generalized selection diversity with normalized threshold test per branch," in *Proc. IEEE Wireless Communications and Networking Conference (WCNC'03)*, Mar. 16-20 2003, vol. 2, pp. 752–756.

[35] A. Papoulis and S. U. Pillai, *Probability, Random Variables and Stochastic Process*, 4th ed. New York: McGraw-Hill, 2002.

[36] X. Zhang and N. C. Beaulieu, "SER and outage of threshold-based hybrid selection/maximal-ratio combining over generalized fading channels," *IEEE Transactions on Communications*, vol. 52, no. 12, pp. 2143–2153, Dec. 2004.

[37] X. Zhang and N. C. Beaulieu, "Threshold-based hybrid selection/maximal-ratio combining over generalized fading channels," in *Proc. IEEE Global Telecommunications Conference (GLOBECOM'04)*, Dallas, TX, USA, Nov 29– Dec. 3 2004, vol. 1, pp. 462–468.

[38] M.-S. Alouini and A. J. Goldsmith, "A unified approach for calculating error rates of linearly modulated signals over generalized fading channels," *IEEE Transactions on Communications*, vol. 47, no. 9, pp. 1324–1334, Sept. 1999.

[39] R. K. Mallik and M. Z. Win, "Analysis of hybrid selection/maximal-ratio combining in correlated Nakagami fading," *IEEE Transactions on Communications*, vol. 50, no. 8, pp. 1372–1383, Aug. 2002.

[40] A. Annamalai, G. K. Deora, and C. Tellambura, "Unified error probability analysis for generalized selection diversity in Rician fading channels," in *Proc. IEEE Vehicular Technology Conference (VTC'02)*, Birmingham, UK, May 2002, vol. 4, pp. 2042–2046.

[41] A. Annamalai and C. Tellambura, "A new approach to performance evaluation of generalized selection diversity receivers in wireless channels," in *Proc. IEEE Vehicular Technology Conference (VTC'01)*, Oct. 2001, vol. 4, pp. 2309–2313.

[42] L. B. Milstein, "Guidelines for evaluation of radio transmission technologies for IMT-2000," *ITU-R M. 1225*, 1997.

[43] JTC(AIR), "Guidelines for system deployment modeling and simulation," in *94.08.01-065R4*.

[44] N. Kong and L. B. Milstein, "SNR of generalized diversity selection combining with nonidentical Rayleigh fading statistics," *IEEE Transactions on Communications*, vol. 48, no. 8, pp. 1266–1271, Aug. 2000.

[45] M. K. Simon and M.-S. Alouini, "A compact performance analysis of generalized selection combining with independent but nonidentically distributed Rayleigh fading paths," *IEEE Transactions on Communications*, vol. 50, no. 9, pp. 1409–1412, Sept. 2002.

[46] M. Schwartz, W. R. Bennett, and S. Stein, *Communication Systems and Techniques*. New York: McGraw-Hill, 1966.

[47] M. K. Simon and M.-S. Alouini, "A unified performance analysis of digital communication with dual selective combining diversity over correlated Rayleigh and Nakagami-*m* fading channels," *IEEE Transactions on Communications*, vol. 47, no. 1, pp. 33–43, Jan. 1999.

[48] Y.-C. Ko, M.-S. Alouini, and M. K. Simon, "Average SNR of dual selection combining over correlated Nakagami-*m* fading channels," *IEEE Communications Letters*, vol. 4, no. 1, pp. 12–14, Jan. 2000.

[49] C. Tellambura, A. Annamalai, and V. K. Bhargava, "Closed form and infinite series solutions for the MGF of a dual-diversity selection combining output in bivariate Nakagami fading," *IEEE Transactions on Communications*, vol. 51, no. 4, pp. 539–542, Apr. 2003.

[50] G. K. Karagiannidis, D. A. Zogas, and S. A. Kotsopoulos, "Performance analysis of triple selection diversity over exponentially correlated Nakagami-*m* fading channels," *IEEE Transactions on Communications*, vol. 51, no. 8, pp. 1245–1248, Aug. 2003.

[51] D. A. Zogas, G. K. Karagiannidis, and S. A. Kotsopoulos, "On the average output SNR in selection combining with three correlated branches over Nakagami-*m* fading

channels," *IEEE Transactions on Wireless Communications*, vol. 3, no. 1, pp. 25–28, Jan. 2004.

[52] Q. T. Zhang and H. G. Lu, "A general analytical approach to multi-branch selection combining over various spatially correlated fading channels," *IEEE Transactions on Communications*, vol. 50, no. 7, pp. 1066–1073, July 2002.

[53] G. K. Karagiannidis, D. A. Zogas, and S. A. Kotsopoulos, "On the multivariate Nakagami-*m* distribution with exponential correlation," *IEEE Transactions on Communications*, vol. 51, no. 8, pp. 1240–1244, Aug. 2003.

[54] M.-S. Alouini and M. K. Simon, "Application of the Dirichlet transformation to the performance evaluation of generalized selection combining over Nakagami-*m* fading channels," *Journal on Communication and Networks*, vol. 1, pp. 5–13, Mar. 1999.

[55] Y. Ma and C. C. Chai, "Unified error probability analysis for generalized selection combining in Nakagami fading channels," *IEEE Journal on Selected Areas in Communications*, vol. 18, no. 11, pp. 2198–2210, Nov. 2000.

[56] A. Annamalai and C. Tellambura, "Error rates of hybrid SC/MRC diversity systems on Nakagami-*m* channels," in *Proc. IEEE Wireless Communications and Networking Conference (WCNC'00)*, Sept. 2000, pp. 227–231.

[57] Y. Ma and S. Pasupathy, "Efficient performance evaluation for generalized selection combining on generalized fading channels," *IEEE Transactions on Wireless Communications*, vol. 3, no. 1, pp. 29–34, Jan. 2004.

[58] A. Annamalai, G. K. Deora, and C. Tellambura, "Theoretical diversity improvement in GSC(N, L) receiver with nonidentical fading statistics," *IEEE Transactions on Communications*, vol. 53, no. 6, pp. 1027–1035, June 2005.

[59] X. Zhang and N. C. Beaulieu, "SER of triple hybrid selection/maximal-ratio combining in exponentially correlated Nakagami fading," *IEE Electronics Letters*, vol. 41, no. 22, pp. 1228–1230, Oct. 2005.

[60] X. Zhang and N. C. Beaulieu, "SER of threshold-based hybrid selection/maximal-ratio combining in equi-correlated Nakagami fading," *IEEE Communications Letters*, vol. 8, no. 9, pp. 552–554, Sept. 2004.

[61] Y. Chen and C. Tellambura, "Distribution functions of selection combiner output in equally correlated Rayleigh, Rician and Nakagami-*m* fading channels," *IEEE Transactions on Communications*, vol. 52, no. 1, pp. 1948–1956, Nov. 2004.

[62] Y. L. Tong, *The Multivariate Normal Distribution*. New York: Springer, 1990.

[63] X. Zhang and N. C. Beaulieu, "Performance analysis of generalized selection combining in generalized correlated Nakagami- *m* fading," *IEEE Transactions on Communications*, vol. 54, no. 11, pp. 2103–2112, Nov. 2006.

[64] L. E. Blumenson and K. S. Miller, "Properties of generalized Rayleigh distributions," *The Annals of Mathematical Statistics*, vol. 34, no. 3, pp. 903–910, 1963.

[65] R. Nabben, "On the Green's matrices of trees," *SIAM Journal on Matrix Analysis and Applications*, vol. 22, no. 4, pp. 1014–1026, 2000.

[66] G. K. Karagiannidis, D. A. Zogas, and S. A. Kotsopoulos, "An efficient approach to multivariate Nakagami-*m* distribution using Green's matrix approximation," *IEEE Transactions on Wireless Communications*, vol. 2, no. 5, pp. 883–889, Sept. 2003.

[67] X. Zhang and N. C. Beaulieu, "SER of threshold-based hybrid selection/maximal-ratio combining in correlated Nakagami fading," *IEEE Transactions on Communications*, vol. 53, no. 9, pp. 1423–1426, Sept. 2005.

[68] X. Zhang and N. C. Beaulieu, "Approximate SER of H-S/MRC in Nakagami fading with arbitrary branch power correlation," *IEEE Transactions on Communications*, vol. 54, no. 1, pp. 56–60, Jan. 2006.

[69] C. C. Tan and N. C. Beaulieu, "Infinite series representations of the bivariate Rayleigh and Nakagami-*m* distributions," *IEEE Transactions on Communications*, vol. 45, no. 10, pp. 1159–1161, Oct. 1997.

[70] Q. T. Zhang, "Maximal-ratio combining over Nakagami fading channels with an arbitrary branch covariance matrix," *IEEE Transactions on Vehicular Technology*, vol. 48, no. 4, pp. 1141–1150, July 1999.

[71] A. Shah and A. M. Haimovich, "Performance analysis of optimum combining in wireless communications with Rayleigh fading and co-channel interference," *IEEE Transactions on Communications*, vol. 46, no. 4, pp. 473–479, Apr. 1998.

[72] A. A. Abu-Dayya and N. C. Beaulieu, "Outage probabilities of diversity cellular systems with cochannel interference in Nakagami fading," *IEEE Transactions on Vehicular Technology*, vol. 41, no. 4, pp. 343–355, Nov. 1992.

[73] J. Cui and A. U. Sheikh, "Outage probability of cellular radio systems using maximal ratio combining in the presence of multiple interferers," *IEEE Transactions on Communications*, vol. 47, no. 8, pp. 1121–1124, Aug. 1999.

[74] A. Shah and A. M. Haimovich, "Performance analysis of maximal ratio combining and comparison with optimum combing for mobile radio communications with cochannel interference," *IEEE Transactions on Vehicular Technology*, vol. 49, no. 4, pp. 1454–1463, July 2000.

[75] V. Aalo and J. Zhang, "Performance analysis of maximal ratio combining in the presence of multiple equal-power cochannel interference in a Nakagami fading channel," *IEEE Transactions on Vehicular Technology*, vol. 50, no. 2, pp. 497–503, Mar. 2001.

[76] C. Chayawan and A. Aalo, "On the outage probability of optimum combining and maximal ratio combining schemes in an interference-limited Rice fading channel," *IEEE Transactions on Communications*, vol. 50, no. 4, pp. 532–535, Apr. 2002.

[77] X. W. Cui, Q. T. Zhang, and Z. M. Feng, "Outage performance for maximal ratio combiner in the presence of unequal-power co-channel interferers," *IEEE Communications Letters*, vol. 8, no. 5, pp. 289–291, May 2004.

[78] J. Cui, D. D. Falconer, and A. U. Sheikh, "Performance evaluation of optimum combining and maximal ratio combining in the preference of cochannel interference and channel correlation for wireless communication system," *Mobile Networks and Applications*, vol. 2, pp. 315–324, Dec. 1997.

[79] Y. Tokgoz and B. D. Rao, "The effects of channel correlation on maximal ratio combining performance in the presence of cochannel interferers," in *Proc. IEEE International Conference on Acoustic, Speech, and Signal Processing (ICASSP'03)*, Apr. 6–10 2003, vol. 4, pp. IV–377–80.

[80] X. Zhang and N. C. Beaulieu, "Outage probability of MRC with equi-power cochannel interferers in correlated Rayleigh fading," *IEEE Communications Letters*, vol. 9, no. 7, pp. 577–579, July 2005.

[81] X. Zhang and N. C. Beaulieu, "Outage probability of MRC with unequal-power cochannel interferers in correlated Rayleigh fading," *IEEE Communications Letters*, vol. 10, no. 1, pp. 7–9, Jan. 2006.

[82] V. Aalo and J. Zhang, "On the effect of co-channel interference on average error rates in Nakagami-fading channels," *IEEE Communications Letters*, vol. 3, no. 5, pp. 136–138, May 1999.

[83] K. Sivanesan and N. C. Beaulieu, "Exact BER analyses of Nakagami/Nakagami and Nakagami/Rayleigh CCI QPSK systems in slow fading," *IEEE Communications Letters*, vol. 8, no. 1, pp. 45–47, Jan. 2004.

[84] K. Sivanesan and N. C. Beaulieu, "Exact BER analysis of bandlimited BPSK with EGC and SC diversity in cochannel interference and Nakagami fading," *IEEE Communications Letters*, vol. 8, no. 10, pp. 623–625, Oct. 2004.

[85] K. Sivanesan and N. C. Beaulieu, "Outage and BER of MRC diversity in bandlimited micro-cellular systems with CCI," *IEEE Communications Letters*, vol. 9, no. 3, pp. 207–209, Mar. 2005.

[86] Y. Ma, T. J. Lim, and S. Pasupathy, "Error probability for coherent and different PSK over arbitrary Rician fading channels with multiple cochannel interferers," *IEEE Transactions on Communications*, vol. 50, no. 3, pp. 429–441, Mar. 2002.

[87] X. Zhang and N. C. Beaulieu, "Outage and error rate of cellular systems using MRC in the presence of multiple interferers and correlated Rayleigh fading," in *Proc. IEEE Global Telecommunications Conference (GLOBECOM'06)*, San Francisco, CA, USA, Nov 27– Dec. 1 2006.

[88] M. J. Gans, "The effect of Gaussian error in maximal ratio combiners," *IEEE Transactions on Communication Technology*, vol. COM-19, no. 4, pp. 492–500, Aug. 1971.

[89] B. R. Tomiuk, N. C. Beaulieu, and A. A. Abu-Dayya, "General forms of maximal ratio diversity with weighting errors," *IEEE Transactions on Communications*, vol. 47, no. 4, pp. 488–492, Apr. 1999.

[90] L. Cao and N. C. Beaulieu, "Closed-form BER results for MRC diversity with channel estimation errors in Ricean fading channels," *IEEE Transactions on Wireless Communications*, vol. 4, no. 4, pp. 1440–1447, July 2005.

[91] R. Annavajjala and L. B. Milstein, "Performance analysis of linear diversity-combining schemes on Rayleigh fading channels with binary signaling and Gaussian weighting errors," *IEEE Transactions on Wireless Communications*, vol. 4, no. 5, pp. 2267–2278, Sept. 2005.

[92] Y. Ma, R. Schober, and S. Pasupathy, "Effect of channel estimation errors on MRC diversity in Rician fading channels," *IEEE Transactions on Vehicular Technology*, vol. 54, no. 6, pp. 2137–2142, Nov. 2005.

[93] R. You, H. Li, and Y. Bar-Ness, "Diversity combining with imperfect channel estimation," *IEEE Transactions on Communications*, vol. 53, no. 10, pp. 1655–1662, Oct. 2005.

[94] L. L. Chong and L. B. Milstein, "Error rate of a multicarrier CDMA system with imperfect channel estimates," in *Proc. IEEE International Conference on Communications (ICC'00)*, 2000, vol. 2, pp. 934–938.

[95] Y. Akyildiz and B. D. Rao, "Maximum ratio combining performance with imperfect channel estimates," in *Proc. IEEE International Conference on Acoustics, Speech, and Signal Processing (ICASSP'02)*, May 2002, vol. 3, pp. 2485–2488.

[96] Y. Tokgoz and B. D. Rao, "The effect of imperfect channel estimation on the performance of maximum ratio combining in the presence of cochannel interference," *IEEE Transactions on Vehicular Technology*, vol. 55, no. 5, pp. 1527–1534, Sept. 2006.

[97] R. N. Bracewell, *The Fourier Transform and Its Applications*, 3rd ed. McGraw-Hill, 2000.

[98] S. Nadarajah and S. Kotz, "Elementary expressions for outage probability," *IEEE Communications Letters*, vol. 10, no. 8, pp. 594, Aug. 2006.

[99] L. Xiao and X. Dong, "Error performance of selection combining and switched combining systems in Rayleigh fading channels with imperfect channel estimation," *IEEE Transactions on Vehicular Technology*, vol. 54, no. 6, pp. 2054–2065, Nov. 2005.

[100] D. S. Shiu, G. J. Foschini, M. J. Gans, and J. M. Kahn, "Fading correlation and its effect on the capacity of multielement antenna systems," *IEEE Transactions on Communications*, vol. 48, no. 3, pp. 502–513, Mar. 2000.

[101] C. N. Chuah, D. Tse, J. M. Kahn, and R. A. Valenzuela, "Capacity scaling in MIMO wireless systems under correlated fading," *IEEE Transactions on Information Theory*, vol. 48, no. 3, pp. 637–650, Mar. 2002.

[102] D. Gesbert, T. Ekman, and N. Christopherser, "Capacity limits of dense palm-sized MIMO arrays," in *Proc. IEEE Global Telecommunications Conference (GLOBECOM'02)*, Nov. 2002, vol. 2, pp. 1187–1191.

[103] T. S. Pollock, T. D. Abhayapala, and R. A. Kennedy, "Antenna saturation effects on MIMO capacity," in *Proc. IEEE International Conference on Communications (ICC'03)*, Anchorage, AK, May 2003, vol. 4, pp. 2301–2305.

[104] L. W. Hanlen and M. Fu, "Capacity of MIMO channels: a volumetric approach," in *Proc. IEEE International Conference on Communications (ICC'03)*, Anchorage, AK, May11-15 2003, vol. 5, pp. 3001–3005.

[105] L. W. Hanlen and M. Fu, "Wireless communication systems with spatial diversity: a volumetric model," *IEEE Transactions on Wireless Communications*, vol. 5, no. 1, pp. 133–142, Jan. 2006.

[106] A. L. Moustakas, H. U. Baranger, L. Balents, A. M. Sengupta, and S. H. Simon, "Communication through a diffusive medium: coherence and capacity," *Science*, vol. 287, no. 5451, pp. 287–290, Jan. 2000.

[107] S. Wei, D. Goeckel, and R. Janaswamy, "On the asymptotic capacity of MIMO systems with fixed length linear antenna arrays," in *Proc. IEEE International Conference on Communications (ICC'03)*, Anchorage, AK, May11-15 2003, vol. 4, pp. 2633–2637.

[108] S. Wei, D. Goeckel, and R. Janaswamy, "On the asymptotic capacity of MIMO systems with antenna arrays of fixed length," *IEEE Transactions on Wireless Communications*, vol. 4, no. 4, pp. 1608–1621, July 2005.

[109] J. H. Winters, "Optimum combining in digital mobile radio with cochannel interference," *IEEE Journal on Selected Areas in Communications*, vol. SAC-2, no. 2, pp. 528–539, July 1984.

[110] J. H. Winters, "On the capacity of radio communication systems with diversity in a Rayleigh fading environment," *IEEE Journal on Selected Areas in Communications*, vol. SAC-5, no. 5, pp. 871–878, June 1987.

[111] J. Zhou, S. Sasaki, S. Muramatsu, H. Kikuchi, and Y. Onozato, "Spatial correlation for a circular antenna array and its applications in wireless communications," in *Proc. IEEE Global Telecommunications Conference (GLOBECOM'03)*, San Francisco, CA, USA, Dec.1-5 2003, vol. 2, pp. 1108–1113.

[112] N. C. Beaulieu and X. Zhang, "On selecting the number of receiver diversity antennas in Ricean fading cochannel interference," in *Proc. IEEE Global Telecommunications Conference (GLOBECOM'06)*, San Francisco, CA, USA, Dec. 27–1 2006.

[113] N. C. Beaulieu and X. Zhang, "On the maximum number of receiver diversity antennas that can be usefully deployed in a cochannel interference dominated environment," *IEEE Transactions on Signal Processing*, to be published.

[114] P. D. Teal, T. D. Abhayapala, and R. A. Kennedy, "Spatial correlation for general distributions of scatters," *IEEE Signal Processing Letters*, vol. 9, no. 10, pp. 305–308, Oct. 2002.

[115] R. H. Clarke and W. L. Khoo, "3-D mobile radio channel statistics," *IEEE Transactions on Vehicular Technology*, vol. 46, no. 3, pp. 798–799, Aug. 1997.

[116] N. C. Beaulieu and Q. Xie, "An optimal lognormal approximation to lognormal sum distributions," *IEEE Transactions on Vehicular Technology*, vol. 53, no. 2, pp. 479–489, Mar. 2004.

[117] X. Dong and N. C. Beaulieu, "Optimal maximal ratio combining with correlated diversity branches," *IEEE Communications Letters*, vol. 6, no. 1, pp. 22–24, Jan. 2002.

[118] A. Annamalai and C. Tellambura, "Analysis of hybrid selection/maximal-ratio diversity combiners with Gaussian errors," *IEEE Transactions on Wireless Communications*, vol. 1, no. 3, pp. 498–512, July 2002.

[119] L. Cao and N. C. Beaulieu, "Bit error rate analysis of hybrid selection/maximal-ratio diversity combining with channel estimation error," in *Proc. IEEE Global Telecommunications Conference (GLOBECOM'04)*, Nov. 29 - Dec. 3 2004, vol. 1, pp. 446–451.

[120] R. G. K. Ladas, "On the solution of a second order linear homogeneous difference equation with variable coefficients," *Journal of Mathematical Analysis and Applications*, vol. 215, no. 1, pp. 32–47, Nov. 1997.

[121] R. K. Mallik, "On the solution of a linear homogeneous difference equation with variable coefficients," *SIAM Journal on Mathematical Analysis*, vol. 31, no. 2, pp. 375–385, 1999.

[122] R. A. Horn and C. R. Johnson, Eds., *Matrix Analysis*. New York: Cambridge University Press, 1985.